INFORMATION TO USERS

This manuscript has been reproduced from the microfilm master. UMI films the text directly from the original or copy submitted. Thus, some thesis and dissertation copies are in typewriter face, while others may be from any type of computer printer.

The quality of this reproduction is dependent upon the quality of the copy submitted. Broken or indistinct print, colored or poor quality illustrations and photographs, print bleedthrough, substandard margins, and improper alignment can adversely affect reproduction.

In the unlikely event that the author did not send UMI a complete manuscript and there are missing pages, these will be noted. Also, if unauthorized copyright material had to be removed, a note will indicate the deletion.

Oversize materials (e.g., maps, drawings, charts) are reproduced by sectioning the original, beginning at the upper left-hand corner and continuing from left to right in equal sections with small overlaps. Each original is also photographed in one exposure and is included in reduced form at the back of the book.

Photographs included in the original manuscript have been reproduced xerographically in this copy. Higher quality 6" x 9" black and white photographic prints are available for any photographs or illustrations appearing in this copy for an additional charge. Contact UMI directly to order.

UMI

A Bell & Howell Information Company
300 North Zeeb Road, Ann Arbor MI 48106-1346 USA
313/761-4700 800/521-0600

Université d'Ottawa · University of Ottawa

PREDICTION OF CRITICAL HEAT FLUX IN BUNDLES USING TUBE LOOK-UP TABLE

by

©XINGDONG CUI

Submitted to the School of Graduate Studies of
the University of Ottawa
in partial fulfilment of
the requirements for the degree of

MASTER OF APPLIED SCIENCE
in
Mechanical Engineering

Ottawa-Carleton Institute for
Mechanical and Aeronautical Engineering

OTTAWA, Ontario, 1997

ABSTRACT

An extensive and systematic literature review on the effect of parameters and geometry on the Critical Heat Flux (CHF) is performed. This review covers most of the flow geometries that have been previously investigated such as tubes, concentric annuli and bundles.

Each of the above geometries is studied individually. The following parameters are found to have a strong effect on CHF in bundles:

- exit quality,
- pressure,
- hydraulic-equivalent diameter,
- heated-equivalent diameter,
- cold wall,
- element spacing (spacers),
- enthalpy or quality imbalance,
- axial heat flux distribution,
- radial heat flux distribution.

It is found that some of the geometric effects on CHF depend on the flow conditions and the CHF type (six types of CHF have been identified for convective boiling).

For each geometry the parametric trends are discussed, a review of the available prediction methods, including CHF

correlations and models, is conducted, and the mechanism of CHF in each geometry is described.

The following trends of CHF in bundles are identified in this study:

(i) in general the CHF in bundles is lower than that in tubes, especially for high quality;

(ii) the geometry effect is the most important factor in bundles.

Based on the observed trends, CHF correction factors are derived for bundles. Finally, a CHF prediction method for bundles based on the correction factors with the AECL-UO lookup table as a reference is proposed.

ACKNOWLEDGEMENTS

I would like to take this opportunity to thank all those who have helped to complete this thesis.

I especially thank my thesis supervisor, Dr. S. C. Cheng whose guidance, advice and support are gratefully acknowledged.

I am also grateful to Dr. D. C. Groeneveld of AECL, who has provided valuable suggestions throughout the course of this work.

My appreciation also goes to the University of Ottawa and to Carleton University for the opportunity to study in these institutions.

TABLE OF CONTENTS

NOMENCLATURE

A	function of G, P, Z and D
B	function of G, P, Z and D
a	two phase multiplier in turbulent intensity equation
a_{ij}	constant taking of value of zero or unity
A_x	cross-sectional area of bundle
b_{ij}	parameter used in Eq.(4.6) when $J_{Gij} > 0$ then $a_{ij}=1$ and $b_{ij}=0$, when $J_{Gij} < 0$ then $a_{ij}=0$ and $b_{ij}=1$, and when $J_{Gij} = 0$ then $a_{ij}=0$ and $b_{ij}=0$
C	constant; parameter in equation (4.2)
CHF	critical heat flux (kW/m^2)
CHF_0	critical heat flux at zero inlet subcooling used in Eqs.(3.8)-(3.14)
C_i	concentration of entrained droplets in the gas core of a subchannel of type i
c_{pf}	specific heat of liquid phase (J/kg.k)
D	tube or shroud diameter (mm or m); or deposition rate of droplets onto the liquid film ($kg/m^2.s$)
D_{he}	heated equivalent diameter = (4 flow area)/(heated perimeter) (mm or m)
D_{hy}	hydraulic equivalent diameter = (4 flow area)/(wetted perimeter) (mm or m)
D_p	average bubble diameter (mm)
d	rod diameter (mm)
E	entrainment rate of droplets from the liquid film ($kg/m^2.s$)

g	acceleration due to gravity (m/s²)
G	mass flux or superficial mass flux (kg/m².s)
G_D	local deposition rate (Mg/m².s)
G_s	axial spacing of the spacers (mm or m)
h	enthalpy (J/kg)
h_{fg}	latent heat (J/kg)
h_{ld}	enthalpy at point of bubble detachment (J/kg)
i_b	turbulent intensity at bubbly layer core interface
J_{gij}	the crossflow of gas from each subchannel of type i to each subchannel of type j per unit length of the bundle
K	function of Z′, R′, W′
K_a	mass transfer coefficient
K_q	as K_a, but in diabatic condition
K_{cij}	mass transfer coefficient for turbulent interchange of entrained drops between subchannel of types i and j
K_{hor}	correction factor used in Eq.(2.17)
k	correction factor, constant
n	fraction of deposition rate on a given surface; the number of elements in a bundle
n_{ij}	number of subchannels of type i bordering on each of the subchannels of type j
P	pressure
P_{cr}	critical pressure
p	perimeter
q_i	heat flux from the ith element in a bundle (kW/m²)
q_{max}	maximum radial heat flux in a bundle (kW/m²)
rms	root mean square error = SQRT(($\sum$(relative error)²)/ number of data points)

R'	$= \rho_g / \rho_f$
Re_l	liquid Reynolds number used in Eq.(2.20)
S_{fij}	area of boundary in the fluid per unit length between each subchannel of type i and each subchannel of type j
S_{si}	solid surface per unit length in each subchannel of type i
T	temperature (K or °C)
t	rod to rod pitch (defined in Fig.3.2)
v'	radial fluctuating velocity (m/s)
v_{li}	radial velocity created by vapour generation (m/s)
W'	$=(\sigma\rho_f/G^2Z)$
W_{dep}	mass flow rate of deposited droplets used in Eq.(3.15)
$W^c_{\Delta p}$	liquid mass flow rate at which entainment ceases.
W_E	entrainment flow rate per unit width (kg/m.s)
W_F	film flow rate per unit width (kg/m.s)
W_{gi}	gas flow rate in each subchannel of type i
W_{LEi}	entrained liquid flow rate in each subchannel
W^c_n	liquid mass flow rate normal to surface.
x	thermodynamic equilibrium quality $=(h-h_f)/h_{fg}$
x_1	average quality in core region
x_2	average quality in bubble layer
x_n	quality at which deposition ceases
x_{n1}	difference of qualities x_n and $x_{\Delta p}$
$x_{\Delta p}$	quality at which entrainment ceases
Z	function of Z', R', W'
Z'	$= Z/D$
z	axial coordinate (mm or m)

Greek Symbols

α	void fraction
σ	surface tension (N/m)
σ'_v	standard deviation of v′
Φ	surface heat flux (kw/m²)
Φ_{oi}	fraction of liquid flowing as film on outer surface for internal heating
ρ	density (kg/m³)
ξ	ratio of heat flux on a rod to the maximum heat flux in the bundle
ψ	$=\frac{1}{2\pi}\exp\left[-\frac{1}{2}\left(\frac{v_{11}}{\sigma_{v'}}\right)-\frac{1}{2}\left(\frac{v_{11}}{\sigma_{v'}}\right)erfc\left(\frac{v_{11}}{\sqrt{2}\sigma_{v'}}\right)\right]$

Subscripts

bun	bundle
c	critical (CHF) conditions
cw	cold wall effect
DO	dryout
DNB	departure from nucleate boiling
e	exit
eq	equilibrium value
f	saturated liquid
g	saturated vapour
h	heated
hy	hydraulic
he	heated
i	inlet; the ith element; inside surface

l	liquid
LF	liquid film
max	maximum
n	normal to surface
nq	corresponds to minimum liquid in the core at CHF section in diabatic conditions
o	outside, outer surface
p	pressure effect
rd	rod
rfd	radial heat flux distribution
s	shroud
sat	saturated condition
sp	spacer effect
sub	subcooled condition
t	rod pitch
T	total flow (liquid+vapour)
w	wetted
x	quality effect

Superscripts

p	value from previous axial segment

LIST OF TABLES

LIST OF FIGURES

1. INTRODUCTION

The Critical Heat Flux (CHF) is characterized by a quick increase of the wall temperature which results from the replacement of liquid by vapor adjacent to the heat transfer surface. This kind of phenomenon has been studied extensively during the past 40 years, as shown by the proliferation of correlations and models, but most of the studies are developed restrictively for round tubes, only some of them can be applied to other geometries.

The development of nuclear power plants generated an increasing interest in CHF in different coolant flow geometries other than round tubes. The CHF is known as one of the factors that limits the maximum power extractable from water-cooled nuclear reactors. Operation at heat flux safely below the CHF remains a major design limitation for nuclear reactors. Hence, the knowledge of the exact occurrence of CHF is essential in increasing the reactor power. Although there are many correlations developed to predict CHF in reactor bundles over past 40 years(e.g., Rogers, 1970), round tube correlations are frequently applied to different geometries present in the reactor recently, such as subchannel-shaped geometries and bundles. This application of tube CHF correlations to the geometries in reactors is a source of possible large errors in CHF predictions, hence large safety margins are required to compensate for these potential errors. Therefore, a prediction method which accounts for the effect of the changes in flow geometry on CHF is needed. The purpose of this study is to develop such a prediction method.

The CHF predication method used in subchannel codes is primarily based on the tube CHF values, but these methods do not take into account the bundle-specific effects such as geometry, enthalpy-imbalance, and radial heat flux distribution. As an initial step toward improving the CHF prediction accuracy in the bundles, this study presents the development of a new CHF prediction method for bundles.

The cost of experimentally investigating the CHF phenomenon in full-scale simulated fuel-bundle geometries is prohibitive, as the experiments on each fuel-bundle geometry would typically cost from 2 to 5 Million dollars. In this study, the experimental results from the literature are used for the analysis.

The differences between tubes and bundles were examined systematically by accounting for the differences in geometric parameters and bundle-specific effects, and based on these observations, a new CHF prediction method for bundles has been proposed. As a reference for comparing the CHF in bundles, the AECL-UO CHF look-up table (Groeneveld et al., 1995) was used in this study. The AECL-UO look-up table is a widely accepted prediction method for tubes.

In this study, the AECL-UO look-up table is used as a reference to predict CHF in reactor bundles. To account for the effects of differences between tubes and bundles on CHF, any variation of each of the characteristic parameters of a bundle needs to be considered. These characteristic parameters are:

- characteristic diameter,
- heated perimeter,
- wetted perimeter,
- the geometric layout of the elements
- spacers,
- radial heat flux distribution.

The approaches taken in this study are:

(i) Examine CHF phenomena in different geometries, such as round tubes, internally heated annuli and bundles.

(ii) Determine the dominating parametric effects on CHF for different geometries, in particular, the bundle-specific effects of cold wall, spacer, radial heat flux distribution, etc.

(iii) Derive a bundle CHF prediction method using the AECL-UO look-up table as a reference and based on correction factors obtained from various parametric effects.

This study is an extension of earlier work by Doerffer(1994), who developed a new method to predict CHF in annuli using the AECL-UO look-up table.

2. CRITICAL HEAT FLUX IN TUBES

2.1 General

In forced convective boiling, the boiling crisis occurs when the heat flux is raised to such a high level that the heated surface can no longer contain continuous liquid contact. It is characterized by a sharp reduction of the local heat transfer coefficient, which results from the replacement of the liquid by vapour adjacent to the heat transfer surface. The boiling crisis manifests itself by a sudden rise in temperature caused by blanking of the heat surface by a stable vapour layer, or by small surface temperature spikes corresponding to the appearance and disappearance of dry patches. The magnitude of the temperature jump during this phenomenon depends on the flow conditions and regimes. To describe this particular condition, different terms have been used:

- *burnout*,
- *dryout*,
- *critical heat flux* (CHF),
- *departure from nucleate boiling* (DNB).

None of these terms gives a general description of the physics. For instance, the term "burnout" implies a physical melting of the heated surface which does not necessarily occur (e.g., at high qualities the temperature excursion is not very important and does

not lead to immediate damage of the surface). The DNB arises when the nucleate boiling is transformed to film boiling in the subcooled or saturated nucleate boiling conditions, so in this case the term "departure from nucleate boiling" is the most appropriate. The term "dryout" is proper when the dryout of the liquid film occurs at high qualities. In this thesis, the aforementioned phenomena will be referred to as the critical heat flux conditions, and the heat flux at which it occurs as the critical heat flux (CHF).

2.2 Heat Transfer Regimes

In flow boiling, flow conditions and regime play a significant role in the CHF mechanism. Collier (1994) pointed out that various hydrodynamic conditions were encountered when a liquid was boiled in a confined tube. The various flow patterns encountered over the length of the tube is shown in the Figure 2.1, in diagrammatic form, together with the corresponding heat transfer regions. These patterns occur when a vertical tube is uniformly heated over its length with a low heat flux and fed with subcooled liquid at its base at such a rate that the liquid is totally evaporated over the length of the tube.

The process of heat transfer is *a single phase convective heat transfer to the liquid phase* (region A), when the liquid is being heated up to the saturation temperature and the wall temperature remains below that necessary for nucleation. At some point along

the tube, the conditions adjacent to the wall are such that the formation of vapour from nucleation sites can occur. Initially vapour formation takes place in the presence of subcooled liquid (region B) and this heat transfer mechanism is known as *subcooled nucleate boiling*. The wall temperature remains essentially constant a few degrees above the saturation temperature, in the subcooled boiling region, B, whilst the mean bulk fluid temperature is increasing to the saturation temperature. The amount by which the wall temperature exceeds the saturation temperature is known as the 'degree of superheat', ΔT_{SAT}, and the difference between the saturation and local bulk fluid temperature is known as the 'degree of subcooling', ΔT_{SUB}.

The transition between the *subcooled nucleate boiling region, B,* and the *saturated nucleate boiling region, C,* is clearly defined from a thermodynamic viewpoint. It is the point at which the liquid reaches the saturation temperature (x=0) found on the basis of simple heat balance calculation. However, subcooled liquid can persist in the liquid core even in the region defined as *saturated nucleate boiling*. Vapour generated in the subcooled region is present at the transition between regions B and C (x=0); thus some of the liquid must be subcooled to ensure that the liquid mixed mean (mixing cup) enthalpy equals that of saturated liquid (h_f). This effect occurs as a result of the radial temperature profile in the liquid and the subcooled liquid flowing in the centre of the channel will only reach the saturation temperature at some distance downstream of the point x=0.

The variable characterizing the heat transfer mechanism, in the regions C to G, is the thermodynamic mass 'quality' (x) of the fluid. The 'quality' of the vapour-liquid mixture at a distance, z is given on a thermodynamic basis as (i.e., thermodynamic quality)

$$x(z)=\frac{h(z)-h_f}{h_{fg}} \tag{2.1}$$

or in terms of heat flux and length (i.e., true quality)

$$x(z)=\frac{4\phi}{DGh_{fg}}(z-z_{SC}) \tag{2.2}$$

where z_{sc} is the length of the tube required to increase the enthalpy of the liquid up to the saturated liquid enthalpy, h_f. In the region of $0<x<1$ and for complete thermodynamic equilibrium, x represents the ratio of the vapour mass flow- rate to the total mass flow-rate. From the thermodynamic definition, Eq.(2.1), x may have both negative values and values greater than unity. The variable x is often referred to as the 'vapour weight fraction'.

A point may be reached where a fundamental transition in the mechanism of heat transfer takes place, when the quality increases through the *saturated nucleate boiling region*. The process of 'boiling' is replaced by the process of 'evaporation'. This transition is preceded by a change in the flow pattern from bubbly or slug flow to annular flow (regions E and F). In the latter regions the thickness of the thin liquid film on the heating surface is often such that the effective thermal conductivity is sufficient to prevent the liquid in contact with the wall being

superheated to a temperature which would allow bubble nucleation. Heat is carried away from the wall by forced convection in the film to the liquid-vapour core interface, where evaporation occurs. The region beyond the transition has been referred to as the *two-phase forced convective region* of heat transfer (regions E and F).

The complete evaporation of the liquid film occurs at some critical value of the quality. This transition is known as 'dryout' and is accompanied by a rise in the wall temperature for channels operating with a controlled surface heat flux. The area between the dryout point and the transition to *dry saturated vapour* (region H) has been defined as the liquid *deficient region* (corresponding to the drop flow pattern) (region G). This condition of 'dryout' often puts an effective limit on the amount of evaporation that can be allowed to take place in a tube at a particular value of heat flux.

2.3 Boiling Map

It is very important to understand, at least qualitatively, the progressive variation of the local heat transfer coefficient along the length of the tube as evaporation proceeds. The local heat transfer coefficient can be established by dividing the surface heat flux (constant over the tube length) by the difference between the wall temperature and the bulk-fluid temperature. Figure 2.1 shows the typical variations of these two temperatures with length along the tube. The variation of the heat transfer

coefficient with length along the tube for the conditions represented in Fig. 2.1 is given in Fig. 2.2 (curve (i), solid line). The heat transfer coefficient is relatively constant in the *single phase convective heat transfer region*, changing only slightly due to the influence of temperature on the liquid physical properties. The temperature difference between the wall and the bulk fluid decreases linearly with length up the point where x=0 in the *subcooled nucleate boiling region*. The heat transfer coefficient, therefore, increases linearly with length in this region. The temperature difference and therefore the heat transfer coefficient remain constant in the *saturated nucleate boiling region*. Because of the reducing thickness of the liquid film in the *two-phase forced convective* region, heat transfer in this region is characterized by an increasing coefficient with increasing length or mass quality. At the dryout point the heat transfer coefficient is suddenly reduced from a very high value in the forced convective region to a value near to that expected for heat transfer by forced convection to dry saturated vapour. As the quality increases through the *liquid deficient region* so that vapour velocity increases and the heat transfer coefficient rises correspondingly. Finally, in the *single-phase vapour region* (x>1) the heat transfer coefficient levels out to that corresponding to convective heat transfer to a single-phase vapour flow.

The above comments have been restricted to the case where a relatively low heat flux is supplied to the walls of the tube. The effect of progressively increasing the surface heat flux whilst keeping the inlet flow-rate constant will now be considered with

reference to Figures 2.2, 2.3 and 2.4. The heat transfer coefficient plotted against mass quality with increasing heat flux as parameter (curves (i)-(vii)) is shown in Figure 2.2. The various regions of two-phase heat transfer in forced convection boiling on a three-dimensional diagram with heat flux, mass quality and temperature as coordinates--'the boiling surface' are shown in Figure 2.3.

The regions of two-phase forced convection heat transfer as a function of quality with increasing heat flux as ordinate (an elevation view of Fig. 2.3 taken in the direction of the arrow) are shown in Figure 2.4.

Curve (i) of Fig. 2.2 represents the conditions shown in Fig. 2.1 for a low heat flux being supplied to the walls of the tube. The temperature pattern shown in Fig. 2.1 will be viewed as the projection in plan view (temperature-quality coordinates) of Fig. 2.3.

Curve (ii) demonstrates the influence of increasing the heat flux. Subcooled boiling is initiated sooner, the heat transfer coefficient in the nucleate boiling region is higher but is unaffected in the two-phase forced convective region. Dryout occurs at a lower mass quality.

Curve (iii) displays the influence of a further increase in heat flux. Again, subcooled boiling is initiated earlier and the heat transfer is again higher in the nucleate boiling region. As the mass quality increases, before the two-phase forced convective

region is initiated and while bubble nucleation is still occurring, an abrupt deterioration in the cooling process takes place. This transition is termed 'departure from nucleate boiling' (DNB).

The mechanism of heat transfer condition where the critical heat flux (DNB or dryout) has been exceeded is dependent on whether the initial condition was the process of 'boiling' (i.e., bubble nucleation in the subcooled or low mass quality regions) or the process of 'evaporation' (i.e., evaporation at the liquid film-vapour core interface in the higher mass quality areas). In the latter case, the 'liquid deficient region' is initiated; in the former case the resulting mechanism is one of 'film boiling (Fig. 2.4).

In Figures 2.2 and 2.4, it can be seen that further increases in heat flux (curves (vi) and (vii)) cause the condition of 'departure from nucleate boiling' (DNB) to occur in the subcooled region with the whole of the saturated or 'quality' region being occupied by firstly 'film boiling' and, in the latter stages, by the 'liquid deficient region'- both relatively inefficient modes of heat transfer.

2.4 CHF Mechanisms

There are six CHF mechanisms, which have been identified, as shown in the following:

(i) Liquid Starvation by Vapour Bridging

For certain combinations of flow geometry and flow conditions, the bubble can be of the same size as the transverse dimension of the flow geometry as shows in Figure 2.5. In this case, a bubble could locally bridge the complete cross section, resulting in a temporary interruption of the supply of liquid and subsequent CHF occurrence due to the blockage of the flow passage or a fraction of the flow passage (Joober, 1993). This mechanism is more likely to occur for:

-low pressure, where the liquid to vapour density-ratio is very high;
-saturated boiling, where bubbles are large;
-low flows, where the size of the discrete vapour cells (bubbles, slugs) is large; and
-narrow flow passages.

For each of these conditions there is a thin liquid film which initially remains between the bubble and the heated wall. If the heat flux is high enough this film will evaporate and as a result a premature CHF occurs.

(ii) Nucleation Induced

This type of CHF is encountered at high subcooling where heat is transferred very efficiently by nucleated boiling. Bubbles grow and collapse at the wall. Some convection will take place between the bubbles. Here CHF (or DNB) occurs at very high surface heat fluxes. It has been suggested (Collier,1981; Tong, 1972; quoted by

Groeneveld, 1995) that the CHF occurrence is due to the spreading of a drypatch following microlayer evaporation under a bubble and coalescence of adjacent bubbles although no definite proof of this is yet available. The occurrence of dryout here depends only on the local surface heat flux and flow conditions and is not affected by upstream heat flux distribution. The surface temperature rise under these conditions is very rapid (fast dryout) and usually results in failure of the heated surface.

(iii) Bubble Clouding

In subcooled and saturated nucleate boiling the number of bubbles generated depends on the heat flux and bulk temperature. The bubble population density near the heated surface increases with increasing heat flux and a so-called bubble boundary layer(Tong, 1965; 1972; quoted by Groenenveld, 1995) often forms a short distance away from the surface. If this layer is sufficiently thick, it can impede the flow of coolant to the heated surface. This in turn leads to a further increase in bubble population until the wall becomes so hot that a vapour patch forms over the heated surface. This type of boiling CHF is also characterized by a fast rise of the heated surface temperature (fast dryout). Physical failure of the heated surface frequently occurs under these conditions.

(iv) Entrainment-Controlled Film Dryout

Figure 2.6 shows the relation between the entrained-droplet flow rate and the local quality. Also shown in this figure is the

hydrodynamic-equilibrium entrainment curve (dotted curve), where the entrainment is balanced by deposition for varying quality. The CHF condition is reached when the entrained-droplet flow equals the total-liquid flow. From this figure it is seen that the entrainment curve increases until crossing the hydrodynamic equilibrium curve and then decreases towards the CHF condition. Hewitt and Hall-Taylor (1970) postulated that, " in the first part of the channel there is net liquid entrainment from the film and in the latter part of the channel there is net liquid deposition. The results are readily understood if it is realized that the flow will always be tending towards the hydrodynamic equilibrium." This type of CHF occurs in annular flow, but for a relatively shorter length and lower burnout qualities than the deposition-controlled film described below. Figure 2.7 illustrates different zones of CHF occurrence, for various local qualities. The entrainment-controlled film dryout may occur either in Zone II or III and is accompanied by a moderate temperature rise. The liquid film depletion in this case may be enhanced by one of the following mechanisms:

- Thermocapillary effect: one of the most important sources of entrainment in annular flow is the surface wave. These waves cause a non-uniform temperature distribution along the liquid-vapour interface, a maximum temperature in the valley and minimum temperature at the wave tip. This in turn causes a surface tension gradient, which draws liquid to the higher surface tension area (wave tips) and eventually leads to a dryout in the wave valley.

- Nucleation induced film breakdown: when nucleation occurs in the annular flow regime, bubbles may cause a dry-patch in the

liquid film if the bubble size is comparable to the film thickness. At high heat flux values, rewetting of this area could be prevented, thus leaking to a CHF condition (N. B., this is unlikely to occur unless a local heat flux spike is present; high turbulence level is annular liquid film usually suppresses nucleation occurrence).

(v) Deposition-Controlled Film Dryout

The entrainment rate strongly depends on film thickness (Hewitt and Hall-Taylor, 1970). Thicker films result in high waves in the liquid film and the tips of the waves eventually become sheared off and entrained. At high qualities, the liquid is thin and liquid entrainment is suppressed. In this region, the liquid-film flow rate is governed by evaporation and deposition. The following equation can be derived from the liquid-film mass balance

$$\frac{CHF}{h_{fg}} = G_D - \frac{dW_{LF}}{dz} \tag{2.3}$$

where W_{LF} is the film flow rate per unit width and G_D is the local deposition rate per unit surface area.

If the last term in the above equation is zero, then the evaporation rate (from the liquid-film vapour interface) just balances the deposition rate and the CHF is said to be deposition controlled. Hewitt and Hall-Taylor(1970) concluded that the CHF for uniformly heated tubes becomes deposition controlled for long tube lengths (L/D>>100). This type of CHF is illustrated in Figure 2.7 by Zone I.

(vi) Annular Film Dryout, No Entrained Droplets.

This type of CHF mechanism occurs only at very low flows and high qualities, where all the liquid is in the liquid film on the walls of the flow geometry. Here, the CHF occurs when the quality approaches 100%.

Any attempts to obtain generalized predictions of the CHF must consider the flow pattern, since the mechanisms of CHF in different flow patterns are not the same, e.g., dryout at annular flow and DNB at bubbly flow.

2.5 Parametric Effects on CHF

It was postulated that the critical heat flux for water in a vertical uniformly heated tube is a function of five independent variables (Collier, 1995), thus,

$$\Phi_c = f(G,\ (\Delta T_{SUB})_i,\ p,\ D,\ z) \qquad (2.4)$$

Since overheating of the tube surface at the critical condition almost invariably begins at the exit of the heated section, it can be argued that display and correlation should be terms of the exit conditions. The thermodynamic state at the tube exit may be such that the fluid is either subcooled or saturated. Either the fluid enthalpy h(z) or the thermodynamic mass quality x(z) may be chosen to characterize the exit conditions. Each of these dependent variables is related to the inlet subcooling via the heat balance

equation thus,

$$h(z)=h_f+\frac{4\phi z}{DG}-(\Delta T_{SUB})_i c_{pf} \tag{2.5}$$

$$x(z)=\frac{1}{h_{fg}}\left[\frac{4\phi z}{DG}-(\Delta T_{SUB})_i c_{pf}\right] \tag{2.6}$$

It is instructive to examine briefly the manner in which the critical heat flux varies with some of the independent variables. Examples of such relations are shown in the following sections:

2.5.1 Effect of Quality and Inlet Subcooling

Figure 2.8 shows the generally decreasing trend of CHF with an increase in quality. This trend continues until at 100% quality the CHF is zero. For a uniformly heated test section the CHF vs. x_{DO} curve can be transferred into a CHF vs. Δh_{in} ($-x_{in}h_{fg}$) as shown in Figure 2.9. Because of the relatively narrow range of inlet subcooling covered in most experiments, this curve is frequently observed to be nearly linear, and shows a continuous increase in CHF with inlet subcooling. Exceptions to these trends been observed at very high flow where both the CHF vs. x_{DO} and CHF vs. Δh_{in} curves can display a minimum, caused by the occurrence of upstream dryout.

2.5.2 Effect of Mass Flux

Figure 2.10 illustrates the effect of mass flux on CHF. The CHF vs. G plot shows a change in slope at low flows, approaching the line

$$\phi = GD_{hy}(h_{fg}+\Delta h_{in}) \ / \ 4L_{he}$$

for a uniform axial heat flux distribution, this line corresponds to $x_{DO} = 1.0$; it thus represents a physical upper limit to the CHF.

The CHF vs. x_{DO} plot shows a crossover of constant G lines; at low x_{DO} values the CHF increases with G while at high x_{DO} values the trend is opposite. This crossover may be explained by considering the CHF mechanisms: At low qualities, CHF is caused by bubble clouding or microlayer evaporation; an increase in mass flux will result in a more efficient removal of vapour nuclei from the wall or will sweep away the bubble boundary layer. This tends to delay CHF. At high qualities, however, dryout is due to liquid film depletion: the higher flow will result in a wavier liquid film and hence increased entrainment which leads to an early liquid film breakdown.

2.5.3 Effect of Pressure

Pressure has a strong effect on CHF primarily because of its effect on thermodynamic properties. Figure 2.11 illustrates the effect for water when the CHF reaches a maximum value between 4 and

7 MPa. The same trend is valid for pool boiling and can be predicted by Zuber's correlation:

$$CHF = Ch_{fg}\rho^{1/2}[\sigma g(\rho_l - \rho_g)]^{1/4}$$

(Hsu and Graham, 1976; quoted by Groeneveld, 1995).

Near the critical pressure the CHF approaches zero since σ, h_{fg} and $\rho_l - \rho_g$ all approach zero while at low pressure ρ_g decreases rapidly with a reduction in P thus also lowering the CHF.

2.5.4 Geometry Effects

(i) Effect of heated length (Figure 2.12): For constant cross section average CHF conditions(i.e., constant p, G, and D) the effect of heated length in simple geometries is usually small if $L_H/D_{hy}>30$ for subcooled inlets or $L_H/D_{hy}>200$ for two-phase inlets. For short test sections, $L_H/D_{hy} < 60 - 80$, CHF increases as L_H/D_{hy} decreases due to the entrance length effect(Rogers, 1966).

(ii) Effect of diameter (Figure 2.13): Many researchers have observed that for round tube geometries, an increase in diameter results in reduction in CHF (constant cross section average CHF condition), e.g., Lee and Obertelli (1963). Figure 2.13 shows that the effect of tube diameter on the relationship between CHF and Δh_{in} and between CHF and x_{DO} for fixed values of G, L_H and p. As the tube diameter is increased, the CHF increase at constant inlet subcooling, and the CHF decreases with increasing tube

diameter for a given exit quality. No satisfactory explanation is yet available but the resultant decrease in shear stress near the wall and higher entrainment rates for larger diameters are expected to be contributing factors (Hewitt and Hall-Taylor, 1970; quoted by Groeneveld, 1995).

2.6 CHF Prediction Methods

2.6.1 CHF Correlations

(i) The Macbeth-Barnett hypothesis: Probably the most general of the empirical correlations is that by Macbeth (1963) and Thompson and Macbeth(1964) based on a hypothesis proposed and tested by Barnett (1963) (Collier 1994). This hypothesis, the 'local conditions hypothesis' suggests that the critical heat flux is solely a function of the mass quality at the point of overheating for a given mass velocity, pressure and tube diameter. Figure 2.14 is a proof of the approximate validity of the hypothesis for uniformly heated round tubes, at least. Barnett and Macbeth made the simplifying assumption that the critical heat flux is a linear function of inlet subcooling, thus

$$\Phi_C = A + B(\Delta h_{SUB})_i \qquad (2.7)$$

where A and B are assumed to be functions of G, p, z, and D. The heat balance equation may be written. (remembering that $(\Delta h_{SUB})_i = (\Delta T_{SUB})_i c_{pf}$)

$$x(z)h_{fg}+(\Delta h_{SUB})_i=\frac{4\phi z}{DG} \tag{2.8}$$

Eliminating $(\Delta h_{SUB})_i$ between Eq.(2.7) and Eq.(2.8)

$$\phi=\frac{A-Bx(z)h_{fg}}{\left[1-\frac{4Bz}{DG}\right]} \tag{2.9}$$

Equation (2.9) indicates a linear relation between ϕ_c and x(z) and implies that

$$\phi_c=M+Nx(z) \tag{2.10}$$

where M and N are assumed to be function of G, p, and D only.

Comparing Eq.(2.9) and Eq.(2.10)

$$A=\frac{M}{1-(4Nz/DGh_{fg})} \tag{2.11}$$

$$B=\frac{-N}{h_{fg}-(4Nz/DG)} \tag{2.12}$$

Substituting these expressions for A and B into Eq.(2.7) gives

$$\phi_c=\frac{M-(N(\Delta h_{SUB})_i/h_{fg})}{1-(4Nz/DGh_{fg})} \tag{2.13}$$

and finally, writing A'=MC' and C'=-DGh_{fg}/4N gives the general

equations

$$\phi_c = \frac{A' + DG(\Delta h_{SUB})_i / 4}{C' + z} \tag{2.14}$$

and

$$\phi_c = \frac{A' - DGh_{fg}x(z)/4}{C'} \tag{2.15}$$

Barnett and Macbeth developed their correlation in terms of Eq.(2.14) rather than Eq.(2.15) since the former has the advantage of being in terms of the independent variables. The values of A' and C' can be correlated in terms of G, D, and p.

(ii) The Katto correlation: Katto (1980, 1981, 1982) and Katto and Ohne(1984) have published a general correlation applicable to a range of fluids which they have progressively improved over the years. The formulation of Katto and Ohne (1984) used the following equation:

$$\phi_C = XG(h_{fg} + K(\Delta h_{SUB})_i) \tag{2.16}$$

The terms X and K are functions of three dimensionless groupings

$Z' = z/D$

$R' = \rho_g \ / \ \rho_f$

$W' = (\sigma\rho_f \ / \ G^2 \ z)$

Five values of X need then to be determined:

$$X_1 = (CW'^{0.043}) / Z'$$

$$X_2 = (0.1R'^{0.133}W'^{0.333}) / (1 + 0.0031Z')$$

$$X_3 = (0.098R'^{0.133}W'^{0.433}Z'^{0.27}) / (1+ 0.0031Z')$$

$$X_4 = (0.0384R'^{0.6}W'^{0.173}) / (1 + 0.28W'^{0.233}Z')$$

$$X_5 = (0.234R'^{0.513}W'^{0.433}Z'^{0.27}) / (1 + 0.0031Z')$$

Table 2.1 Choice of X and K Values for Katto and Ohne (1984) correlation

For	$R' < 0.15$		$R' > 0.15$	
If	$X_1 < X_2$	$X = X_1$	$X_1 < X_5$	$X = X_1$
	$X_1 > X_2$ & $X_2 < X_3$	$X = X_2$	$X_1 > X_5$ & $X_5 > X_4$	$X = X_5$
	$X_1 > X_2$ & $X_2 > X_3$	$X = X_3$	$X_1 > X_5$ & $X_5 < X_4$	$X = X_4$
	$K_1 > K_2$	$K = K_1$	$K_1 > K_2$	$K = K_1$
	$K_1 < K_2$	$K = K_2$	$K_1 < K_2$ & $K_2 < K_3$	$K = K_2$
			$K_1 < K_2$ & $K_2 > K_3$	$K = K_3$

The value of C is given by

$C = 0.25$ for $Z' < 50$

$C = 0.25 + 0.0009(Z' - 50)$ for $50 < Z' < 150$

$C = 0.34$ for $Z' > 150$

Three values of K also need to be established:

$$K_1 = 0.261/(CW'^{0.043})$$

$$K_2 = \{0.833[0.0124 + (1/Z')]\} / (R'^{0.133}W'^{0.333})$$

$$K_3 = \{1.12[1.52W'^{0.233} + (1/Z')]\} / (R'^{0.6}W'^{0.173})$$

The appropriate values of X and K are then chosen according to Table 2.1.

The correlation is valid over the following ranges of data:

$0.01 < z < 8.8$ m

$0.001 < D < 0.038$ m

$5 < Z' < 880$

$0.0003 < R' < 0.41$

$3\times10^{-9} < W' < 2\times10^{-2}$

2.6.2 CHF Models

Early attempts to obtain generalized predictions of the CHF for liquids flowing inside of tubes were often based on the assumption that the underlying mechanism was essentially the same as for pool boiling. All investigators have now concluded that this is not the case and that the appropriate model depends on the two-phase flow pattern that exists at the CHF conditions(see section 2.4).

In addition to recognizing the probable flow pattern, the orientation of the line must also be considered. In horizontal flow, except at very high mass fluxes, the liquid and vapor

distributions are not uniform circumferentially, and this leads to lower CHF.

2.6.2.1 Bubbly flow model

The mechanism most generally accepted as leading to CHF at low qualities is that of bubble crowding and vapour blanketing at the wall. The bubble layer near the wall is assumed to become so thick that it inhibits enthalpy transport between the fluid in the core and the liquid near the wall.

Weisman and Pei (1983) attempted to develop a model for the interchange between the core region and bubbly layer and relating this to the conditions at which vapour blanketing occurs. The model is based on the following postulates:

(i) Under subcooled and low quality conditions, CHF is a local phenomenon.

(ii) During subcooled and low quality boiling, the bubbly layer builds up in thickness along the channel until it fills the region close to the wall where the turbulent eddy size is insufficient to transport the bubbles radially. At the CHF location, the bubbly layer is assumed to be at this maximum thickness.

(iii) CHF occurs then the volume fraction of steam in the bubbly layer just exceeds the volume fraction (critical void

fraction) at which an array of ellipsoidal bubbles can be maintained without significant contact between the bubbles.

(iv) The volume fraction of steam in the bubbly layer is determined by a balance between the outward flow of vapour and the inward flow of liquid at the bubbly layer core interface. This is reasonable based on the supposition that liquid entering the bubbly layer may be taken as eventually reaching the wall. This implies that the interstices between the bubbly layer are filled with turbulent liquid and that this turbulence level is enhanced by the presence of the bubbles and the boiling process. The critical turbulent transport rate then appears at the edge of the bubbly layer where the liquid turbulence enhancement is substantially below that found within the layer.

The predictive equation is found as

$$\Phi_{DNB}=h_{fg}G(x_2-x_1)i_b\psi\left(\frac{h_f-h_{ld}}{h_l-h_{ld}}\right) \tag{2.17}$$

where

$$\psi=\frac{1}{2\pi}\exp\left[-\frac{1}{2}\left(\frac{v_{11}}{\sigma_{v'}}\right)-\frac{1}{2}\left(\frac{v_{11}}{\sigma_{v'}}\right)erfc\left(\frac{v_{11}}{\sqrt{2}\sigma_{v'}}\right)\right] \tag{2.18}$$

$$i_b = 0.462 Re^{-0.1}(k)^{0.6}\left(\frac{D_p}{D}\right)^{0.6}\left[1 + a\left(\frac{\rho_l - \rho_g}{\rho_g}\right)\right] \qquad (2.19)$$

An iterative procedure is required for computing the predicted value of Φ_{DNB} since the function of ψ, on the RHS of the predictive equation (eq. 2.17) depends on Φ. A value for Φ is assumed and levy's model (1966) is used to calculate the location, z_d, and the enthalpy h_{ld}, at the bubble departure point. An iterative approach is then used to calculate x_{avg}, and h_l, at the z_{CHF}, which is at the end of the tube. The values of i_b and ψ are then computed. By assuming α_2=0.82 at z_{CHF}, x_2 is evaluated at z_{CHF} thus allowing x_1 and ρ_1 to be determined at this evaluation.

where the ranges of parameters are:

P 20-205 bars,

G 3500000-49000000 kg/m².h,

L 0.35-360 cm,

D 0.115-3.75 cm,

$\alpha_{CHF} \leq 0.6$.

The model provides good accuracy when applied to

(i) uniformly heated water data at a variety of conditions and from a variety of sources,

(ii) non-uniformly heated tests,

(iii) data at the high mass velocities of industrial interest,

(iv) CHF data obtained with fluid other than water.

2.6.2.2 Annular flow model

In adiabatic annular flow, liquid droplets are continuously entrained from the liquid film on the tube surface. At the same time, some of the liquid droplets suspended in the vapor core are deposited on the liquid film. For a long unheated tube, the rate of deposition is in equilibrium with the rate of entrainment, and the film thickness remains constant.

The theoretically based prediction of high-void CHF by determination of the conditions at which the annular film dries out was first suggested by Isbin(1959), Isbin and Vandewater et al.(1961). These workers postulated that under diabetic conditions, the liquid film flow in a round tube is determined by an integral balance between entrainment, evaporation, and deposition.

Whalley(1977) proposed his differential mass balances on the film flow and entrained liquid flow as

$$\frac{dW_E}{dz}=\pi d_o(E-D) \tag{2.20}$$

and

$$\frac{dW_{LE}}{dz}=\pi d_o\left(D-E-\frac{\phi}{h_{fg}}\right) \tag{2.21}$$

Integration of the forgoing equation requires appropriate procedures for determination of the entrainment and deposition rates. The deposition rate D is determined from the product of a

mass transfer or deposition coefficient K and droplet concentration C; that is,

$$D=KC \tag{2.22}$$

The entrainment rate is based on the observation that under equilibrium conditions during adiabatic operation, the entrainment and deposition rates are equal. Since under these conditions E=D and D=KC,

$$E=KC_E \tag{2.23}$$

The value of C_E is often taken as a function of the dimensionless group $(\tau m/\sigma)$. Calculation of the entrainment rate requires a knowledge of the interfacial shear stress and film thickness. Use is made of the so-called triangular relationship, which allows W_F, m, and dp/dz to be related in a way that knowledge of any two allows the third to be calculated.

2.6.2.3 Other models

Over the years, hundreds of ad hoc correlations have been developed for the prediction of CHF in vertical flow. Most of them are applicable for a limited range of flow conditions only. However, prediction methods for CHF in horizontal flow are scarce and inaccurate; they are generally valid for a limited range of flow parameters only. One of the reasons for the poor performance of horizontal CHF correlations is the scarcity of horizontal CHF

data.

Researchers (Collier et al, 1994 , Rogers, 1982, and Wong et al.,1990) stated that in horizontal channels, gravitational forces act on both the vapour phase and the liquid phase in a direction perpendicular to the fluid stream, causing asymmetric phase distribution and possibly phase separation. This maldistribution of void can have a severe effect on heat transfer in general and CHF in particular.

For flows with high mass velocities, the effect of tube orientation on CHF is negligible but for intermediate and low flows, the CHF for horizontal flow can be considerably lower. Figure 2.15 illustrates the possible CHF occurrences in a horizontal tube. Upstream dryout occurs in the low-quality region where bubbles coalesce and form a continuous vapour cushion along the upper portion of the tube. As vaporization continues downstream, the increase stream velocity causes higher-amplitude waves to form on the liquid-vapour interface. The faster-moving vapour stream impinges on the waves and thus causes liquid to be entrained in the vapour-core region. Some of the entrained liquid is deposited onto the upper portion of the tube and, finally, the liquid will again cover the full circumference of the tube and annular flow is established.

The CHF mechanisms are identified in three different quality regions:

(i) At very low qualities, bubbles that are produced at the

wall could form ribbons of vapour along the upper surface of the channel under low flow conditions. These vapour ribbons act as barriers and inhibit the replenishment of liquid lost by draining and evaporation, thus causing a premature occurrence of the CHF condition and a subsequent steep rise in the wall temperature.

(ii) At low and intermediate qualities, the flow in the evaporating channel is characterized by alternating large splashing waves which carry the liquid to the upper surface of the channel. There is little or no droplet entrainment activity and, thus, no replenishment of the liquid film at the top of the channel. As a result, the liquid film at the upper surface is subjected to drainage and evaporation which will finally dryout if sufficient time is given before the next splashing wave touches the upper surface.

(iii) At high qualities, the flow pattern is probably annular. Figure 2.15 shows a horizontal annular flow in air and water, for typical liquid film and vapour velocities. The annular liquid film at the top of the channel is thinner as a result of draining along the circumferential direction. At the bottom of the channel, larger-amplitude waves give rise to a significant droplet entrainment into the vapour core. Little entrainment occurs at the top of the channel because here the liquid film is much smoother. When the heat flux reaches the critical value, the liquid film at the top of the channel will become completely depleted, thus resulting in "dryout".

To determine the CHF for horizontal flow, Groeneveld et al.

(1986) suggested that the CHF for vertical flow be multiplied by a correction factor K_{hor}.

$$CHF_{hor}=K_{hor}\cdot CHF_{table}. \qquad (2.24)$$

where CHF_{table} is the critical heat flux value obtained from the look-up table. Several methods for deriving an expression for K_{hor} were introduced by Wong et al. (1990).

(i) Mass-flux Threshold Method

The correction factor K_{hor} is strongly dependent on the flow conditions. Groeneveld (1982) suggested that for values of mass flux below G_{min} the flow is fully-stratified and hence the CHF for horizontal flow is zero for K_{hor} =0. On the other hand, as mass velocities in horizontal flow are high ($G>G_{max}$), the effect of the tube orientation on CHF becomes insignificant and hence CHF_{hor} may be assumed equal to the CHF for vertical flow (CHF_{ver}). For $G_{min}<G<G_{max}$, K_{hor} takes the following form:

$$K_{hor}=\left(\frac{G-G_{min}}{G_{max}-G_{min}}\right)^{0.62} \qquad (2.25)$$

where $K_{hor}=0$ for $G<G_{min}$

$K_{hor}=1$ for $G>G_{max}$

The G_{min} is mass-flux threshold for fully-stratified flow, and G_{max} is mass flux threshold for onset of noticeable stratification, which can be derived from the flow-regime map (Wong, 1990).

$$G_{\min}=\frac{(gD\rho_g(\rho_l-\rho_g))^{0.5}}{X_a}\left(\frac{1}{0.65+1.11X_{LM}^{0.6}}\right)^2 \tag{2.26}$$

where X_a is the actual quality. The Lockhart-Martinelli parameter is defined by

$$X_{LM}=\left(\frac{1-X_a}{X_a}\right)^{0.9}\left(\frac{\mu_l}{\mu_g}\right)^{0.1}\left(\frac{\rho_g}{\rho_l}\right)^{0.5} \tag{2.27}$$

and

$$G_{\max}=\left[\frac{gD_{1.2}\rho_l(\rho_l-\rho_g)}{0.092(1-X_a)^{1.8}\mu_l^{0.2}}f_2(X_{LM})^2\right]^{0.556} \tag{2.28}$$

$$f_2(X_{LM})=\exp[A+B\ln(X_{LM})+C\ln^2(X_{LM})] \tag{2.29}$$

where

A=-0.3470, B=+0.2920, C=-0.0556

(ii) Forced-balance and Transit-time Approach

Wong et al. (1990) developed a model to determine the correction factor K_{hor} using the transit-time approach. The transit time taken for a droplet or bubble to travel across the channel is compared to the transit time to travel along the channel. This transit-time ratio serves as a measure of void migration and hence

a measure of the void accumulation near the top of the channel. Some simplified approaches were utilized in the development of the transit-time ratio for various types of flow regimes such as droplet flow and bubbly flow, thus Wong et al. developed the following equation to calculate the correction factor K_{hor}:

$$K_{hor}=1-\exp\left[-\left(\frac{T_t}{a}\right)^b\right] \tag{2.30}$$

The best correlation appears to be with the use of T_1 with b=0.5 and a=3.0.

$$K_{hor}=1-\exp\left[-\left(\frac{T_1}{3}\right)^{0.5}\right] \tag{2.31}$$

where T_1 is the turbulent to buoyancy force ratio,

$$T_1=0.046Re_l^{-0.2}\left(\frac{1-x_e}{1-\varepsilon}\right)^2\frac{G^2}{gD\rho_l(\rho_l-\rho_g)\epsilon^{0.5}} \tag{2.32}$$

and ϵ is the cross-sectional average void fraction,

$$\epsilon=(D_i/D)^{0.5}$$

and Re_l is the liquid Reynold number.

2.6.3 Table Look-up Method

Since most empirical correlations and analytical models have a limited range of application, the need for a more general technique is obvious. Attempts have been made in the USSR to construct a standard table of CHF values for given geometry. The table development work has been continued at Chalk River Nuclear Laboratories and was completed at the University of Ottawa. Groeneveld et al.(1986) developed a standard look-up table based on the western data base which has a wider range of applications, for vertical water-cooled tubes, at discrete value of pressure (P), mass flux (G), and quality (X), covering the range of 0.1 - 20MPa, 0 - 7500kg/m^2.s, (zero flow refers to pool-boiling conditions) and -50 to 100% vapor quality (negative quality refers to subcooled conditions). The UO-AECL lookup table also provided the correction factor K_n for the effect of diameter factor, bundle factor, grid spacer factor, heated length factor, axial flux distribution factor, flow factor (horizontal flow and vertical flow).

Compared to other available prediction methods, the tabular approach has the following advantages:

(i) greater accuracy,
(ii) wider range of application,
(iii) correct asymptotic behaviour,
(iv) requires less computing time, and
(v) easily updated if additional data becomes available.

The prediction results of UO-AECL lookup table are in good agreement with the experimental data in tubes, however, further investigations are needed for the CHF prediction in bundles.

2.6 Summary

In this chapter, the mechanisms of CHF are presented and the methods of predicting CHF in tubes are introduced. The three approaches are:

a) Empirical correlations
b) CHF models
c) Table lookup method

The table lookup method is recommended for its wide range of application and better accuracy.

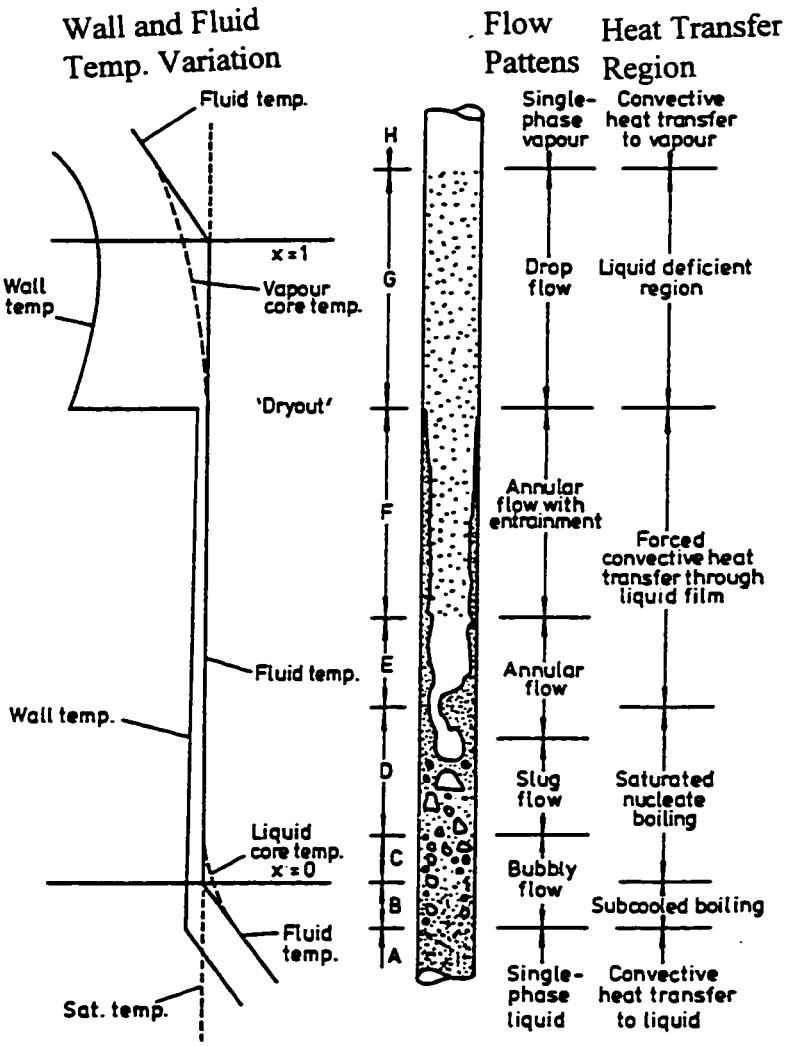

Figure 2.1 Regions of heat transfer in convective boiling. From Collier (1994).

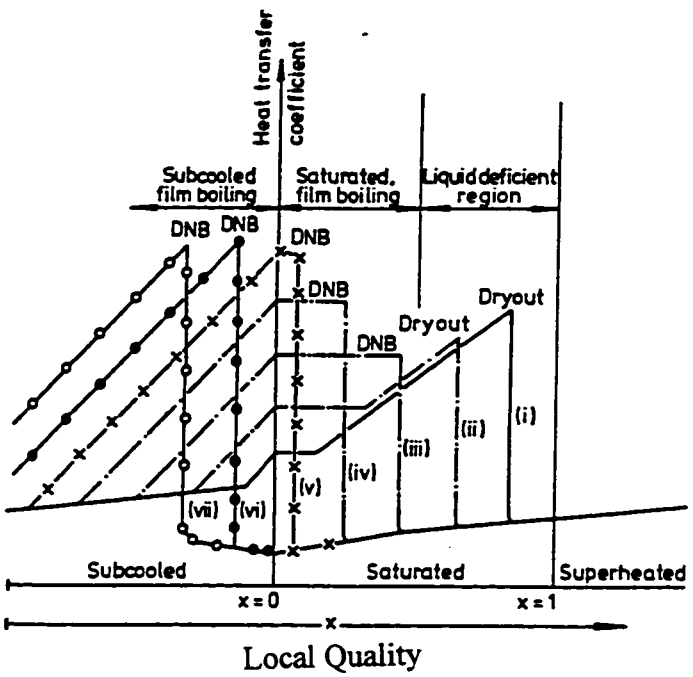

Figure 2.2 Variation of heat transfer coefficient with quality with increasing heat flux as parameter. From Collier(1994).

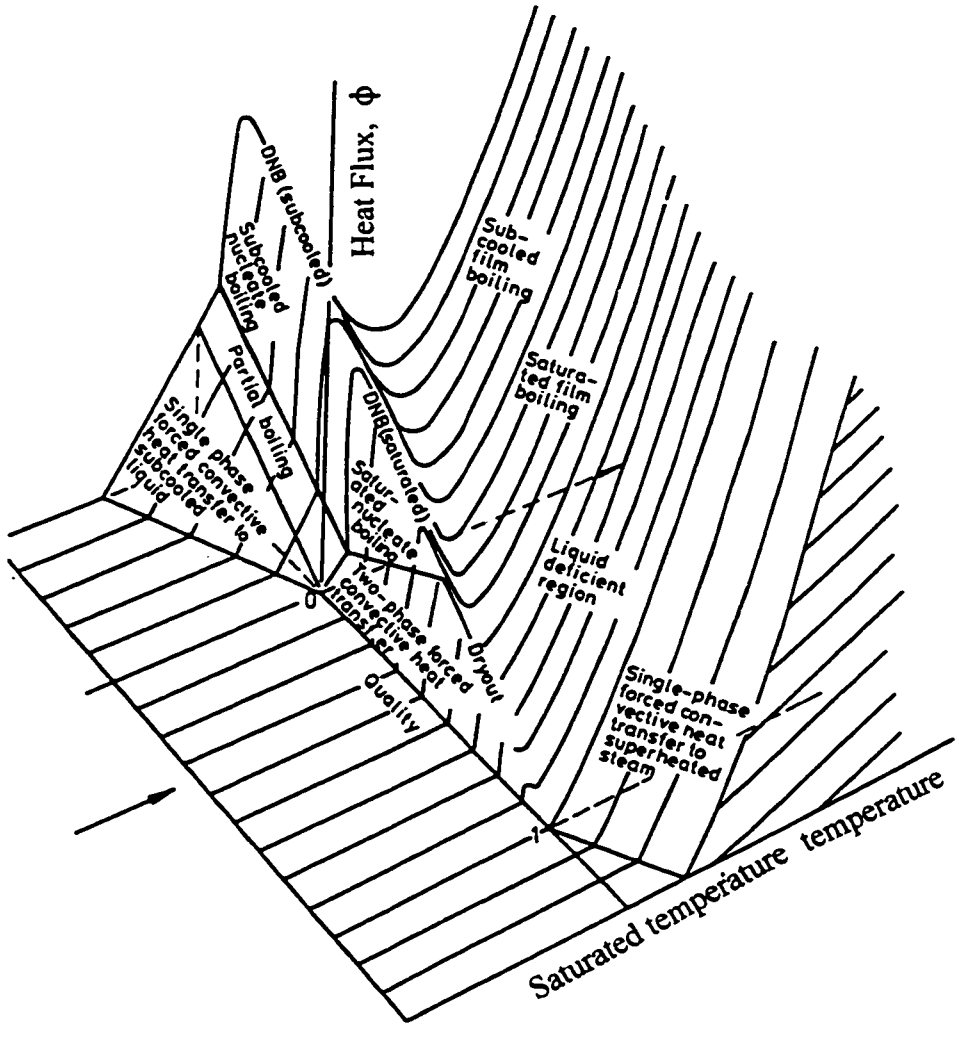

Figure 2.3 Forced convection boiling surface. From Collier (1994).

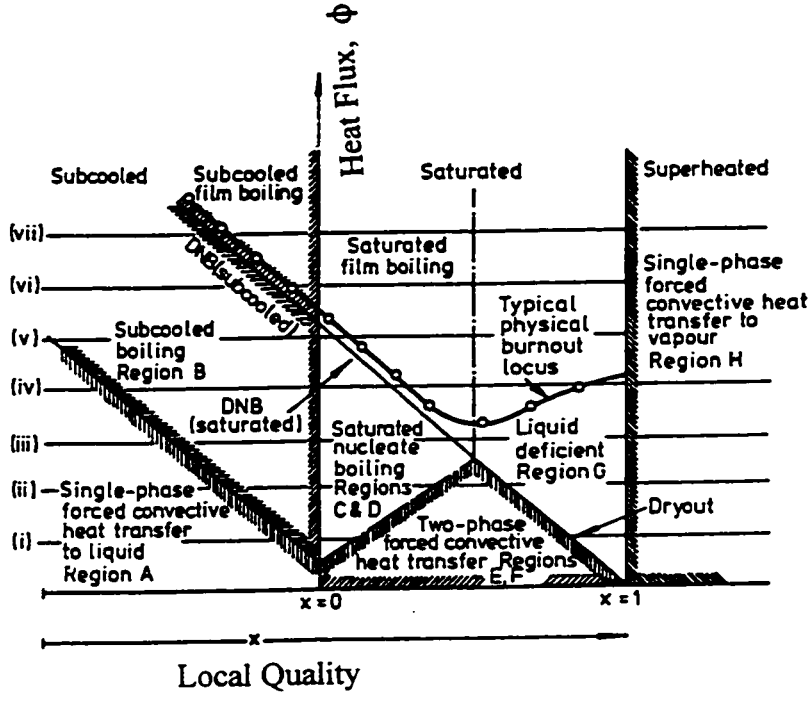

Figure 2.4 Regions of two-phase forced convective heat transfer as a function of quality with increasing heat flux as ordinate. From Collier (1994).

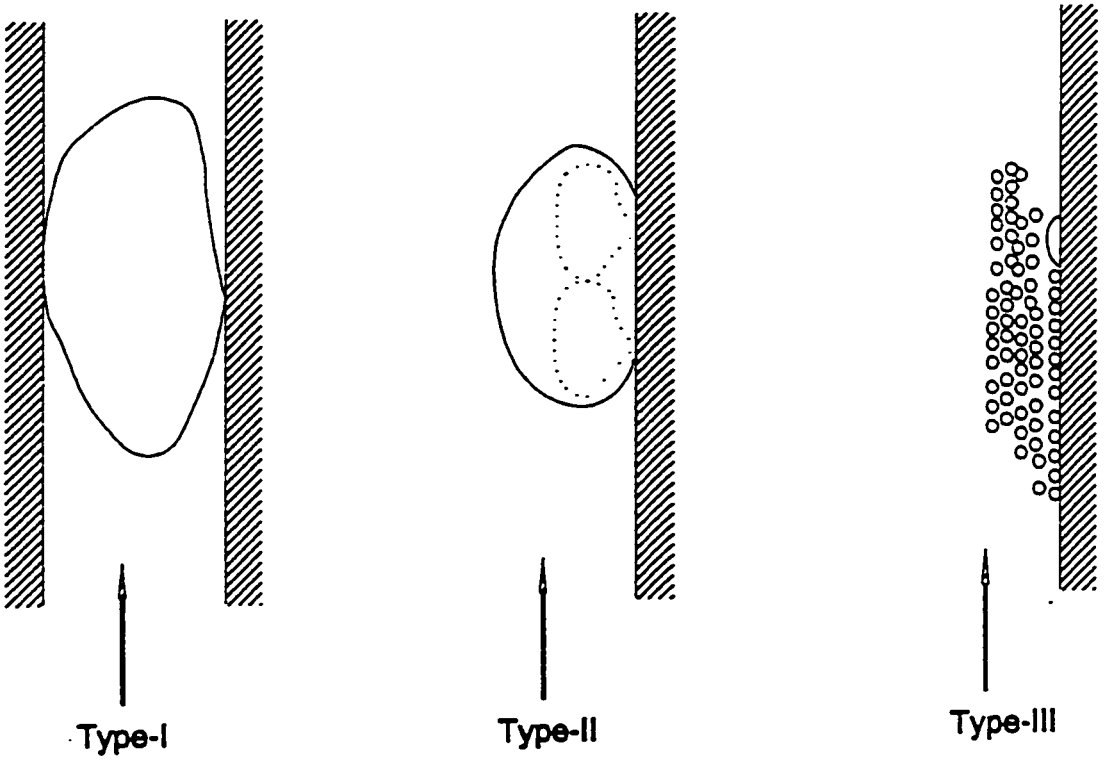

Figure 2.5 CHF in Forced convective boiling and subcooled conditions. From Joober (1993).

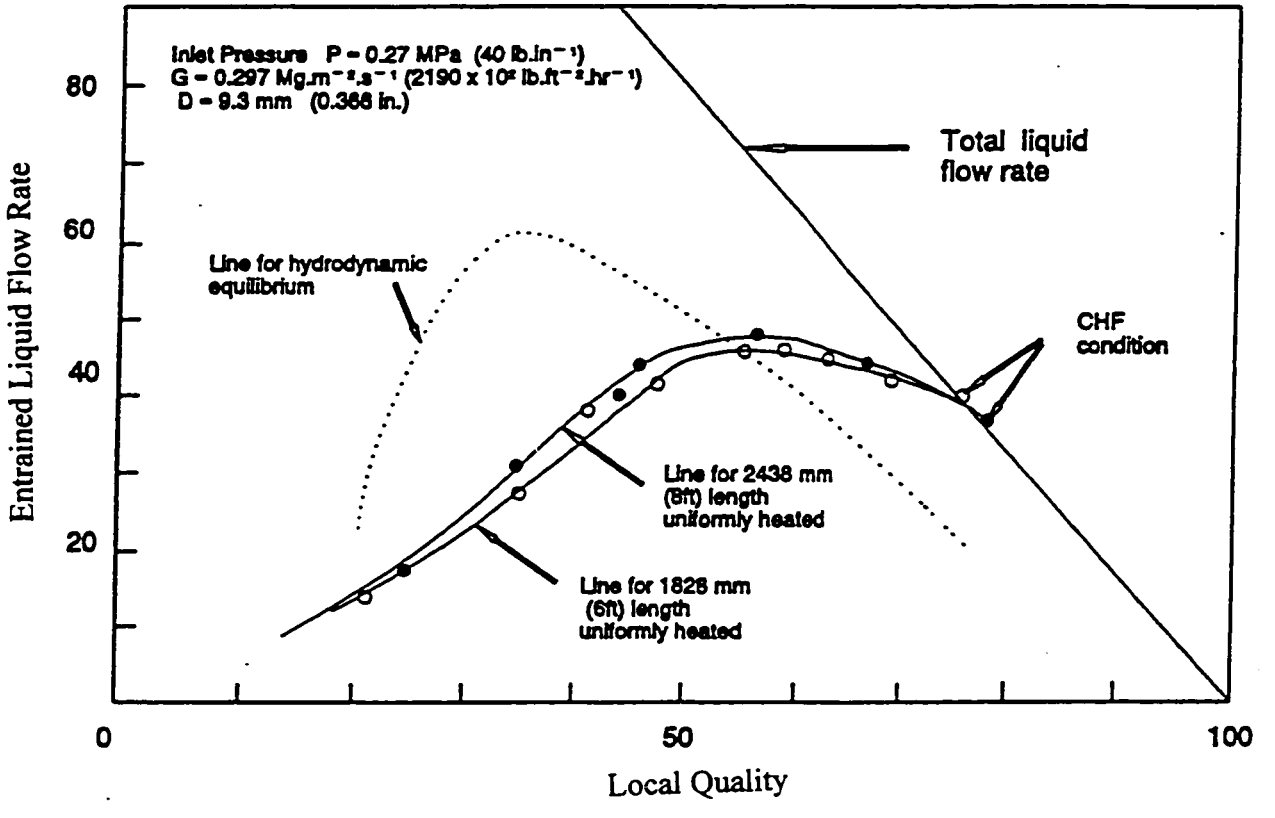

Figure 2.6 Entrainment curves for boiling in a tube with subcooled water at the inlet (the CHF occurs at the exit). From Hewitt and Hall-Taylor (1970).

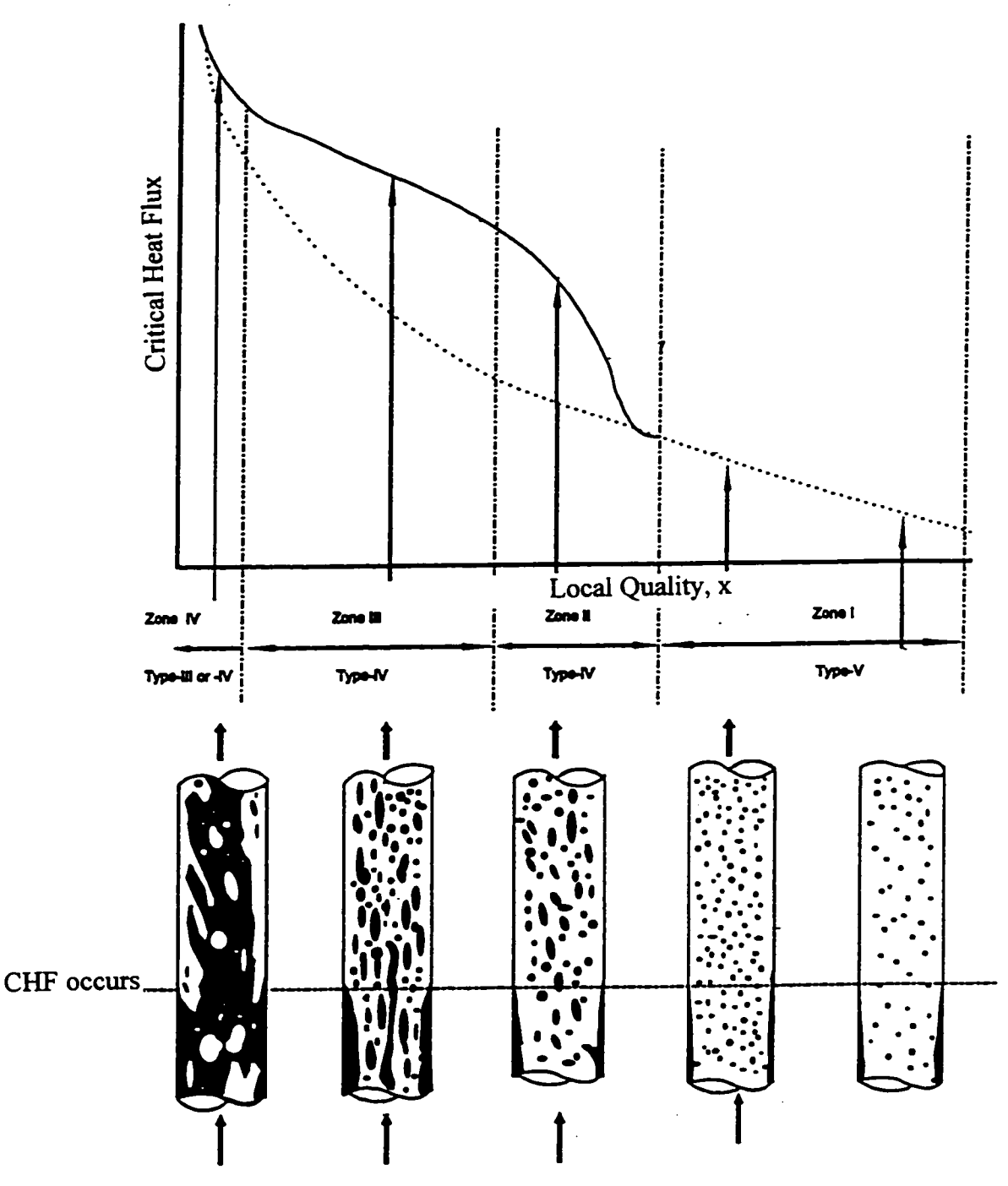

Figure 2.7 CHF types in forced convective boiling for positive qualities and for uniformly heated tubes. From Hewitt and Hall-Taylor (1970).

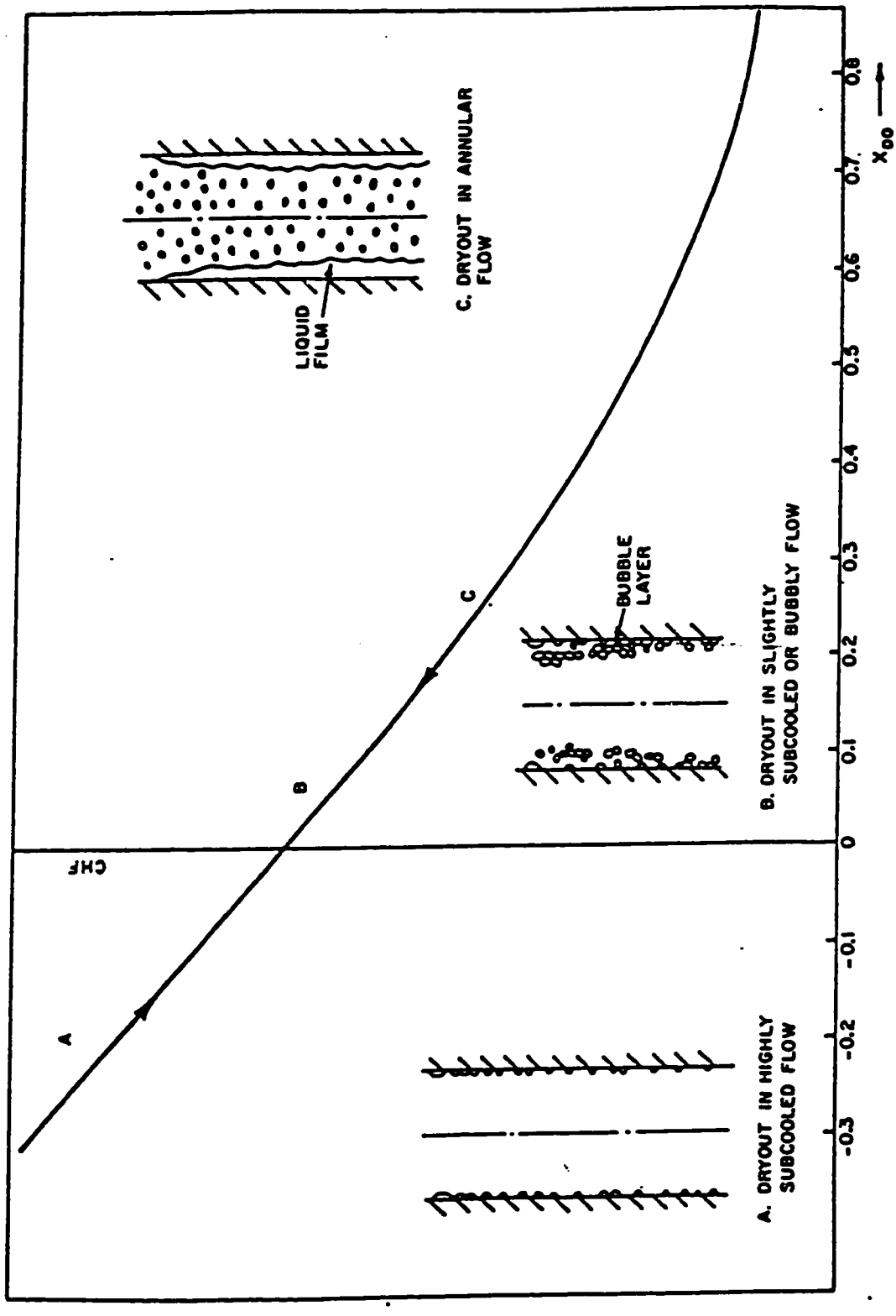

Figure 2.8 Effect of quality on critical heat flux. From Groeneveld (1995).

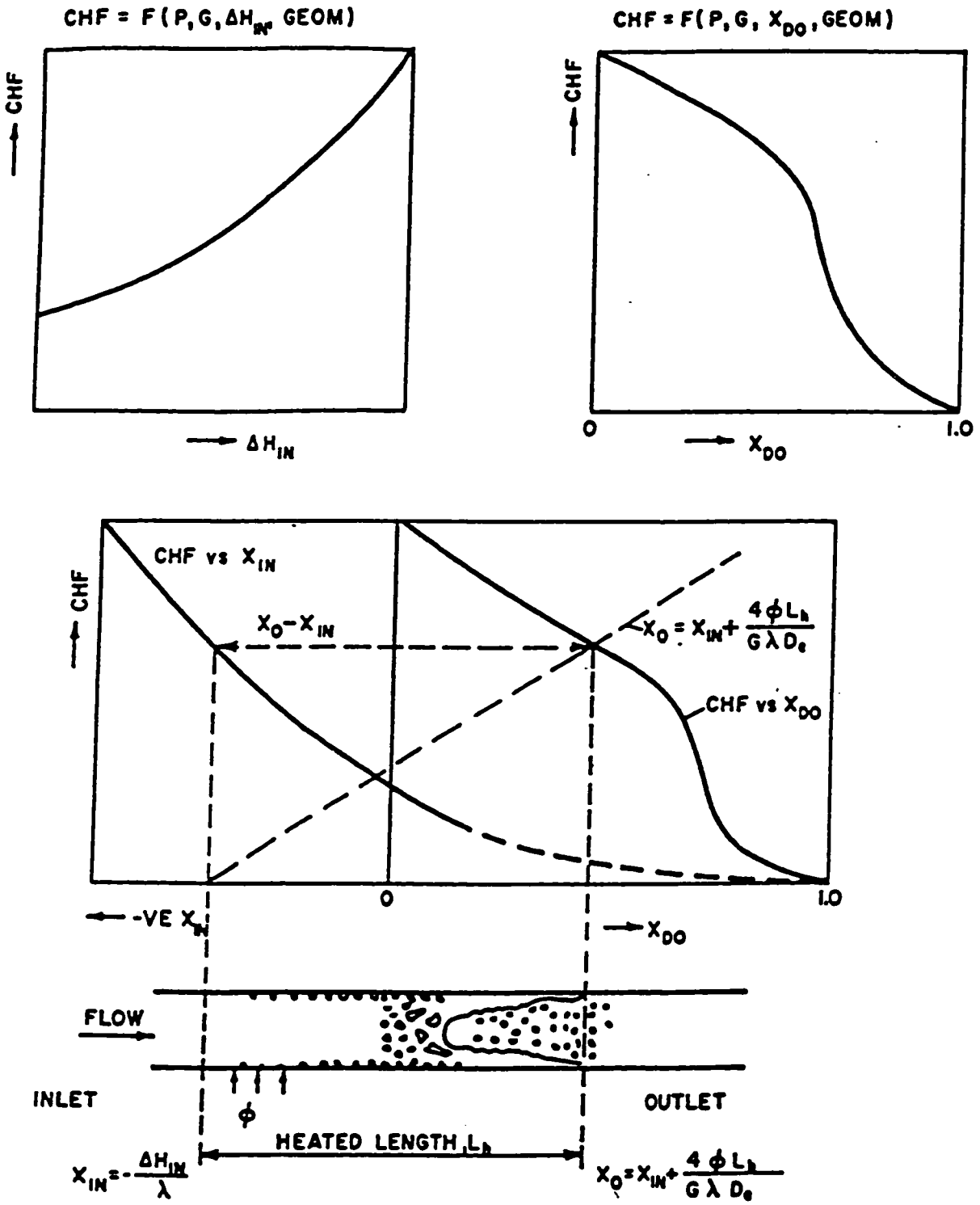

Figure 2.9 Transformation of CHF vs. Δh_{in} into CHF vs. X_{DO}. From Groeneveld (1995).

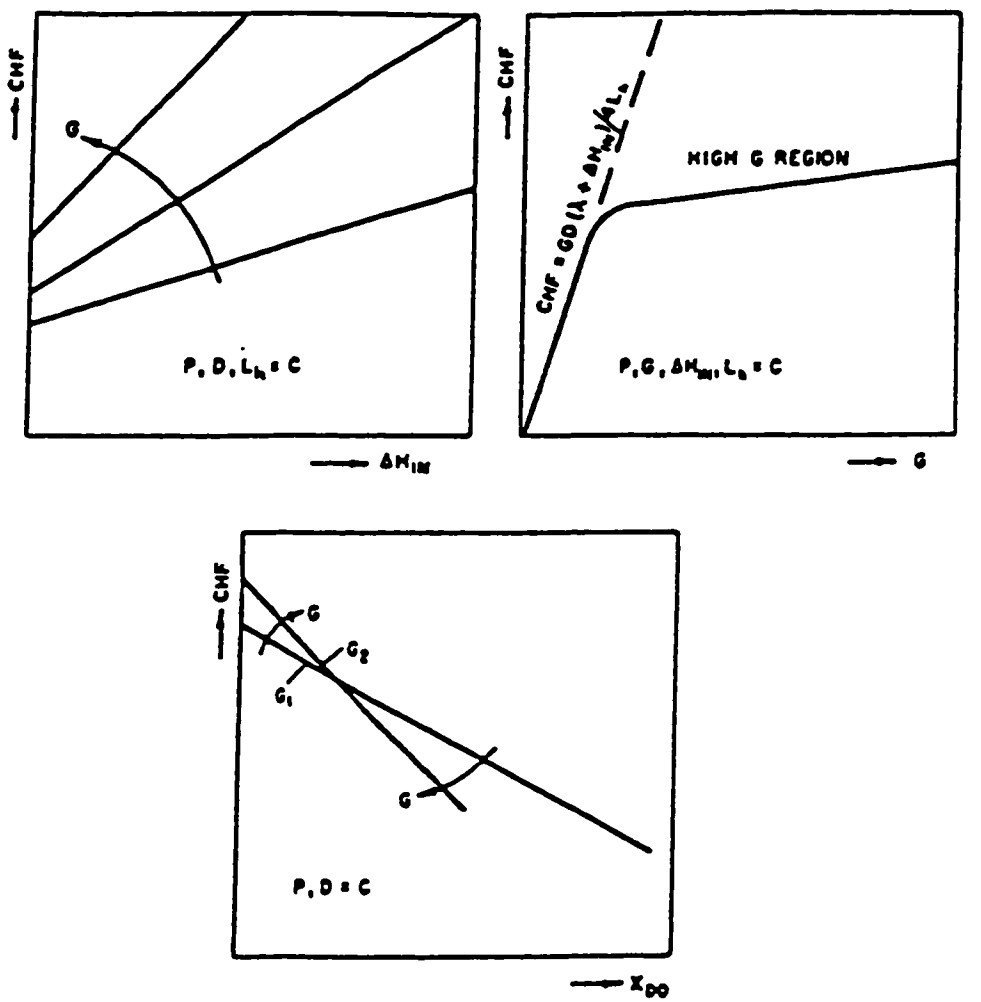

Figure 2.10 Effect of mass flux on CHF. Form Groeneveld (1995).

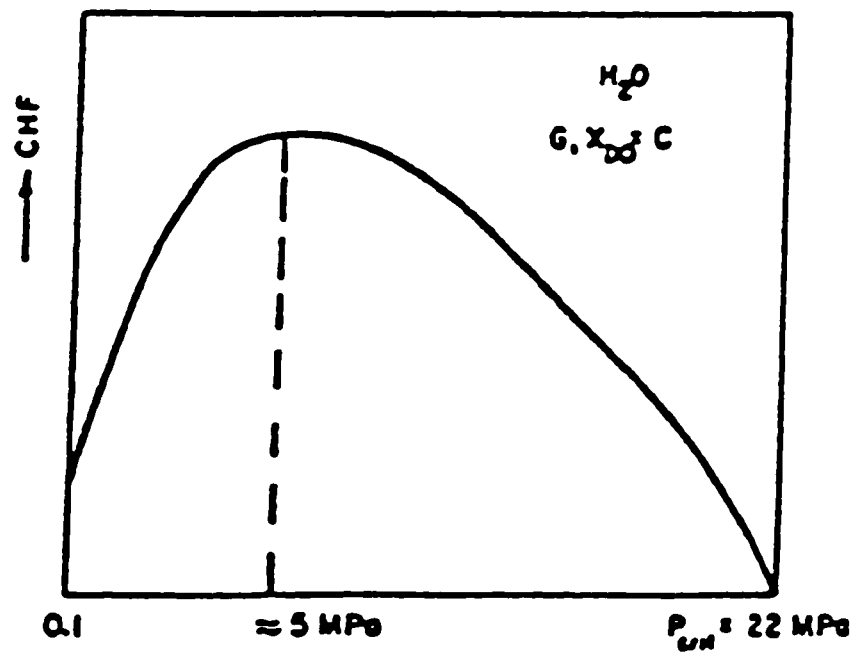

Figure 2.11 Effect of pressure on CHF.
From Groeneveld (1995).

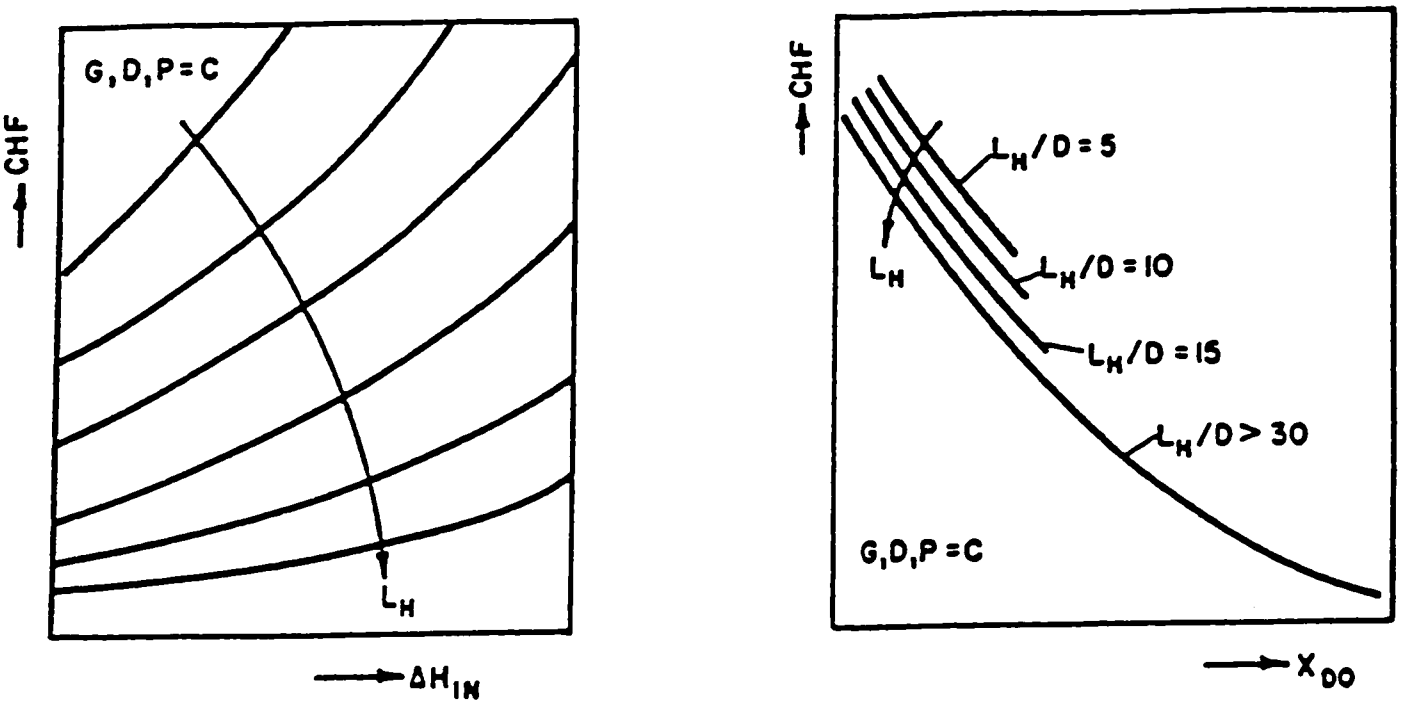

Figure 2.12 Effect of heated length on CHF.
From Groeneveld (1995).

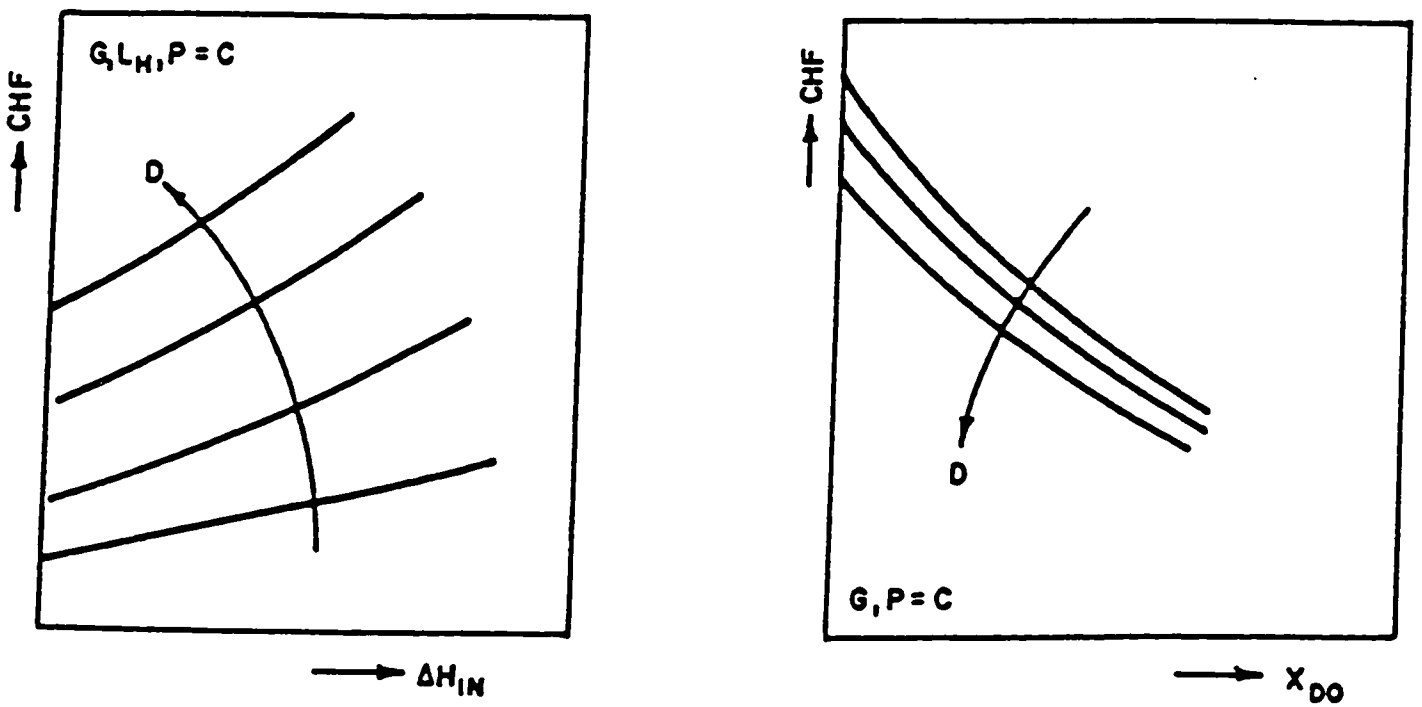

Figure 2.13 Effect of diameter on CHF.
From Groeneveld (1995).

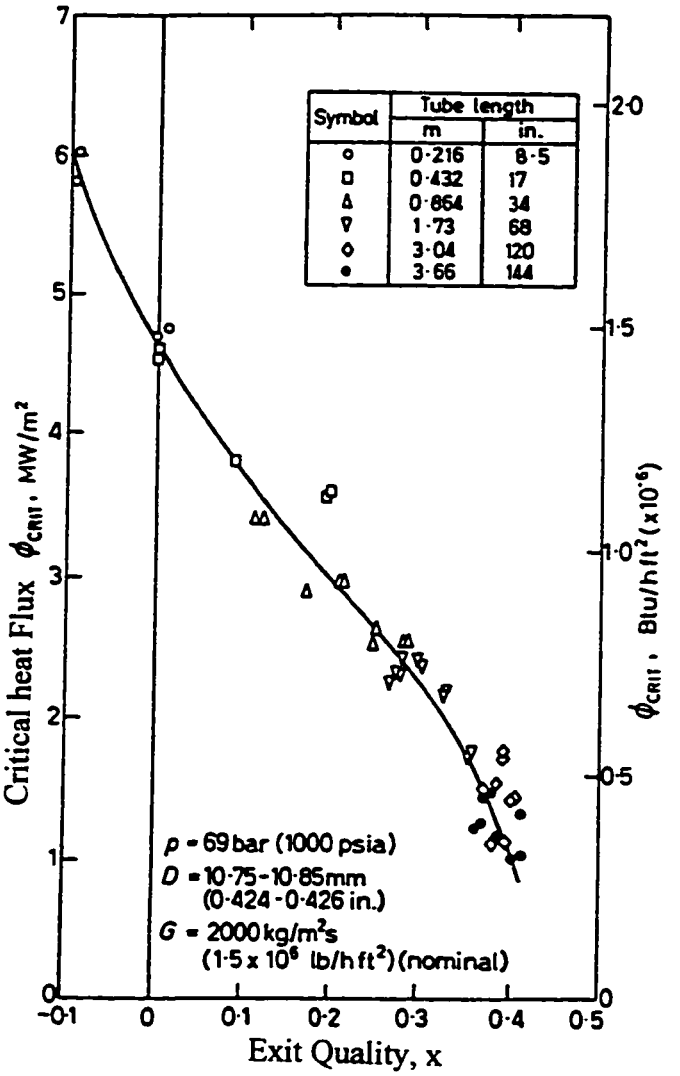

Figure 2.14 The effect of tube length on CHF at fixed exit conditions. From Collier (1994).

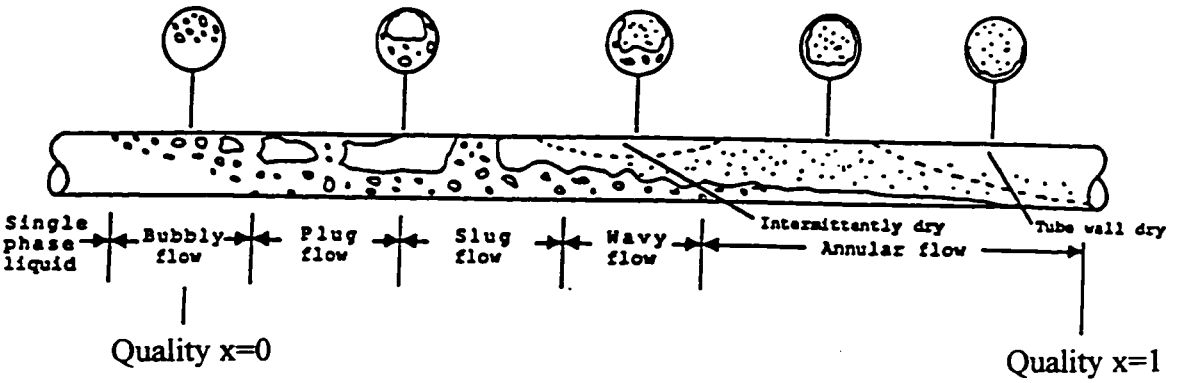

Figure 2.15 Flow regimes for horizontal flow. From Becker (1971).

3. CRITICAL HEAT FLUX IN INTERNALLY HEATED ANNULI

3.1 General

The CHF in internally heated annuli is more complicated than that in tubes. The geometry and the adjacent unheated wall have a pronounced role in the prediction of CHF. The prediction method of CHF in annuli can be used to predict CHF in rod bundles, since they have some similarities if the rod bundles are served as the internal tube in the annuli. As an initial step towards improving the understanding of CHF in rod bundles, this chapter presents the CHF predictions in internally heated annuli.

3.2 Difference Between Tubes and Internally Heated Annuli

In a round tube, the tube wall is heated and the fluid flows inside the tube. In internally heated annuli, the inner tube is heated and the fluid flows in the annular section between the heated and unheated wall. The geometry factors have more effect on the CHF prediction in annuli than in tubes since the annular section is usually narrow. Apparently, in an annulus heated on one surface only, a thick liquid film collects on the unheated surface, starving the heated surface of liquid, and hastening CHF. The higher CHF for tube than for an annulus is presumably the result of the non-uniformly distributed shear stress between heated and unheated wall (Rogers, 1966).

In order to distinguish the difference of CHF mechanism between tubes and concentric annuli, an insight into the physical mechanisms leading to CHF is needed. Doerffer et al. (1994) suggested that it can be discussed for the two limiting quality regions.

The CHF phenomenon is a very local one in the low and negative exit qualities regions, and therefore, in this situation, the presence of an unheated wall in annuli does not have any significant effect on CHF. That is why the CHF values in annuli are quite close to those obtained in tubes in these regions.

The CHF is related with a dryout of the liquid film on the heated surface in the positive quality range in annular flow. In this case, CHF values are much lower than those in tubes at the corresponding exit conditions. This is a result of several combined effects described below:

(i) The total wetted perimeter is heated in tubes, while in internally heated annuli, only a part of the wet perimeter is heated. So, in tubes, the evaporation of liquid film can reduce the film thickness at a constant rate around the whole perimeter. In annuli, however, evaporation only takes place on the heated inner wall, while the liquid film on the unheated outer tube is not subjected to evaporation but flows along the channel at an almost constant flowrate. Therefore, a significant fraction of the liquid phase does not participate in the cooling processing of the heated wall. This explains why the CHF occurs at much lower critical qualities in annuli compared with the values for tubes at the same

CHF value, pressure, and mass flux.

(ii) There is a uniform shear stress distribution of the liquid film around the perimeter in tubes, however, in internally heated annuli, the liquid film is subjected to the non-uniformly distributed shear stress between heated and unheated surfaces. The inner surface experiences higher shear stress than the outer one. This results in a thinner liquid film, higher entrainment rate and faster depletion on the heated surface than that on the unheated surface.

(iii) The deposition rate is uniform and totally reaches the heated surface in tubes. While, in internally heated annuli, the deposition on the heated surface is lower, since the evaporation process on the heated wall creating a radial mass flow of vapor produces a lift force to droplets preventing them from earlier deposition on this surface and pushes them into farther downstream region i.e., post-dryout region.

Rogers(1966) also stated that CHF for an internally heated annulus is less than that for an externally heated annulus, attributed to the higher shear stress on the inner surface than the outer surface, which causes entrainment from the film. And the CHF for an annulus heated on both surfaces approaches that for a tube, attributed also to the higher shear stress on the inner surface.

Attention should also be paid to the significant role that the gap size plays on the CHF in annuli. Tolubinskiy et al. (1977) pointed out that the geometry affects the CHF in narrow annuli and

that the closeness of the annuli walls interferes with disengagement of vapor from the heated surface. Some parts of the annular cross section become vapor-locked, which reduces the CHF at low pressure. However, the specific volume of the stream decreases with an increase in pressure, and this reduces the probability of a vapor lock. It is also found that the CHF increases significantly when the annulus width is increased to a certain value, but there is only an insignificant rise in CHF with further increases in width.

3.3 Observed Parametric Trends

3.3.1 Effect of Pressure

The behavior of CHF=f(P) in annuli is similar to that in tubes. Thus, while a monotonic reduction in q_{cr} was observed upon increase in pressure from 20 bar to 200 bar in all the studies of critical heat flux in tubes, the curve of q_{cr} in annuli exhibits a peak which shifts upon variations in the operation variables and annuli width from 1/3 to 2/3 P_{cr}. At high subcooling and high mass flowrate, the peak of the curve of CHF=f(P) is shifted toward lower pressure (Tolubinskiy et al., 1977).

Meanwhile, Doerffer et al. (1994) pointed out that in the positive-quality range, the effect of pressure is much stronger in tubes than in annuli. In the high-pressure range, q_{cr} values in both cases become closer to each other. For negative qualities, the pressure effect is similar in both geometries, and the differences

in CHF values are much smaller than for positive qualities.

3.3.2 Effect of Mass Flux

The general trends of CHF experimental data against mass flux in annuli show that the CHF increases with the mass flux, which suggests a similar mass flux effect in annuli and tubes(Doerffer, 1994). At low qualities, the effect of mass flux on CHF is smaller, and finally vanishes with increase in the inner tube diameter, i.e., with reduction in the annulus width, which means the mass flux effect in annuli depends on gap size. The effect of mass flux with a larger gap size is more pronounced (Tolubinskiy et al., 1977).

3.3.3 Effect of Quality

As the flow qualities increase, the values of CHF decreases linearly with low mass flux. The non-linear trend is observed when the mass flux is larger.

Doerffer stated that the effect of quality on CHF appears much stronger in annuli than in tubes, especially in the positive-quality region. This may be due to the large parasitic liquid film flow on the unheated surface, which reduces the film flowrate on the heated surface and the deposition rate onto the heated surface. The values of CHF in annuli and tubes are closer to each other at the DNB-type conditions (i.e., at the low or negative qualities),

where the unheated wall effect does not play a significant role. The CHF is a more local phenomenon.

The quality effect seems to be the strongest one among all the parametric factors in annuli.

3.3.4 Geometry Effects

3.3.4.1 Effect of unheated wall

The CHF value in annuli is usually lower than in tubes at the same exit quality. This is partly because of the existence of a thick cold liquid film build up on the unheated wall which does not contribute to the heat removal from the heating surface. Also, for the same reason, the CHF occurs at much lower qualities in annuli compared with the values in tubes at the same CHF value, pressure and mass flux.

3.3.4.2 Effect of gap size

Generally, the CHF increases initially with the gap size, reaches its maximum value at a specific gap size, and then decreases with the gap size. However, Tolubinskiy (1977) pointed out that the CHF increases significantly with gap size before it is equal to 2.0 mm, but further increase in gap size produces only an insignificant rise in CHF.

3.3.4.3 Effect of L/D_{hy} ratio

The global effect of the L/D_{hy} ratio on CHF is that the CHF decreases with increase in the L/D_e ratio. The effect of L/D_{hy} on CHF depends on the mass flux and gap size, but for larger gap size the effect becomes less pronounced or is unclear. Also, the effect of L/D_{hy} is difficult to determine precisely because of the experimental conditions and upstream effect.

3.4 CHF Prediction Methods

3.4.1 CHF Correlations

(i) Barnett's correlation (1966) was based on 830 CHF data obtained in water at pressure of 1000 psia, and collected from 13 sources. For these data points his correlation predicts CHF with an rms error of 7.4%. Barnett found his correlation superior to the annuli CHF correlation of Janssen and Kervinen (1963), Bertoletti et al. (1965), Becker (1966), and Tong et al. (1964), which predicted CHF for Barnett's data base with rms errors of 16.1%, 14.8%, 15.3%, and 60.2%, respectively. Barnett's correlation has the following form:

$$CHF\times 10^{-6}=\frac{A+B\Delta H_i}{C+L} \qquad (3.1)$$

the equation (3.1) is for a pressure of 1000 psia (69 bar).

where:

$$A = 67.45 D_{hy}^{0.68} (G \times 10^{-6})^{0.192} [1 - 0.744 e^{-6.512 D_{he} G \times 10^{-6}}] \quad (3.2)$$

$$B = 0.2587 D_{hy}^{1.261} (G \times 10^{-6})^{0.817} \quad (3.3)$$

$$C = 185.0 D_{he}^{1.415} (G \times 10^{-6})^{0.212} \quad (3.4)$$

This correlation uses British units and its data base covers the following range:

Δh_i:	0 to 412 Btu/lb	(0 to 0.958 MJ/kg)
G:	0.14 to 6.20 lb/(hr.ft)x10^{-6}	(190 to 8430 kg/m^2.s)
L:	24.00 to 108.0 in	(0.61 to 2.74 m)
D_i:	0.375 to 3.798 in	(9.52 to 96.5 mm)
D_o:	0.551 to 4.006 in	(14.0 to 101.6 mm)

For the pressure other than 1000 psia, but within the range of 600 to 1400 psia, Eq.(3.1) is modified to

$$CHF \times 10^{-6} = \frac{A\left(\frac{H_{fg}}{649}\right) + B\Delta H_{in}}{C + L} \quad (3.5)$$

where H_{fg} is in Btu/lb.

Equation (3.1) was formulated for the inlet conditions. To predict the CHF for a given exit conditions this equation is transferred via the heat balance equation

$$x_c = \frac{1}{H_{fg}}\left(\frac{4L\,CHF}{D_{he}G} - \Delta H_{in}\right) \tag{3.6}$$

into the following form:

$$CHF \times 10^{-6} = \frac{A - x_c B H_{fg}}{C + L - \frac{4BL}{D_{he}G}\times 10^{6}} \tag{3.7}$$

(ii) Katto (1979) developed a prediction method for CHF in annuli based on 310 CHF data points collected from 25 sources in the following fluids: water, Freon-12, Freon-114, acetone, toluene, sodium and monoisopropyl-biphenyl. A similar set of equations as those for tubes (Katto, 1978) were used for annuli. Katto (1979) proposed separate equations for the three regimes:

H-regime

$$\frac{CHF_o}{GH_{fg}} = 0.12\left(\frac{\rho_g}{\rho_f}\right)^{0.133}\left(\frac{\sigma\rho_f}{G^2 L}\right)^{1/3}\frac{1}{1+0.0081 L/D_{he}} \tag{3.8}$$

L-regime

$$\frac{CHF_o}{GH_{fg}} = 0.25\left(\frac{\sigma\rho_f}{G^2L}\right)^{0.043}\frac{1}{L/D_{he}} \tag{3.9}$$

N-regime

$$\frac{CHF_o}{GH_{fg}} = 0.22\left(\frac{\rho_g}{\rho_f}\right)^{0.133}\left(\frac{\sigma\rho_f}{G^2L}\right)^{0.433}\frac{(L/D_{he})^{0.171}}{1+0.0081L/D_{he}} \tag{3.10}$$

The regimes were distinguished by the following criteria:

-between L and H regimes

$$\frac{L}{D_{he}} = \frac{1}{0.48\left(\frac{\rho_g}{\rho_f}\right)^{0.133}\left(\frac{\sigma\rho_f}{G^2L}\right)^{0.29} - 0.0081} \tag{3.11}$$

-between H and N regimes

$$\frac{L}{D_{he}} = \frac{0.0206}{\left(\frac{\sigma\rho_f}{G^2L}\right)^{0.584}} \tag{3.12}$$

The above equations refer to CHF at zero inlet subcooling (i.e., subscript 0). When liquid is subcooled then the CHF can be calculated as:

$$CHF = CHF_o\left(1 + K\frac{\Delta H_{in}}{H_{fg}}\right), \tag{3.13}$$

where K is dimensionless parameter independent of Δh_{in}.

L-regime: $K_L=1.0$

H-regime: $K_H=1.8(130D/L)^{5.0(\rho g/\rho f)}$

N-regime: $K_N=0.664(\rho_g/\rho_f)^{-0.6}$

The correlation covers the following range of parameters:

L:	0.0762 - 8.84 m,
D_i:	5 - 96.4 mm,
D_o:	12.7 - 101 mm,
ρ_g/ρ_f:	0.000058 - 0.16.

Equations (3.8) through (3.13) were formulated for the inlet conditions. To predict the CHF at exit conditions Equation (3.6) is applied and yields

$$CHF=\frac{CHF_o(1-kx_c)}{1-\frac{4Lk\,CHF_o}{GH_{fg}D_{he}}} \tag{3.14}$$

3.4.2 CHF Models

Kirillov and Smogalev (1972, quoted by Doerffer et al., 1994) gave an analytical droplet-diffusion model describing the dryout-type CHF in tubes, which introduced the new parameter x_n, the quality at which droplet deposition from the core stream onto the channel wall deteriorates markedly or ceases completely, for adiabatic two-phase flow. This approach was subsequently used to develop a CHF prediction model for annuli (Kirillov and Smogalev,

1972).

Figure 3.1 shows that a formation of annular flow (internally heated) takes place between 1 to 2. Between 2 to 3 droplets from the wavy liquid films become entrained in the vapor core as a result of interaction between the films and the core flow. At 3 liquid entrainment ceases and a fairly smooth liquid film begins. In the region from 3 to 4 (i.e., to the section, where CHF occurs) the core flow consists of the vapor and the liquid droplets. If the effect of the vapor thrust velocity (due to the film evaporation) on droplet deposition is neglected, then deposition will continue until the liquid mass flow rate in the core flow reaches its minimum value, which corresponding to the quality x_n.

The mass flow rate of deposited droplets in this region is

$$W_{dep} = W_{\Delta P}^{c} - W_{n}^{c} \tag{3.15}$$

Deposition on the inner surface is

$$W_{i,\,dep} = n_i W_{dep} \tag{3.16}$$

and on the outer (unheated) surface is

$$W_{o,\,dep} = n_o W_{dep} \tag{3.17}$$

where

$$n_i = \frac{r_i}{r_i + r_o} \qquad and \qquad n_o = \frac{r_o}{r_i + r_o} \tag{3.18}$$

A normal component of the vapor flow, $q''/(H_{fg}\rho_g)$, decreases the

droplet deposition onto the inner surface in the ratio K_q/K_a as follows:

$$W_{i,\,dep} = n_i W_{dep} \frac{K_q}{K_a} \tag{3.19}$$

The droplets mass flow rate in the core stream, at which mass transfer deteriorates, is

$$W_{nq}^{c} = W_{n}^{c} + n_i W_{dep}\left(1 - \frac{K_q}{K_a}\right) \tag{3.20}$$

For the onset of CHF it is necessary that

$$W_c = W_{nq}^{c} + W_{o,f} \tag{3.21}$$

Eq.(3.15) and Eq.(3.20) with the following relation

$$W_{\Delta p}^{c} = W_{\Delta p} E_{\Delta p} \tag{3.22}$$

and assuming

$$K_q = K_a - \frac{q_i}{H_{fg}\rho_g} \tag{3.23}$$

introduced to Eq.(3.21), which is divided by the total mass flow rate, W_T, yields

$$x_c = x_n - n_i[(1 - x_{\Delta P})E_{\Delta P} - 1 + x_n]\frac{q_i}{K_a H_{fg}\rho_g} - \frac{W_{o,f}}{W_T} \tag{3.24}$$

where

$$\frac{W_c}{W_T}=1-x_c, \qquad \frac{W_n^c}{W_T}=1-x_n \quad and \quad \frac{W_{\Delta P}}{W_T}=1-x_{\Delta P}$$

Rearranging Eq.(3.24) with an assumption $E_{\Delta P}$ = 1, yields the following equation:

$$CHF_i=\frac{r_i+r_o}{r_i}\times\frac{K_a H_{fg}\rho_g}{x_{ni}}\times(x_n-\phi_{oi}-x_c) \tag{3.25}$$

where the heat flux q_i becomes the CHF in an internally heated annulus.

3.4.3 Correlation Based on Observed Parametric Effects

Doerffer et al. (1994) analyzed the parametric effect on the CHF in annuli, they found that the effect of critical quality, gap size and pressure are the strongest influencing factors. Therefore, a correlation with the correction factors of critical quality, gap size and pressure, based on the tube CHF look-up table of Groenenveld et al. (1986), was proposed as

$$CHF_{an}=CHF_{D=8}\times k_x\times k_\delta\times k_p \tag{3.26}$$

where:

- $CHF_{D=8}$ is the CHF for a tube with an ID of 8 mm, as predicted by the tube CHF look-up table of Groeneveld et al. (1986), at given pressure, quality and mass flux.

- k_x accounts for the differences in CHF mechanism between tubes and annuli, resulting in a strong quality effect

  -for $x_e \leq 0.025$ $\quad k_x = 0.81$

  -for $x_e > 0.025$ $\quad k_x = 0.859 - 16.179x_e^{1.5} + 15.6x_e^2 - 7.195x_e^2 \ln(x_e)$,

-k_δ accounts for the gap effect

  -for $\delta < 4.26$ mm

$$k_\delta = 0.2872 + 1.209\delta^2 - 1.156\delta^{2.5} + 0.2873\delta^3$$

  -for $4.26 \leq \delta \leq 6.27$ mm

$$k_\delta = 1.2672 - 0.0298\delta$$

  -for $6.27 < \delta \leq 8.26$ mm

$$k_\delta = 0.75$$

-k_p accounts for the pressure effect

  -for P<3.30 MPa $\quad k_p = 0.9$

  -for $3.3 \leq P \leq 10.5$ MPa $\quad k_p = 0.808 + 0.0278P$

  -for P>10.5 MPa $\quad k_p = 1.1$

Doerffer (1994) also pointed out that correlation (3.21) is based on the critical quality, x_e, which is an average value over the whole flow area of an annulus. However, if a rod-centered

subchannel approach were used, the critical quality would be much greater. The CHF in internally heated annuli is controlled by the phenomena occurring in the vicinity of the heated surface. The subchannel can be defined as the region between the heated surface and the surface where the maximum velocity occurs. It is known that the same CHF value occurs in tubes at much higher exit quality than in annuli, hence such a subchannel approach may model CHF in annuli closer to that in tubes. It was therefore assumed that the CHF in an annulus would occur when the rod-centered subchannel quality was $x_c' = x_c + \Delta x_c$, for which $CHF_{an}(P, G, x_c) = CHF_{D=8}(P, G, x_c')$. The following correlation for Δx_c was found:

$$\Delta x_c = 0.658 - 0.33 \times P^{0.428} \times G^{0.108} \times \delta^{-0.453} \times D_{he}^{0.37} + 0.208 \times e^{-18.5 \times (Xc - 0.35)^2} \qquad (3.27)$$

where P in (MPa), G in (Mg/m^2s), δ in(mm), and D_{he} in (cm).

3.4.4 General Approach Applicable to All Flow Geometries

Two reports (i.e., Bethke and Zeggel, 1993a, and Bobkov, 1993, quoted by Doerffer, 1994) present an attempt to generalize the flow geometry description by some universal variables, and then to use them for CHF prediction for annuli and rod bundles based on CHF Look-up tables for tubes. Bethke and Zeggel proposed to use a characteristic length - so called "inscribed diameter" while Bobkov introduced an elementary heat cell. These two concepts are described below.

(i) Bethke and Zeggel approach:

The definition of a characteristic length or inscribed diameter of the second order, D_2, for annuli and rod bundles is shown in Figure 3.2. For rod bundles it can be calculated according to the formula

$$D_2 = D(2t/D - 1) \qquad (3.28)$$

where D and t are rod diameter and rod-to-rod pitch, respectively.

Doerffer pointed out that this dimension better characterizes the location of heated perimeter (important from CHF point of view) than the hydraulic equivalent diameter, when applied to CHF look-up table prediction.

Furthermore, Bethke and Zeggel (1993) concluded that the application of any equivalent diameter depends on the prevailing flow regime at CHF location. They recommended, for the DNB-type CHF and for deposition controlled CHF in the annular flow, to use the equivalent hydraulic diameter as the diameter of an equivalent circular tube. The reason for this is, in the regime of bubbly boiling, the hydraulics of the flow core affects motion and distribution of bubbles and, hence, the onset of departure from nucleate boiling. On the other hand, motion and distribution of droplets in the vapour core flow affect the annular flow and, hence, the deposition controlled CHF. But, between these two regimes, the equivalent tube diameter should be calculated taking into account the surface tension and the shear stress, which, together, define the force controlled equivalent diameter, D_f.

To derive D_f the following forces acting at the vapour-liquid interface are considered:

- surface tension force, which tends to smooth the interface and to prevent droplet entrainment, is given by

$$F_\sigma = \sigma \Delta z = \sigma_\infty \Delta z \frac{1}{1 + \frac{2\delta}{r}} \tag{3.29}$$

where σ_∞ is the surface tension at plane surface, Δz is the axial length, δ is the distance between the equimolecular interface and the surface of tension, and r is the radius of the surface of tension.

- shear force, which agitates the interface causing waves and entrainment, can be assessed from

$$F_\tau = \tau \pi D \Delta z = 0.0395 \frac{\pi \rho \upsilon^{0.25}}{u^{-7/4}} \frac{D}{D_{he}^{0.25}} \Delta z \tag{3.30}$$

where u is the average vapour velocity in the flow core, and τ is the shear stress at the interface.

An assumption that the shear force to surface tension force ratios in a circular tube and other flow geometry (i.e., in annuli or rod bundles) are the same, yields the force controlled equivalent diameter

$$D_f = \left(\frac{D}{D_{he}^{0.25}} \right) \tag{3.31}$$

Bethke and Zeggel (1993) proposed the following CHF prediction in annuli:

$$CHF_{an} = CHF_{D=8} \left(\frac{0.008}{D} \right)^{1/3} \tag{3.32}$$

where D in (m) can be either the inscribed diameter of the second order, D_2, or D_f, depending on the flow regime.

(ii) Bobkov approach

Bobkov (1993) formulated the elementary heat cell for any type of flow geometry as shown in Figure 3.3. Each type is characterized by the thermal boundary layer curvature parameter, R_0, defined as

$$R_O = \frac{Y_{th,av}}{R_{he}} \tag{3.33}$$

where $Y_{th,av}$ is the average thickness of thermal boundary layer over the perimeter (i.e., gap size for annuli), and R_{he} is the heat transfer surface radius, which depends on heat supply (i.e., for round tube $R_{he}=D/2$, for internally heated annulus $R_{he} = D_i/2$).

To predict CHF in the concentric internally heated annuli, first the exit quality displacement, Δx_c, should be calculated

according to

$$\Delta x_c = 0.05(R_O + 1)^2 \left(1 - \frac{P}{P_{cr}}\right), \tag{3.34}$$

where

$$R_O = \frac{2\delta}{D_i} \tag{3.35}$$

then the CHF lookup table value for the 8 mm tube is used with the correlation for the equivalent heated diameter as follows:

$$CHF_{an} = CHF_{D=8}(P,\ G,\ D_{he},\ x_c + \Delta x_c)\ . \tag{3.36}$$

3.5 Recommendation

In this chapter, the differences of CHF between tube and annuli are discussed, the parametric effects on CHF are presented and the prediction method is given. The three perdition methods are:

i) empirical correlation,
ii) CHF model in annuli, and
iii) CHF prediction in annuli using tube look-up table.

Among the CHF prediction methods in annuli, Eq.(3.24) is recommended. Note that Eq.(3.24) not only has good prediction accuracy, but also gives correct parametric and asymptotic trends (see Figure 3.4).

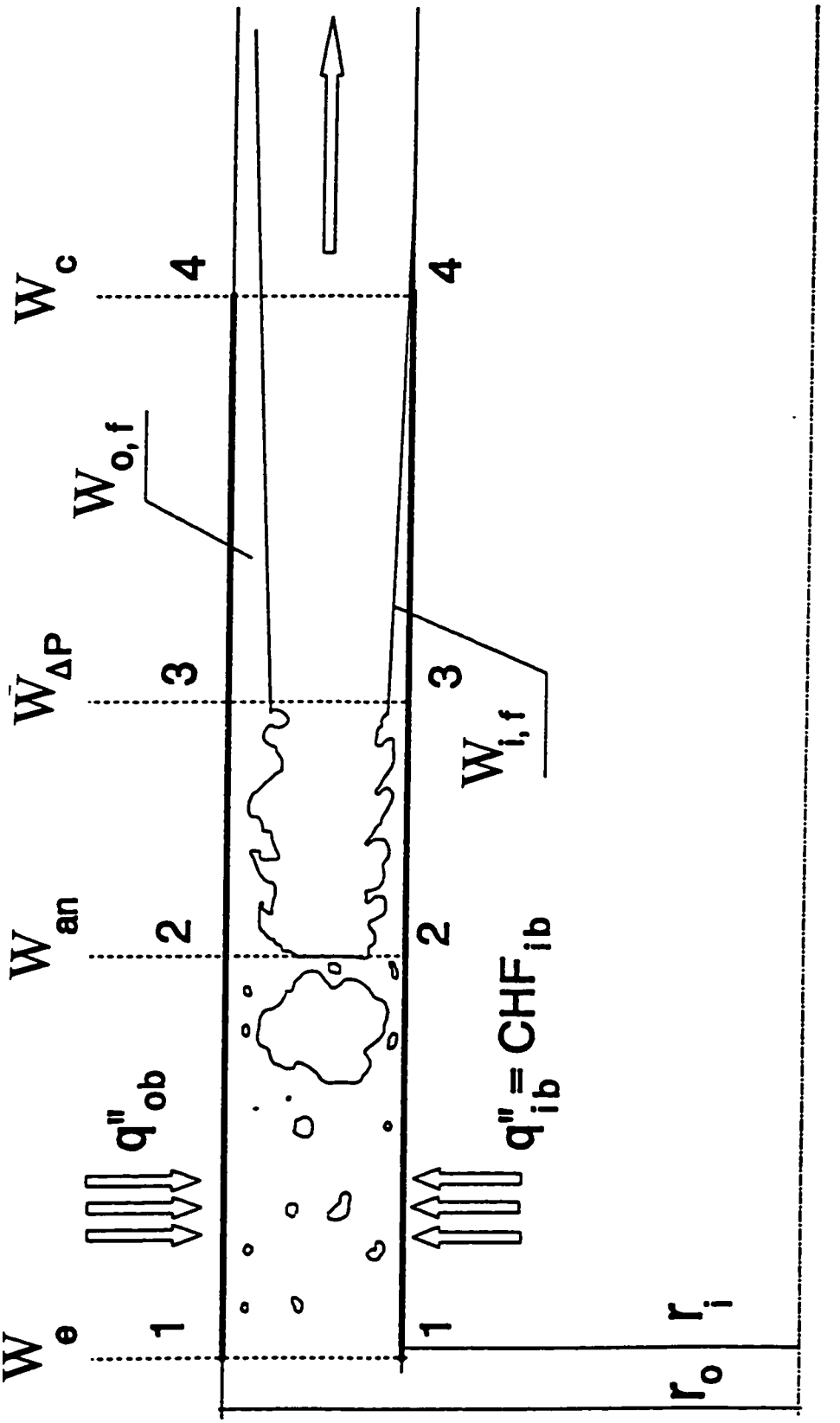

Figure 3.1 Schematic of flow patterns in annulus for Kirillov and Smogalev's model (1972). From Doerffer (1994).

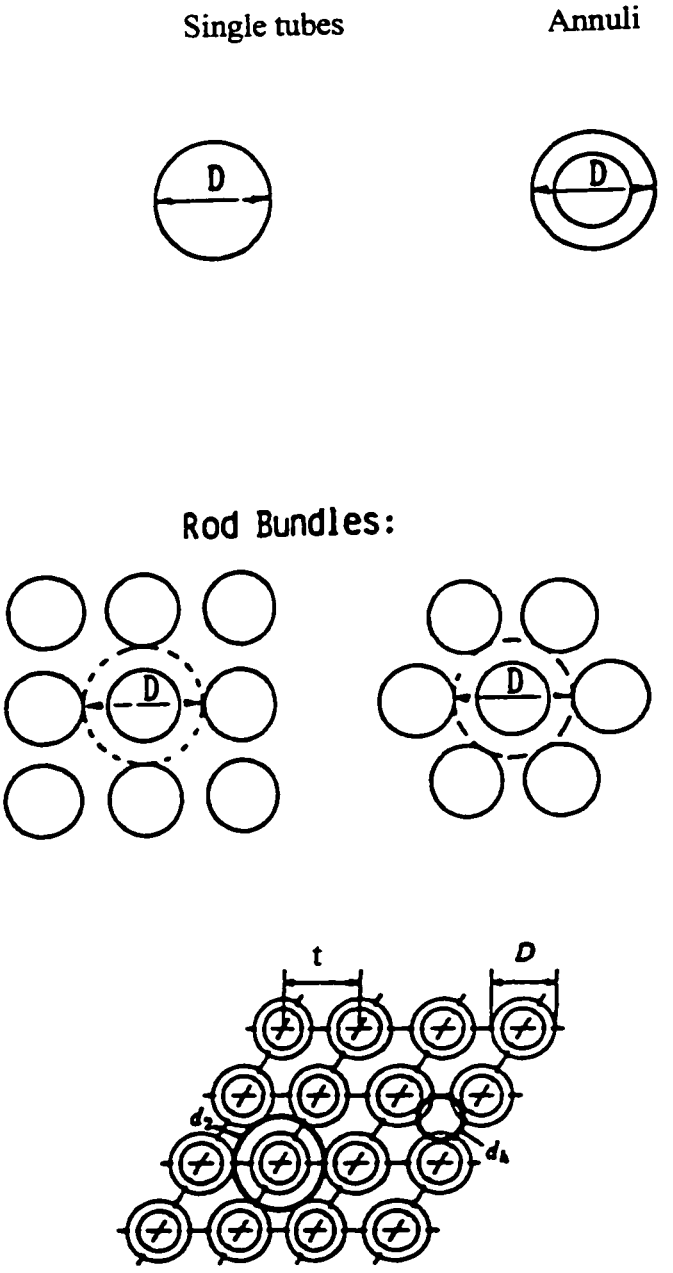

Figure 3.2 Definition of characteristic dimension - inscribed diameter of 2nd order for various flow geometries by Bethke and Zeggel (1993). From Doerffer (1994).

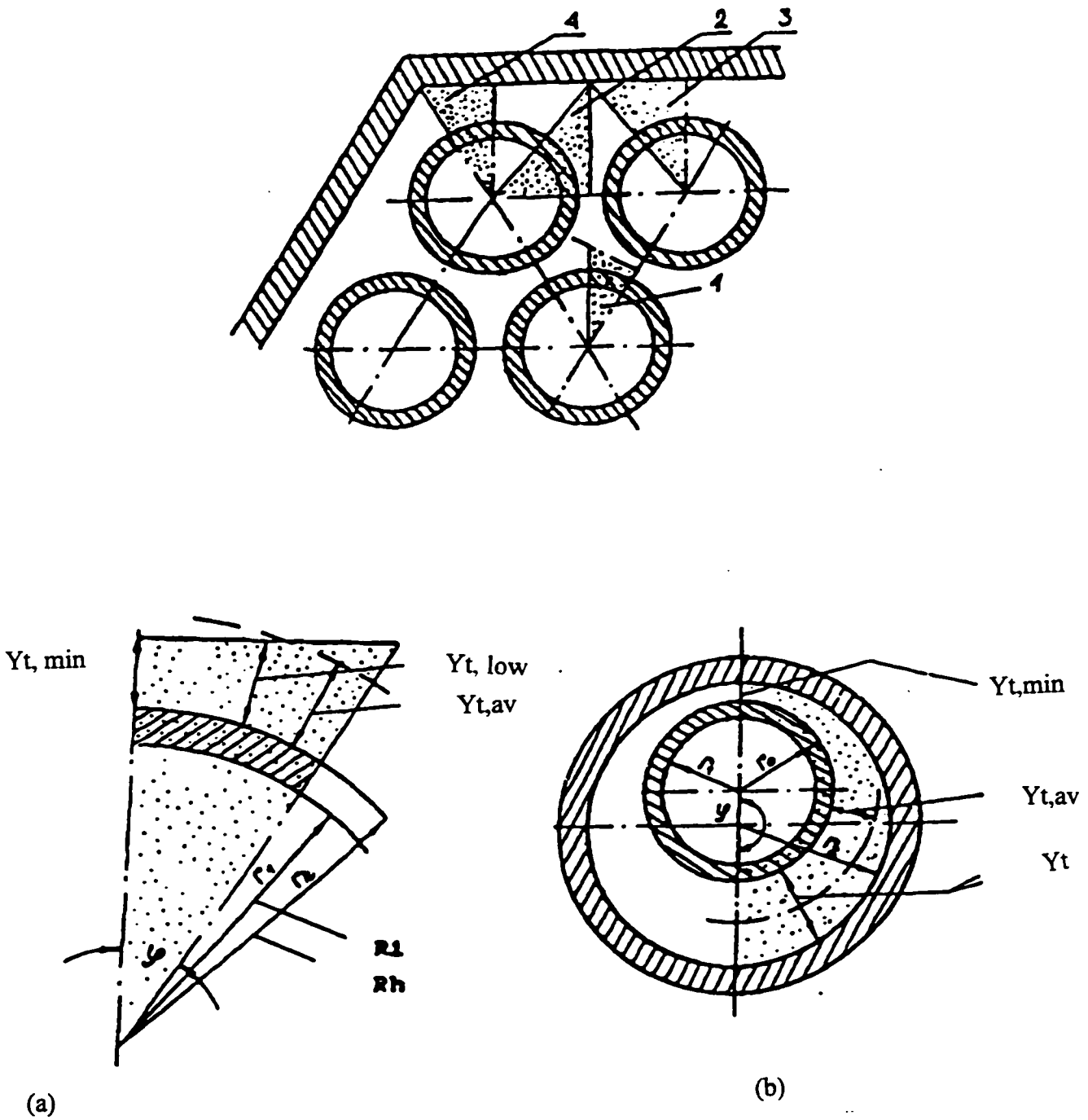

Figure 3.3 Definition of elementary heat cell for different flow geometries. (Bobkov, 1993, quoted by Doerffer, 1994)

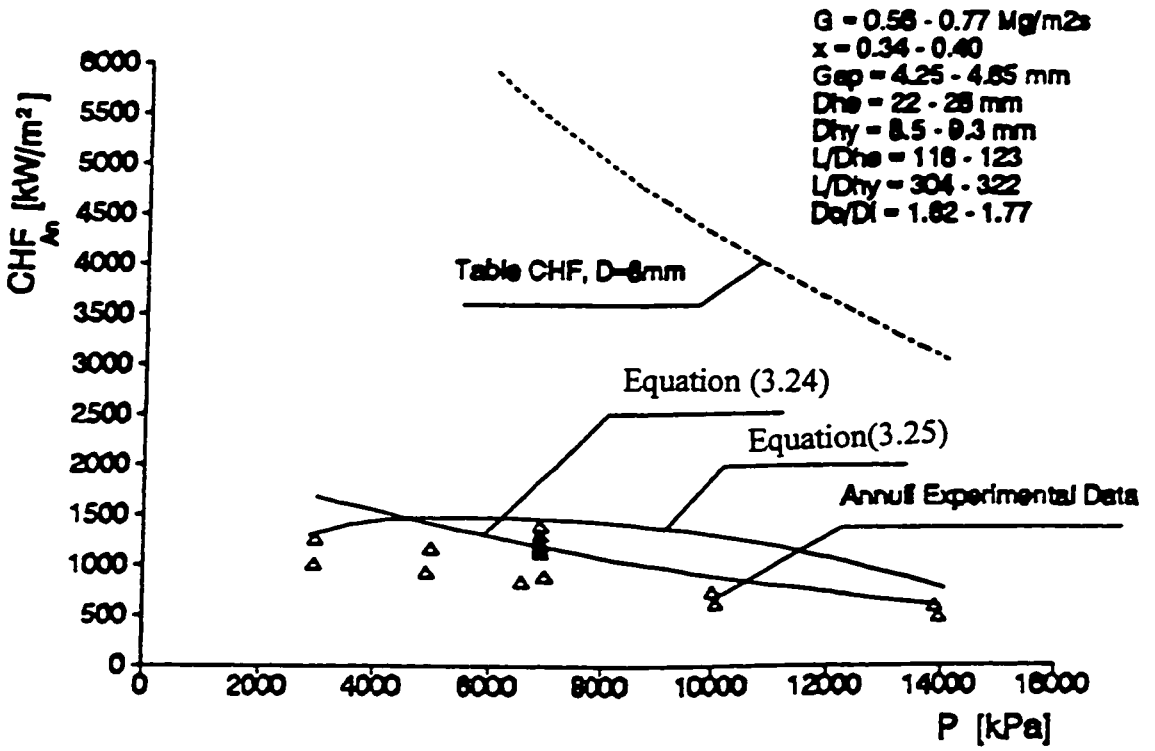

Figure 3.4 Comparison of CHF in annuli and tubes against pressure. From Doerffer(1994)

4. CRITICAL HEAT FLUX IN BUNDLES

4.1 General

In water-cooled nuclear-power reactors the fuel element is often in the form of a bundle of small diameter rods spaced one from another by helically wrapped wires or by grid type spacers. A considerable number of electrically heated models of such elements have been tested in various laboratories and the detailed results have been compiled, correlated and discussed. The reactor technology appears to be well established, however, detailed behaviors of coolant in the fuel channels are not thought to be well understood. In order to solve various problems, the related physical phenomena should be thoroughly investigated.

When dealing with the dryout phenomenon for critical power evaluation, dryout mechanism as shown in Figure 4.1 has to be studied in addition to the balance of mass, energy, and momentum between subchannels. The liquid film flow on the fuel rod surface decreases due to vaporization and entrainment by steam flow. There are three processes which control the film flow rate, i.e.

(i) Evaporation of the film: This tends to decrease the liquid film flowrate.

(ii) Droplet entrainment: This high speed vapor may strip droplets off the wavy surface of the film. With high heat flux, nucleate boiling may occur, with the subsequent entrainment of

liquid droplets into the vapor core. Both these processes tend to decrease the liquid film flowrate.

(iii) Droplet deposition: Droplets carried in the vapor core can rejoin the liquid film. This is a mass transfer process which is driven by concentration gradient of droplets, i.e. from high concentration in the vapor core to lower concentration near the film.

If the fuel rod surface is directly exposed to vapor, heat transfer is highly degraded and surface temperature rises steeply. This is dryout phenomenon. Physically, the condition for dryout corresponds to the situation where the heating surface is not completely covered by a liquid film. Since surface tension prevents an infinitely thin film, there exists a critical film thickness below which the film will break up to expose the heated surface. However, disturbances from the core flow tend to destabilize the film by inducing waves on the film surface and result in a larger critical film thickness. If flow distribution is nonuniform, it may cause nonuniformity in liquid film flow and cause dryout. The entrained liquid droplets can deposit on the fuel surface due to steam flow turbulence. This deposit increases the critical power for dryout. The vapor generated on or in the boundary layer near the wall surface has a velocity component away from the rod surface. The drag force by this surface component works to prevent the liquid droplets from depositing on the rod surface. Although drag force is very small under normal conditions, it can not be ignored when very high heat flux appears or very high surface temperature is expected. These phenomena are also highly depended

on the geometry of the flow path.

It should be noted that the gap size in bundles affects the CHF in the two-phase flow regime. Becker (1967) suggested that the bundles with a small value of t/d will be more restrictive to cross flow and the CHF will be small. As t/d increases, the CHF will increase until the inter-element spacing is sufficiently wide that crossflow is not restricted. At this point CHF would be insensitive to increasing element-to-element clearance. Actually, Rogers(1966) described that, with helical spacers, for element spacings (t - d) of about 1.88 mm, and larger, the critical heat fluxes approach those of annuli, but for element spacings below 1.88 mm, they decrease significantly with element spacing. The low CHF in the closely-spaced bundles can be attributed mainly to poor mixing between the sub-channels of the bundles. The complex flow passage geometry of these bundles produces non-uniform mass velocities in the various sub-channels. The different heated perimeter, and the non-uniform radial heat flux, produce no uniform heat inputs to the sub-channels. These factors, and the poor mixing between sub-channels, results in significantly different enthalpy rises, and hence qualities, at a given axial position in the sub-channels. Therefore, for a given heat flux, critical conditions can be reached in a certain sub-channel, when the bundle average enthalpy (quality) is well below the critical value for similar conditions in an annulus.

4.2 Differences in Mechanisms Between Annuli and Bundles

In internally heated annuli, the heat flux is uniform, the annular section between the tubes is the flow area, and there are not subchannels. In bundles, the rod bundles are contained in a flow tube and the fluid is heated by the bundle elements, each element may have different heat flux. The heat flux is not uniform across the cross section. In subchannel analysis, however, elements are assumed to be contained in the subchannels. This allows the flow within a subchannel to be treated as one dimensional in the axial direction, together with the assumptions about the velocity and void fraction profiles across the cross section.

There are usually two ways to divide the bundle into subchannels, i.e., the conventional flow centered subchannel and the rod centered subchannel. The conventional flow centered subchannels (Figure 4.2) are best suited for the liquid continuous regime in the lower part of the bundle. However, in the annular flow regime the rod centered subchannels have some advantages for keeping track of the liquid films around the rod.

CANDU rod bundles are spaced at regular intervals by wart spacers, although there are spacers in some annuli, too. However, the spacer effect in both annuli and bundles are quite different due to the geometry differences. Properly designed spacers can significantly improve the bundle critical power performance. Shiralkar et al. (1992) pointed out that differences of the order of 10% in critical power are not uncommon. Nishida (1992) stated that the spacer has the following effects on liquid film flow.

i. The film thickness has its minimum in the vicinity of the spacer due to flow area reduction. However, it should be noted that dryout does not always occur at the point of minimum film thickness, but at the point of minimum flow rate.

ii. At very low droplet concentration, an increase of gas-liquid interfacial shear stress owing to the spacer resulted in more entrained droplets, which led to decrease of the film thickness behind the spacer. On the other hand, at a high droplet concentration, the film thickness behind the spacer increased due to the larger number of deposited droplets.

iii. On increasing the number of installed spacers, thicker films were generated by a sum of increased droplet deposition rate at each spacer. This trend could be attributed to higher critical powers with more spacers.

Figure 4.3 shows a schematic of the variation on thermal margin along the length of the bundle. Because of downstream benefits provided by the spacers, the limiting conditions typically occur just upstream of a spacer. Unfortunately, this is one of the main sources of uncertainty today. Figure 4.4 shows the various ways in which the spacer affects the flow distribution. Two major mechanisms are: film thinning immediately upstream of the spacer element and enhancement of downstream turbulence. The spacer also serves to collect impinging droplets and provides runoff of liquid to the rod. Uneven resistance in spacer cells can cause large

crossflows. The spacer element also causes mechanical entrainment of the film at the contact points. The relative importance of these effects depends on the design of the spacer.

In an equilibrium flow in a rod bundle, there are no lateral pressure difference between subchannels as the time average value and no unidirectional crossflow from one subchannel to the adjacent ones. Then flow rates of both liquid and vapor in each subchannel do not vary in the axial direction. In a non-equilibrium flow, on the contrary, flow redistributions occur along the channel axis so as to approach the equilibrium flow.

Under the two-phase flow condition, the crossflow has been divided into the following three categories (Sato, 1992): (See Figure 4.5)

(i)Turbulent mixing: An inter-subchannel mixing due to turbulence of the fluids. By this mixing, momentum and energy transfer between subchannels take place, but no net mass transfer results.

(ii) Void drift: A cross flow resulting from the tendency of a two-phase flow to approach an equilibrium condition. This phenomenon causes a net transfer of liquid and vapor from one subchannel to another in an attempt to attain the equilibrium.

(iii)Diversion crossflow: A crossflow occurring in a non-equilibrium flow due to lateral pressure gradients between subchannels. Such pressure gradients may be induced by difference

of subchannel geometry or obstructions such as spacers.

This subdivision is greatly affected by the description for single-phase flow; turbulent mixing and diversion crossflow were originally used in the description of inter-subchannel mixing of single-phase coolants (Rogers et al., 1968, 1972). Unlike single-phase flow, the crossflow processes of two-phase flow are complex and difficult to sort out into identifiable mechanisms. However, the above subdivision can be considered to be useful in the development of subchannel analysis if these three types of cross flow are superimposed on one another.

In reactor bundles, the non-uniform flow rate in the different sub-channel geometry plays a significant role in CHF. It also results in significant diversion cross flows in the region near the entrance of a bundle, and the initial flow distribution and resulting diversion cross flow is strongly affected by upstream conditions as well as the perturbation caused by the bundle end-plate.

4.3 Flow and Enthalpy Imbalance

In rod bundles, as the void fraction in the coolant flow effects the thermal-hydraulic characteristics, thus changing heat flux, coolant flow, pressure, and temperature, the void fraction is the most significant factor. Lahey, Jr. et al. (1971) conducted a series of experiments and concluded that:

i. There is a significant flow and enthalpy variation in the various subchannels of a rod bundles.

ii. Cross-flow enthalpy increases monotonically with subchannel quality beyond the bubbly-annular transition region, where there is a drop in the cross-flow enthalpy due to liquid slugging in this flow regime.

McPherson(1971) described a method for comparing bundle critical power behavior based on the enthalpy rise rate imbalance and on experimental evidence of the effect of this imbalance on bundle critical power. McPherson stated that the greater the difference between the maximum and mean qualities, the lower is the mean coolant quality at dryout and the lower the critical channel power. The bundle enthalpy imbalance number(BEIN) is defined as

$$BEIN = \frac{(dH/dL)_{max} - (dH/dL)_{mean}}{(dH/dL)_{mean}} \tag{4.1}$$

The normalized critical heat flux corresponding to the lowest BEIN for a given arrangement is defined as the bundle performance number, P(BEIN). If the relative critical heat flux of a reference bundle is given by the performance number, $P(BEIN_1)$, then the critical correlation for a second bundle with performance number $P(BEIN_2)$ is

$$\phi_{BL} = \frac{P(BEIN_2)}{P(BEIN_1)} f(P, G, X, geometry) \tag{4.2}$$

where ϕ_{BL} is the boiling length average heat flux. This correlation

is applied to the second bundle to find the CHF at the conditions and then the critical power calculated.

Sato (1992) pointed out that the fluid turbulence mixing causes an inter-subchannel mixing, thus momentum and energy transfer take place between subchannels. Since turbulent mixing occurs even when a subchannel flow is in equilibrium, it is generally considered that turbulent mixing results from turbulence in the ventilated two subchannels, and the eddy diffusivity of two-phase flow is a significant parameter.

When a two-phase flow in a rod bundle is not in equilibrium, a flow redistribution occurs along the channel axis, approaching the equilibrium state. Since significant transverse variations of quality do occur in a rod bundle, with the gas seeking the more open high velocity central region of the bundle and the liquid passing through the lower velocity region adjacent to the shroud wall in order to reach the kinetic balance, a void drift takes place and results in a net transport of liquid and vapor from one subchannel to another in an attempt to attain the equilibrium. In order to see the relation of flow distributions to flow pattern, Sato (1992) conducted an experiment using air-liquid in two channels with different diameters (Figure 4.6). The results are shown in Figure 4.7. We can see that in a bubbly flow, such as the photograph (a) of Figure 4.7, bubble density of one subchannel was similar to that of another subchannel and, thus, uniform flow resulted. When the flow pattern became slug or churn flow, void drift took place drastically with increasing air flow rate, resulting in a high air flow rate and a lower water flow rate on

the larger subchannel side and vice versa on the smaller subchannel side, as seen from the photographs (b) and (c) of Figure 4.7. After reaching the ultimately non-uniform flow distribution, the activity of void drift decreased with a further increase of air flow rate, and eventually the flow pattern of both subchannels became similar to each other, as shown in the photograph (d) of Figure 4.7. In view of flow pattern, it can be said that a heterogeneity of flow is a cause of the transverse variation of flow distributions.

Diversion crossflow is a forced transfer of mass from one subchannel to another as a result of transverse pressure gradient. Such pressure gradient may be induced by differences of subchannel geometry or obstruction such as spacers. Since it may be understood that diversion crossflow takes place superimposing on turbulent mixing and void drift, the extraction of it from an overall crossflow is very difficult.

4.4 Parametric Effects on CHF in Bundles

4.4.1 Effect of Pressure

In round tubes, CHF is a decreasing function of pressure in the range of interest in nuclear reactors. In bundles, CHF generally decreases with increasing pressure, but is not as sensitive to pressure as in tubes and annuli. Some researchers have reported bundles which are insensitive to pressure. Rogers(1970, quoted by Atkinson, 1981) suggested that this decreased sensitivity can be related to the dryout of the liquid film in the following

way. As pressure decreases, (ρ_f/ρ_g) increases, which in turn increases the void fraction. This increase in the void enhances the non-uniformity of flow in the bundle subchannels. Also, droplet entrainment is promoted due to the increased slip ratio. This increased entrainment depletes the liquid film on the heater surfaces, causing a decrease in the critical quality and CHF, when compared with tubes. This decrease offsets the increase in CHF observed in tubes and annuli with the subsequent lowered sensitivity to pressure.

4.4.2 Effect of Mass Flux

In round tubes, CHF is an increasing function of mass flux in the low and negative quality region, but a decreasing function of mass flux in the high quality region. In bundles, CHF has the similar trend as in tubes, but is more sensitive to mass flux than in tubes and annuli, since higher mass flux can influence the cross flow in bundles, and the enthalpy imbalance. The enthalpy imbalance in bundles is caused by the difference of enthalpy in each subchannel. If the mass flux is higher, the turbulent mixing among subchannels is better, then the cross flow will be increased, and the CHF will be increased.

4.4.3 Effect of Quality

In round tubes, the CHF is a decreasing function of quality. In bundles, the effect of quality on CHF is more pronounced than in

tubes, especially in positive quality region. This is due to the large parasitic liquid film flow on the unheated surface, which reduces the film flow rate on the heated surfaces, and the entrained liquid fraction. But this effect is not sensitive at DNB-type conditions (i.e., at low or negative qualities), where the unheated wall effect does not play a significant role.

4.4.4 Geometry Effects

In round vertical tubes, the mixing of vapor and liquid occurs without restriction and the circumferential heat flux distribution is generally uniform so that the thickness of the liquid film is more or less constant around the tube. In bundle geometries, the flowrate in some subchannels can be smaller than in others. Also, in two-phase flow conditions, the rods act as restrictions to crossflow and inter-channel mixing of liquid and vapor. Thus, due to the enthalpy imbalance, some subchannels may have less liquid available for the fuel element surfaces, implying that dryout will occur in these subchannels first. Thus, the critical condition will be reached at a bulk quality which is lower than the quality in an equivalent round tube under the same inlet conditions. Becker (1967) suggests that those bundles with a small value of t/d will be more restrictive to cross flow. Also, the crossflow will be not restricted when the inter-element spacing is sufficiently wide. Another important parameter in the horizontal bundles of CANDU reactor affecting CHF is the ratio of outer clearance (between fuel rod and pressure tube) and internal bundle clearance, which results in potential by-pass of coolant around the bundle, thus reducing

CHF (Rogers, 1970).

4.4.4.1 Effect of unheated wall

At a given exit quality, the critical heat flux in a channel having one unheated wall is usually lower than that in a totally-heated channel (Huang, 1993). This is because of the existence of a thick, cold liquid film build up along an unheated wall which does not contribute to the heat removal from the heating surface. The deterioration of CHF in a subchannel containing the cold wall is modeled by replacing the heated equivalent diameter with the hydraulic diameter of the channel during the evaluation of CHF. This comes from the premise that the effective flow rate for heat transfer of a channel including a cold wall is proportional to the ratio of the heated perimeter to the wetted perimeter of the channel. This consideration will increase the bulk enthalpy in the channel and result in the reduction of CHF.

4.4.4.2 Effect of spacer

In a rod or tube bundle the relative position of rods or tubes is usually maintained by spacers. Two basically different types of spacers are commonly used for rod bundles having predominantly axial flows. Helical wires are attached to the rods for the entire length of the bundle. This is called the wire wrap spacing design. Grid spacers, honeycomb or egg-crate grids, are arranged on the rods at fixed planes of the bundle. For bundles with wide rod-to-

rod spacing, the grid spacers are usually used. The grid spacer acts as flow obstruction in the bundle and causes increased pressure drop due to its form drag and skin friction. The grid spacers also tend to increase the local wall heat transfer. The heat transfer augmentation of grid spacers has been observed in single phase flow and two phase flow. However, the understanding of the heat transfer mechanism and the ability to predict the heat transfer downstream of the grid spacer are still very limited. Groeneveld (1980) points out that the following trends can be inferred from the experimental studies:

(a) Ferrule type spacer grids, which are made up of concentric rings fitting tightly around the heater rods, have the minimal effect on critical power. Two opposing effects were observed for this type of spacer: (i) the liquid film on the heated rods was stripped off, thus, the critical power was reduced, and (ii) the turbulence and crossflow downstream were generated by the reduction in flow area. This mixing reduced the subchannel enthalpy and flow imbalance in neighboring subchannels and hence increase the critical power.

(b) The grid spacer producing the largest flow obstruction did not necessarily result in the largest increase in critical power.

(c) The maximum increase in critical power due to grid spacers usually occurred at high flows, high qualities and short axial grid spacings.

(d) Although an increase in critical power due to rod spacing

devices was observed in most studies, detrimental effects could also be present. The much larger beneficial effect of spacers usually overshadowed the detrimental effect in most studies.

(e) CHF was mainly found to take place preferentially just upstream of a rod spacing device in the experimental studies.

The CHF was influenced by rod spacing devices in rod bundles primarily by affecting the phase distribution. Some insight into the spacer effect on CHF is given by Groeneveld (1980).

(1) Film flow rate on unheated surface: A significant fraction of the liquid flow in a fuel bundle assembly can be on the unheated wall. The liquid film thickness on the unheated surface is about three times that of the heated rods; this liquid film does not take part in the heat transfer in the bundle: it reduces the amount of liquid available for cooling of the heated rods. To counteract this effect, rod spacing devices have been designed which will trip the liquid film off the unheated surface.

(2) Enthalpy and flow imbalance: Considerable mass flux and enthalpy imbalance between adjacent subchannels can be present due to unequal subchannel power input and hydraulic resistance.

(3) Entrained liquid fraction: Hewitt (1970, quoted by Groeneveld,1980)) had shown that in annular flow, a very large fraction of the liquid was entrained in the core of the flow channel. CHF could be increased by directing this entrained liquid

towards the heated surface by using twisted tapes or mixing vanes attached to the rod spacing devices.

(4) Breakup of bubble boundary layer: In the bubbly flow regime, the density of bubble population increases with heat flux and a bubble boundary layer is often formed a short distance away from the surface. This layer can be so thick that it impedes the flow of liquid to the heated surface and this eventually will lead the CHF condition. The presence of rod spacing devices, which contact the rods over large sections of the rod periphery, tends to increase the turbulence near the heated surface and break up the bubble boundary layer.

(5) Flow regime transitions: In horizontal two-phase flow, a more homogeneous phase distribution across the bundle can result from the improved subchannel mixing downstream of spacing devices. This tends to counteract the effect of eccentricity and flow stratification.

4.4.4.3 Effect of segmented bundles

Atkinson (1981) stated that for segmented fuel channels the end plate in bundles of CANDU reactors tends to strip the liquid film from the fuel element surfaces and to redistribute the flow of both vapor and liquid among the subchannels. Also, the 50cm fuel bundles are placed in the fuel channel while the reactor is operating by automatic fueling machines. The angular orientation of the bundle

is completely random, so that the flow passages in the end plates are generally not aligned. The effect that the end plates have on dryout would depend on the inter-element spacing, the relative alignment of the end plates, the void fraction, etc. and is very unpredictable. Atkinson proposed a correlation for CANDU reactors which based on full scale, electrically heated CANDU bundles with end-plate. However, Rogers (1970, quoted by Atkinson, 1981) pointed out that, when the CHF results for smooth, vertical bundles are compared with segmented bundles of the same length, the position of the dryout in the bundle may change, but the magnitude of the critical heat flux is not substantially different.

4.4.5 Effect of Radial Heat Flux Distribution

The effect of radial heat flux distribution can be rationalized using the steady flow energy equation in the following argument. A uniformly heated round tube of diameter D_{he} and length L has a coolant mass flux of G, with saturated liquid at the inlet (X_{in}=0), and measured CHF, ϕ. Under these conditions, the critical quality is

$$x_{rd} = 4 \ (L/D_{he}) (\phi/h_{fg}G)$$

For a rod bundle with uniform radial heat flux distribution, equivalent diameter D_{he} and length L, assuming that the flow of coolant is uniformly distributed across the bundle, so that the mass flux is a constant, Atkinson (1981) chose a stream tube which includes all the heating elements and whose flow crossection is

$$A_x \cdot (P_{he}/P_{tot}) \tag{4.3}$$

Outside of this heated stream tube is an unheated flow (next to the flow tube wall). The arbitrary restriction of no mixing between the unheated stream tube and the unheated flow is imposed. If the ratio of the vapor flow to the total flow in the stream tube at the critical condition is assumed equal to x_{rd}, then the critical heat flux for the bundle is defined by

$$\phi \cdot L \cdot P_{he} = GA_x \cdot (P_{he}/P_{tot})\,(x_{rd} \cdot h_{fg}) = GA_x \cdot x_c \cdot h_{fg}, \tag{4.4}$$

i.e.,

$$x_c = x_{rd} \cdot (P_{he}/P_{tot}) = x_{rd} \cdot \eta \tag{4.5}$$

This idea can be extended to bundles with radial heat flux depression. Becker (1967) suggested that the elements with depression heat flux can be thought of as 'partly cold rods', i.e.,

$$\eta = \frac{d\sum_{i=1}^{n} (q_i/q_{max})}{nd + D_s} \tag{4.6}$$

4.4.6 Effect of Axial Heat Flux Distribution

The axial heat flux distribution has a significant effect on CHF, especially on the location of CHF. Usually the CHF takes place at the exit of the bundles with a uniform axial heat flux

distribution, but it will occur at the place where the local quality equals the critical quality for a nonuniform heat flux distribution. The effect of nonuniform heating on CHF can be predicted based on one of the following hypotheses:

(i) Total power hypothesis: The total power hypothesis suggests that the total power that can be generated to a nonuniformly heated geometry is the same as that for a similar geometry with uniform heating.

(ii) Local conditions hypothesis: The local condition hypothesis states that it is only the local heat flux and local quality at the location of CHF that control the onset of CHF, and the upstream history is not important. It is immaterial that whether the heat flux is distributed uniformly or nonuniformly and whether the inlet flow conditions are saturated or subcooled.

(iii) Boiling length average heat flux hypothesis: For high quality regions, where the annular flow regime typically occurs, the CHF depends not only on local flow conditions, but also on the upstream history. The boiling length average(BLA) heat flux hypothesis is a tentative modification of the local condition hypothesis to take the history effect into account. It assumes that CHF occurs when the BLA heat flux reaches a certain critical value. Compared with the local condition hypothesis, the BLA hypothesis predicts the CHF and dryout location more accurately for systems with non-uniform AFD.

The BLA heat flux is the integral average of surface heat flux

over the portion of the heat flux surface on which boiling occurs

$$q_{BLA}=\frac{\int_{z_x=0}^{z} q\,dz}{z-z_{x=0}} \tag{4.7}$$

where $z_{x=0}$ is the axial location where the quality x=0. At x<0, the BLA heat flux is equivalent to the local heat flux.

(iv) The 'F-factor' method: A consequence of the failure of the "local condition" hypothesis for non-uniform heat flux distributions is that the value of the local critical heat flux must depend, to some degree, on the heat flux profile upstream of the point considered(Collier et al., 1994).

To correct the effect of axial heat flux nonuniformity, Tong et al.'s F-factor (1968,1972) is widely used

$$F=\frac{C}{\phi_{c,n}[1-\exp(-C\times Z_{CHF,n})]}\times\int_{Z_{ONB}}^{Z_{CHF,n}}\phi(z)\exp[-C\times(Z_{CHF,n}-Z)]dz \tag{4.8}$$

where

$$C=\frac{5.91(1-X_{CHF})^{4.31}}{G^{0.478}}\quad(m^{-1}) \tag{4.9}$$

4.5 CHF Prediction Methods in Bundles

4.5.1 General

In water cooled nuclear power reactors the fuel element is often in the form of a cluster of small diameter rods spaced one from another by spacers. A considerable number of electrically heated models of such fuel elements have been tested in various laboratories. Analysis of thermo-hydraulic conditions within a multi-rod cluster can be handled at various levels of detail.

(i) *Mixed flow correlation approach*

In this approach the entire channel is assumed to behave in a one-dimensional manner with 'average' properties being ascribed to the variables such as mass flow-rate, quality and heat flux. No attempt is made to consider any two-dimensional 'fine structure' within the channel. This method is the practical design approach and in engineering practice. The correlation used must be developed from experiments with the actual geometry of the fuel bundle. The actual coolant is preferably used in the experiments or an alternative coolant can be used if appropriate scaling rules have been established (Atkinson and Rogers, 1982). An early attempt at such a correlation was that of Macbeth (1964) and Barnett (1966).

(ii) *Sub-channel analyses*

Under this general heading, an attempt is made to sub-divide

the rod cluster into a number of parallel interacting flow subchannels between rods. The equations of mass, momentum and energy conservation are solved to give radial and axial variations in quality (or fluid enthalpy) and mass flow-rate. Interchange of mass, heat, and momentum is allowed between neighboring sub-channels. The mass, heat and momentum interchange between subchannels must be defined by appropriate empirical equations established by separate experiments. Once the local enthalpy and flow conditions at each sub-channel node have been established, suitable constitutive relations in the form of empirical correlations are used to define the heat transfer regime, including the CHF, so as to provide the local temperature of the rod surface. Details of such calculations have been given by Weisman and Bowring (1975). Bowring (1979) has published a subchannel dryout correlation (WSC-2) for use with sub-channel analysis computer codes. AECL (Atomic Energy of Canada Ltd.) also developed a sub-channel code, ASSERT, for the CHF computation for CANDU reactor.

(iii) *Phenomenological analyses*

Under this general heading, an attempt is made to model the kinetics of the various physical processes which occur. Clearly such analyses must relate to the actual flow patterns present and, more important, they must be able to handle departures from hydrodynamic equilibrium (i.e., not 'fully developed' flows). To illustrate these points an example of the Phenomenological model developed by Whalley (1978) for two-phase flow in a vertical cluster is given in following section. Attention must be paid that

the Phenomenological analysis does not really represent a separate approach from sub-channel analysis, since the Phenomenological method must be applied on a sub-channel basis if they have any use.

4.5.2 CHF Correlations

Macbeth (1964) applied the 'local conditions' hypothesis to a selection of data from uniformly heated vertical rod clusters and obtained the following correlation for 69 bar only

$$\phi_{CRIT} \times 10^{-6} = \frac{A + B(\Delta h_{SUB})}{C + z} \tag{4.10}$$

where

$A = 67.6 D_{he}^{0.83} (Gx10^{-6})^{0.57}$

$B = 0.25 D_{he} (Gx10^{-6})$

$C = 47.3 D_{he}^{0.57} (Gx10^{-6})^{0.27}$

The eq. (4.10) and parameters A, B and C use British units. Attention should be also paid that the eq. (4.10) was for a specified type of bundle geometry, with vertical uniform sub-channels. This correlation would not bee valid for CANDU fuel bundles with their non-uniform sub-channel bundle end plates and horizontal configuration.

Barnett (1966) showed that Eq.(4.10) can predict a wide range

of rod bundle data with remarkable accuracy. In annular channels, the CHF appears to vary qualitatively in the same general manner as for round tube. The CHF may be assumed to be a function of six independent variables thus:

$$\Phi_{CRIT} = f(G, (\Delta h_{SUB}), P, D_i, D_o, z)$$

where D_i and D_o are the internal and external diameters of the annulus respectively.

For rod bundles the values of D_i and D_o are defined as follows:

'equivalent' $D_i = D_{rd}$, the rod diameter (inches)

'equivalent' $D_o = [D_{rd}(D_{rd}+D_h^*)]^{0.5}$ (inches)

where

$$D_h^* = \frac{4\times(flow\ area)}{S\times(heated\ rod\ perimeter)}, \qquad and \qquad S = \sum_{rods} \xi$$

ξ is the ratio of heat flux on a rod to the maximum heat flux in the bundles. If all the rods carry the same heat flux, $D_h^* = D_h$; and

$$A = 64.04 D_{he}^{1.058} (Gx10^{-6})^{0.511}$$
$$B = 0.204 D_{he}^{1.277} (Gx10^{-6})^{0.872}$$
$$C = 60.41 D_{he}^{2.241} (Gx10^{-6})^{0.388}$$

All parameters above are in British units.

4.5.3 Subchannel Method

Subchannel analysis is a pragmatic method to predict flow behavior and thermal performance inside of a rod bundle. Especially in two-phase flow conditions, conservation equations of mass, energy and momentum are written one-dimensionally on a subchannel base taking account of crossflows between the neighboring subchannels.

Subchannel analysis dates back to the late 1950s, as stated by Shiralkar et al. (1992), The first generation of computer codes based on this concept include COBRA, HAMBO and MIXER. These are based on the mixture equations for two-phase flow with allowance for phase slip, which represented the state of the art at the time. The largest uncertainty in these models is the interaction between the subchannels caused by pressure difference across the cross section and by turbulent mixing across the gaps between rods.

Methods for two-phase flow analysis improved further in the seventies and eighties, primarily due to the advances being made in safety analysis. Two fluid models were developed and considerable effort was expended in modeling of the interfacial shear and heat transfer for the various flow regimes. The THERMIT code was perhaps the first to embody a full two-fluid model for subchannel analysis. The current trend is towards multi-field modeling of the continuous and dispersed phases, with further refinement of the basic two-phase flow models.

The two-fluid model has been extended to encompass multiple fields. In general, this means separate representation of the continuous and dispersed fields. In the annular flow regime, the liquid film, vapor and droplets are each represented by a set of conservation equations. In subcooled boiling, there is a superheated liquid layer which generates saturated vapor bubbles at the heated surface, while the bulk liquid is subcooled. It is customary to account for the superheated liquid through an energy partition model for the wall heat flux, rather than as a separate field. In the bubbly flow regime, the two sets of conservation equations for the liquid degenerate into one set present the continuous bulk liquid, and the vapor bubble present the dispersed field.

The advent of three-field modeling has raised a question about the optimum geometrical representation of the subchannels. The conventional flow centered subchannels (Figure 4.2) are best suited for the liquid continuous regime in the first part of the bundle. However, in the annular flow regime the rod centered subchannels have some advantages for keeping track of the liquid films around the rod. The main disadvantage of this scheme is that there is no data on turbulent mixing transfer across the large subchannel boundaries. Lines of zero shear have to be assumed as the bounding surfaces. Moreover, while deposition of droplets is based on the region surrounding the rod, the entrainment rates could be different on different sides of the rod if the velocity is different. On the other hand, in a conventional subchannel, the different surfaces within a subchannel could have very different rates of heat generation and surface characteristics, and using a

single average film is not appropriate. Thus it is important to individually model each film as a separate field. Examples of such multi-field analytical models are the FIDAS, MULTI, COBRAG and ASSERT codes.

4.5.4 CHF Models

The first successful attempt to extend dryout modeling to rod bundles is credited to Whalley (1978). The approach is basically the same as that used for a round tube, but the mass balance accounts for (a) turbulent two-phase mixing between adjacent subchannels and (b) transfer of entrained liquid between subchannels by cross flow.

The equation then are

$$\frac{dW_{LEi}}{dz}=S_{Si}(E_i-D_i)+\sum_{j=1}^{n}k_{cij}S_{Fij}(C_j-C_i)n_{ji}+\sum_{j=1}^{n}a_{ij}\frac{W_{LEi}}{W_{Gi}}J_{Gji}n_{ji}+\sum_{j=1}^{n}b_{ij}\frac{W_{LEj}}{W_{Gj}}J_{Gji}n_{ji} \qquad (4.11)$$

turbulent mixing between subchannels

Transfer of entrained liquid between subchannels due to gas crossflow

the deposition rate D_i can be written as

$$D_i=k_iC_i$$

the entrainment rate E_i can be written as

$$E_i=k_iC_{Ei}$$

Whalley uses rod-centered subchannels (Figure 4.8). This has the advantage of allowing the liquid film around each rod to be treated individually. This channel arrangement is particularly adaptable to triangular-pitch lattices.

Lim and Weisman (1988) also used conventional sub-channels, which they argue are more appropriate than rod-centered channels, for boiling reactors having a square rod array. Their approach may be understood by referring to Figure 4.9, which shows the subchannels into which a typical rod bundle is divided. The solid lines debark the regions in which the vapor mass fluxes and concentration of droplets are considered to be uniform. The dotted lines debark the subchannels in which entrainment deposition calculations are carried out.

The calculations from the previous length step will have provided: (a) the mass flux and quality of the vapor-droplet mixture entering the segment and (b) the liquid film flow rates on each of the rods facing the channel. The quality and mass flux at the inlet to each of the four subchannels is set equal to the channel values at the segment inlet. Mass balance equations are then written for each of the subchannels to obtain the quality, $x(i, j)$, and liquid film mass flux at the subchannel exit, $G_f(i, j)$. That is

$$G^{p}(i, j)h_{fg}[x(i, j) - x^{p}(i, j)] = \frac{4}{D_e}\phi(i, j)(\Delta z) \qquad (4.12)$$

$$G_{LE}(i,j)-G_{LE}^{p}(i,j)=\frac{4}{D_{hy}}(\Delta z)\left[D(i,j)-E(i,j)-\frac{\phi(i,j)}{h_{fg}}\right] \qquad (4.13)$$

where the superscript "p" indicates the values from the previous length step.

The deposition rate, D(i, j) is obtained from

$$D(i,j) = k\ C(i,j) \qquad (4.14)$$

While the entrainment rate, E(i, j) is obtained from

$$E(i,j) = kC_{eq}(i,j) \qquad (4.15)$$

4.6 Summary

In this chapter, the differences of the CHF mechanism between annuli and bundles are discussed and the parametric effects on CHF in bundles are presented. The CHF prediction methods are also introduced. The three approaches for predicting CHF in bundles are:

i) Mixed flow correlation approach
ii) Sub-channel analyses
iii) Phenomenological analyses

The CHF prediction in bundles is very complex. The applicable range of the mixed flow approach is narrow, while the sub-channel and the phenomenological methods are difficult to use and time

consuming. The need is obvious for a simple method, applicable to a wide parametric range and with accurate prediction. The development of such a new method to predict CHF in bundles using the tube look-up table as a reference is given in the next chapter.

Table 4.1: Summary of parametric effect on CHF in bundles

Parameters		Observed Effect	Physical Explanation
Pressure		CHF is generally a decreasing function of pressure, but is not as sensitive to pressure as in tubes.	When pressure decreases, the void fraction increases, the non-uniformity of flow in the bundle is enhanced. Also, droplets entrainment is promoted due to the increased slip ratio. Therefore, the CHF is decreased. This decrease offsets the increase in CHF observed in tubes. Rogers (1970)
Mass flux		CHF increases with mass flux increases, and is more sensitive than in tubes.	The mass flux can influence the cross flow in bundles, and higher mass flux leads to better mixing and evens the enthalpy imbalance in bundles, then the CHF will be increased.
Quality		CHF is a deceasing function of quality, and is more sensitive than in tubes.	There is a parasitic liquid film flowing on the unheated surface, which passby the liquid film flow rate on heated surfaces in bundles. Then the CHF in bundles is lower than that in tubes.
Geometry	Unheated wall	CHF is lower in bundles than in tubes, since there is an unheated wall.	The deterioration of CHF in a subchannel containing the unheated wall is due to the existence of a thick, cold liquid film built up along an unheated surface which does not contribute to the heat removal from the heating surfaces.
	Spacer	The existence of spacers can improve the CHF in bundles.	Rod spacing devices can influence the CHF in rod bundles primarily by affecting phase distribution, such as film flow rate on unheated surface, enthalpy and flow imbalance, entrained liquid fraction, etc. Groeneveld (1980)
Flow transient		The flow transient can deteriorate the CHF in bundles.	The liquid film is thinner at higher flow rate and thicker at low flow rate in bundles. When flow rate decreases quickly during the flow transient, the film thickness is still thin, then the CHF occurs prematurely.

Table 4.1 (concluded)

Parameters	Observed Effect	Physical Explanation
Radial heat flux distribution	CHF can be increased by the radial heat flux distribution	The CHF occurs in the subchannel which has the highest quality or enthalpy in bundles, it is usually the inner subchannel, which has the lower flow rate and higher quality. The effect of RFD can smooth the enthalpy among the subchannels in bundles by reducing the heat flux at the inner subchannel, and then, increase the CHF in bundles.
Axial heat flux distribution	The axial heat flux distribution has a significant effect on the CHF, especially on the location of CHF.	The CHF occurs only when the quality reaches the critical quality, the CHF usually occurs at the exit of uniform axial heat flux distribution bundles, where the enthalpy or quality is higher than the previous section of the bundle, and the CHF might occur at the middle of the bundle where the critical quality is reached due to the effect of axial heat flux distribution.

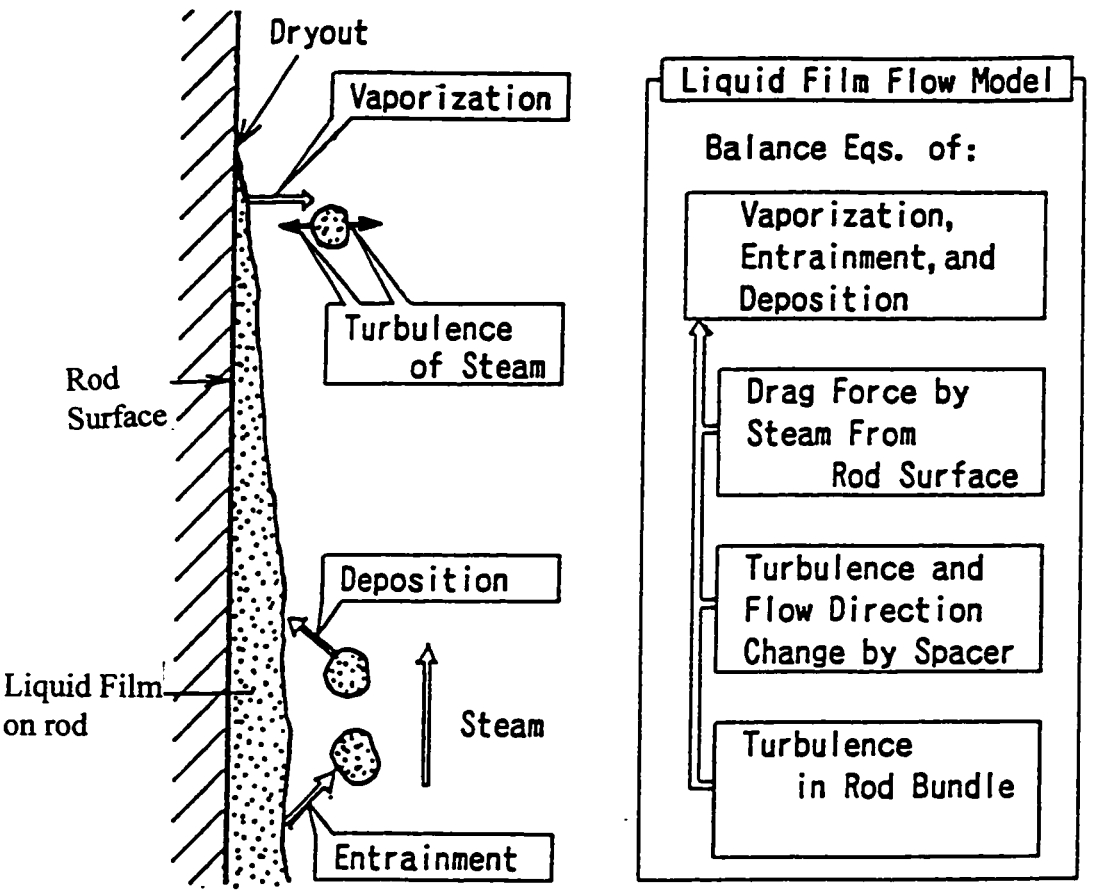

Figure 4.1 Dryout phenomena and factors affecting CHF. From Kitayama (1992).

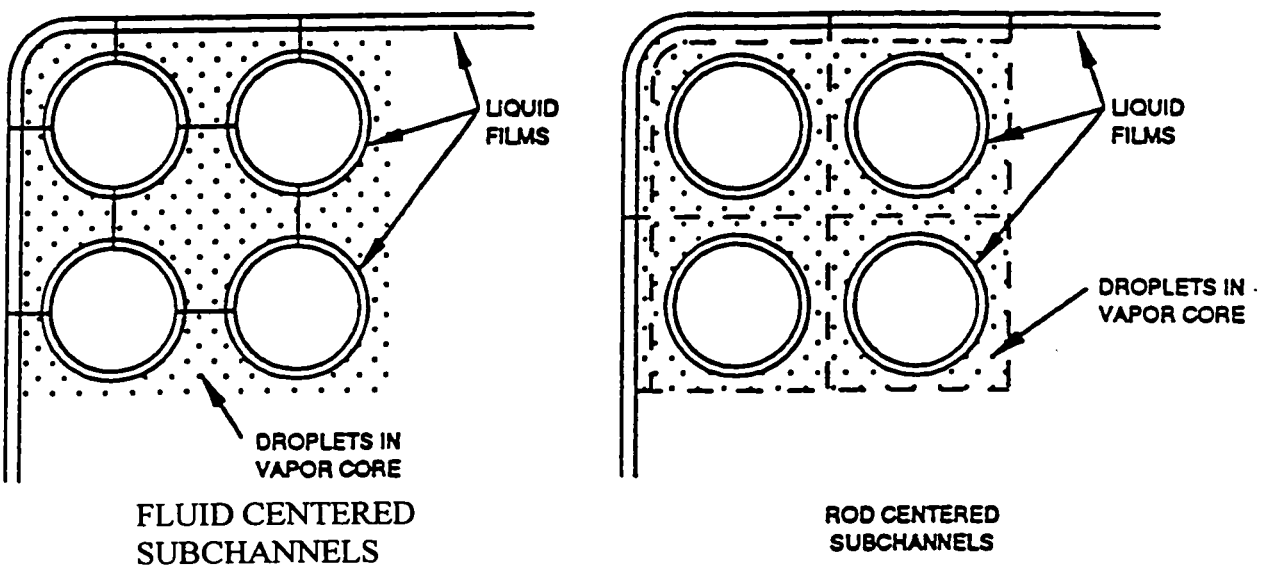

Figure 4.2 Subchannel arrangements. From Shiralkar et al. (1992).

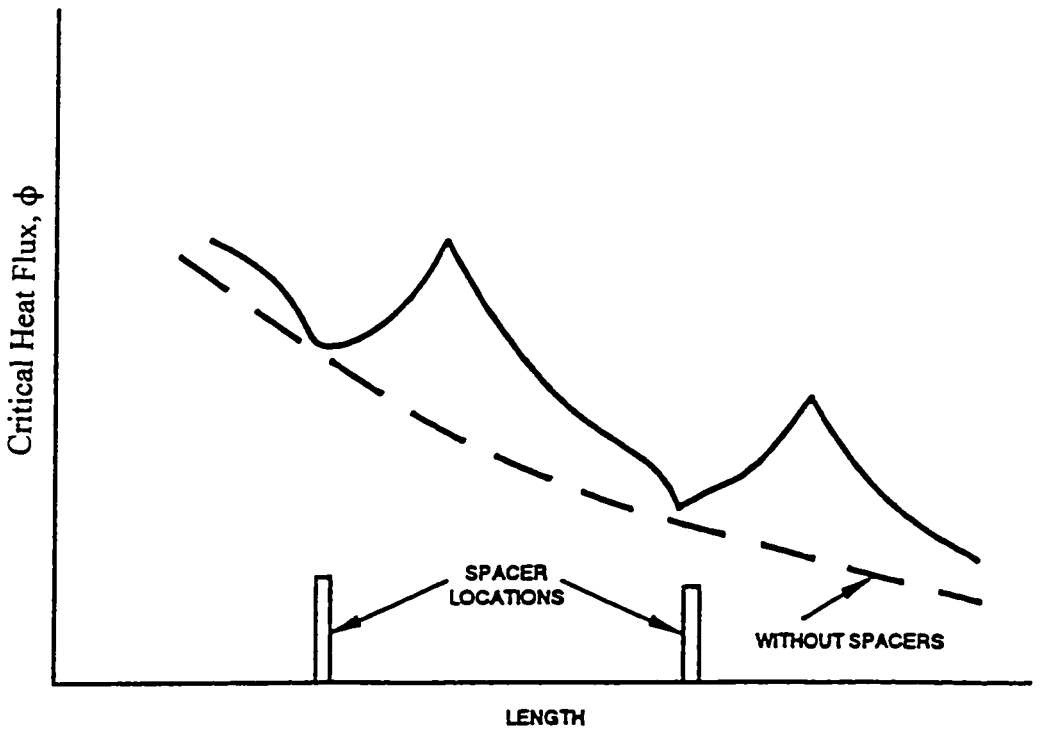

Figure 4.3 Variation of thermal margin along bundle length. From Shirlkar et al. (1992).

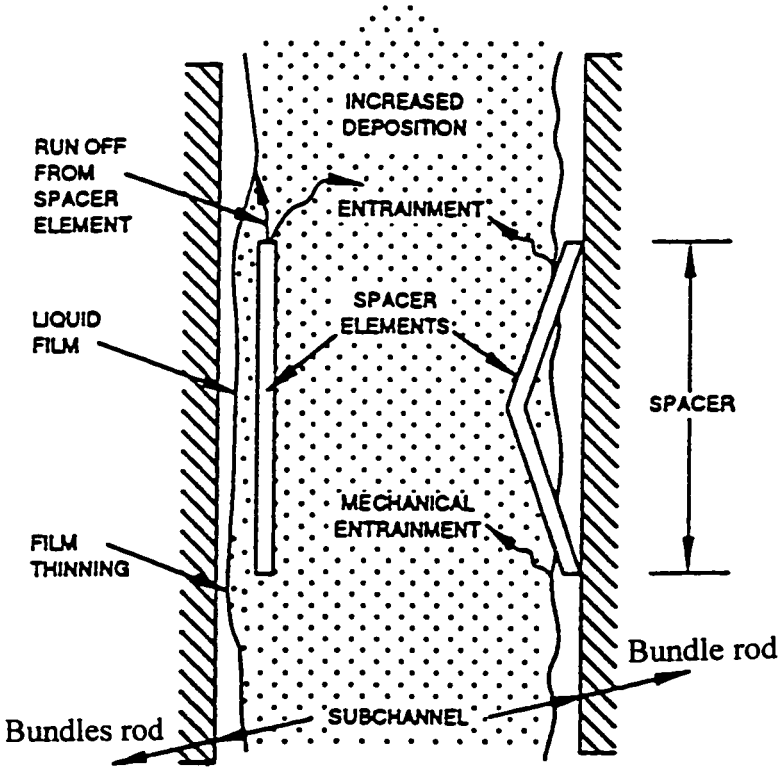

Figure 4.4 Spacer interaction. From Shiralkar et al. (1992).

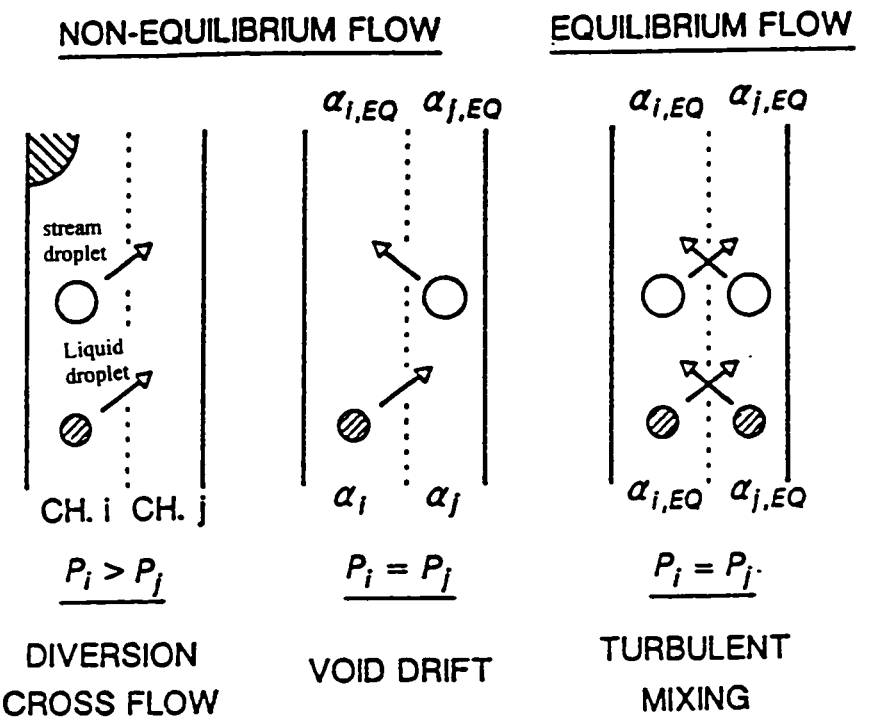

Figure 4.5 Three types of crossflow between subchannels. From Sato (1992).

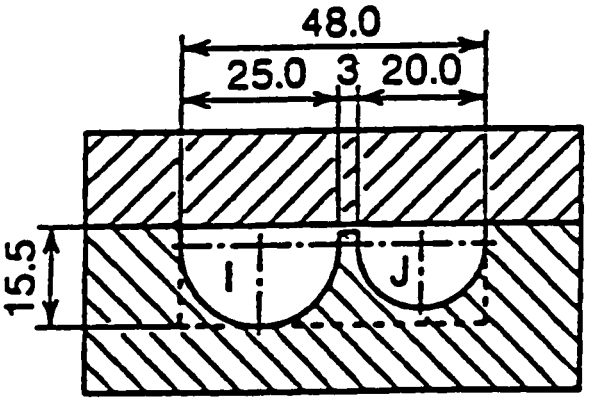

Figure 4.6 Cross section of the test section used by Sato et al. (1992).

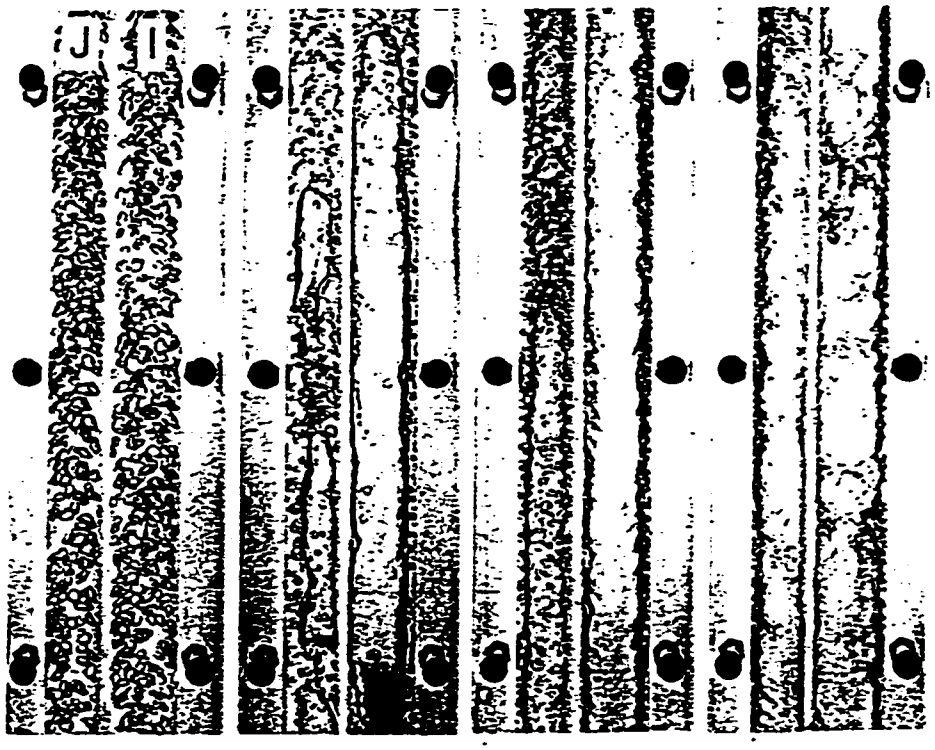

(a) j_g=0.35m/s (b) j_g=1.0m/s (c) j_g=4.0m/s (d) j_g=7.5m/s

Figure 4.7 A series of flows observed in Figure 4.6 at J_L=1.0 m/s. From Sato et al. (1992).

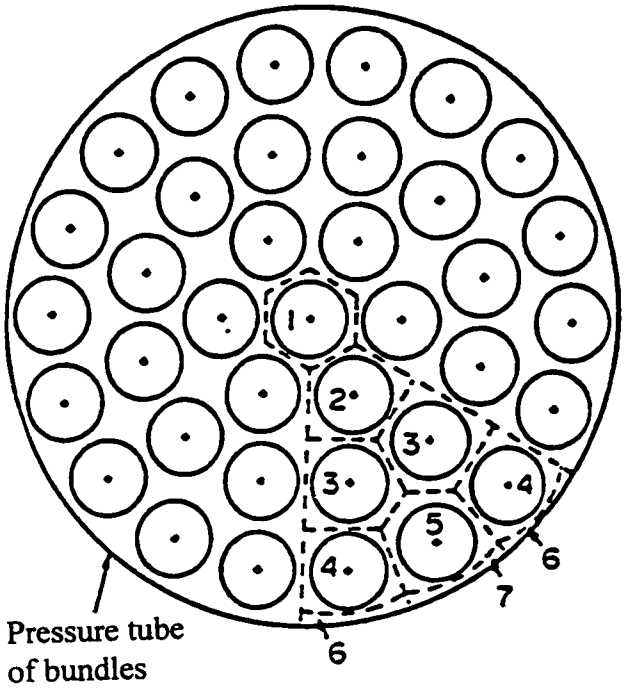

Figure 4.8 Thirty-seven-rod bundle used by Walley (1977).

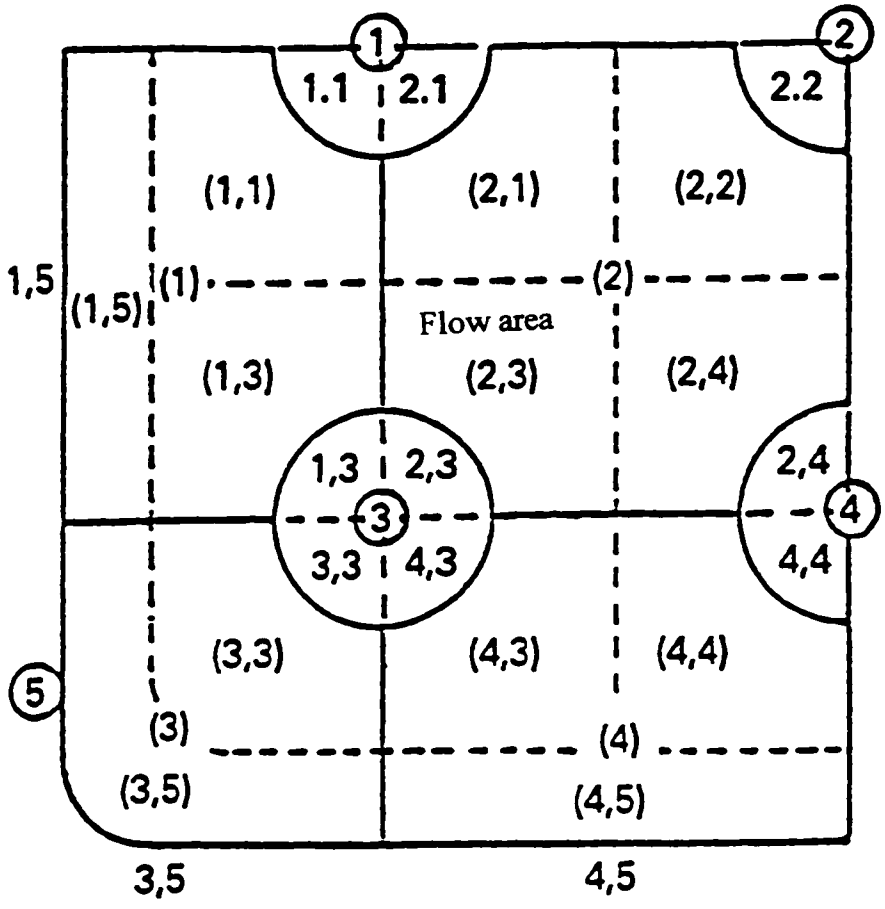

Figure 4.9 Typical channel and subchannel arrangement. From Lim et al. (1988).

5. DEVELOPMENT OF A BUNDLE CHF CORRELATION USING THE CHF LOOK-UP TABLE

5.1 General

This chapter uses observed trends and correction factors to derive a new CHF correlation in bundles. Due to the lack of reliable CHF experimental data in bundles with the same enthalpy distribution coupled with the complexity of CHF phenomena in general, the task of deriving an accurate CHF correlation for a bundle is by no means easy.

Since the tube CHF has been measured extensively (especially the CHF in an 8 mm tube), these CHF values are generally used as a reference and CHF values in other geometries are related to the tube values by applying correction factors. The following general form for the bundle CHF correlation is proposed:

$$CHF_{bun} = CHF_{D=8} \times k_i \times k_j \times k_k \cdots \qquad (5.1)$$

where k_i, k_j and k_k are correction factors to account for specific differences between the CHF occurrence in tubes and bundles. Equation (5.1) will have the same parametric and asymptotic trends as the CHF look-up table. This is the advantage of using this approach rather than an empirical correlation, which frequently gives the wrong asymptotic trends due to their limited range of application. The correction factors are discussed in the sections below.

5.2 CHF Data Base

To reveal the CHF characteristics in bundles and to develop a new CHF prediction method, available CHF experimental data in bundles with vertical upflow were collected and checked for internal consistency. A data bank of 929 CHF points was created, consisting of the water-CHF data of Owen et al.(1969), Bowditch et al.(1972), Smyth et al.(1967), and Edwards et al.(1965).

The distributions of the data against some parameters are shown in the histograms, i.e., Figures 5.1 to 5.3. The ranges of flow parameters and geometric dimension of the bundle for each data set are shown in Table 5.2, and the CHF experimental data are tabulated in Appendix A.

Table 5.1 Comparison of the Selected Data

	Owen	Bowditch	Smyth	Edwards
Subchannel arrangement	Same	Same	Same	Same
Rod distribution	Same	Same	Same	Same
Element Spacing	Same	Same	Same	Same
Axial Heat Flux Distribution	Same	Same	Same	Same
Radial Heat Flux Distribution	Same	Same	Same	Same
Spacer Device	Same	Same	Same	Same
Bundle orientation	Same	Same	Same	Same
Correlatable	Yes	Yes	Yes	Yes

The enthalpy imbalance in the bundle plays a significant role in the CHF prediction, and must be taken into account in the

development of CHF correlation. Table 5.1 shows that the selected data base have the same bundle geometry, power distribution, spacing device and orientation, so they can be used as the data base for the correlation development.

5.3 Parametric Effects on CHF

5.3.1 Effect of Pressure

The distribution of the available data with respect to pressure (see Figure 5.1) shows that the majority of CHF experiments were carried out at pressure of about 4.5 MPa, 5.8 MPa and 7 MPa with some in a lower pressure range.

In round tubes, CHF is a decreasing function of pressure in the range of interest here. In bundles, CHF generally decreases with increasing pressure, but is not as sensitive to pressure as in tubes and annuli. Some researchers have reported bundles which are insensitive to pressure (see section 4.4.1). Then a correction factor would be needed, since CHF from the look-up tables is quite sensitive to pressure.

5.3.2 Effect of Mass Flux

The distribution of the available CHF data with respect to mass flux (see Figure 5.2) shows that the majority of CHF experiments were carried out at lower mass fluxes (i.e., below 4

Mg/m²s), with a gradually decreasing number of experiments in the higher mass flux range.

The CHF is proportional to mass flux at low quality regime, but is inversely proportional to mass flux at high quality regime (see section 4.4.2). The CHF shows the same trend with mass flux in the tube lookup table (Groeneveld, 1995). So the mass flux has similar effect on CHF in bundles compared with in tubes.

5.3.3 Effect of Quality

The majority of bundle CHF data were obtained in the positive-quality range, most of them are located between 0.2 - 0.6 (see Figure 5.3).

It was found for a given data base that both the $CHF_{bun.exp}$ and $CHF_{bun.exp}/CHF_{D=8}$ show a decreasing trend with the exit quality, x_e (compare Figures 5.4 and 5.5). The CHF also shows a decreasing trend with the quality in the tube lookup table (Groeneveld, 1995) for the same parameter range. Thus, it appears that the effect of x_e on CHF must be stronger in bundles than in tubes.

This may be due to a large parasitic liquid film flow on the unheated surface, which decreases the film flow rate on the heated surface and the total amount of liquid taking part in the heat transfer in bundles. The values of the CHF in bundles and tubes are closer to each other at the DNB-type condition (i.e., at low qualities), where the unheated wall effect does not play a

significant role. The enthalpy imbalance at high quality regime also plays an important role.

5.3.4 Effect of Radial Heat Flux Distribution (RFD)

A set of selected data was used to verify the effect of radial heat flux distribution on the CHF in bundles, by comparing the data obtained in bundles having the same geometry and same pressure, mass flux, and quality value with uniform and non-uniform radial heat flux distributions. The CHF occurs in the "hottest" subchannel, which usually is the inside subchannel in bundles with uniform RFD, and outside subchannel with the non-uniform RFD. The result suggests that the radial heat flux distribution has a significant effect on CHF in bundles. The CHF in bundles which has radial heat flux distribution is greater than those without it (see Figure 5.6).

5.3.5 Effect of Spacer

The distance between elements in bundles is maintained by the spacer, and the spacer has a pronounced effect on CHF in bundles. The detail of the spacer effect can be seen in section 4.4.4.2.

5.4 CHF Prediction Methods

The geometry and special effects in bundles are very complex,

these including equivalent diameter and element spacing effect, cold wall effect, spacer effect, radial heat flux distribution effect, etc. Some of the CHF correlations for bundles can be found in the literature, but they can only be used for limited conditions.

Ulrych (1985) showed in his paper that CHF lookup tables have a much wider range of application not just for tubes. With the proper choice of a characteristic diameter to replace the tube diameter, the applicability of the tables can be extended to more complex geometries. Mainly data from the open literature were used for verification of his method.

The parametric and asymptotic trends of the Ulrych prediction method were examined and its prediction was compared against the CHF data bank to find out how good is this method.

5.4.1 Ulrych Method

For both Russian(1977) and Groeneveld(1983) CHF lookup tables in tubes, in the diameter range of 4 mm < D < 8 mm, the critical heat flux for diameters other than 8 mm may be obtained from the table values $CHF_{D=8}$ by

$$CHF = CHF_{D=8} \cdot (8 / D)^{n}. \qquad (5.2)$$

The Russian publication (1977) recommended n = 0.5 while Groeneveld(1983) proposed n = 1/3, and Ulrych gave n = 0.404.

The CHF table in tubes can be used for different geometries, provided a proper selection of the equivalent diameter is made to replace D in Equation(5.2).

The Ulrych prediction method was based on CHF data obtained in bundles and covering the following ranges:

Pressure	30 to 196 bar
Mass velocity	500 to 5000 kg/m²s
Subcooling at CHF	-75K to 0
Quality at CHF	0 to 100 %

Approximately 1600 CHF measurements were collected.

Ulrych concluded that, for equivalent hydraulic diameters between 2.5 mm and 80 mm, the use of the diameter of second order (see Figure 5.7) in bundles,

$$D_2 = d(2(t/d) - 1) \qquad (5.3)$$

as the equivalent diameter gives a much better prediction than the use of equivalent hydraulic diameter when using the CHF tables to predict CHF in bundles. where t is the element spacing shown in Figure 5.7.

5.4.2 Assessment of the Ulrych Method

To reveal the CHF trends predicted by the Ulrych method,

calculation was performed and its results are shown in Table 5.3. The Ulrych method shows correct parameter and asymptotic trends but gives a considerable discrepancy compared with the experimental data (see Figures 5.8 and 5.9).

5.4.3 Correlation Based on Observed Parametric Effects

Due to the poor accuracy exhibited by the Ulrych method, and to ensure the correct trends, a new CHF correlation was developed for bundles, using the 8-mm tube CHF look-up table of Groeneveld et al. (1995) as a reference in order to ensure the correct parametric and asymptotic trends.

The examination of the CHF data for bundles (section 5.3) showed that critical quality, cold wall, radial heat flux distribution, and spacer have influence on the $CHF_{bun.exp}$ values. Therefore, correction factors account for these effects were used in the proposed correlation.

5.4.3.1 Correction factors

(i) Quality correction factor, k_x

Figure 5.10 shows that as the quality increases the ratio between the CHF in bundles and the corresponding value from the AECL-UO CHF look-up table for an 8 mm tube decreases. The following expression represents the quality correction factor:

$$k_x = 0.980371 - 3.41556x + 5.82044x^2 - 3.30131x^3 \quad \text{for } x < 0.65 \qquad (5.4)$$

$$k_x = 0.33 \quad \text{for } x > 0.65$$

This equation was obtained with all the 929 data points from the data base. The general decrease in CHF with quality may be explained in terms of phase distribution. In general, the ratio $CHF_{bun.exp}/CHF_{D-8}$ is close to one for the very low quality and subcooled region (where the bulk temperature is the most important parameter and is relatively unaffected by the presence of an unheated wall, the CHF is the DNB type in this region). This ratio decreases gradually in the positive quality region (due to the strong effect of the thicker liquid film on the unheated wall and the enthalpy imbalance in subchannels, and the CHF is entrainment controlled) and the ratio is least for the high quality region where the CHF is deposition controlled (in this region, the presence of the liquid located on the unheated surface is felt most severely and has the greatest detrimental effect on CHF).

(ii) Spacer correction factor, k_{sp}

Many types of grid spacers have been used in bundles to maintain the rod-to-rod spacing, and some are designed to promote the mixing of coolant and enhance heat transfer. Lin et al. (1992) suggested that for a uniform axial heat flux with a larger grid spacer loss coefficient, the following correlation is used for the spacer effect in bundles:

$$k_{sp} = 1 + 1.7923\,(G_s/D_{hy})^{-0.3962} \qquad (5.5)$$

where G_s is the axial spacing of spacers, and equation(5.5) is recommended by Lin et al.(1992) for PWR fuel bundle spacers and is not really relevant for the bundles considered here.

(iii) Radial heat flux distribution and
cold wall correction factor, k_{rfd}

The effect of cold wall plays a very important role in the CHF phenomenon in bundles. Guide tubes or shroud tubes, which cannot generate thermal energy in bundles, would decrease the CHF level since coolant through cold walls will bypass the heated region and cannot be used for heat transfer.

Becker et al. (1967, quoted by Atkinson, 1981) suggested that the elements with depressed heat flux can be thought of as 'partly cold rods', and can use the following correction factor to account for its effect in bundles.

$$k_{rfd} = \frac{d\sum_{i=1}^{n}(q_i/q_{max})}{nd+D_s} \qquad (5.6)$$

where q_i, and q_{max} are the heat flux on the ith element and the maximum heat flux in the bundles, respectively, and D_s is the shroud diameter. Equation(5.6) for k_{rfd}, while allowing for radial heat flux distribution in a crude way, ignores the effect of sub-

channel enthalpy imbalance arising from difference sub-channel flow geometries.

5.4.3.2 Correlation proposed

The following correlation is proposed for the prediction of CHF in bundles:

$$CHF_{bun} = CHF_{D=8} \cdot k_p \cdot k_x \cdot k_{sp} \cdot k_{rfd} \qquad (5.7)$$

where:

- $CHF_{D=8}$ is the CHF for a tube with an ID of 8 mm, as predicted by the tube CHF look-up table of Groeneveld et al.(1995), at given pressure, mass flux, and critical quality.
- k_p pressure correction factor,

  $k_p = 1.13474 - 2.2685 \times 10^{-5} \cdot p$ (p in kPa)
- k_x quality correction factor given by Eq.(5.4).
- k_{sp} spacer correction factor given by Eq.(5.5).
- k_{rfd} cold wall and RFD correction factor given by Eq.(5.6).

Noted that the CHF_{bun} is the bundle redial-average heat flux and that the quality on which it is based is also the bundle radial-average quality.

The above correlation has been created by all 929 experimental data from the data base and found to have the correct parametric and asymptotic trends (see Figures 5.8 and 5.9). The rms error of 929 experimental CHF data is 9% at constant inlet conditions, and

20% at constant exit conditions. The rms error for each set of experiment data is shown in Table 5.3. This equation is a considerable improvement over the current use of tube CHF values. More correction factors could be introduced to Eq.(5.7) to account for other effects which are ignored in this work but could be important in some cases (e.g., the outer clearance between bundle and shroud tube, the horizontal orientation of bundle, D_{hy} and the axial heat flux distribution). Further improvement can be made in the future, when additional experimental data become available.

Equation (5.7) can be used for vertical up flow in bundles which has the similar geometry with the bundles used in this study (shown in Table 5.2), and within the following parameter ranges:

p:	1.48 - 7.0	(MPa)
G:	0.267 - 4.11	(Mg/m^2s)
x_c:	0.014 - 0.781	

5.4.4 Application of the Proposed Correlation

5.4.4.1 General

Equation(5.7) is a local-condition type correlation, which is based on the local (or cross sectional average) (Groeneveld, 1996) enthalpy or quality at the CHF location, i.e.,

CHF = f(P, G, X, local geometry)

Since in most cases, the CHF is a local phenomenon and is relatively insensitive to the inlet condition, and it can be easily modified to account for separate effects, such as the spacer, axial heat flux distribution effects.

Groeneveld (1996) pointed out that "the critical heat flux prediction methods based on local quality have two different applications.

(i) When applied to determine the CHF margins, the CHF is always evaluated based on given inlet conditions (as illustrated in Figure 5.11); the margins or errors must be calculated based on the 'constant inlet conditions approach' or the 'heat balance method'. This thus corresponds to use the look-up table only for determining the CHF vs. X relationship.

(ii) When applied in reactor safety analysis, the user frequently compares the local heat flux with a predicted CHF based on a local quality ('direct substitution method'). If the heat flux is greater than the CHF, an excursion into the post-CHF regime will be encountered. The quality, heat flux and sheath temperature are calculated values obtained from the safety code and will vary with time, location and boundary conditions.

Hence this is really a special case of the heat balance method, except here the heat balance method is more difficult to apply because of the complex transients during a loss of coolant accident (LOCA).

In summary, the user would normally first calculate the quality, via a heat balance method or a safety code, and subsequently evaluate the CHF at this condition. ..."

Note that Eq.(5.7) is based on the critical quality, x_e, which is an average value over the whole flow area in bundles. However in reality, the CHF occurs in the subchannel which has the highest quality, the quality displacement or enthalpy imbalance should be taken into account. The methods (Bobkov, 1993 and McPherson, 1971), which account for the enthalpy imbalance, are described in sections 3.4.4 and 4.3, respectively.

5.4.4.2 Errors

Groeneveld (1996) suggested that the error must be based on the parameters being kept constant in the experiment, i.e., the inlet condition. The CHF quality is a calculated quality, based on the measured CHF and hence cannot be predicted prior to the experiment.

Groeneveld et al. (1986) have described two different methods of predicting the CHF and their errors using the local-condition type correlation:

(i) constant exit quality approach or the direct substitution method, and

(ii) constant inlet conditions approach or the heat

balance method.

Method (i) is applied when predicting CHF for a given system, but the prior knowledge of the enthalpy or quality at CHF, which is a dependent parameter, is required.

Method (ii) is applied when the exit quality is unknown or assessing the error of a CHF prediction correlation. It needs to find the CHF from the intersection of the CHF vs. X curve and satisfying the heat balance.

A simple case of a uniformly heated bundle having fixed inlet condition and operating at a given heat flux for the two above methods is shown in Figure 5.11. It first shows that the CHF vs. X_c curve in the bundle is obtained from the CHF vs. X_c curve in the tube by the correction factors and then shows how to determine the two CHFs and their errors based on constant inlet and constant exit conditions. The CHF_1 value is obtained at a constant quality ($X=X_1$) by method (i) but it does not satisfy the heat balance relationship. CHF_2 is obtained by method (ii) from the intersection of the CHF vs. X curve in the bundle and the heat balance line ($x=x_2$). q_1 is the experimental data. The method (i) tends to give a much higher prediction error than method (ii). The difference depends on the slope of the CHF vs. X curve; it is least for a zero slope and reaches a maximum for a steep negative slope.

Equation(5.7) was examined by the experimental data based on both constant inlet condition and constant exit condition. The results are shown in Table 5.3. Equation(5.7) gives not only a

quite good CHF prediction in bundles but also correct parametric and asymptotic trends (Figures 5.8 and 5.9).

5.5 Recommendation

A thorough analysis of the CHF prediction methods for bundles given in the literature shows that these methods are not accurate. They gives neither good prediction accuracy when applied to a large CHF data base nor correct parametric and asymptotic trends.

The correlation developed during this study is superior. Note that Eq.(5.7) exhibits correct asymptotic and parametric trends and gives a good CHF prediction for parameters covered within the data base.

Table 5.2 CHF Data Base for Bundles

Parameter	Owen et al. (1969)	Edwards et al. (1965)	Smyth et al. (1967)	Bowdith et al. (1972)
P [MPa]	4.34 - 6.96	6.723 -6.929	3.38 - 6.79	1.48 - 6.88
G [Mg/m²s]	0.67 - 4.11	0.267 - 2.441	0.68 - 2.4	0.549 - 3.1
x_{exit}	0.181 - 0.643	0.28 - 0.781	0.207 - 0.506	0.159 - 0.667
Shroud ID [m]	0.1306	0.1306	0.1289	0.1289
Element OD [m]	0.0159	0.0159	0.0159	0.0159
Equivalent wetted diameter [m]	0.01072	0.01071	0.01902	0.0101
Equivalent heated diameter [m]	0.01346	0.01346	0.02681	0.0127
Element spacing (t) [mm]	0.01908	0.01908	0.01908	0.01908
Heated length	3.66	3.66	3.66	3.66
No. of elements	37	37	37	37
Perimeter heated [m]	1.7982	1.7982	1.5984	1.7982
Perimeter wetted [m]	2.2585	2.2585	2.2532	2.2532
Flow area [cm²]	60.49	60.49	57.03	57.03
Spacing devices	Grids	Grids	Grids	Grids
Grid spacing[mm] G_s	300*	300*	300*	300*
k_{rfd}	~0.6	~0.6	~0.6.	~0.6
k_{sp}	1.5	1.5	1.5	1.5
Radial heat flux distribution	1.00/0.662/0.566/0.0 1.00/0.639/0.640/0.0 1.00/0.656/0.568/0.0 1.00/0.660/0.571/0.0 1.00/0.656/0.568/0.0	1.00/0.648/0.565/0.0	1.00/0.639/0.557/0.0	1.00/0.66/0.60/0.0
Axial heat flux distribution	Uniform	Uniform	Uniform	Uniform
No. of CHF	497	104	119	209

* these values are not given by the experiment report.
~ approximately.

Table 5.3 Accuracy of CHF Prediction Method in Bundles

Data Base	Correlation	Error (%)		Number of CHF Data
		Inlet Conditions	Exit Conditions	
		Rms	Rms	
Owen et al. (1969)	Eq. (5.7)	7	17	497
	Ulrych	22	70	
Bowdith et al. (1972)	Eq. (5.7)	6	16	209
	Ulrych	21	65	
Smyth et al. (1967)	Eq. (5.7)	6	17	119
	Ulrych	38	110	
Edwards et al. (1965)	Eq. (5.7)	9	20	104
	Ulrych	35	100	

$$Avg. = \frac{1}{n}\sum E \cdot 100\%$$

where an error, E, is defined as

$$E = \frac{(CHF_{pred.} - CHF_{exp.})}{CHF_{exp}}$$

and

$$Rms = \sqrt{\frac{1}{n}\sum E^2 \cdot 100\%}$$

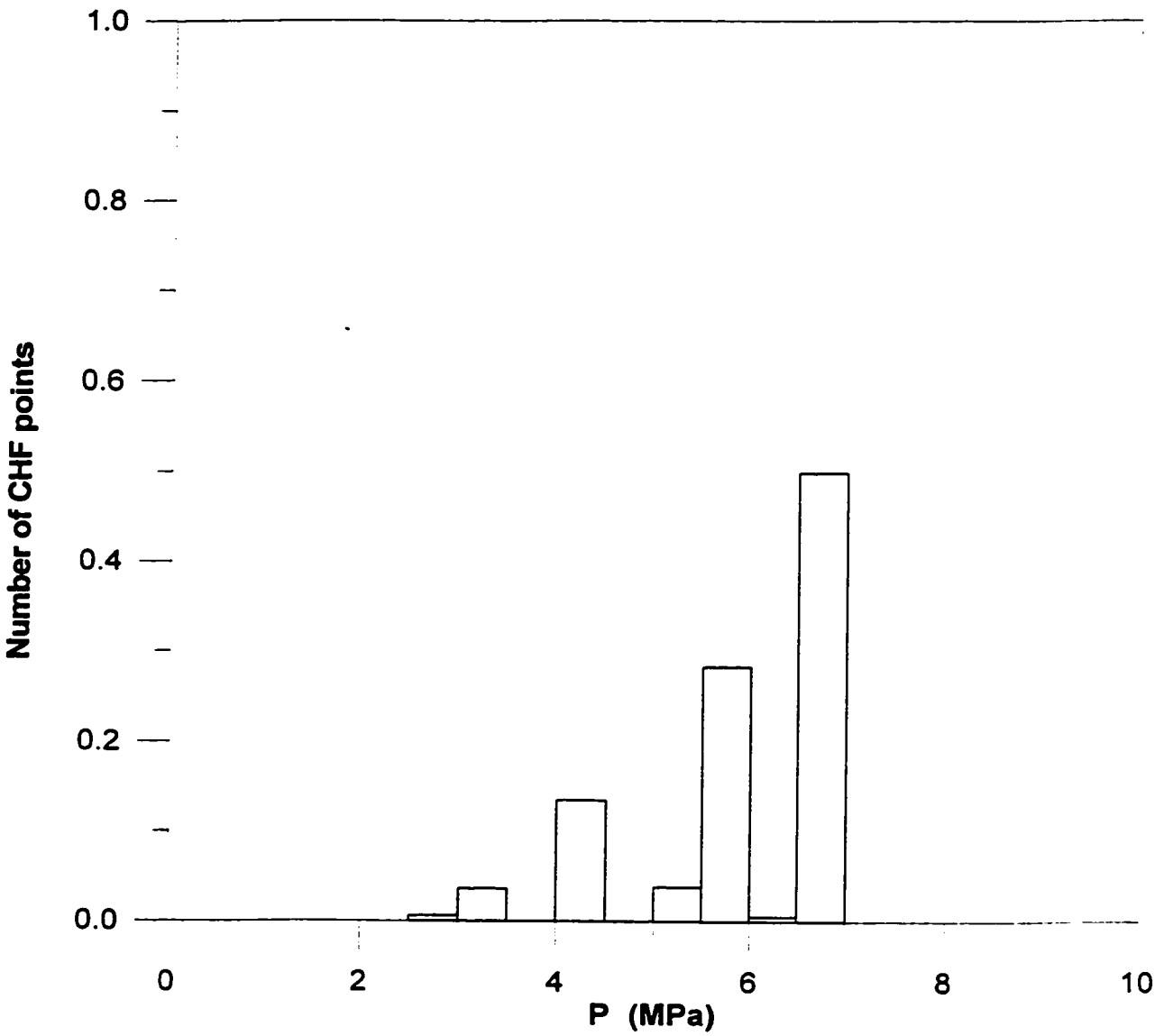

Figure 5.1 Bundle CHF data distribution against pressure

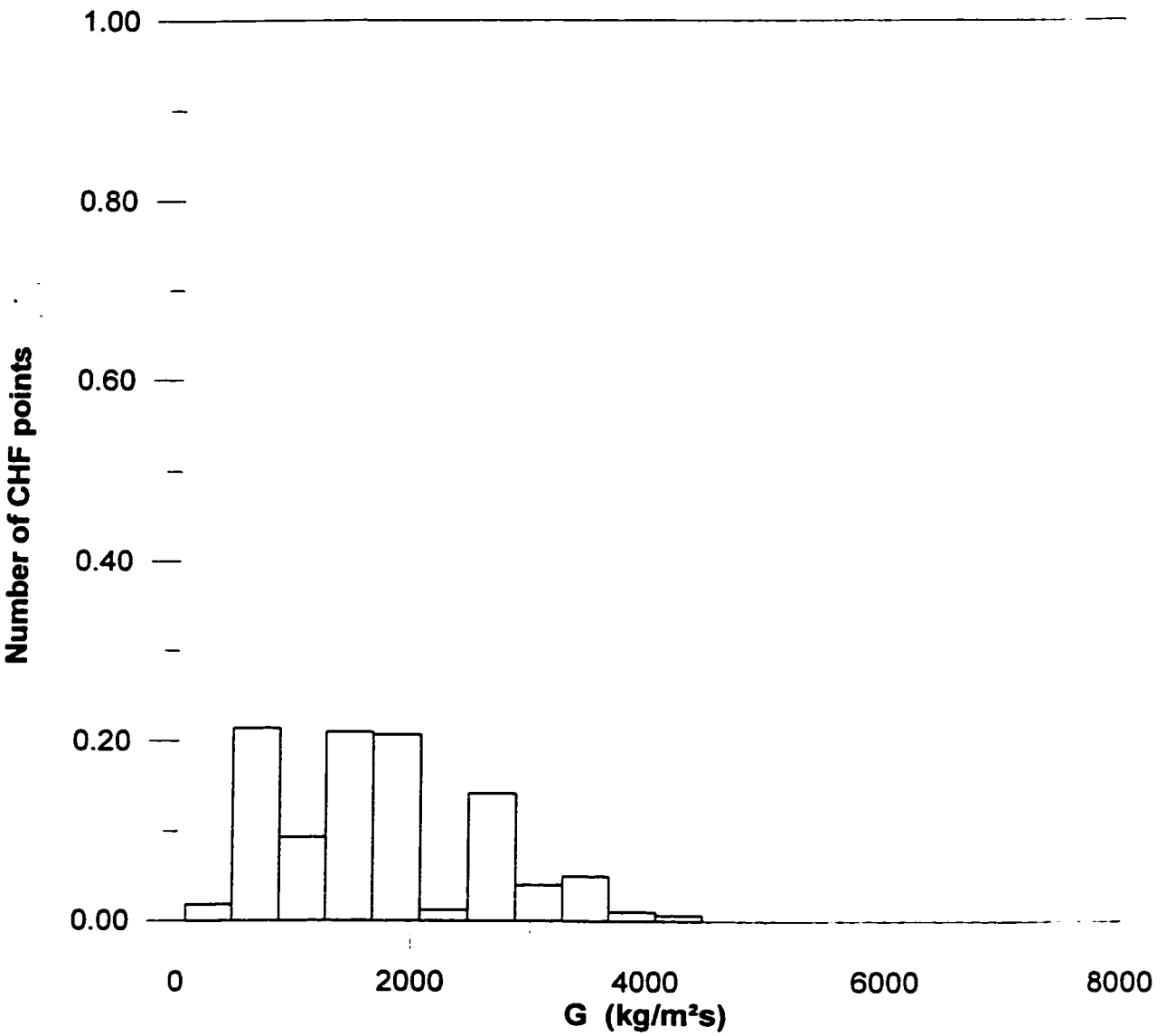

Figure 5.2 Bundle CHF data dirtribution against mass flux

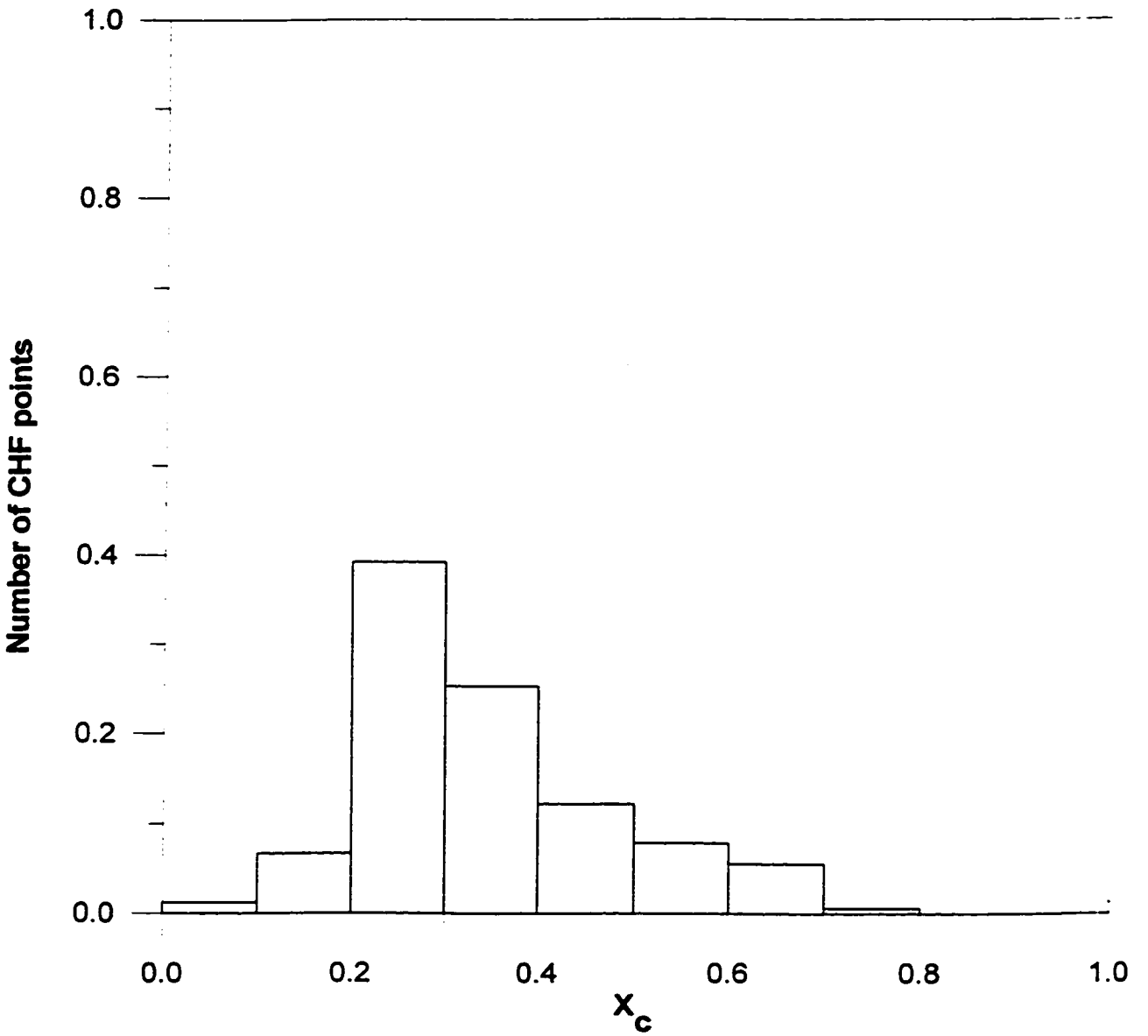

Figure 5.3 Bundle CHF data distribution against exit quality

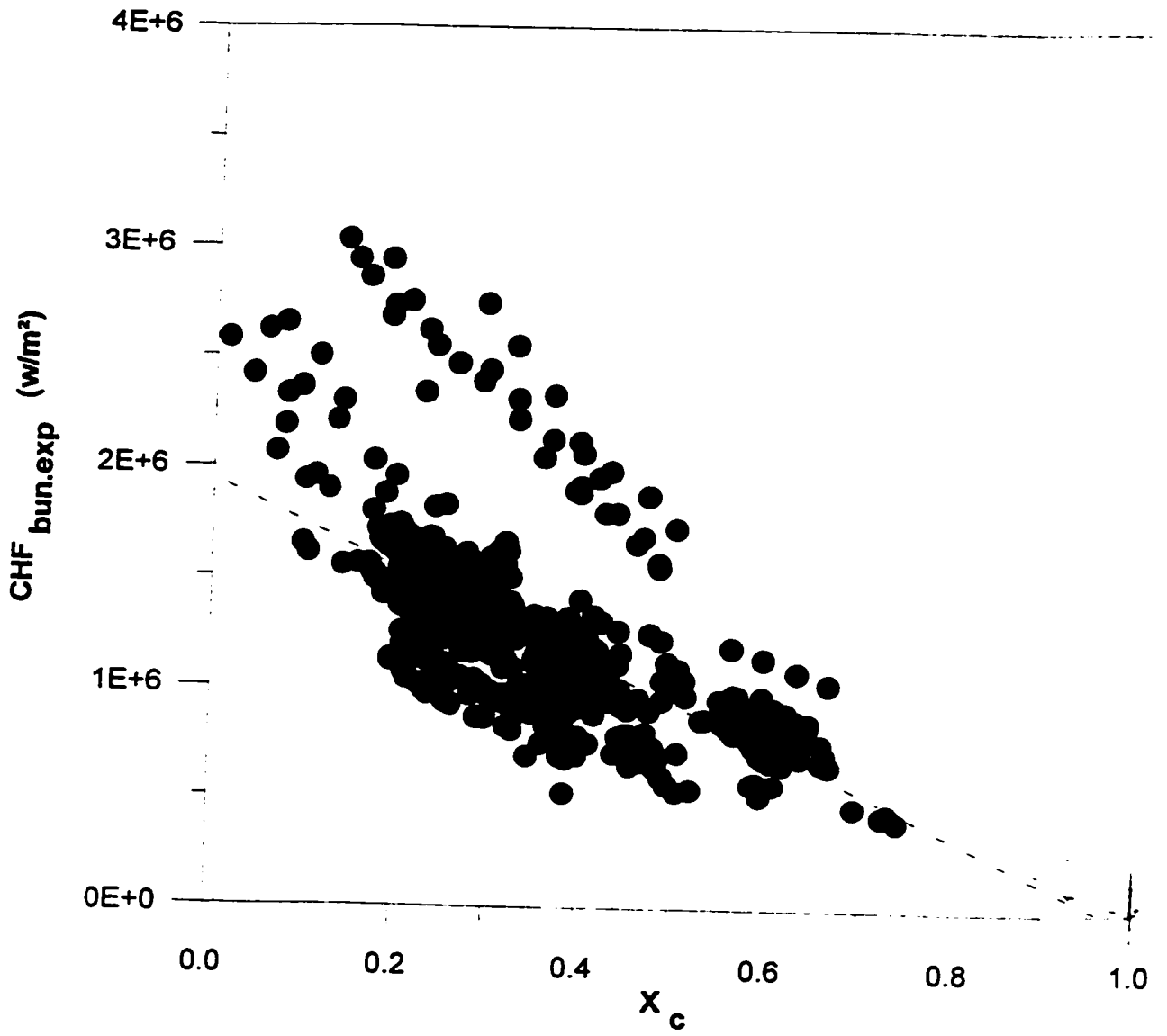

Figure 5.4 CHF in bundles vs. exit quality

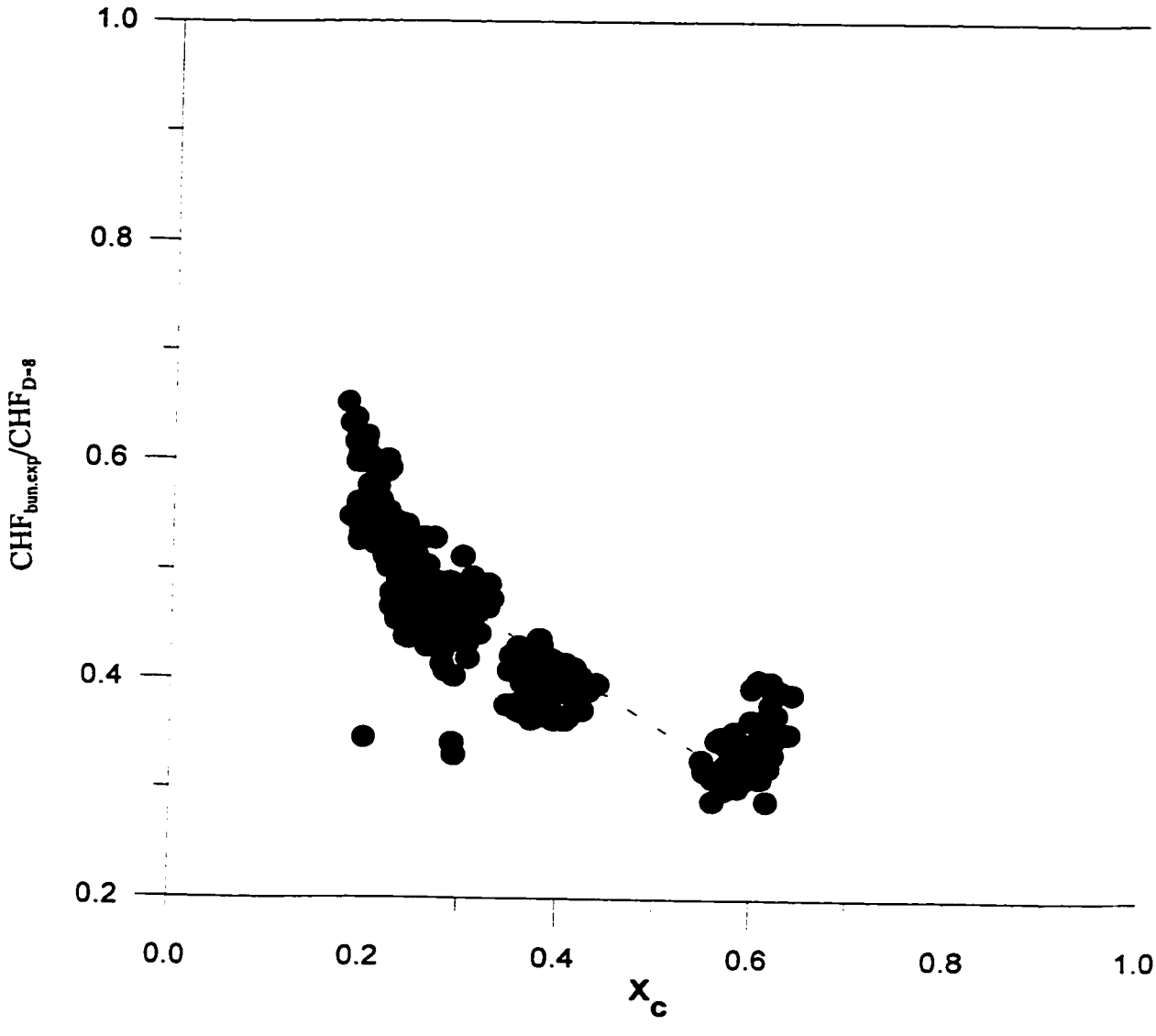

Figure 5.5 $CHF_{bun.exp}/CHF_{D-8}$ ratio against quality

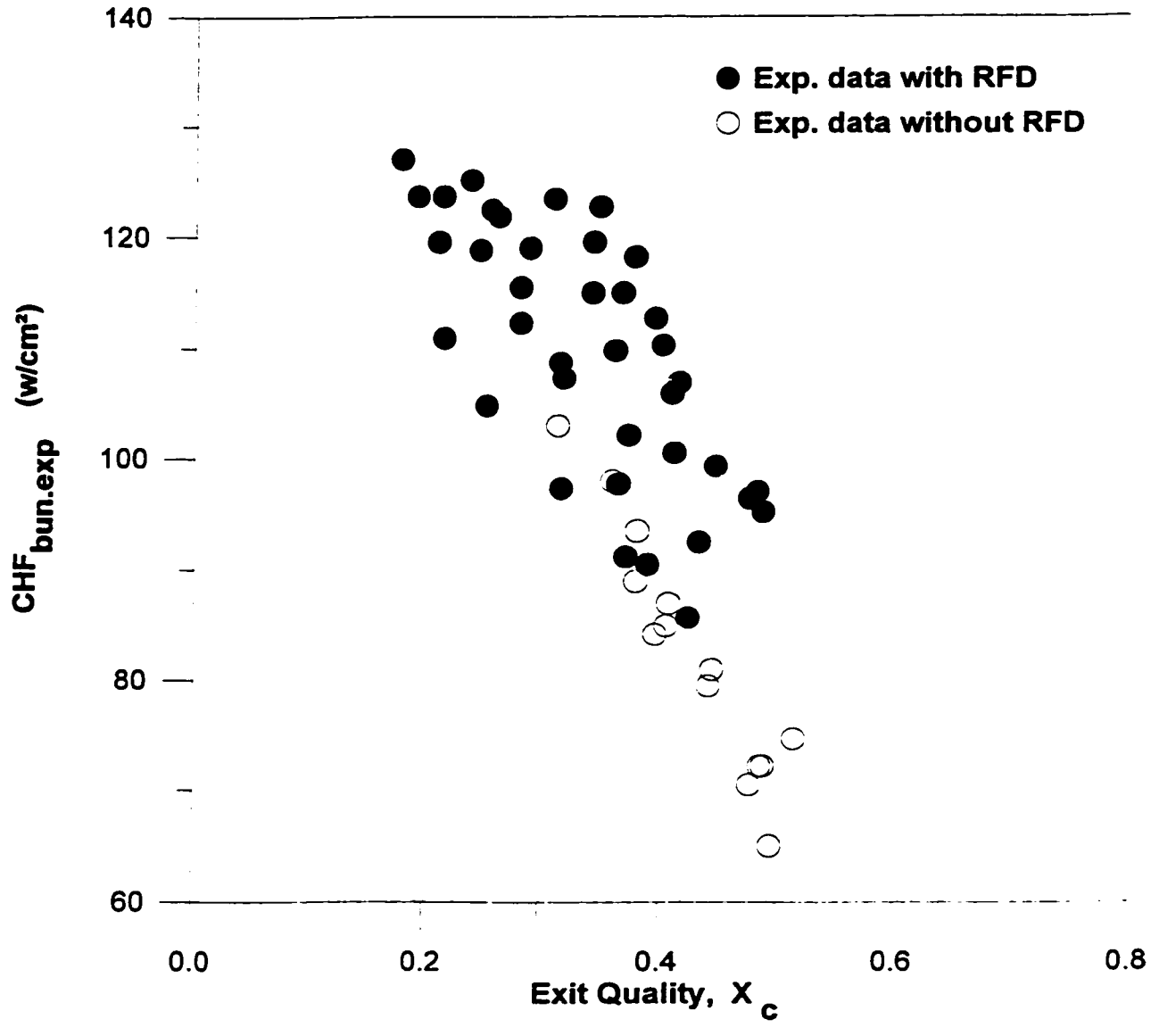

Figure 5.6 Effect of RFD on bundle CHF

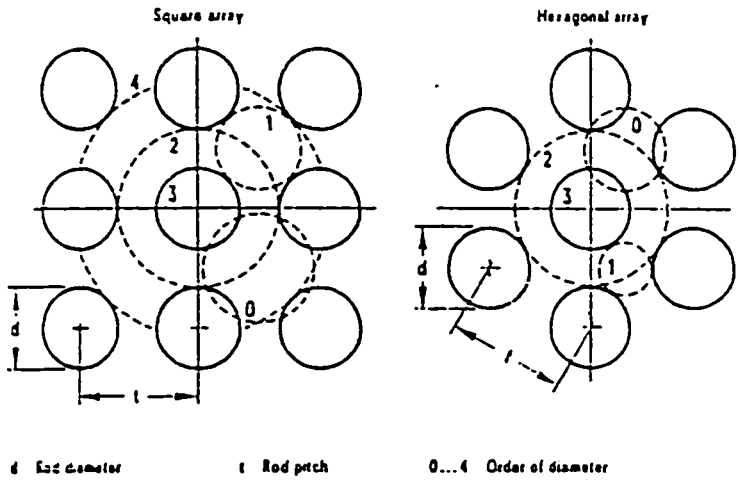

Figure 5.7 Possible characteristic length in rod bundles (Ulrych, 1985)

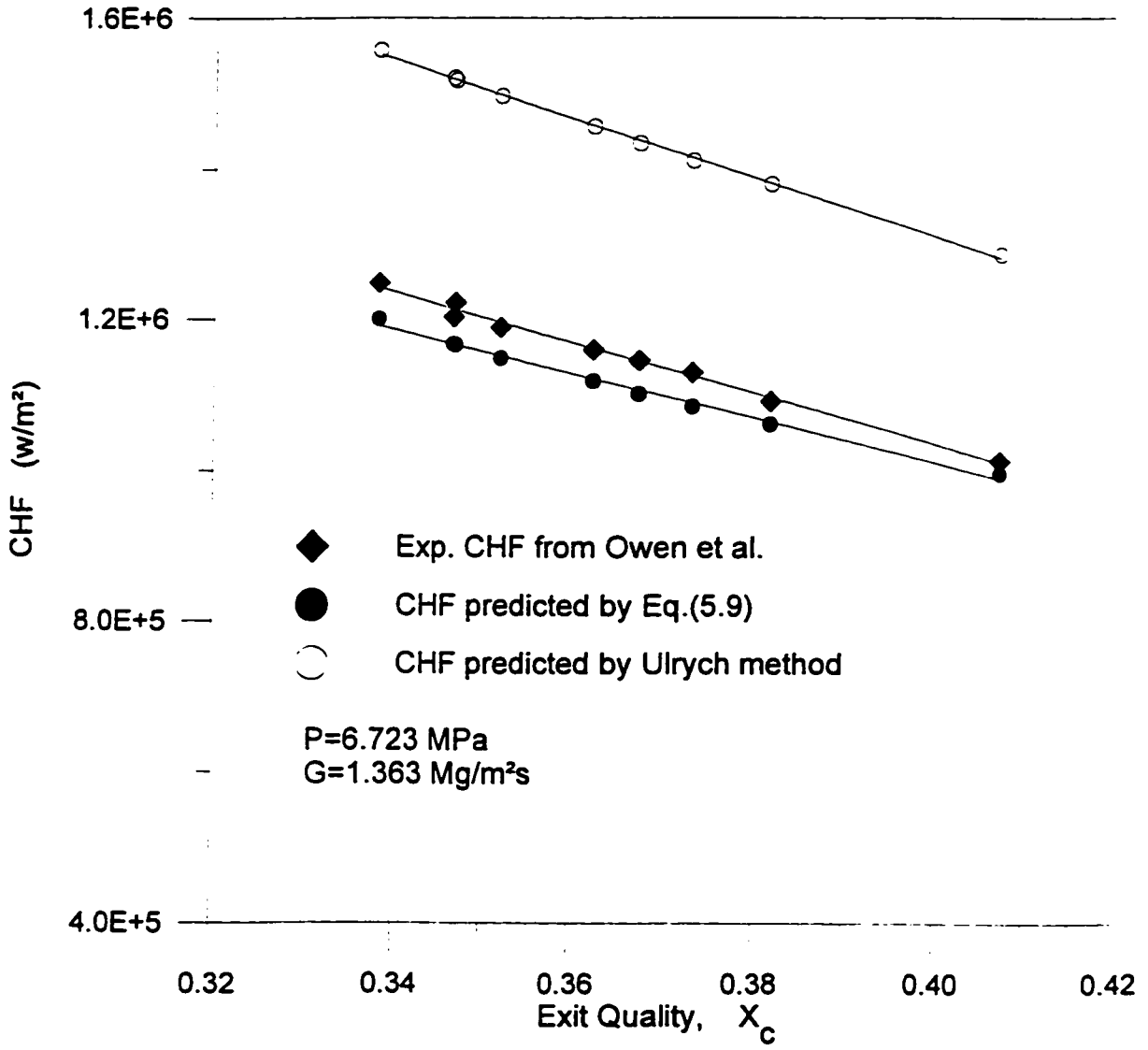

Figure 5.8 Comparison of Ulrych method and Eq.(5.7) with experimental data for P=6.723 MPa, G=1.363 Mg/m²s

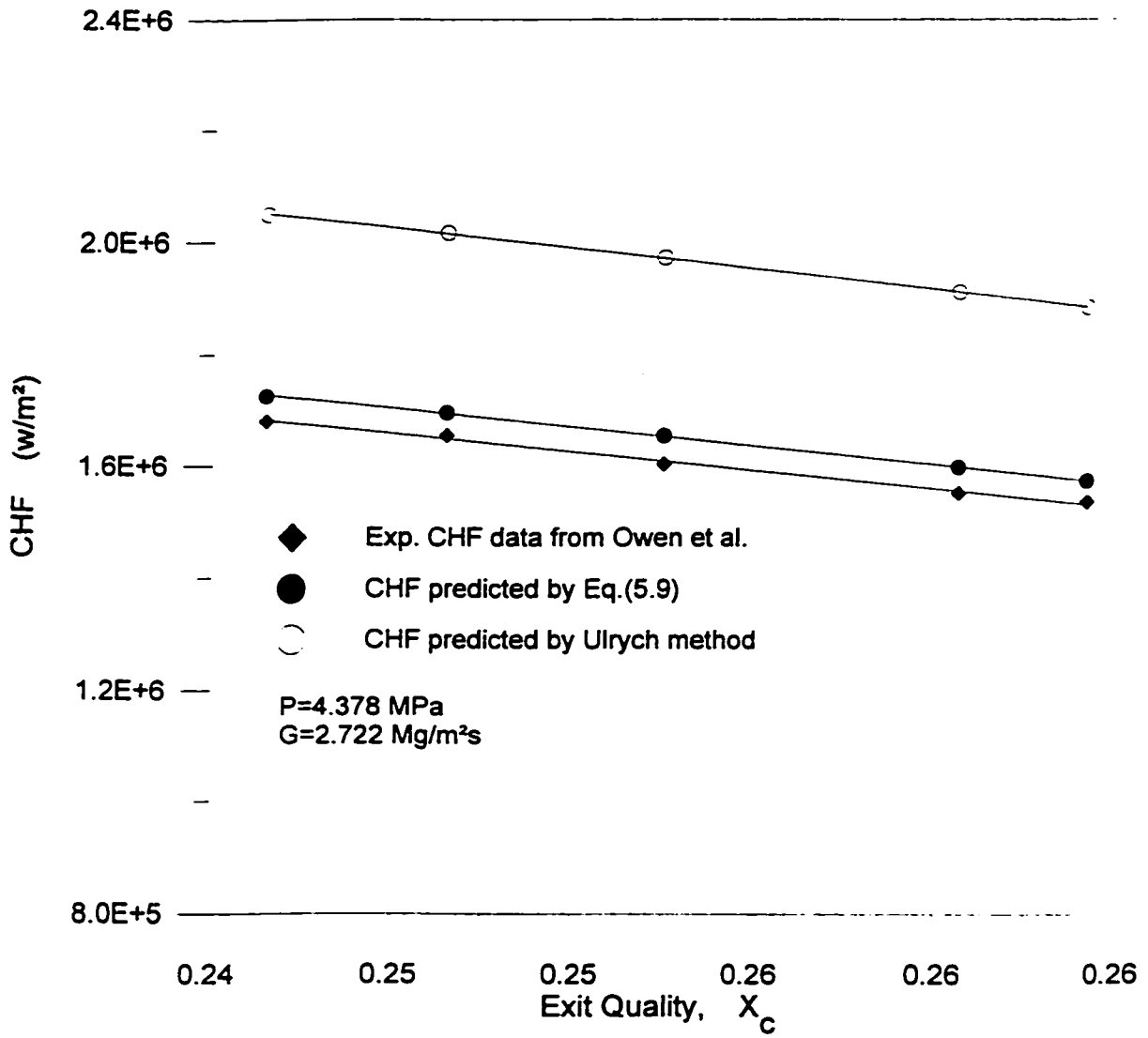

Figure 5.9 Comparison of Ulrych method and Eq.(5.7) with experimental data for P=4.378 MPa, G=2.722 Mg/m²s

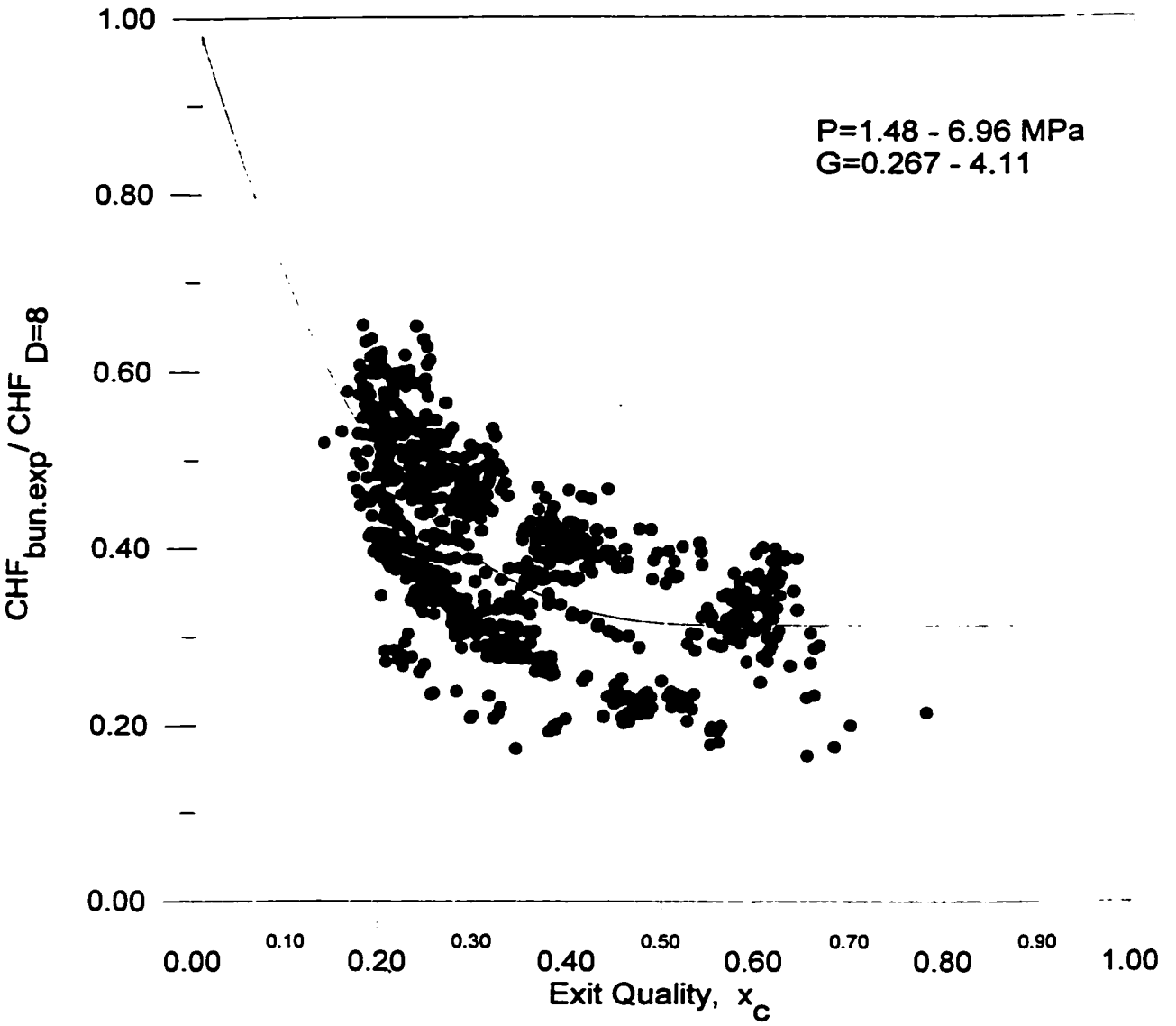

Figure 5.10 $CHF_{bun.exp} / CHF_{D=8}$ vs. exit quality

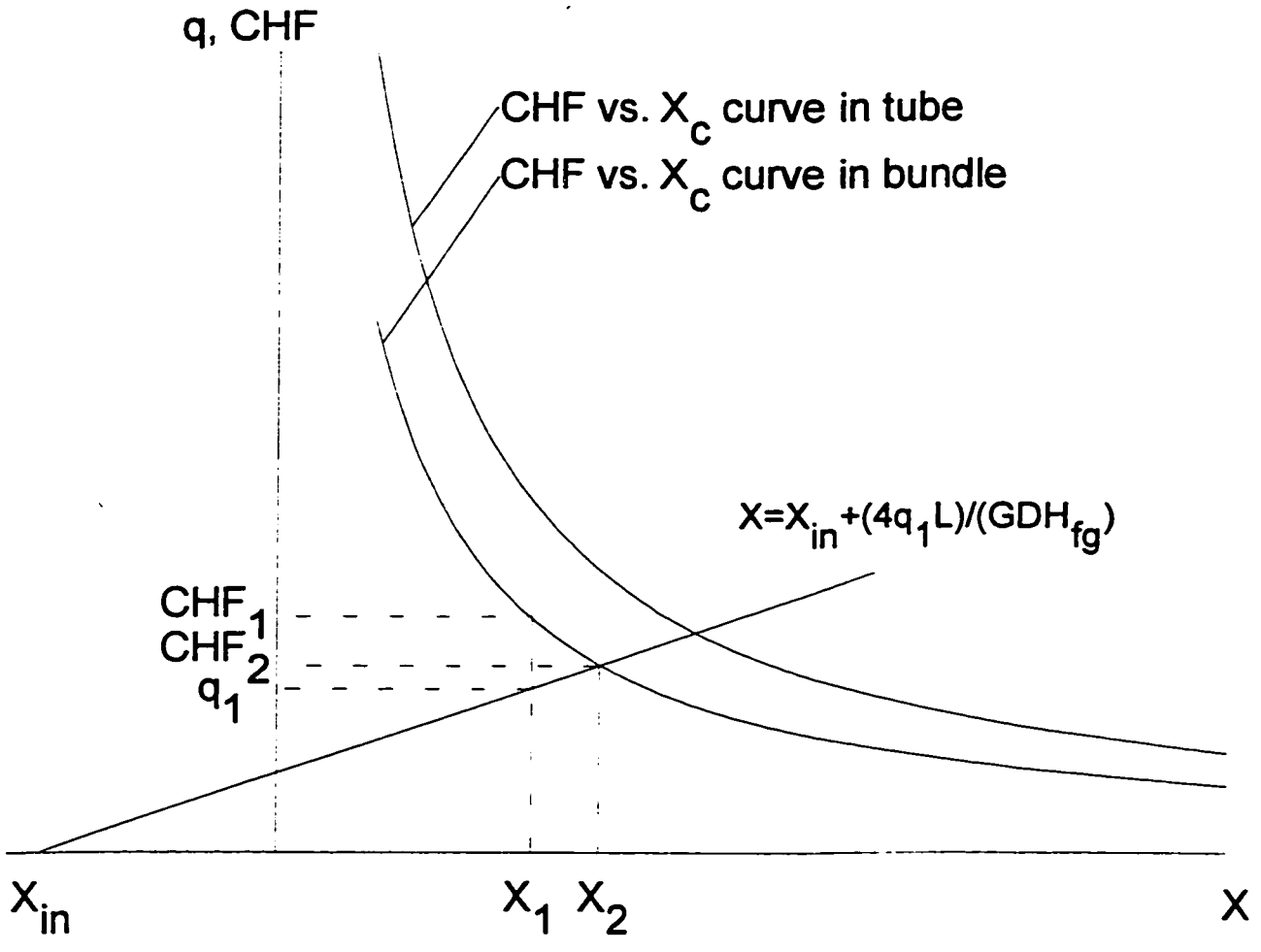

Figure 5.11 CHF values for a uniformly heated bundle

6. CONCLUSIONS AND FINAL REMARKS

An extensive review of CHF in tubes, annuli and bundles is given in this study. The physical mechanisms of CHF were discussed to better understand the CHF behavior in bundles, and also its differences with tubes. The CHF value in a tube is always larger than that of a bundle under normal condition due to the effects of geometry and enthalpy imbalance.

The physical phenomena responsible for CHF in bundles are much more complex. It is recognized that the following effects distinguish CHF in bundles from tubes:

(i) equivalent diameters,
(ii) cold wall,
(iii) element spacing (spacer),
(iv) pressure,
(V) quality,
(vi) radial and axial heat flux distributions, and
(Vii) enthalpy or quality imbalance.

The experimental CHF data, obtained in bundles, were collected from the literature and used as the basis for analysis. The tube CHF look-up table (Groeneveld, 1995) was taken as the reference for analysis and construction of a new CHF prediction method for bundles. The prediction method uses the table CHF as a base with correction factors obtained from observed bundle-specific effects. The tube CHF lookup table is simple, accurate, and applicable to a

very wide parameter range and gives correct parametric trends.

The new prediction method (Equatin (5.7), developed in this study) predicts CHF in bundles with good accuracy. The rms error is 9% for the constant inlet condition and 20% for the constant exit condition, and it also shows correct parametric and asymptotic trends. Equation (5.7) is based on the same enthalpy imbalance and includes the effects of exit quality, spacer, cold wall, and radial heat flux distribution, except the effects of axial heat flux distribution and geometry. It is basically a correction to the tube CHF look-up table.

Equation(5.7) is limited to the data range and the similar geometry of the bundles used in this study. The ultimate goal is to derive a new CHF prediction method which can be used in the subchannel analysis (such as a rod-centered subchannel approach where $CHF_{bun}(P,G,X_c)=CHF_{D=8}(P,G,X_c')$, $X_c'=X_c+\Delta X_c)$, and general analytical CHF prediction methods valid for different cases of CHF occurrence, when more experimental data become available in the future.

REFERENCES

1. Atkinson, J. C.(1981), "Critical Heat Flux in Horizontal and Vertical 37-element Nuclear Fuel Bundles." Thesis of M. Eng., Carleton University.

2. Atkinson, J. C. and Rogers, J. T. (1982), "Critical Heat Flux in Vertical and Horizontal 37-Element Nuclear Fuel Bundles", Proc. Third Annual Conference, Canadian Nuclear Society, p. A22, June, 1982.

3. Barnett, P. G.(1963), "An Investigation Into Validity of Certain Hypotheses Implied by Various Burnout Correlations". AEEW-R 214.

4. Barnett, P. G. (1966), "A Correlation of Burnout Data for Uniformly Heated Annuli and Its Use for Predicting Burnout in Uniformly Heated Rod Bundles", AEEW-R-463, Winfrith.

5. Barnett, P. G. (1968), " A Comparison of the Accuracy of Some Correlations for Burnout in Annuli and Rod Bundles," AEEW-R-558, Winfrith.

6. Becker, K.M.(1966), "A Correlation for Burnout Predictions in Vertical Rod Bundles", S-349.

7. Becker, K. M. (1967), "A Burnout Correlation for Flow Boiling of Water in Vertical Rod Bundles", Aktiebolaget Atomenergi, AE-276, Stockholm.

8. Becker, K. M. (1969), "Burnout Conditions for Large Rod Bundles with Radial and Axial Flux Distributions", S-401 FRIGG PM-48.

9. Bertoletti, S. et al. (1965), "Heat Transfer Crisis with Steam-Water Mixture", Energia Nuclear, 12(3), pp121-172.

10. Bethke, S, and Zeggel, W. (1993a), "Interpretation of CHF Bundle Tests by CHF Tables', International Working Group Meeting on CHF Fundamentals, Braunschweig, Germany, March 3-4.

11. Bethke, S. et al. (1993b), "Interpretation of CHF Bundle Tests by CHF Tables." International Working Group Meeting on CHF Fundamentals. Braunschweig. March 3-4, 1993.

12. Bobkov, V.P. (1993), "Boiling Crisis in Channels of Different Cross-sectional Geometry, Description of Mode." International Working Group Meeting on CHF Fundamentals, Braunschweig, Germany, March 3-4.

13. Bowditch, F. H. et al. (1972), "9 MW Rig High Pressure Water Heat Transfer and Flow Resistance Measurements on a 36-rod, 12 ft Long Cluster Simulating a Prototype SGHWR Fuel Element with Pin Heat Flux Tilt", United Kingdom Atomic Energy Authority Report AEEW-R 812, Oct.

14. Bowring, R. W. (1979), "WSC-2 a Subchannel Dryout Correlation for Water-cooled Clusters over the Pressure Range 3.4-16.9 MPa(500-2300 pia) ", AEEW-R983, UKAEA Winfrith.

15. Chang, S. H., (1989), "Transient-effects Modelling of Critical Heat Flux". Nuc. Eng. and Des. Vol 113, pp51-57.

16. Collier, J. G. et al (1994), "Convection Boiling and Condensation", Clarendon Press. Oxford. Third edition.

17. Doerffer, S. (1994), Groeneveld, D. C., Cheng, S. C., Rudzinski, K. F. "A comparison of Critical Heat Flux in Tubes and Annuli." Nuclear Engineering and Design, Vol.149, pp167-175.

18. Edwards, P. A. et al.(1965), "6 MW Rig Burnout Data on Simulated S.G.H.W.R. Steam Generating Channels Heat Series NOS. 1 TO 6", United Kingdom Atomic Energy Authority Report AEEW-R 454.

19. Groeneveld, D. C. et al (1980), "Spacing Devices for Nuclear Fuel Bundles: A Survey of Their Effect on CHF, Post-CHF Heat Transfer and Pressure Drop", ARD-TD-158.

20.Groeneveld, D. C. et al (1982), "A general CHF Prediction Method for Water, Suitable for Reactor Accident Analysis. CENG Report DRE/STT/82-2-E/DG.

21. Groeneveld, D. C. et al (1986), "1986 AECL-UO Critical Heat Flux Lookup Table." Heat Transfer Engineering, vol.7, no.1-2.

22. Groeneveld, D. C. (1995), "CANDU Reactor Thermalhydraulics Course." ARD-TD-567.

23. Groeneveld, D. C. et al.(1995), "The 1995 Look-up Table for

Critical Heat Flux in Tubes." Nuclear Engineering and Design, Vol.163, pp1-23.

24. Groeneveld, D. C. (1996), "On the Definition of Critical Heat Flux Margin." Nuclear Engineering and Design, Vol.163. pp245-247.

25. Groeneveld, D. C. (1996), "Reply to the Letter to the Editor from Todreas and Hejlzar on the paper entitled 'The 1995 CHF look-up table...'." Nuclear engineering and design, Vol.163, pp27-28.

26. Hewitt, G. F. and Hall-Taylor, N. S. (1966), "Annular two-phase flow", Pergamon Press, Oxford.

27. Huang, D. H. (1993), "Development of Bundle Correlation Method and its Application to Predicting CHF in Rod Bundles", Nuc. Eng. and Des., Vol. 139, pp206-5-220.

28. Isbin, H. S. (1959), "Two Phase Heat Transfer, Two-phase Burnout, USAEC Report AECU-4305 University of Minnesota, Minneapolis, MN.

29.Isbin, H. S. and Vandewater, R. (1961) Trans. ASME, J. Heat Transfer Vol.83 pp149.

30. Janssen, E. Levy, S. and Kervinen, J.A. (1963), "Investigations of burnout in Internally heated annulus cooled by water at 600 to 1450 PSIA", ASMS Paper No. 63-WA-149, November.

31. Joober, K. (1993), "The effect of Flow Geometry on Critical

Heat Flux", M. A. Sc., University of Ottawa.

32.Katto, Y. (1978), "A generalized Correlation of Critical Heat Flux for the Forced Convection Boiling in Vertical Uniformly Heated Round Tubes", Int. J. Heat Mass Transfer vol 21, pp.1527.

33. Katto, Y.(1979), "Generalizen Correlations of Critical Heat Flux for the Forced Convection Boiling in Vertical Uniformly Heated Annuli." J. Heat Mass Transfer, Vol.22, pp.575-584.

34. Katto, Y. (1980), "General Features of CHF of Forced Convective Boiling in Uniformly Heated Vertical Tubes with Zero Inlet Subcooling", Int. J. Heat Mass Transfer, vol 23, 493-504.

35. Katto, Y. (1981), "General Features of CHF of Forced Convective Boiling in Uniformly Heated Rectangular Channel", Int. J. Heat Mass Transfer, vol 24, 1413-1419.

36. Katto, Y. (1982), "An analytical Investigation on CHF of Flow Boiling in Uniformly Heated Vertical Tubes with Special Reference to Governing Dimensionless Groups", Int. J. Heat Mass Transfer, vol 25, 1353-1361.

37. Katto, Y. and Ohne, H. (1984), "An Improved Version of the Generalized Correlation of Critical Heat Flux for Forced Convection Boiling in Uniformly Heated Vertical Tubes",Int. J. Heat Mass Transfer, vol 27, 1641-1648.

38. Kirillov, P.L. and Smogalev, I.P. (1969), " Calculating the

Heat Exchange Crisis for a Vapour-liquid Mixture on the Basis of a Droplet-diffusion Model", Institute of physics and power, Obninsk, USSR, report no. FEI-181.

39. Kirillov, P. L. and Smogalev, I. P. (1972), "Calculation of Heat-transfer Crisis for Annuli Two-phase Flow of a Steam-liquid Mixture through an Annuli Channel", Translation from report FEI-297 of the Physics and Power-engineering Institute, Obnisk, USSR (1972), as report AECL-4752 of chalk river laboratories(1974).

40. Lahey, Jr R. T. et al.(1971), "Mass Flux and Enthalpy Distribution in a Rod Bundle for Single- and Two-Phase Flow Conditions", Journal of Heat Transfer, May 1971, pp197.

41. Lee, D. H. and Obertelli, J. D. (1963), "An Experimental Investigation of Forced Convection Boiling in High Pressure Water. Part I", AEEW-R, 213.

42. Levy, S. (1966), "Forced Convection Subcooled Boiling-Prediction on Vapour Volumetric Fraction, GEAP-5157, General Electric Company.

43. Lim, J. C., Weisman, J. (1988), "A phenomenologically Based Prediction of Rod-bundle Dryout. Nuclear" Eng. and Des., Vol.105, pp363-371.

44. Lim, J. C., Weisman, J. (1990), "A phenomenologically Based Prediction of the Critical Heat Flux in Channels Containing an Unheated Wall." Int. J. Heat mass transfer, Vol.33, no.1, pp203-

205.

45. Lin, W. S. et al.(1992), "Bundle Critical Power Predictions under Normal and Abnormal Conditions in Pressurized Water Reactors", Nucl. Tech. Vol. 98, pp.354-364, June 1992.

46. Macbeth, R. V.(1963), "Burn-out analysis. Part 4. Application of a Local Condition Hypothesis to World Data for Uniformly Heated Round Tubes and Rectangular Channels". AEEW-R 267.

47. Macbeth, R. V.(1964), "Burnout Analysis-Part 5. Examination of Published World Data for Rod Bundles". AEEW-R 358.

48. McPherson, G. D. (1971), "The Use of Enthalpy Imbalance in Evaluating the Dryout Performance of Fuel Bundles", AECL-3968.

49.Nishida, K. et al (1992), "Effect of Spacing Structures on Critical Power in a Nuclear Fuel Bundle", Thermal Hydraulic of Nuclear Reactors, Vol.I, M. Merilo, editor American Nuclear Society, LaGrange, Park, IL.

50. Owen, O. R. et al.(1969), " 9 MW Rig High Pressure Water Heat Transfer and Flow Resistance Measurements on 36-rod, 12 ft. Long Clusters Simulating an SGHW Reactor Fuel Element of Single Enrichment", United Kingdom Atomic Energy Authority Report AEEW-R 643.

51. Rogers, J. T. (1966), "Heat transfer limitations on Nuclear Reactor Fuel Elements", The Canadian Journal of Chemical

Engineering, pp 289.

52. Rogers, J. T. (1968), "Coolant Interchange Mixing in Reactor Fuel Bundles - Single-Phase Coolant, Heat Transfer in Rod Bundles", ASME, New York, Dec., 1968.

53. Rogers, J. T. (1970), "Kanupp Reactor Critical Power Ratio Analysis by 'CPP', a BASIC Language Computer Program", CGE Technical Report R70CAP14.

54. Rogers, J. T. et al. (1972), "Mixing by Turbulent Interchange in Fuel Bundles", Correlations and Inferences, ASME Paper, 72-HT-53.

55. Rogers, J. T. et al. (1982), "Flow Boiling Critical Heat Flux in a Vertical Annulus at Low Pressure and Velocities", In Proc. 7th Int. Heat Transfer Conf., Munich, Vol. 4, pp339-344.

56. Sato Y. (1992), "Crossflow of Gas-liquid Mixture Between Subchannels", Thermal Hydraulic of Nuclear Reactors, Vol.I, M. Merilo, editor American Nuclear Society, LaGrange, Park, IL.

57. Shiralkar, B. S. (1992), "Recent Trends in Subchannel Analysis", Thermal Hydraulic of Nuclear Reactors, Vol.I, M. Merilo, editor American Nuclear Society, LaGrange, Park, IL.

58.Smyth, R. T. et al. (1967), "Dryout and Pressure Drop Experiments on a Simulated S.G.H.W.R. Channel with Five Unheated Rods 6 MW Rig Test Series No.47", United Kingdom Atomic Energy

Authority Report AEEW-R 757, July.

59. Tolubinskiy, V. I. et al. (1977), "Boiling Crisis in Concentric and Eccentric Annuli." HEAT TRANSFER-Soviet Research, Vol.9, no.1.

60. Tong, L. S., Currin, H. B. and Engel, F. C. (1964), "DNB(Burnout) Studies in an Open Lattice Core", W.C.A.P.-3736.

61. Tong L. S.(1968), "An Evaluation of the Departure from Nucleate Boiling in Bundles of Reactor Fuel Rods." Nucl. Sci.and Eng., Vol.33, pp7-15.

62. Tong, L. S.(1972), "Boiling Crisis and Critical Heat Flux", USAEC Report TID-25887, Westinghouse Electricity Corporation.

63. Ulrych, G.(1985), "Application of Tube Critical Heat Flux Tables to Annuli and Rod Bundles. Proceedings of third international topical meeting on reactor thermal hydraulics." Rhode Island, USA Oct. 15-18.

64. Weisman, J and Bowring, R. W. (1975), "Methods for Detailed Thermal and Hydraulic Analysis of Water-cooled Reactors", Nuc. Sci. & Engng. vol. 57, pp255-276.

65. Weisman, J and Pei, B. S. (1983), "Prediction of Critical Heat Flux in Flow Boiling at Low Qualities", Int. J. Heat Mass Transfer. vol. 26, 1463-1477.

66. Walley, P. B. (1977) "The Calculation of Dryout in a Rod

Bundle", Int. Multiphase Flow, Vol.3, pp501-515.

67. Whalley, P. B.(1978), "The Calculation of Dryout in a Rod Bundle-a Comparison of Experimental and Calculated Results." Int. Multiphase Flow, Vol.4, pp427-431.

APPENDIX A: Experimental CHF data in bundles

1. Owen et al.(1969), (1).

RFD: 1.00/0.662/0.566/0.0

P (kPa)	G (kg/m²s)	Xc	Xin	CHF (w/m²)
6.72E+03	1.36E+03	4.13E-01	-5.10E-02	1.07E+06
6.72E+03	6.84E+02	6.10E-01	-1.00E-01	8.27E+05
6.72E+03	6.84E+02	6.43E-01	-7.51E-02	8.31E+05
6.72E+03	1.36E+03	3.86E-01	-6.13E-02	1.03E+06
6.72E+03	1.36E+03	3.53E-01	-1.80E-01	1.24E+06
6.74E+03	1.37E+03	3.51E-01	-1.69E-01	1.21E+06
6.72E+03	2.04E+03	2.75E-01	-1.25E-01	1.38E+06
6.69E+03	2.04E+03	2.74E-01	-1.26E-01	1.38E+06
6.72E+03	2.72E+03	2.23E-01	-1.08E-01	1.53E+06
6.72E+03	2.72E+03	2.19E-01	-1.11E-01	1.52E+06
6.76E+03	3.40E+03	1.93E-01	-9.22E-02	1.64E+06
6.74E+03	3.40E+03	1.91E-01	-9.31E-02	1.64E+06
6.76E+03	1.36E+03	3.64E-01	-1.32E-01	1.14E+06
6.74E+03	2.04E+03	2.82E-01	-9.83E-02	1.31E+06
6.74E+03	2.04E+03	2.82E-01	-9.47E-02	1.20E+06
6.74E+03	2.72E+03	2.40E-01	-6.79E-02	1.42E+06
6.70E+03	2.72E+03	2.40E-01	-6.32E-02	1.39E+06
6.74E+03	3.40E+03	2.04E-01	-6.17E-02	1.54E+06
6.72E+03	3.74E+03	1.89E-01	-7.11E-02	1.65E+06
6.74E+03	2.04E+03	3.06E-01	-5.90E-02	1.26E+06
6.69E+03	2.04E+03	2.99E-01	-6.37E-02	1.25E+06
6.76E+03	1.36E+03	3.94E-01	-8.22E-02	1.10E+06
6.72E+03	1.37E+03	3.95E-01	-9.18E-02	1.13E+06
6.74E+03	1.36E+03	3.70E-01	-1.44E-01	1.19E+06
6.72E+03	1.37E+03	3.76E-01	-1.49E-01	1.22E+06
6.69E+03	2.04E+03	2.97E-01	-7.92E-02	1.30E+06
6.72E+03	2.72E+03	2.33E-01	-9.09E-02	1.49E+06
6.72E+03	2.72E+03	2.33E-01	-9.09E-02	1.49E+06
6.72E+03	1.36E+03	3.74E-01	-1.33E-01	1.17E+06

Cont'd

P (kPa)	G (kg/m²s)	Xc	Xin	CHF (w/m²)
6.72E+03	2.04E+03	2.60E-01	-1.54E-01	1.43E+06
6.74E+03	2.72E+03	2.48E-01	-5.57E-02	1.39E+06
6.76E+03	2.72E+03	2.51E-01	-5.89E-02	1.42E+06
6.76E+03	2.04E+03	3.12E-01	-5.00E-02	1.25E+06
6.72E+03	6.99E+02	6.08E-01	-1.68E-01	9.19E+05
6.72E+03	7.00E+02	6.01E-01	-1.71E-01	9.16E+05
6.72E+03	6.89E+02	6.25E-01	-1.16E-01	8.65E+05
6.72E+03	6.89E+02	6.21E-01	-1.08E-01	8.49E+05
6.76E+03	6.85E+02	6.21E-01	-1.52E-01	8.96E+05
6.72E+03	6.80E+02	6.31E-01	-1.20E-01	8.64E+05
6.72E+03	6.84E+02	6.21E-01	-9.38E-02	8.28E+05
6.69E+03	6.85E+02	6.23E-01	-9.71E-02	8.36E+05
6.74E+03	1.36E+03	3.02E-01	-1.14E-01	1.14E+06
6.72E+03	6.80E+02	6.17E-01	-1.31E-01	6.61E+05
6.72E+03	6.86E+02	6.14E-01	-9.45E-02	8.23E+05
6.72E+03	6.89E+02	6.21E-01	-9.43E-02	8.30E+05
6.72E+03	6.84E+02	6.27E-01	-8.95E-02	8.20E+05
6.76E+03	6.81E+02	6.24E-01	-7.73E-02	8.07E+05
6.76E+03	6.80E+02	6.11E-01	-9.20E-02	8.36E+05
6.79E+03	6.75E+02	6.15E-01	-6.86E-02	8.08E+05
6.79E+03	6.75E+02	6.18E-01	-6.86E-02	8.11E+05
5.76E+03	6.84E+02	6.11E-01	-1.14E-01	8.75E+05
5.79E+03	6.84E+02	5.95E-01	-1.35E-01	8.89E+05
5.76E+03	1.36E+03	3.57E-01	-1.45E-01	1.21E+06
5.76E+03	1.36E+03	3.55E-01	-1.48E-01	1.21E+06
5.72E+03	1.36E+03	3.73E-01	-1.11E-01	1.17E+06
5.86E+03	1.36E+03	3.98E-01	-6.80E-02	1.11E+06
5.72E+03	1.36E+03	3.96E-01	-6.27E-02	1.11E+06
5.76E+03	2.04E+03	2.91E-01	-8.03E-02	1.34E+06
5.76E+03	2.04E+03	2.77E-01	-1.15E-01	1.42E+06
5.76E+03	2.04E+03	2.66E-01	-1.38E-01	1.46E+06
5.76E+03	1.37E+03	3.91E-01	-1.09E-01	1.21E+06
5.76E+03	1.36E+03	3.82E-01	-1.24E-01	1.22E+06
5.76E+03	2.04E+03	2.86E-01	-1.16E-01	1.45E+06

Cont'd

P (kPa)	G (kg/m²s)	Xc	Xin	CHF (w/m²)
5.79E+03	2.04E+03	2.86E-01	-1.13E-01	1.44E+06
5.79E+03	2.72E+03	2.36E-01	-8.41E-02	1.53E+06
5.76E+03	2.72E+03	2.43E-01	-7.07E-02	1.51E+06
5.76E+03	2.72E+03	2.51E-01	-5.59E-02	1.47E+06
5.76E+03	2.72E+03	2.44E-01	-6.20E-02	1.47E+06
5.86E+03	2.04E+03	3.03E-01	-6.92E-02	1.33E+06
5.76E+03	2.03E+03	3.00E-01	-7.71E-02	1.36E+06
5.72E+03	1.37E+03	3.80E-01	-1.09E-01	1.19E+06
5.75E+03	1.36E+03	3.69E-01	-1.40E-01	1.23E+06
5.76E+03	1.36E+03	3.65E-01	-1.72E-01	1.30E+06
5.76E+03	1.36E+03	3.51E-01	-1.99E-01	1.33E+06
5.76E+03	2.04E+03	2.59E-01	-1.70E-01	1.55E+06
5.76E+03	2.04E+03	2.60E-01	-1.67E-01	1.54E+06
5.76E+03	2.72E+03	2.49E-01	-5.00E-02	1.43E+06
5.86E+03	2.72E+03	2.49E-01	-5.68E-02	1.46E+06
6.76E+03	1.36E+03	3.99E-01	-7.17E-02	1.08E+06
6.72E+03	2.72E+03	2.40E-01	-8.00E-02	1.47E+06
6.76E+03	3.40E+03	2.03E-01	-7.51E-02	1.60E+06
6.72E+03	3.40E+03	1.94E-01	-9.55E-02	1.68E+06
6.72E+03	3.41E+03	2.14E-01	-5.15E-02	1.53E+06
6.72E+03	3.40E+03	2.00E-01	-8.75E-02	1.66E+06
6.72E+03	3.75E+03	1.95E-01	-6.31E-02	1.64E+06
6.72E+03	3.75E+03	2.01E-01	-5.65E-02	1.63E+06
6.72E+03	3.75E+03	1.90E-01	-7.87E-02	1.71E+06
6.72E+03	4.09E+03	1.84E-01	-5.72E-02	1.67E+06
6.69E+03	4.09E+03	1.87E-01	-5.43E-02	1.68E+06
5.76E+03	4.09E+03	1.85E-01	-4.81E-02	1.66E+06
5.76E+03	3.40E+03	2.11E-01	-5.28E-02	1.59E+06
5.76E+03	3.40E+03	1.95E-01	-7.97E-02	1.66E+06
5.79E+03	3.40E+03	1.99E-01	-7.94E-02	1.67E+06
5.76E+03	2.72E+03	2.22E-01	-1.26E-01	1.67E+06
5.76E+03	2.72E+03	2.24E-01	-1.23E-01	1.67E+06
5.76E+03	2.72E+03	2.25E-01	-1.10E-01	1.61E+06
5.76E+03	2.72E+03	2.34E-01	-1.01E-01	1.61E+06

Cont'd

P (kPa)	G (kg/m²s)	Xc	Xin	CHF (w/m²)
5.76E+03	2.72E+03	2.34E-01	-9.16E-02	1.60E+06
5.76E+03	3.74E+03	1.94E-01	-5.79E-02	1.67E+06
5.76E+03	3.74E+03	1.93E-01	-5.81E-02	1.66E+06
5.69E+03	3.74E+03	1.94E-01	-4.96E-02	1.63E+06
5.76E+03	3.74E+03	2.00E-01	-4.45E-02	1.61E+06
5.76E+03	3.74E+03	2.02E-01	-4.30E-02	1.62E+06
5.76E+03	4.09E+03	1.92E-01	-4.19E-02	1.69E+06
6.72E+03	4.11E+03	1.81E-01	-6.53E-02	1.72E+06
6.72E+03	3.40E+03	2.08E-01	-6.57E-02	1.59E+06
6.72E+03	3.41E+03	2.04E-01	-7.22E-02	1.60E+06
4.38E+03	1.36E+03	3.73E-01	-8.92E-02	1.19E+06
4.38E+03	1.36E+03	3.91E-01	-5.20E-02	1.14E+06
4.38E+03	2.72E+03	2.32E-01	-9.41E-02	1.67E+06
4.38E+03	2.72E+03	2.29E-01	-9.44E-02	1.66E+06
4.38E+03	2.72E+03	2.35E-01	-7.73E-02	1.60E+06
4.38E+03	6.75E+02	5.79E-01	-1.28E-01	8.98E+05
4.38E+03	6.73E+02	5.75E-01	-1.33E-01	8.98E+05
4.38E+03	1.37E+03	3.59E-01	-1.29E-01	1.26E+06
4.38E+03	2.72E+03	2.39E-01	-7.46E-02	1.61E+06
4.38E+03	6.85E+02	5.65E-01	-1.91E-01	9.76E+05
4.41E+03	6.86E+02	5.69E-01	-1.85E-01	9.74E+05
6.72E+03	3.40E+03	2.08E-01	-5.63E-02	1.53E+06
6.72E+03	3.40E+03	2.10E-01	-5.32E-02	1.52E+06
4.38E+03	2.72E+03	2.47E-01	-4.87E-02	1.51E+06
4.38E+03	2.73E+03	2.44E-01	-5.27E-02	1.53E+06
4.38E+03	2.04E+03	2.85E-01	-7.72E-02	1.39E+06
4.38E+03	2.03E+03	2.82E-01	-8.76E-02	1.42E+06
4.38E+03	2.04E+03	2.76E-01	-1.24E-01	1.54E+06
4.38E+03	2.04E+03	2.68E-01	-1.30E-01	1.53E+06
4.38E+03	2.04E+03	2.66E-01	-1.32E-01	1.54E+06
4.38E+03	2.04E+03	2.94E-01	-5.56E-02	1.34E+06
4.38E+03	1.36E+03	3.76E-01	-8.25E-02	1.18E+06
4.38E+03	1.37E+03	3.66E-01	-1.15E-01	1.24E+06
4.38E+03	1.36E+03	3.48E-01	-1.63E-01	1.31E+06

Cont'd

P (kPa)	G (kg/m²s)	Xc	Xin	CHF (w/m²)
5.76E+03	2.72E+03	2.29E-01	-8.32E-02	1.50E+06
5.76E+03	2.72E+03	2.25E-01	-1.04E-01	1.59E+06
5.76E+03	2.72E+03	2.21E-01	-1.15E-01	1.62E+06
4.38E+03	1.36E+03	3.73E-01	-1.27E-01	1.28E+06
4.38E+03	2.04E+03	2.93E-01	-1.01E-01	1.51E+06
4.40E+03	2.04E+03	2.94E-01	-8.40E-02	1.45E+06
4.38E+03	2.04E+03	3.07E-01	-5.62E-02	1.39E+06
4.38E+03	2.04E+03	3.19E-01	-3.98E-02	1.38E+06
4.38E+03	2.72E+03	2.53E-01	-5.03E-02	1.55E+06
4.38E+03	2.72E+03	2.58E-01	-4.21E-02	1.54E+06
4.38E+03	2.72E+03	2.48E-01	-6.79E-02	1.60E+06
4.38E+03	2.71E+03	2.43E-01	-8.13E-02	1.65E+06
4.38E+03	2.72E+03	2.37E-01	-9.06E-02	1.68E+06
4.38E+03	2.04E+03	2.81E-01	-1.28E-01	1.58E+06
5.76E+03	2.04E+03	2.80E-01	-1.37E-01	1.51E+06
5.76E+03	2.04E+03	2.99E-01	-7.93E-02	1.37E+06
4.38E+03	6.78E+02	5.61E-01	-1.34E-01	8.88E+05
4.38E+03	6.71E+02	5.73E-01	-1.10E-01	8.63E+05
4.38E+03	6.70E+02	5.85E-01	-1.02E-01	8.67E+05
4.38E+03	6.78E+02	5.93E-01	-8.12E-02	8.58E+05
4.38E+03	6.82E+02	5.94E-01	-4.56E-02	8.20E+05
4.38E+03	6.81E+02	5.96E-01	-4.67E-02	8.23E+05
4.38E+03	6.81E+02	5.53E-01	-1.65E-01	9.20E+05
4.38E+03	6.85E+02	5.50E-01	-1.89E-01	9.54E+05
5.76E+03	3.40E+03	2.04E-01	-7.54E-02	1.68E+06
5.80E+03	3.40E+03	2.06E-01	-6.26E-02	1.61E+06
5.78E+03	3.40E+03	2.12E-01	-4.98E-02	1.58E+06
5.76E+03	3.40E+03	1.94E-01	-9.32E-02	1.73E+06
5.78E+03	3.40E+03	1.97E-01	-8.67E-02	1.71E+06
5.76E+03	2.04E+03	2.89E-01	-1.15E-01	1.46E+06
5.76E+03	2.04E+03	2.93E-01	-1.06E-01	1.45E+06
5.76E+03	2.04E+03	2.94E-01	-9.91E-02	1.42E+06
5.76E+03	2.03E+03	3.14E-01	-5.64E-02	1.33E+06
5.76E+03	2.72E+03	2.36E-01	-8.02E-02	1.52E+06

Concluded

P (kPa)	G (kg/m²s)	Xc	Xin	CHF (w/m²)
4.38E+03	6.80E+02	5.72E-01	-8.31E-02	8.36E+05
4.38E+03	6.89E+02	5.61E-01	-7.59E-02	8.24E+05

2. Owen et al.(1969), (2).

RFD: 1.00/0.639/0.640/0.0
AFD: consine

P (kPa)	G (kg/m²s)	Xc	Xin	CHF (w/m²)
5.76E+03	6.80E+02	5.61E-01	-1.46E-01	5.66E+05
5.76E+03	6.77E+02	5.64E-01	-1.41E-01	5.70E+05
5.78E+03	1.36E+03	2.28E-01	-1.33E-01	1.18E+06
5.79E+03	2.04E+03	2.44E-01	-1.07E-01	1.31E+06
5.76E+03	6.84E+02	5.52E-01	-1.08E-01	5.23E+05
5.76E+03	6.80E+02	5.61E-01	-1.02E-01	5.20E+05
5.77E+03	6.85E+02	2.61E-01	-1.13E-01	5.43E+05
5.76E+03	6.86E+02	5.60E-01	-1.29E-01	5.56E+05
5.76E+03	6.81E+02	5.52E-01	-1.61E-01	5.71E+05
5.76E+03	6.82E+02	5.53E-01	-1.67E-01	5.80E+05
5.76E+03	1.35E+03	3.38E-01	-1.06E-01	1.10E+06
5.76E+03	1.36E+03	3.12E-01	-1.66E-01	1.20E+06
5.76E+03	1.36E+03	3.12E-01	-1.58E-01	1.17E+06
5.74E+03	1.36E+03	3.28E-01	-1.37E-01	1.14E+06
5.79E+03	1.36E+03	3.28E-01	-1.22E-01	1.12E+06
5.78E+03	1.36E+03	3.48E-01	-5.29E-02	1.08E+06
5.76E+03	1.36E+03	3.59E-01	-5.79E-02	1.04E+06
5.79E+03	2.04E+03	2.69E-01	-4.41E-02	1.17E+06
5.79E+03	2.04E+03	2.62E-01	-5.91E-02	1.20E+06
5.79E+03	2.04E+03	2.53E-01	-7.68E-02	1.23E+06
5.79E+03	2.04E+03	2.44E-01	-9.90E-02	1.28E+06
5.77E+03	2.04E+03	2.36E-01	-1.22E-01	1.34E+06
5.76E+03	2.04E+03	2.26E-01	-1.46E-01	1.40E+06
5.79E+03	2.04E+03	2.15E-01	-1.72E-01	1.46E+06
5.76E+03	1.36E+03	3.24E-01	-1.24E-01	1.12E+06
5.76E+03	2.72E+03	1.96E-01	-1.07E-01	1.52E+06
5.76E+03	2.72E+03	2.01E-01	-9.51E-02	1.48E+06
5.79E+03	2.72E+03	2.10E-01	-8.17E-02	1.45E+06
5.76E+03	3.41E+03	2.09E-01	-5.18E-02	1.35E+06
5.76E+03	3.41E+03	1.87E-01	-5.33E-02	1.76E+06

Cont'd

P (kPa)	G (kg/m²s)	Xc	Xin	CHF (w/m²)
5.76E+03	2.72E+03	2.15E-01	-6.56E-02	1.42E+06
5.76E+03	2.72E+03	2.19E-01	-4.76E-02	1.54E+06
5.74E+03	3.06E+03	1.39E-01	-4.96E-02	1.85E+06
5.76E+03	3.06E+03	1.89E-01	-5.12E-02	1.83E+06
5.76E+03	3.06E+03	1.78E-01	-6.31E-02	1.87E+06
5.76E+03	3.06E+03	1.65E-01	-8.39E-02	1.93E+06
5.76E+03	3.06E+03	1.82E-01	-4.71E-02	1.78E+06
5.79E+03	3.06E+03	1.84E-01	-4.96E-02	1.81E+06
5.76E+03	3.40E+03	1.84E-01	-3.64E-02	1.90E+06
5.72E+03	6.85E+02	5.18E-01	-6.27E-02	7.30E+05
5.79E+03	6.82E+02	5.22E-01	-5.36E-02	7.16E+05
5.76E+03	6.81E+02	5.21E-01	-4.05E-02	6.99E+05
5.76E+03	1.36E+03	3.46E-01	-5.98E-02	1.02E+06
5.72E+03	1.36E+03	3.56E-01	-4.08E-02	9.89E+05
5.76E+03	1.35E+03	3.62E-01	-2.99E-02	9.70E+05
5.76E+03	1.35E+03	3.64E-01	-3.11E-02	9.79E+05
5.76E+03	2.03E+03	2.64E-01	-5.76E-02	1.20E+06
5.81E+03	2.04E+03	2.59E-01	-4.02E-02	1.31E+06
5.75E+03	2.72E+03	2.11E-01	-5.98E-02	1.58E+06
5.65E+03	2.72E+03	2.04E-01	-3.92E-02	1.68E+06
5.77E+03	3.40E+03	1.79E-01	-4.02E-02	1.89E+06
6.72E+03	1.37E+03	3.17E-01	-8.88E-02	9.72E+05
6.72E+03	1.36E+03	3.14E-01	-4.91E-02	1.02E+06
6.72E+03	1.36E+03	3.31E-01	-2.78E-02	1.01E+06
6.72E+03	1.36E+03	3.42E-01	-1.43E-02	9.94E+05
6.72E+03	1.36E+03	3.36E-01	-1.15E-01	8.88E+05
6.72E+03	1.36E+03	3.17E-01	-1.53E-01	7.22E+05
6.74E+03	1.36E+03	3.09E-01	-1.20E-01	1.02E+06
6.72E+03	6.75E+02	5.09E-01	-1.07E-01	7.29E+05
6.76E+03	6.85E+02	4.99E-01	-1.57E-01	7.80E+05
6.74E+03	6.89E+02	5.15E-01	-7.16E-02	7.06E+05
6.72E+03	6.85E+02	5.21E-01	-5.50E-02	6.90E+05
6.69E+03	6.82E+02	5.29E-01	-3.45E-02	6.73E+05
6.72E+03	2.04E+03	2.43E-01	-9.18E-02	1.20E+06

Cont'd

P (kPa)	G (kg/m²s)	Xc	Xin	CHF (w/m²)
6.76E+03	2.02E+03	2.75E-01	-3.86E-02	1.11E+06
6.70E+03	2.04E+03	2.59E-01	-3.34E-02	1.22E+06
6.70E+03	2.03E+03	2.67E-01	-2.19E-02	1.20E+06
6.69E+03	2.04E+03	2.54E-01	-7.31E-02	1.17E+06
6.74E+03	2.03E+03	2.35E-01	-1.15E-01	1.25E+06
6.72E+03	2.04E+03	2.00E-01	-1.74E-01	1.34E+06
6.72E+03	2.04E+03	2.07E-01	-1.62E-01	1.32E+06
6.72E+03	2.72E+03	1.80E-01	-1.34E-01	1.50E+06
6.76E+03	2.72E+03	1.81E-01	-1.32E-01	1.48E+06
6.72E+03	2.72E+03	1.98E-01	-1.01E-01	1.43E+06
6.72E+03	2.72E+03	2.08E-01	-8.11E-02	1.37E+06
6.76E+03	2.72E+03	2.10E-01	-5.67E-02	1.49E+06
6.69E+03	2.73E+03	2.05E-01	-3.79E-02	1.40E+06
6.72E+03	2.72E+03	2.06E-01	-2.61E-02	1.53E+06
6.72E+03	3.40E+03	2.07E-01	-2.71E-02	1.41E+06
6.76E+03	3.40E+03	2.10E-01	-2.52E-02	1.40E+06
6.70E+03	3.40E+03	2.02E-01	-4.29E-02	1.49E+06
6.72E+03	3.40E+03	1.78E-01	-6.47E-02	1.70E+06
6.69E+03	3.06E+03	1.87E-01	-8.53E-02	1.46E+06
6.69E+03	3.06E+03	1.84E-01	-7.09E-02	1.62E+06
6.76E+03	3.07E+03	2.02E-01	-6.07E-02	1.41E+06
6.72E+03	3.06E+03	2.01E-01	-4.32E-02	1.53E+06
6.72E+03	3.06E+03	2.06E-01	-3.52E-02	1.51E+06
6.69E+03	3.05E+03	2.31E-01	-1.56E-02	1.32E+06
6.69E+03	3.06E+03	1.84E-01	-9.90E-02	1.52E+06
5.76E+03	1.37E+03	2.92E-01	-1.52E-01	1.11E+06
5.76E+03	3.06E+03	2.04E-01	-7.49E-02	1.60E+06
4.38E+03	3.06E+03	1.98E-01	-5.46E-02	1.50E+06
4.41E+03	3.06E+03	1.92E-01	-6.69E-02	1.54E+06
4.38E+03	3.06E+03	1.89E-01	-6.96E-02	1.54E+06
4.38E+03	3.06E+03	1.99E-01	-5.20E-02	1.49E+06
4.38E+03	3.06E+03	2.03E-01	-4.65E-02	1.48E+06
4.41E+03	3.06E+03	2.06E-01	-3.86E-02	1.45E+06
5.07E+03	3.06E+03	2.07E-01	-5.15E-02	1.49E+06

Cont'd

P (kPa)	G (kg/m²s)	Xc	Xin	CHF (w/m²)
5.07E+03	3.06E+03	2.05E-01	-5.98E-02	1.52E+06
5.07E+03	3.07E+03	2.10E-01	-4.69E-02	1.48E+06
5.07E+03	3.06E+03	2.14E-01	-3.70E-02	1.44E+06
5.07E+03	3.06E+03	2.14E-01	-3.98E-02	1.46E+06
5.76E+03	3.06E+03	2.09E-01	-6.31E-02	1.52E+06
5.76E+03	2.04E+03	2.43E-01	-9.34E-02	1.25E+06
5.76E+03	1.36E+03	3.34E-01	-6.34E-02	9.90E+05
5.79E+03	2.72E+03	2.07E-01	-8.78E-02	1.46E+06
4.38E+03	2.72E+03	2.06E-01	-6.76E-02	1.46E+06
4.38E+03	2.72E+03	2.11E-01	-5.66E-02	1.41E+06
4.38E+03	2.72E+03	1.76E-01	-4.57E-02	1.83E+06
4.38E+03	2.72E+03	2.16E-01	-5.38E-02	1.42E+06
4.38E+03	2.72E+03	1.98E-01	-8.63E-02	1.50E+06
4.38E+03	2.72E+03	2.04E-01	-7.30E-02	1.46E+06
4.41E+03	2.72E+03	2.00E-01	-8.00E-02	1.47E+06
6.72E+03	2.04E+03	2.21E-01	-1.28E-01	1.25E+06
6.72E+03	1.36E+03	3.05E-01	-1.10E-01	9.91E+05
6.72E+03	1.36E+03	3.21E-01	-7.93E-02	9.50E+05
5.72E+03	1.36E+03	3.43E-01	-4.58E-02	9.66E+05
5.76E+03	1.36E+03	2.93E-01	-1.54E-01	1.11E+06
5.76E+03	2.04E+03	2.20E-01	-1.42E-01	1.35E+06
6.72E+03	2.72E+03	1.99E-01	-1.09E-01	1.45E+06
5.76E+03	2.04E+03	2.27E-01	-1.28E-01	1.32E+06
5.72E+03	2.04E+03	2.34E-01	-1.10E-01	1.28E+06
5.76E+03	2.04E+03	2.63E-01	-4.76E-02	1.15E+06
5.76E+03	2.04E+03	2.81E-01	-2.46E-02	1.13E+06
5.76E+03	2.04E+03	2.42E-01	-9.07E-02	1.24E+06
5.76E+03	1.37E+03	3.48E-01	-1.86E-02	9.14E+05
5.76E+03	1.36E+03	3.60E-01	-3.84E-02	9.39E+05
5.76E+03	1.36E+03	3.31E-01	-5.43E-02	9.57E+05
5.77E+03	1.36E+03	3.24E-01	-8.21E-02	1.01E+06
5.76E+03	1.36E+03	3.04E-01	-1.19E-01	1.06E+06
5.78E+03	1.36E+03	2.89E-01	-1.65E-01	1.13E+06
4.38E+03	1.36E+03	3.39E-01	-3.23E-02	9.80E+05

Concluded

P (kPa)	G (kg/m²s)	Xc	Xin	CHF (w/m²)
4.41E+03	1.37E+03	3.15E-01	-7.47E-02	1.03E+06
4.37E+03	1.36E+03	3.30E-01	-5.12E-02	1.00E+06
4.45E+03	1.36E+03	3.26E-01	-5.72E-02	1.00E+06
4.41E+03	1.36E+03	3.04E-01	-1.12E-01	1.10E+06
4.41E+03	1.36E+03	3.14E-01	-9.54E-02	1.08E+06
4.39E+03	1.37E+03	3.15E-01	-8.46E-02	1.06E+06
4.38E+03	2.04E+03	2.34E-01	-9.53E-02	1.31E+06
4.34E+03	2.04E+03	2.35E-01	-9.37E-02	1.31E+06
4.39E+03	2.04E+03	3.35E-01	-1.20E-01	1.37E+06
4.38E+03	2.04E+03	2.47E-01	-6.32E-02	1.23E+06
4.41E+03	2.04E+03	2.43E-01	-7.55E-02	1.26E+06
4.38E+03	2.03E+03	2.59E-01	-4.15E-02	1.18E+06
6.21E+03	3.06E+03	2.01E-01	-7.13E-02	1.49E+06
6.23E+03	3.06E+03	2.11E-01	-5.98E-02	1.48E+06
6.31E+03	3.06E+03	2.18E-01	-3.79E-02	1.39E+06
6.21E+03	3.06E+03	1.82E-01	-2.62E-02	1.79E+06
6.27E+03	3.06E+03	1.86E-01	-2.08E-02	1.75E+06
6.26E+03	3.06E+03	1.97E-01	-6.47E-02	1.43E+06

3. Owen et al.(1969), (3).

RFD: 1.00/0.660/0.571/0.0

P (kPa)	G (kg/m²s)	Xc	Xin	CHF (w/m²)
5.76E+03	1.36E+03	3.94E-01	-1.35E-01	1.28E+06
5.76E+03	2.04E+03	3.02E-01	-1.18E-01	1.52E+06
5.76E+03	2.72E+03	2.40E-01	-1.08E-01	1.68E+06
5.76E+03	2.72E+03	2.54E-01	-8.03E-02	1.61E+06
5.76E+03	2.72E+03	2.73E-01	-4.90E-02	1.55E+06
5.76E+03	2.04E+03	3.29E-01	-5.52E-02	1.36E+06
5.76E+03	1.36E+03	4.19E-01	-6.78E-02	1.17E+06
5.76E+03	1.36E+03	4.41E-01	-2.11E-02	1.11E+06
5.76E+03	1.36E+03	3.91E-01	-1.38E-01	1.27E+06
5.76E+03	1.36E+03	4.01E-01	-1.17E-01	1.25E+06
5.76E+03	1.37E+03	4.08E-01	-8.97E-02	1.20E+06
5.76E+03	1.36E+03	4.15E-01	-7.24E-02	1.17E+06
5.76E+03	1.36E+03	4.32E-01	-3.37E-02	1.12E+06
5.76E+03	1.36E+03	4.40E-01	-2.39E-02	1.12E+06
5.76E+03	2.04E+03	3.16E-01	-6.75E-02	1.38E+06
5.79E+03	2.04E+03	3.12E-01	-8.49E-02	1.43E+06
5.76E+03	2.05E+03	2.92E-01	-1.15E-01	1.47E+06
5.76E+03	2.04E+03	2.78E-01	-1.44E-01	1.52E+06
5.76E+03	2.04E+03	2.79E-01	-1.40E-01	1.51E+06
5.76E+03	2.04E+03	3.28E-01	-3.57E-02	1.31E+06
5.76E+03	2.04E+03	3.28E-01	-5.28E-02	1.37E+06
5.76E+03	2.72E+03	2.54E-01	-6.43E-02	1.53E+06
5.79E+03	2.72E+03	2.67E-01	-3.56E-02	1.45E+06
5.79E+03	2.72E+03	2.56E-01	-5.38E-02	1.49E+06
5.76E+03	2.72E+03	2.48E-01	-7.63E-02	1.55E+06
5.76E+03	2.72E+03	2.34E-01	-9.97E-02	1.60E+06
5.76E+03	3.40E+03	2.18E-01	-5.11E-02	1.62E+06
5.76E+03	3.41E+03	2.05E-01	-8.37E-02	1.74E+06
5.76E+03	3.40E+03	2.09E-01	-7.49E-02	1.71E+06
5.76E+03	3.40E+03	2.17E-01	-5.96E-02	1.68E+06

Cont'd

P (kPa)	G (kg/m²s)	Xc	Xin	CHF (w/m²)
5.76E+03	3.40E+03	2.26E-01	-3.90E-02	1.59E+06
5.76E+03	2.73E+03	2.26E-01	-1.20E-01	1.67E+06
5.76E+03	2.04E+03	2.69E-01	-1.57E-01	1.54E+06
5.76E+03	2.04E+03	2.65E-01	-1.59E-01	1.53E+06
5.76E+03	1.36E+03	3.65E-01	-1.70E-01	1.29E+06
5.76E+03	1.36E+03	3.69E-01	-1.69E-01	1.30E+06
5.76E+03	1.36E+03	3.85E-01	-1.52E-01	1.29E+06
5.76E+03	1.36E+03	3.65E-01	-1.83E-01	1.32E+06
5.79E+03	6.75E+02	5.81E-01	-1.87E-01	9.14E+05
5.76E+03	6.78E+02	6.19E-01	-7.19E-02	8.25E+05
5.76E+03	6.81E+02	6.11E-01	-4.05E-02	7.81E+05
5.76E+03	6.75E+02	6.23E-01	-6.26E-02	8.17E+05
5.76E+03	6.80E+02	6.10E-01	-9.54E-02	8.45E+05
5.76E+03	6.97E+02	5.97E-01	-1.18E-01	8.79E+05
5.76E+03	6.78E+02	5.91E-01	-1.44E-01	8.78E+05
5.76E+03	6.86E+02	5.78E-01	-1.23E-01	8.47E+05
5.76E+03	6.70E+02	5.72E-01	-1.60E-01	8.67E+05
6.72E+03	1.36E+03	3.81E-01	-1.55E-01	1.24E+06
6.72E+03	1.36E+03	3.83E-01	-1.43E-01	1.21E+06
6.72E+03	2.04E+03	2.90E-01	-1.08E-01	1.37E+06
6.72E+03	2.72E+03	2.40E-01	-7.98E-02	1.47E+06
6.72E+03	3.41E+03	2.04E-01	-6.89E-02	1.50E+06
6.72E+03	1.36E+03	4.10E-01	-5.41E-02	1.07E+06
6.72E+03	1.36E+03	4.26E-01	-2.78E-02	1.04E+06
6.72E+03	1.36E+03	4.21E-01	-3.44E-02	1.05E+06
6.72E+03	1.36E+03	4.08E-01	-7.89E-02	1.12E+06
6.72E+03	1.36E+03	3.84E-01	-1.09E-01	1.13E+06
6.72E+03	1.36E+03	3.82E-01	-1.10E-01	1.14E+06
6.72E+03	1.36E+03	3.76E-01	-1.36E-01	1.18E+06
6.72E+03	1.36E+03	3.57E-01	-1.73E-01	1.22E+06
6.72E+03	2.03E+03	2.76E-01	-1.31E-01	1.40E+06
6.72E+03	2.04E+03	2.66E-01	-1.57E-01	1.46E+06
6.72E+03	2.04E+03	3.00E-01	-8.34E-02	1.32E+06
6.72E+03	2.04E+03	3.32E-01	-2.21E-02	1.22E+06

Cont'd

P (kPa)	G (kg/m²s)	Xc	Xin	CHF (w/m²)
6.72E+03	2.04E+03	3.09E-01	-5.96E-02	1.27E+06
6.72E+03	2.04E+03	3.16E-01	-5.32E-02	1.27E+06
6.72E+03	2.72E+03	2.63E-01	-4.12E-02	1.40E+06
6.72E+03	2.72E+03	2.50E-01	-6.07E-02	1.43E+06
6.72E+03	2.72E+03	2.32E-01	-9.86E-02	1.52E+06
6.72E+03	2.72E+03	2.25E-01	-1.14E-01	1.56E+06
6.72E+03	2.72E+03	2.13E-01	-1.41E-01	1.64E+06
6.72E+03	3.41E+03	1.98E-01	-9.39E-02	1.68E+06
6.72E+03	3.41E+03	2.16E-01	-5.56E-02	1.56E+06
6.72E+03	3.40E+03	2.00E-01	-8.46E-02	1.64E+06
6.72E+03	3.41E+03	2.26E-01	-3.82E-02	1.52E+06
6.72E+03	3.41E+03	2.24E-01	-4.45E-02	1.54E+06
6.72E+03	6.77E+02	6.26E-01	-5.41E-02	7.77E+05
6.72E+03	6.82E+02	6.08E-01	-8.14E-02	7.96E+05
6.72E+03	6.77E+02	5.98E-01	-1.13E-01	8.12E+05
6.72E+03	6.84E+02	6.00E-01	-1.43E-01	8.58E+05
6.72E+03	6.88E+02	5.82E-01	-1.70E-01	8.74E+05
6.72E+03	6.80E+02	5.76E-01	-1.93E-01	8.85E+05
6.72E+03	6.80E+02	6.40E-01	-2.42E-02	7.61E+05
4.38E+03	1.36E+03	4.00E-01	-7.04E-02	1.20E+06
4.38E+03	1.36E+03	4.23E-01	-2.70E-02	1.14E+06
4.38E+03	1.36E+03	4.08E-01	-4.60E-02	1.16E+06
4.38E+03	1.36E+03	3.80E-01	-1.01E-01	1.23E+06
4.37E+03	1.36E+03	3.63E-01	-1.23E-01	1.24E+06
4.38E+03	2.04E+03	2.90E-01	-1.04E-01	1.51E+06
4.38E+03	2.04E+03	2.94E-01	-8.65E-02	1.45E+06
4.38E+03	2.04E+03	2.02E-01	-6.92E-02	1.42E+06
4.38E+03	2.04E+03	3.08E-01	-4.48E-02	1.35E+06
4.38E+03	2.72E+03	2.51E-01	-4.87E-02	1.52E+06
4.38E+03	2.72E+03	2.45E-01	-6.61E-02	1.58E+06
4.38E+03	2.71E+03	2.38E-01	-8.50E-02	1.64E+06
4.38E+03	2.72E+03	2.56E-01	-3.91E-02	1.50E+06
4.38E+03	2.04E+03	2.78E-01	-1.27E-01	1.55E+06
4.38E+03	1.36E+03	3.56E-01	-1.58E-01	1.31E+06

Concluded

P (kPa)	G (kg/m²s)	Xc	Xin	CHF (w/m²)
4.38E+03	1.36E+03	3.57E-01	-1.52E-01	1.30E+06
4.41E+03	6.70E+02	5.37E-01	-1.94E-01	9.17E+05
4.38E+03	6.78E+02	5.27E-01	-1.79E-01	8.98E+05
4.38E+03	6.80E+02	5.78E-01	-8.62E-02	8.45E+05
4.38E+03	6.75E+02	5.75E-01	-1.22E-01	8.81E+05
4.38E+03	6.77E+02	5.69E-01	-1.40E-01	8.99E+05
4.38E+03	6.84E+02	6.15E-01	-5.07E-02	8.50E+05

4. Owen et al.(1969), (4).

RFD: 1.00/0.656/0.568/0.0

P (kPa)	G (kg/m²s)	Xc	Xin	CHF (w/m²)
6.72E+03	1.36E+03	3.95E-01	-9.25E-02	1.13E+06
6.72E+03	1.36E+03	3.97E-01	-7.58E-02	1.09E+06
6.76E+03	1.36E+03	4.00E-01	-5.94E-02	1.06E+06
6.72E+03	1.36E+03	4.19E-01	-2.25E-02	1.01E+06
6.72E+03	1.36E+03	3.89E-01	-1.06E-01	1.15E+06
6.72E+03	1.36E+03	3.72E-01	-1.41E-01	1.19E+06
6.72E+03	1.36E+03	3.64E-01	-1.55E-01	1.20E+06
6.72E+03	1.36E+03	3.60E-01	-1.77E-01	1.25E+06
6.72E+03	2.72E+03	2.44E-01	-7.71E-02	1.48E+06
5.76E+03	1.36E+03	3.82E-01	-1.48E-01	1.28E+06
6.72E+03	2.04E+03	2.70E-01	-1.28E-01	1.38E+06
6.72E+03	2.72E+03	2.25E-01	-1.01E-01	1.50E+06
6.72E+03	2.72E+03	2.50E-01	-6.20E-02	1.44E+06
6.96E+03	2.69E+03	2.54E-01	-4.42E-02	1.35E+06
6.76E+03	2.72E+03	2.60E-01	-3.04E-02	1.34E+06
6.72E+03	3.40E+03	2.05E-01	-7.29E-02	1.61E+06
6.72E+03	3.40E+03	2.24E-01	-3.85E-02	1.52E+06
6.72E+03	3.41E+03	2.12E-01	-5.65E-02	1.56E+06
6.72E+03	1.36E+03	3.83E-01	-1.20E-01	1.16E+06
6.72E+03	2.72E+03	2.17E-01	-1.15E-01	1.54E+06
6.72E+03	2.72E+03	2.08E-01	-1.44E-01	1.63E+06
6.76E+03	3.40E+03	1.94E-01	-9.74E-02	1.68E+06
6.72E+03	3.40E+03	2.03E-01	-7.56E-02	1.61E+06
6.72E+03	3.40E+03	1.96E-01	-8.52E-02	1.63E+06
6.72E+03	3.41E+03	2.14E-01	-4.71E-02	1.51E+06
6.72E+03	3.41E+03	2.16E-01	-5.34E-02	1.56E+06
5.76E+03	1.36E+03	4.16E-01	-6.99E-02	1.17E+06
5.76E+03	1.36E+03	4.22E-01	-3.76E-02	1.11E+06
5.76E+03	1.36E+03	4.25E-01	-2.25E-02	1.08E+06
5.76E+03	1.36E+03	4.07E-01	-9.06E-02	1.20E+06
5.76E+03	1.36E+03	3.98E-01	-1.16E-01	1.24E+06

Cont'd

P (kPa)	G (kg/m²s)	Xc	Xin	CHF (w/m²)
5.76E+03	1.36E+03	3.85E-01	-1.41E-01	1.21E+06
5.76E+03	1.36E+03	3.76E-01	-1.60E-01	1.29E+06
5.76E+03	1.35E+03	3.76E-01	-1.81E-01	1.24E+06
4.38E+03	1.36E+03	3.74E-01	-1.55E-01	1.26E+06
4.38E+03	1.36E+03	2.93E-01	-1.23E-01	1.33E+06
4.38E+03	1.36E+03	2.95E-01	-1.02E-01	1.28E+06
4.38E+03	1.36E+03	4.08E-01	-7.06E-02	1.23E+06
4.38E+03	1.36E+03	4.17E-01	-4.63E-02	1.18E+06
4.38E+03	1.36E+03	4.18E-01	-2.47E-02	1.13E+06
6.72E+03	1.36E+03	3.72E-01	-1.53E-01	1.22E+06
6.72E+03	2.04E+03	2.80E-01	-1.17E-01	1.37E+06
6.72E+03	2.04E+03	2.61E-01	-1.50E-01	1.43E+06
6.72E+03	2.04E+03	2.57E-01	-1.64E-01	1.44E+06
6.72E+03	2.04E+03	2.93E-01	-8.89E-02	1.32E+06
6.71E+03	2.04E+03	3.03E-01	-5.37E-02	1.23E+06
6.72E+03	2.03E+03	3.14E-01	-3.33E-02	1.20E+06
6.72E+03	6.81E+02	5.84E-01	-1.37E-01	8.36E+05
6.72E+03	6.88E+02	5.75E-01	-1.68E-01	8.68E+05
6.72E+03	6.69E+02	5.83E-01	-1.96E-01	8.87E+05
6.72E+03	6.78E+02	5.85E-01	-1.12E-01	8.02E+05
6.76E+03	6.82E+02	6.02E-01	-8.52E-02	7.95E+05
6.74E+03	6.86E+02	5.87E-01	-5.14E-02	7.42E+05
5.76E+03	1.36E+03	4.07E-01	-4.40E-02	1.09E+06
5.76E+03	1.36E+03	4.11E-01	-4.09E-02	1.09E+06
5.76E+03	6.82E+02	6.05E-01	-1.04E-01	8.55E+05
5.76E+03	6.78E+02	6.16E-01	-7.76E-02	8.32E+05
5.76E+03	6.74E+02	6.15E-01	-6.32E-02	8.09E+05
5.76E+03	6.73E+02	6.19E-01	-5.12E-02	7.97E+05
5.76E+03	6.88E+02	6.15E-01	-1.33E-01	9.01E+05
5.77E+03	6.82E+02	5.84E-01	-1.63E-01	9.04E+05
5.76E+03	6.85E+02	5.80E-01	-1.79E-01	9.22E+05
5.76E+03	2.72E+03	2.50E-01	-4.16E-02	1.40E+06
5.79E+03	2.72E+03	2.42E-01	-6.39E-02	1.47E+06
5.76E+03	2.72E+03	2.44E-01	-5.79E-02	1.45E+06

Cont'd

P (kPa)	G (kg/m²s)	Xc	Xin	CHF (w/m²)
5.76E+03	2.72E+03	2.29E-01	-8.32E-02	1.50E+06
5.76E+03	2.72E+03	2.25E-01	-1.04E-01	1.59E+06
5.76E+03	2.72E+03	2.21E-01	-1.15E-01	1.62E+06
4.38E+03	1.36E+03	3.73E-01	-1.27E-01	1.28E+06
4.38E+03	2.04E+03	2.93E-01	-1.01E-01	1.51E+06
4.40E+03	2.04E+03	2.94E-01	-8.40E-02	1.45E+06
4.38E+03	2.04E+03	3.07E-01	-5.62E-02	1.39E+06
4.38E+03	2.04E+03	3.19E-01	-3.98E-02	1.38E+06
4.38E+03	2.72E+03	2.53E-01	-5.03E-02	1.55E+06
4.38E+03	2.72E+03	2.58E-01	-4.21E-02	1.54E+06
4.38E+03	2.72E+03	2.48E-01	-6.79E-02	1.60E+06
4.38E+03	2.71E+03	2.43E-01	-8.13E-02	1.65E+06
4.38E+03	2.72E+03	2.37E-01	-9.06E-02	1.68E+06
4.38E+03	2.04E+03	2.81E-01	-1.28E-01	1.58E+06
5.76E+03	2.04E+03	2.80E-01	-1.37E-01	1.51E+06
5.76E+03	2.04E+03	2.99E-01	-7.93E-02	1.37E+06
4.38E+03	6.78E+02	5.61E-01	-1.34E-01	8.88E+05
4.38E+03	6.71E+02	5.73E-01	-1.10E-01	8.63E+05
4.38E+03	6.70E+02	5.85E-01	-1.02E-01	8.67E+05
4.38E+03	6.78E+02	5.93E-01	-8.12E-02	8.58E+05
4.38E+03	6.82E+02	5.94E-01	-4.56E-02	8.20E+05
4.38E+03	6.81E+02	5.96E-01	-4.67E-02	8.23E+05
4.38E+03	6.81E+02	5.53E-01	-1.65E-01	9.20E+05
4.38E+03	6.85E+02	5.50E-01	-1.89E-01	9.54E+05
5.76E+03	3.40E+03	2.04E-01	-7.54E-02	1.68E+06
5.80E+03	3.40E+03	2.06E-01	-6.26E-02	1.61E+06
5.78E+03	3.40E+03	2.12E-01	-4.98E-02	1.58E+06
5.76E+03	3.40E+03	1.94E-01	-9.32E-02	1.73E+06
5.78E+03	3.40E+03	1.97E-01	-8.67E-02	1.71E+06
5.76E+03	2.04E+03	2.89E-01	-1.15E-01	1.46E+06
5.76E+03	2.04E+03	2.93E-01	-1.06E-01	1.45E+06
5.76E+03	2.04E+03	2.94E-01	-9.91E-02	1.42E+06
5.76E+03	2.03E+03	3.14E-01	-5.64E-02	1.33E+06
5.76E+03	2.72E+03	2.36E-01	-8.02E-02	1.52E+06

Concluded

P (kPa)	G (kg/m²s)	Xc	Xin	CHF (w/m²)
5.76E+03	1.36E+03	3.92E-01	-1.02E-01	1.19E+06
6.72E+03	2.04E+03	2.88E-01	-8.59E-02	1.30E+06
5.76E+03	2.04E+03	2.57E-01	-1.76E-01	1.57E+06
5.76E+03	2.72E+03	2.38E-01	-8.57E-02	1.56E+06
5.76E+03	2.72E+03	2.48E-01	-6.20E-02	1.49E+06
5.76E+03	3.40E+03	2.09E-01	-5.93E-02	1.62E+06
5.76E+03	2.72E+03	2.25E-01	-1.21E-01	1.67E+06
5.76E+03	2.04E+03	3.12E-01	-4.61E-02	1.29E+06
5.76E+03	2.04E+03	2.57E-01	-1.66E-01	1.53E+06

5. Bowdith et al.(1972).

RFD: 1.00/0.660/0.600/0.0

P (kPa)	G (kg/m²s)	Xc	Xin	CHF (w/m²)
5.86E+03	1.37E+03	3.92E-01	-3.22E-02	1.02E+06
5.86E+03	1.37E+03	3.79E-01	-4.11E-02	1.04E+06
5.86E+03	1.37E+03	3.79E-01	-6.63E-02	1.08E+06
5.86E+03	1.37E+03	3.61E-01	-1.09E-01	1.14E+06
5.86E+03	1.37E+03	3.54E-01	-1.26E-01	1.16E+06
5.86E+03	2.05E+03	2.81E-01	-4.96E-02	1.19E+06
5.86E+03	2.08E+03	2.63E-01	-7.61E-02	1.23E+06
5.86E+03	2.08E+03	2.55E-01	-9.14E-02	1.26E+06
5.86E+03	2.09E+03	2.42E-01	-1.19E-01	1.31E+06
5.86E+03	2.75E+03	2.21E-01	-5.61E-02	1.34E+06
5.86E+03	2.75E+03	2.05E-01	-8.01E-02	1.38E+06
5.86E+03	2.75E+03	1.92E-01	-9.95E-02	1.42E+06
5.86E+03	3.09E+03	1.78E-01	-9.86E-02	1.49E+06
5.86E+03	3.09E+03	2.00E-01	-6.26E-02	1.43E+06
5.86E+03	3.09E+03	2.02E-01	-5.67E-02	1.41E+06
5.86E+03	3.09E+03	1.86E-01	-7.95E-02	1.45E+06
5.86E+03	3.10E+03	1.72E-01	-1.13E-01	1.56E+06
5.86E+03	2.74E+03	1.90E-01	-1.15E-01	1.48E+06
5.86E+03	2.74E+03	1.80E-01	-1.27E-01	1.49E+06
5.86E+03	2.06E+03	2.20E-01	-1.82E-01	1.47E+06
5.86E+03	2.06E+03	2.31E-01	-1.58E-01	1.42E+06
5.86E+03	1.37E+03	3.37E-01	-1.72E-01	1.24E+06
5.86E+03	1.04E+03	4.04E-01	-1.91E-01	1.09E+06
5.86E+03	1.04E+03	4.19E-01	-1.69E-01	1.08E+06
5.86E+03	1.04E+03	4.32E-01	-1.34E-01	1.04E+06
6.83E+03	2.75E+03	1.74E-01	-1.53E-01	1.52E+06
6.83E+03	3.09E+03	1.59E-01	-1.40E-01	1.56E+06
6.82E+03	1.38E+03	2.95E-01	-2.27E-01	1.22E+06
6.83E+03	1.38E+03	3.03E-01	-2.11E-01	1.20E+06
6.83E+03	1.37E+03	3.13E-01	-1.78E-01	1.14E+06
6.83E+03	1.37E+03	3.29E-01	-1.39E-01	1.09E+06

Cont'd

P (kPa)	G (kg/m²s)	Xc	Xin	CHF (w/m²)
6.85E+03	1.39E+03	3.79E-01	-3.24E-02	9.50E+05
6.83E+03	1.37E+03	3.50E-01	-9.04E-02	1.02E+06
6.83E+03	1.04E+03	4.52E-01	-6.49E-02	9.06E+05
6.83E+03	1.04E+03	4.31E-01	-1.08E-01	9.46E+05
6.83E+03	1.04E+03	4.16E-01	-1.41E-01	9.78E+05
6.83E+03	1.04E+03	4.05E-01	-1.64E-01	9.97E+05
6.83E+03	1.04E+03	3.80E-01	-2.23E-01	1.06E+06
6.83E+03	1.04E+03	4.46E-01	-7.80E-02	9.22E+05
6.83E+03	6.94E+02	5.91E-01	-5.16E-02	7.53E+05
6.83E+03	6.92E+02	5.66E-01	-1.19E-01	8.01E+05
6.83E+03	6.93E+02	5.31E-01	-2.06E-01	8.65E+05
6.83E+03	5.50E+02	6.00E-01	-2.44E-01	7.85E+05
6.83E+03	5.51E+02	6.23E-01	-1.70E-01	7.39E+05
6.83E+03	5.51E+02	6.67E-01	-4.25E-02	6.59E+05
4.48E+03	2.75E+03	2.01E-01	-7.74E-02	1.43E+06
4.48E+03	2.76E+03	2.08E-01	-6.26E-02	1.40E+06
4.48E+03	2.75E+03	1.94E-01	-9.21E-02	1.47E+06
5.89E+03	1.04E+03	4.64E-01	-6.15E-02	9.58E+05
5.86E+03	1.04E+03	4.75E-01	-2.01E-02	9.02E+05
5.86E+03	1.04E+03	4.43E-01	-1.04E-01	1.00E+06
5.86E+03	6.94E+02	5.35E-01	-1.72E-01	8.66E+05
5.86E+03	6.90E+02	5.55E-01	-1.41E-01	8.46E+05
5.86E+03	6.93E+02	5.65E-01	-1.04E-01	8.16E+05
5.86E+03	6.92E+02	5.84E-01	-5.76E-02	7.82E+05
5.86E+03	5.50E+02	6.58E-01	-4.08E-02	6.76E+05
5.86E+03	5.56E+02	6.37E-01	-7.18E-02	6.95E+05
5.86E+03	5.56E+02	6.13E-01	-1.47E-01	7.44E+05
5.86E+03	5.51E+02	5.91E-01	-2.07E-01	7.77E+05
5.86E+03	2.75E+03	2.08E-01	-7.55E-02	1.37E+06
6.83E+03	2.75E+03	2.16E-01	-7.21E-02	1.34E+06
6.83E+03	2.75E+03	2.23E-01	-5.16E-02	1.28E+06
6.83E+03	2.75E+03	2.05E-01	-8.98E-02	1.37E+06
6.79E+03	2.75E+03	1.87E-01	-1.16E-01	1.42E+06
6.79E+03	3.10E+03	1.77E-01	-1.12E-01	1.52E+06

Cont'd

P (kPa)	G (kg/m²s)	Xc	Xin	CHF (w/m²)
6.83E+03	3.09E+03	1.91E-01	-9.01E-02	1.47E+06
6.83E+03	3.09E+03	2.09E-01	-5.19E-02	1.36E+06
6.83E+03	3.09E+03	2.00E-01	-7.11E-02	1.42E+06
6.83E+03	2.06E+03	2.73E-01	-6.09E-02	1.16E+06
6.83E+03	2.12E+03	2.49E-01	-8.81E-02	1.21E+06
6.83E+03	2.06E+03	2.28E-01	-1.40E-01	1.29E+06
6.83E+03	2.06E+03	2.18E-01	-1.70E-01	1.36E+06
6.83E+03	2.06E+03	2.14E-01	-1.79E-01	1.37E+06
6.81E+03	1.04E+03	5.03E-01	-6.55E-02	9.97E+05
6.82E+03	1.37E+03	4.29E-01	-4.01E-02	1.09E+06
6.83E+03	2.05E+03	3.17E-01	-6.69E-02	1.33E+06
6.84E+03	1.75E+03	2.65E-01	-6.26E-02	1.53E+06
6.79E+03	3.10E+03	2.46E-01	-6.34E-02	1.62E+06
6.83E+03	3.10E+03	2.38E-01	-8.20E-02	1.68E+06
6.83E+03	2.75E+03	2.53E-01	-9.65E-02	1.63E+06
6.83E+03	2.08E+03	2.98E-01	-9.82E-02	1.38E+06
6.83E+03	1.38E+03	4.08E-01	-7.25E-02	1.12E+06
6.83E+03	1.37E+03	4.00E-01	-1.00E-01	1.16E+06
6.83E+03	1.37E+03	3.82E-01	-1.32E-01	1.20E+06
6.84E+03	1.38E+03	3.68E-01	-1.69E-01	1.25E+06
6.83E+03	2.06E+03	2.79E-01	-1.26E-01	1.42E+06
6.83E+03	2.06E+03	2.70E-01	-1.54E-01	1.48E+06
6.83E+03	2.75E+03	2.31E-01	-1.23E-01	1.65E+06
6.83E+03	2.75E+03	2.37E-01	-1.07E-01	1.60E+06
6.83E+03	2.75E+03	2.48E-01	-9.23E-02	1.58E+06
6.83E+03	2.75E+03	2.51E-01	-7.67E-02	1.52E+06
6.83E+03	2.74E+03	2.70E-01	-3.98E-02	1.44E+06
6.83E+03	3.09E+03	2.50E-01	-4.38E-02	1.53E+06
6.83E+03	3.09E+03	2.50E-01	-5.32E-02	1.58E+06
6.83E+03	2.08E+03	3.26E-01	-3.47E-02	1.25E+06
6.83E+03	1.04E+03	5.14E-01	-4.08E-02	9.72E+05
6.83E+03	1.04E+03	5.08E-01	-6.72E-02	1.01E+06
6.83E+03	1.04E+03	4.89E-01	-1.00E-01	1.04E+06
5.86E+03	1.37E+03	4.44E-01	-3.38E-02	1.16E+06

Cont'd

P (kPa)	G (kg/m²s)	Xc	Xin	CHF (w/m²)
4.48E+03	1.37E+03	4.41E-01	-4.99E-02	1.26E+06
4.52E+03	1.38E+03	4.23E-01	-8.23E-02	1.30E+06
4.48E+03	1.37E+03	4.14E-01	-1.05E-01	1.33E+06
4.48E+03	1.38E+03	4.00E-01	-1.45E-01	1.40E+06
4.48E+03	2.06E+03	3.22E-01	-9.51E-02	1.62E+06
4.48E+03	2.06E+03	3.19E-01	-8.46E-02	1.56E+06
4.49E+03	2.06E+03	3.25E-01	-6.41E-02	1.50E+06
4.48E+03	2.07E+03	3.12E-01	-1.05E-01	1.62E+06
4.48E+03	2.07E+03	3.19E-01	-1.03E-01	1.66E+06
4.48E+03	1.04E+03	5.12E-01	-2.56E-02	1.04E+06
4.48E+03	1.04E+03	5.06E-01	-5.56E-02	1.09E+06
4.48E+03	1.04E+03	4.94E-01	-8.49E-02	1.12E+06
4.48E+03	1.04E+03	4.75E-01	-1.69E-01	1.25E+06
4.48E+03	1.04E+03	4.87E-01	-1.38E-01	1.22E+06
4.48E+03	6.89E+02	4.16E-01	-7.07E-02	8.85E+05
4.48E+03	6.91E+02	6.13E-01	-3.20E-02	8.33E+05
4.46E+03	6.93E+02	5.90E-01	-1.30E-01	9.34E+05
4.48E+03	6.89E+02	5.95E-01	-1.57E-01	9.69E+05
4.48E+03	5.50E+02	6.44E-01	-1.82E-01	8.51E+05
4.48E+03	5.48E+02	4.71E-01	-1.16E-01	8.04E+05
4.48E+03	5.49E+02	6.58E-01	-8.04E-02	7.56E+05
4.48E+03	5.47E+02	6.62E-01	-2.88E-02	7.07E+05
2.87E+03	5.48E+02	6.13E-01	-5.09E-02	7.34E+05
2.89E+03	5.52E+02	6.25E-01	-2.68E-02	7.24E+05
2.87E+03	5.49E+02	6.09E-01	-9.37E-02	7.77E+05
2.86E+03	5.49E+02	5.77E-01	-1.44E-01	7.99E+05
2.86E+03	6.08E+02	5.42E-01	-1.10E-01	9.05E+05
2.88E+03	6.90E+02	5.48E-01	-8.96E-02	8.87E+05
2.89E+03	6.90E+02	5.54E-01	-6.05E-02	8.53E+05
2.89E+03	6.92E+02	5.69E-01	-1.58E-02	8.14E+05
2.90E+03	1.04E+03	4.61E-01	-3.12E-02	1.03E+06
2.90E+03	1.04E+03	4.52E-01	-5.20E-02	1.05E+06
2.86E+03	1.04E+03	4.45E-01	-7.23E-02	1.08E+06
2.86E+03	1.04E+03	4.44E-01	-8.52E-02	1.11E+06

Cont'd

P (kPa)	G (kg/m²s)	Xc	Xin	CHF (w/m²)
2.87E+03	1.04E+03	4.30E-01	-1.44E-01	1.20E+06
2.86E+03	1.37E+03	3.87E-01	-4.98E-02	1.21E+06
2.89E+03	1.38E+03	3.83E-01	-7.84E-02	1.20E+06
2.88E+03	1.38E+03	3.76E-01	-9.15E-02	1.30E+06
2.88E+03	1.38E+03	3.70E-01	-1.16E-01	1.35E+06
2.92E+03	2.07E+03	2.86E-01	-9.13E-02	1.57E+06
2.86E+03	2.07E+03	2.90E-01	-6.66E-02	1.49E+06
2.86E+03	2.07E+03	2.75E-01	-1.15E-01	1.63E+06
1.48E+03	6.91E+02	4.60E-01	-1.11E-01	8.58E+05
1.48E+03	6.93E+02	4.49E-01	-1.21E-01	8.60E+05
1.48E+03	6.93E+02	4.62E-01	-8.40E-02	8.23E+05
1.48E+03	6.88E+02	4.90E-01	-2.72E-02	7.73E+05
1.48E+03	1.04E+03	3.61E-01	-5.14E-02	9.30E+05
1.48E+03	1.04E+03	3.52E-01	-7.20E-02	9.55E+05
1.48E+03	1.04E+03	3.48E-01	-9.25E-02	9.94E+05
1.48E+03	1.04E+03	3.39E-01	-1.24E-01	1.05E+06
1.51E+03	1.38E+03	2.79E-01	-1.17E-01	1.19E+06
1.50E+03	1.38E+03	2.81E-01	-1.03E-01	1.15E+06
1.48E+03	1.38E+03	2.81E-01	-9.16E-02	1.12E+06
1.50E+03	1.38E+03	2.85E-01	-7.73E-02	1.08E+06
1.48E+03	1.38E+03	2.91E-01	-6.57E-02	1.07E+06
1.51E+03	1.38E+03	2.88E-01	-5.40E-02	1.03E+06
1.48E+03	5.52E+02	5.16E-01	-7.67E-02	7.11E+05
1.48E+03	5.62E+02	5.42E-01	-1.08E-02	6.74E+05
1.41E+03	5.54E+02	5.39E-01	-4.28E-02	7.04E+05
1.48E+03	5.53E+02	5.41E-01	-4.39E-02	7.04E+05
1.48E+03	5.49E+02	5.21E-01	-1.19E-01	7.64E+05
5.86E+03	6.89E+02	6.22E-01	-1.07E-01	8.85E+05
5.86E+03	6.89E+02	6.25E-01	-9.10E-02	8.70E+05
5.86E+03	6.87E+02	6.31E-01	-1.26E-01	9.16E+05
5.86E+03	6.93E+02	6.17E-01	-1.54E-01	9.42E+05
5.86E+03	2.06E+03	2.91E-01	-1.40E-01	1.51E+06
5.86E+03	2.07E+03	2.96E-01	-1.24E-01	1.53E+06
5.86E+03	2.06E+03	3.17E-01	-6.04E-02	1.37E+06

Cont'd

P (kPa)	G (kg/m²s)	Xc	Xin	CHF (w/m²)
5.86E+03	2.06E+03	3.03E-01	-9.01E-02	1.43E+06
5.86E+03	6.89E+02	5.93E-01	-1.94E-01	9.56E+05
5.86E+03	6.92E+02	5.83E-01	-2.09E-01	9.66E+05
5.83E+03	6.87E+02	6.23E-01	-1.18E-01	8.97E+05
5.86E+03	6.88E+02	6.02E-01	-1.66E-01	9.31E+05
5.86E+03	2.75E+03	2.55E-01	-6.72E-02	1.56E+06
5.86E+03	2.75E+03	2.64E-01	-4.96E-02	1.52E+06
5.86E+03	2.76E+03	2.49E-01	-7.80E-02	1.59E+06
5.86E+03	2.75E+03	2.51E-01	-8.65E-02	1.64E+06
5.86E+03	3.09E+03	2.28E-01	-7.28E-02	1.64E+06
5.86E+03	3.10E+03	2.38E-01	-5.20E-02	1.58E+06
5.86E+03	3.09E+03	2.22E-01	-8.50E-02	1.67E+06
5.86E+03	2.75E+03	2.43E-01	-9.68E-02	1.65E+06
6.83E+03	2.75E+03	2.60E-01	-4.65E-02	1.42E+06
6.83E+03	2.75E+03	2.49E-01	-6.88E-02	1.47E+06
6.83E+03	2.75E+03	2.47E-01	-8.88E-02	1.56E+06
6.83E+03	2.75E+03	2.27E-01	-1.19E-01	1.61E+06
6.83E+03	3.09E+03	2.26E-01	-8.52E-02	1.63E+06
6.88E+03	3.09E+03	2.30E-01	-6.71E-02	1.55E+06
6.83E+03	3.10E+03	2.38E-01	-5.02E-02	1.51E+06
6.83E+03	3.09E+03	2.23E-01	-7.77E-02	1.57E+06
6.83E+03	2.06E+03	3.15E-01	-4.45E-02	1.25E+06
6.81E+03	2.06E+03	3.00E-01	-7.73E-02	1.32E+06
6.83E+03	2.06E+03	2.87E-01	-1.14E-01	1.39E+06
6.83E+03	2.06E+03	2.77E-01	-1.56E-01	1.51E+06
6.83E+03	1.37E+03	3.67E-01	-2.03E-01	1.33E+06
6.83E+03	1.37E+03	3.75E-01	-1.75E-01	1.28E+06
6.83E+03	1.37E+03	3.84E-01	-1.47E-01	1.24E+06
6.83E+03	1.37E+03	3.87E-01	-1.18E-01	1.17E+06
6.83E+03	1.37E+03	4.30E-01	-2.55E-02	1.06E+06
6.83E+03	6.89E+02	6.19E-01	-9.49E-02	8.29E+05
6.84E+03	6.87E+02	6.03E-01	-1.36E-01	8.57E+05
6.83E+03	6.91E+02	5.77E-01	-2.17E-01	9.28E+05
4.48E+03	6.99E+02	5.70E-01	-1.68E-01	9.66E+05

Concluded

P (kPa)	G (kg/m²s)	Xc	Xin	CHF (w/m²)
4.48E+03	6.91E+02	5.89E-01	-1.15E-01	9.11E+05
4.48E+03	6.90E+02	6.00E-01	-7.99E-02	8.76E+05
4.48E+03	1.37E+03	4.15E-01	-6.60E-02	1.23E+06
4.48E+03	1.37E+03	4.05E-01	-9.26E-02	1.28E+06
4.48E+03	1.38E+03	3.82E-01	-1.29E-01	1.32E+06
4.48E+03	2.06E+03	2.91E-01	-1.06E-01	1.54E+06
4.48E+03	2.07E+03	2.97E-01	-9.48E-02	1.52E+06
4.48E+03	2.07E+03	3.03E-01	-6.90E-02	1.44E+06

6. Smyth et al.

RFD: 1.00/0.639/0.557/0.0

P (kPa)	G (kg/m²s)	Xc	Xin	CHF (w/m²)
3.46E+03	1.71E+03	2.44E-01	-4.70E-02	1.09E+06
3.46E+03	1.71E+03	2.49E-01	-4.68E-02	1.11E+06
3.50E+03	2.06E+03	2.19E-01	-4.15E-02	1.18E+06
3.47E+03	2.06E+03	2.31E-01	-3.97E-02	1.23E+06
3.45E+03	1.03E+03	3.29E-01	-5.25E-02	8.63E+05
3.45E+03	1.03E+03	3.22E-01	-4.49E-02	8.27E+05
3.45E+03	1.03E+03	3.27E-01	-4.47E-02	8.40E+05
3.38E+03	7.01E+02	3.45E-01	-1.02E-01	6.92E+05
3.38E+03	7.03E+02	3.87E-01	-5.34E-02	6.82E+05
3.38E+03	7.03E+02	3.98E-01	-5.31E-02	6.98E+05
3.50E+03	6.82E+02	3.80E-01	-8.46E-02	6.95E+05
3.50E+03	6.82E+02	3.89E-01	-8.32E-02	7.06E+05
3.46E+03	6.82E+02	3.81E-01	-8.26E-02	6.95E+05
3.45E+03	6.82E+02	3.85E-01	-8.31E-02	7.02E+05
3.48E+03	1.03E+03	3.00E-01	-8.76E-02	8.78E+05
3.45E+03	1.03E+03	2.98E-01	-8.60E-02	8.72E+05
3.45E+03	1.37E+03	2.56E-01	-8.43E-02	1.02E+06
3.45E+03	1.36E+03	2.59E-01	-8.30E-02	1.02E+06
3.46E+03	1.71E+03	2.27E-01	-8.92E-02	1.19E+06
3.50E+03	1.71E+03	2.26E-01	-8.62E-02	1.17E+06
3.48E+03	1.93E+03	2.07E-01	-8.64E-02	1.25E+06
3.47E+03	1.92E+03	2.08E-01	-7.35E-02	1.19E+06
3.48E+03	1.92E+03	2.16E-01	-7.40E-02	1.23E+06
3.45E+03	1.92E+03	2.21E-01	-5.44E-02	1.17E+06
3.45E+03	1.92E+03	2.25E-01	-5.31E-02	1.18E+06
3.46E+03	1.92E+03	2.36E-01	-3.42E-02	1.14E+06
3.50E+03	1.36E+03	2.83E-01	-4.04E-02	9.67E+05
6.72E+03	1.02E+03	3.72E-01	-7.91E-02	8.81E+05
6.72E+03	1.03E+03	3.67E-01	-8.23E-02	8.78E+05
6.72E+03	1.37E+03	2.99E-01	-7.73E-02	9.86E+05

Cont'd

P (kPa)	G (kg/m²s)	Xc	Xin	CHF (w/m²)
6.72E+03	1.37E+03	2.99E-01	-7.40E-02	9.72E+05
6.72E+03	1.37E+03	3.04E-01	-7.40E-02	9.86E+05
6.72E+03	1.37E+03	2.84E-01	-1.09E-01	1.03E+06
6.72E+03	1.37E+03	2.81E-01	-1.09E-01	1.02E+06
6.72E+03	1.37E+03	2.87E-01	-1.09E-01	1.04E+06
6.72E+03	1.03E+03	3.53E-01	-1.20E-01	9.27E+05
6.72E+03	1.03E+03	3.38E-01	-1.32E-01	9.27E+05
6.72E+03	1.03E+03	3.42E-01	-1.32E-01	9.34E+05
6.72E+03	1.03E+03	3.17E-01	-1.78E-01	9.70E+05
6.72E+03	1.03E+03	3.21E-01	-1.75E-01	9.71E+05
6.72E+03	1.03E+03	3.75E-01	-5.67E-02	8.46E+05
6.72E+03	1.37E+03	3.15E-01	-4.97E-02	9.53E+05
6.72E+03	1.38E+03	3.17E-01	-4.64E-02	9.53E+05
6.72E+03	1.37E+03	3.30E-01	-3.14E-02	9.46E+05
6.73E+03	1.72E+03	2.88E-01	-2.25E-02	1.02E+06
6.72E+03	1.72E+03	2.72E-01	-4.88E-02	1.05E+06
6.72E+03	1.72E+03	2.71E-01	-4.56E-02	1.04E+06
6.72E+03	1.71E+03	2.49E-01	-8.61E-02	1.10E+06
6.72E+03	1.72E+03	2.48E-01	-8.28E-02	1.08E+06
6.72E+03	1.72E+03	2.51E-01	-8.45E-02	1.10E+06
6.76E+03	1.71E+03	2.39E-01	-1.08E-01	1.13E+06
6.72E+03	1.71E+03	2.37E-01	-1.07E-01	1.12E+06
6.72E+03	2.05E+03	2.11E-01	-9.47E-02	1.20E+06
6.72E+03	2.05E+03	2.12E-01	-9.47E-02	1.20E+06
6.72E+03	2.05E+03	2.19E-01	-8.03E-02	1.17E+06
6.72E+03	2.06E+03	2.18E-01	-8.03E-02	1.17E+06
6.72E+03	2.06E+03	2.35E-01	-5.12E-02	1.12E+06
6.72E+03	2.06E+03	2.38E-01	-5.12E-02	1.13E+06
6.72E+03	2.05E+03	2.42E-01	-3.97E-02	1.10E+06
6.72E+03	2.05E+03	2.54E-01	-2.95E-02	1.11E+06
6.72E+03	2.40E+03	2.30E-01	-2.67E-02	1.17E+06
6.72E+03	2.39E+03	2.34E-01	-2.33E-02	1.17E+06
6.72E+03	2.40E+03	2.22E-01	-4.00E-02	1.19E+06
6.72E+03	2.39E+03	2.21E-01	-4.00E-02	1.19E+06

Cont'd

P (kPa)	G (kg/m²s)	Xc	Xin	CHF (w/m²)
6.72E+03	2.39E+03	2.16E-01	-5.32E-02	1.23E+06
6.72E+03	2.40E+03	2.15E-01	-4.99E-02	1.21E+06
6.72E+03	2.40E+03	2.22E-01	-3.67E-02	1.19E+06
6.72E+03	2.05E+03	2.28E-01	-6.75E-02	1.16E+06
6.72E+03	2.05E+03	2.28E-01	-6.58E-02	1.15E+06
6.72E+03	1.71E+03	2.59E-01	-6.80E-02	1.08E+06
6.72E+03	1.71E+03	2.53E-01	-6.68E-02	1.08E+06
6.72E+03	1.38E+03	3.21E-01	-3.48E-02	9.32E+05
6.62E+03	1.37E+03	3.36E-01	-2.27E-02	9.43E+05
6.72E+03	1.37E+03	2.95E-01	-9.30E-02	1.01E+06
6.72E+03	1.37E+03	2.96E-01	-9.11E-02	1.01E+06
6.72E+03	1.03E+03	3.55E-01	-1.04E-01	9.00E+05
6.72E+03	1.03E+03	3.50E-01	-1.03E-01	8.86E+05
6.72E+03	1.03E+03	3.56E-01	-1.04E-01	9.01E+05
6.72E+03	1.03E+03	3.22E-01	-1.57E-01	9.37E+05
6.72E+03	1.03E+03	3.32E-01	-1.61E-01	9.66E+05
6.72E+03	1.03E+03	3.44E-01	-1.60E-01	9.86E+05
6.72E+03	1.03E+03	3.26E-01	-1.58E-01	9.50E+05
6.72E+03	6.85E+02	4.59E-01	-7.58E-02	6.97E+05
6.72E+03	6.85E+02	4.64E-01	-7.58E-02	7.05E+05
6.69E+03	6.89E+02	4.59E-01	-5.23E-02	6.72E+05
6.72E+03	6.85E+02	4.65E-01	-4.99E-02	6.72E+05
6.72E+03	6.85E+02	4.75E-01	-5.15E-02	6.88E+05
6.72E+03	6.84E+02	4.57E-01	-7.44E-02	6.93E+05
6.72E+03	6.84E+02	4.63E-01	-7.42E-02	7.00E+05
6.72E+03	6.84E+02	4.38E-01	-1.04E-01	7.07E+05
6.72E+03	6.84E+02	4.38E-01	-1.06E-01	7.09E+05
6.72E+03	6.81E+02	4.68E-01	-1.06E-01	7.43E+05
6.72E+03	6.81E+02	4.69E-01	-1.06E-01	7.45E+05
6.72E+03	6.80E+02	4.55E-01	-1.30E-01	7.58E+05
6.72E+03	6.80E+02	4.63E-01	-1.30E-01	7.69E+05
6.72E+03	6.80E+02	4.49E-01	-1.32E-01	7.53E+05
6.72E+03	6.80E+02	4.61E-01	-1.32E-01	7.69E+05
6.72E+03	6.80E+02	4.45E-01	-1.61E-01	7.85E+05

Concluded

P (kPa)	G (kg/m²s)	Xc	Xin	CHF (w/m²)
6.72E+03	6.80E+02	4.51E-01	-1.64E-01	7.98E+05
6.72E+03	6.80E+02	4.42E-01	-1.62E-01	7.84E+05
6.72E+03	6.80E+02	4.53E-01	-1.62E-01	7.98E+05
6.72E+03	6.88E+02	4.74E-01	-5.80E-02	6.97E+05
6.72E+03	6.88E+02	4.77E-01	-5.63E-02	6.99E+05
6.72E+03	6.88E+02	4.73E-01	-5.82E-02	6.96E+05
6.72E+03	6.88E+02	4.83E-01	-5.80E-02	7.09E+05
6.76E+03	6.86E+02	4.80E-01	-4.29E-02	6.82E+05
6.76E+03	6.86E+02	5.06E-01	-4.09E-02	7.13E+05
6.72E+03	6.86E+02	4.85E-01	-3.69E-02	6.81E+05
6.72E+03	6.90E+02	4.74E-01	-8.03E-02	7.28E+05
6.72E+03	6.90E+02	4.79E-01	-8.34E-02	7.39E+05
6.72E+03	6.90E+02	4.80E-01	-7.38E-02	7.29E+05
6.72E+03	1.02E+03	3.65E-01	-6.33E-02	8.34E+05
6.72E+03	1.02E+03	3.74E-01	-6.15E-02	8.48E+05
6.72E+03	1.02E+03	3.74E-01	-5.19E-02	8.27E+05
6.79E+03	1.02E+03	3.82E-01	-3.29E-02	8.05E+05
6.72E+03	1.02E+03	3.85E-01	-3.37E-02	8.13E+05
6.76E+03	1.02E+03	3.76E-01	-4.50E-02	8.19E+05
6.76E+03	1.02E+03	3.83E-01	-4.48E-02	8.32E+05
6.72E+03	1.03E+03	3.42E-01	-1.17E-01	9.00E+05

7. Edwards et al.(1965).

RFD: 1.00/0.648/0.565/0.0

P (kPa)	G (kg/m²s)	Xc	Xin	CHF (w/m²)
6.84E+03	7.45E+02	4.10E-01	-1.71E-01	7.52E+05
6.84E+03	7.45E+02	4.06E-01	-1.72E-01	7.48E+05
6.92E+03	7.15E+02	4.55E-01	-7.42E-02	6.52E+05
6.85E+03	7.15E+02	4.55E-01	-7.56E-02	6.55E+05
6.83E+03	7.27E+02	3.92E-01	-2.31E-01	7.86E+05
6.84E+03	7.27E+02	3.99E-01	-2.23E-01	7.86E+05
6.83E+03	1.36E+03	2.62E-01	-1.27E-01	9.24E+05
6.83E+03	1.36E+03	2.62E-01	-1.31E-01	9.28E+05
6.84E+03	1.36E+03	2.90E-01	-8.10E-02	8.71E+05
6.85E+03	1.36E+03	2.90E-01	-7.75E-02	8.66E+05
6.83E+03	1.36E+03	2.56E-01	-1.43E-01	9.39E+05
6.82E+03	1.38E+03	2.36E-01	-1.70E-01	9.72E+05
6.92E+03	1.68E+03	2.56E-01	-6.49E-02	9.36E+05
6.87E+03	1.68E+03	2.54E-01	-7.03E-02	9.43E+05
6.88E+03	1.68E+03	2.13E-01	-1.40E-01	1.04E+06
6.86E+03	1.70E+03	2.25E-01	-1.22E-01	1.02E+06
6.85E+03	1.70E+03	2.32E-01	-1.04E-01	9.89E+05
6.70E+03	2.03E+03	2.41E-01	-3.99E-02	1.00E+06
6.67E+03	2.03E+03	2.32E-01	-5.28E-02	1.02E+06
6.63E+03	2.03E+03	2.10E-01	-9.05E-02	1.07E+06
6.66E+03	2.05E+03	1.96E-01	-1.19E-01	1.13E+06
6.87E+03	2.43E+03	2.13E-01	-4.99E-02	1.09E+06
6.94E+03	2.56E+03	1.96E-01	-5.76E-02	1.12E+06
6.99E+03	1.03E+03	3.60E-01	-6.53E-02	7.50E+05
6.93E+03	1.02E+03	3.62E-01	-7.06E-02	7.59E+05
6.90E+03	1.02E+03	3.28E-01	-1.52E-01	8.11E+05
6.90E+03	1.03E+03	2.99E-01	-2.14E-01	8.64E+05
6.86E+03	7.15E+02	4.87E-01	-9.92E-02	7.21E+05
6.86E+03	7.15E+02	4.88E-01	-9.92E-02	7.22E+05
6.81E+03	7.41E+02	4.50E-01	-1.77E-01	8.05E+05

Cont'd

P (kPa)	G (kg/m²s)	Xc	Xin	CHF (w/m²)
6.81E+03	7.41E+02	4.51E-01	-1.79E-01	8.08E+05
6.81E+03	6.99E+02	4.57E-01	-2.29E-01	8.26E+05
6.83E+03	6.99E+02	4.57E-01	-2.31E-01	8.28E+05
6.86E+03	1.03E+03	3.82E-01	-9.92E-02	8.59E+05
6.85E+03	1.03E+03	3.82E-01	-9.55E-02	8.50E+05
6.75E+03	1.03E+03	3.50E-01	-1.56E-01	9.00E+05
6.81E+03	1.03E+03	3.51E-01	-1.60E-01	9.10E+05
6.79E+03	1.03E+03	3.41E-01	-1.89E-01	9.46E+05
6.79E+03	1.03E+03	3.42E-01	-1.85E-01	9.42E+05
6.90E+03	1.41E+03	3.10E-01	-7.95E-02	9.41E+05
6.83E+03	1.41E+03	3.10E-01	-7.73E-02	9.40E+05
6.83E+03	1.41E+03	2.78E-01	-1.38E-01	1.01E+06
6.83E+03	1.41E+03	2.81E-01	-1.34E-01	1.01E+06
6.83E+03	1.41E+03	2.95E-01	-9.89E-02	9.60E+05
6.79E+03	1.41E+03	2.98E-01	-9.51E-02	9.60E+05
6.76E+03	1.71E+03	2.78E-01	-5.68E-02	1.00E+06
6.79E+03	1.71E+03	2.81E-01	-5.14E-02	9.05E+05
6.79E+03	1.72E+03	2.59E-01	-9.33E-02	1.05E+06
6.84E+03	1.72E+03	2.65E-01	-9.19E-02	1.06E+06
6.83E+03	1.72E+03	2.45E-01	-1.27E-01	1.10E+06
6.83E+03	1.72E+03	2.45E-01	-1.27E-01	1.10E+06
6.83E+03	2.05E+03	2.49E-01	-4.78E-02	1.05E+06
6.79E+03	2.05E+03	2.53E-01	-4.21E-02	1.05E+06
6.83E+03	2.02E+03	2.46E-01	-5.90E-02	1.07E+06
6.81E+03	2.02E+03	2.49E-01	-5.70E-02	1.07E+06
6.77E+03	2.08E+03	2.29E-01	-8.06E-02	1.11E+06
6.77E+03	2.08E+03	2.30E-01	-7.70E-02	1.11E+06
6.80E+03	6.92E+02	5.32E-01	-1.96E-03	6.23E+05
6.80E+03	5.53E+02	5.27E-01	-1.96E-03	6.19E+05
6.81E+03	6.92E+02	5.10E-01	-4.78E-02	6.66E+05
6.83E+03	6.92E+02	5.34E-01	-3.47E-02	6.66E+05
6.83E+03	7.19E+02	4.81E-01	-1.17E-01	7.41E+05
6.87E+03	7.19E+02	4.84E-01	-1.14E-01	7.42E+05
6.82E+03	1.03E+03	4.20E-01	-2.14E-02	7.83E+05

Cont'd

P (kPa)	G (kg/m²s)	Xc	Xin	CHF (w/m²)
6.81E+03	1.04E+03	3.83E-01	-7.54E-02	8.19E+05
6.83E+03	1.04E+03	3.59E-01	-1.20E-01	8.65E+05
6.81E+03	1.03E+03	3.69E-01	-1.04E-01	8.47E+05
6.72E+03	1.36E+03	3.25E-01	-5.85E-02	9.04E+05
6.74E+03	1.36E+03	3.37E-01	-4.01E-02	8.89E+05
6.80E+03	1.37E+03	2.98E-01	-1.09E-01	9.67E+05
6.80E+03	1.37E+03	3.06E-01	-1.02E-01	9.67E+05
6.85E+03	1.36E+03	2.80E-01	-1.52E-01	1.01E+06
6.85E+03	1.36E+03	2.86E-01	-1.47E-01	1.02E+06
6.83E+03	1.71E+03	2.76E-01	-7.91E-02	1.05E+06
6.78E+03	1.72E+03	2.74E-01	-7.70E-02	1.04E+06
6.79E+03	1.71E+03	2.85E-01	-6.07E-02	1.02E+06
6.79E+03	1.72E+03	2.75E-01	-5.88E-02	1.01E+06
6.79E+03	2.03E+03	2.56E-01	-4.96E-02	1.07E+06
6.86E+03	2.03E+03	2.56E-01	-4.61E-02	1.06E+06
6.74E+03	2.01E+03	2.40E-01	-8.58E-02	1.14E+06
6.72E+03	2.02E+03	2.43E-01	-8.21E-02	1.14E+06
6.79E+03	1.72E+03	2.87E-01	-4.02E-02	9.75E+05
6.79E+03	1.72E+03	2.82E-01	-4.40E-02	9.72E+05
6.93E+03	1.71E+03	2.95E-01	-2.54E-02	9.42E+05
6.86E+03	1.70E+03	3.03E-01	-1.37E-02	9.33E+05
6.85E+03	2.02E+03	2.71E-01	-2.14E-02	1.02E+06
6.86E+03	2.01E+03	2.75E-01	-7.85E-03	9.82E+05
6.79E+03	2.44E+03	2.33E-01	-2.70E-02	1.10E+06
6.81E+03	2.44E+03	2.34E-01	-2.51E-02	1.10E+06
6.83E+03	2.43E+03	2.45E-01	-1.17E-02	1.08E+06
6.83E+03	2.43E+03	2.42E-01	-1.17E-02	1.07E+06
6.78E+03	2.82E+02	7.00E-01	-1.73E-01	4.25E+05
6.79E+03	2.67E+02	6.83E-01	-1.29E-01	3.73E+05
6.86E+03	2.73E+02	6.55E-01	-1.19E-01	3.64E+05
6.87E+03	2.78E+02	7.81E-01	-1.76E-02	3.83E+05
6.81E+03	4.75E+02	6.54E-01	-2.51E-02	5.59E+05
6.93E+03	4.77E+02	6.62E-01	-1.18E-02	5.53E+05
6.86E+03	5.09E+02	6.06E-01	-1.33E-01	6.47E+05

Concluded

P (kPa)	G (kg/m²s)	Xc	Xin	CHF (w/m²)
6.85E+03	4.83E+02	6.08E-01	-2.66E-01	7.19E+05
6.86E+03	4.75E+02	6.15E-01	-2.61E-01	7.26E+05
6.90E+03	6.73E+02	4.89E-01	-1.05E-01	6.89E+05
6.83E+03	6.77E+02	4.88E-01	-1.10E-01	6.98E+05
6.90E+03	6.80E+02	4.52E-01	-1.88E-01	7.51E+05
6.90E+03	6.75E+02	4.61E-01	-1.78E-01	7.45E+05

APPENDIX B: The 1995 look-up talbe for critical flux in tubes.

P (kPa)	G (kg/m²s)	Quality -0.5	-0.4	-0.3	-0.2	-0.15	-0.1	-0.1	0	0.05	0.1	0.15	0.2	0.25	0.3	0.35	0.4	0.45	0.5	0.6	0.7	0.8	0.9	1
100	0	6604	5931	5779	5230	4593	3419	2247	1066	421	298	207	158	142	130	120	111	103	99	84	74	68	67	0
100	50	7325	6618	6468	5729	4940	3881	2618	1526	787	754	683	635	620	609	600	591	582	570	513	401	288	253	0
100	100	7920	7193	7039	6140	5206	4124	2942	1947	1159	1137	1123	1107	1093	1084	1078	1070	1060	1037	961	747	550	416	0
100	300	8359	7581	7395	6216	5232	4206	3475	2792	1693	1665	1651	1598	1536	1502	1475	1378	1243	1151	979	751	626	550	0
100	500	8554	7663	7455	6223	5261	4305	3768	3204	2040	1887	1883	1875	1798	1725	1714	1615	1486	1418	1155	752	558	415	0
100	1000	8850	7809	7462	6263	5387	4626	4129	3527	2528	2286	2280	2211	2129	2028	1870	1655	1632	1631	1434	850	428	206	0
100	1500	9417	8302	7563	6292	5432	4734	4216	3606	2652	2427	2405	2292	2195	2084	1905	1857	1856	1856	1597	839	348	109	0
100	2000	10635	9440	8016	6306	5434	4739	4218	3616	2693	2487	2446	2333	2212	2054	1950	1918	1889	1815	1466	674	183	62	0
100	2500	11843	10902	8701	6372	5443	4745	4220	3631	2743	2548	2505	2367	2217	1985	1846	1779	1693	1582	1162	494	80	12	0
100	3000	12864	11763	9397	6497	5452	4751	4239	3651	2795	2606	2572	2418	2245	1941	1738	1596	1472	1315	842	341	61	15	0
100	3500	13813	12522	10017	6666	5504	4827	4277	3662	2843	2652	2624	2470	2282	1937	1684	1449	1264	1059	581	220	70	33	0
100	4000	14726	13194	10671	7016	5660	4908	4310	3688	2947	2727	2685	2530	2327	1960	1638	1316	1098	891	503	239	108	51	0
100	4500	15610	13867	11347	7492	5902	5006	4338	3707	3060	2820	2738	2560	2353	2026	1696	1378	1145	939	591	324	151	71	0
100	5000	16463	14483	11918	7906	6242	5266	4412	3738	3157	2893	2777	2599	2401	2097	1798	1496	1262	1054	693	398	194	92	0
100	5500	17292	15192	12473	8240	6513	5487	4529	3813	3242	2952	2824	2663	2454	2156	1863	1587	1355	1149	776	466	238	113	0
100	6000	18101	15833	13017	8614	6772	5668	4684	3933	3349	3040	2892	2699	2492	2167	1912	1662	1437	1230	853	530	282	135	0
100	6500	18895	16681	13566	8992	7060	5876	4856	4103	3439	3089	2934	2718	2502	2208	1968	1731	1511	1305	925	592	326	157	0
100	7000	19671	17331	14079	9355	7349	6087	5029	4223	3505	3132	2965	2741	2507	2251	2019	1792	1577	1374	993	651	369	179	0
100	7500	20429	17962	14562	9712	7643	6288	5181	4300	3559	3176	2996	2765	2530	2291	2066	1848	1638	1436	1056	708	413	201	0
100	8000	21169	18557	15017	10057	7939	6507	5370	4375	3617	3220	3027	2793	2550	2326	2108	1898	1693	1495	1116	763	458	223	0
300	0	6608	5940	5746	5024	4349	3432	2433	1596	1575	1029	665	467	317	234	194	178	171	170	149	143	143	90	0
300	50	7338	6635	6481	5644	4951	3882	2842	2003	1987	1443	1123	938	813	745	708	686	660	642	601	472	391	300	0
300	100	7980	7239	7099	6174	5211	4235	3225	2431	2076	1574	1291	1258	1230	1211	1190	1168	1118	1081	1026	866	669	473	0
300	300	8373	7593	7461	6403	5447	4544	3889	3371	2433	2095	2071	1995	1895	1828	1771	1636	1494	1447	1203	857	695	564	0
300	500	8561	7677	7508	6414	5498	4667	4234	3832	2863	2479	2435	2333	2185	2072	1869	1700	1539	1463	1188	764	574	521	0
300	1000	8870	7823	7525	6430	5590	4931	4585	4189	3285	2845	2750	2553	2388	2283	1968	1766	1586	1545	1174	677	439	288	0

Cont'd

P (kPa)	G (kg/m²s)	Quality -0.5	-0.4	-0.3	-0.2	-0.15	-0.1	-0.1	0	0.05	0.1	0.15	0.2	0.25	0.3	0.35	0.4	0.45	0.5	0.6	0.7	0.8	0.9	1
300	1500	9431	8302	7605	6438	5610	4985	4609	4209	3339	2922	2834	2618	2424	2301	2021	1924	1615	1525	1103	568	220	131	0
300	2000	10661	9448	8032	6454	5629	4995	4615	4210	3370	2948	2863	2678	2462	2320	2066	1771	1571	1410	1029	490	143	60	0
300	2500	11855	10910	8722	6547	5663	5004	4622	4225	3415	2979	2869	2687	2528	2282	2016	1700	1524	1327	957	407	74	23	0
300	3000	12869	11772	9430	6735	5786	5087	4656	4239	3462	3021	2879	2801	2595	2245	1927	1627	1380	1180	777	333	61	19	0
300	3500	13823	12533	10082	7036	6024	5320	4744	4249	3515	3073	2895	2816	2584	2154	1816	1543	1258	1043	610	264	77	34	0
300	4000	14738	13207	10742	7495	6343	5601	4851	4254	3520	3102	2908	2652	2389	2044	1809	1461	1166	935	545	275	111	51	0
300	4500	15623	13881	11412	8034	6702	5832	4927	4266	3525	3110	2926	2671	2405	2064	1846	1490	1203	978	610	340	152	69	0
300	5000	16476	14503	11994	8435	7062	6098	5000	4275	3530	3141	2959	2703	2432	2116	1867	1577	1303	1088	710	411	191	90	0
300	5500	17305	15210	12558	8809	7372	6360	5090	4277	3536	3178	2988	2730	2482	2156	1914	1667	1402	1187	799	477	237	112	0
300	6000	18115	15851	13102	9216	7692	6645	5211	4287	3543	3194	3003	2762	2510	2238	2025	1742	1488	1273	879	543	283	136	0
300	6500	18909	16700	13639	9605	8015	6908	5346	4308	3577	3229	3029	2792	2554	2291	2073	1809	1565	1351	954	608	329	159	0
300	7000	19683	17350	14151	9975	8325	7175	5592	4450	3642	3268	3058	2823	2587	2337	2115	1868	1634	1422	1024	669	374	182	0
300	7500	20443	17982	14645	10356	8630	7427	5870	4662	3727	3302	3090	2849	2613	2376	2152	1920	1697	1486	1089	728	420	204	0
300	8000	21187	18581	15122	10747	8936	7656	6117	4840	3803	3338	3118	2872	2635	2407	2185	1966	1753	1545	1150	784	465	227	0
500	0	6613	5962	5710	4879	4200	3469	2595	1783	1697	1174	786	535	374	278	226	207	191	183	151	150	149	140	0
500	50	7339	6650	6458	5568	4962	3983	3168	2424	2249	1728	1380	1145	1005	921	865	826	793	754	611	493	476	359	0
500	100	7984	7254	7089	6195	5267	4489	3688	2975	2478	1780	1683	1623	1566	1525	1492	1440	1391	1292	1158	1045	875	539	0
500	300	8381	7602	7468	6589	5783	5098	4547	4089	3396	2921	2801	2679	2527	2409	2050	1799	1552	1489	1188	1049	919	607	0
500	500	8567	7692	7517	6629	5876	5250	4853	4452	3784	3247	3074	2888	2695	2498	2187	1887	1593	1414	959	774	622	554	0
500	1000	8877	7837	7533	6650	5991	5531	5273	4873	4075	3452	3256	2975	2923	2629	2277	1911	1547	1385	962	635	445	301	0
500	1500	9445	8303	7616	6664	5994	5576	5323	4909	4093	3456	3313	3293	3154	2782	2260	1811	1453	1268	911	543	271	232	0
500	2000	10666	9456	8053	6677	6037	5601	5327	4911	4104	3460	3407	3406	3261	2790	2184	1696	1383	1164	852	335	137	65	0
500	2500	11863	10915	8754	6839	6141	5645	5331	4913	4138	3605	3545	3527	3335	2696	1991	1535	1290	1067	605	298	72	29	0
500	3000	12878	11781	9493	7189	6430	5789	5366	4915	4182	3750	3725	3662	3428	2621	1871	1427	1224	963	570	283	61	21	0
500	3500	13835	12543	10196	7654	6789	6006	5430	4939	4271	3726	3712	3652	3350	2426	1700	1330	1214	972	541	271	82	35	0
500	4000	14752	13220	10867	8155	7143	6293	5553	4951	4152	3593	3578	3485	3154	2345	1798	1428	1234	973	555	301	115	51	0
500	4500	15636	13895	11520	8688	7556	6584	5670	4963	4006	3513	3501	3404	3064	2352	1871	1498	1261	1016	624	358	153	68	0
500	5000	16490	14524	12118	9138	7969	6877	5748	4922	3913	3408	3159	2840	2783	2354	1903	1579	1337	1111	719	420	190	88	0
500	5500	17320	15228	12689	9580	8334	7180	5765	4815	3863	3407	3157	2816	2690	2362	1964	1676	1434	1210	810	482	235	111	0
500	6000	18130	15869	13234	10022	8690	7517	5754	4632	3880	3494	3361	3079	2727	2371	2025	1767	1519	1300	893	548	282	135	0
500	6500	18923	16718	13768	10439	9036	7799	5735	4402	3899	3494	3368	3093	2749	2389	2084	1837	1599	1379	971	615	330	159	0
500	7000	19697	17368	14281	10822	9366	8112	6026	4577	3945	3496	3388	3096	2791	2408	2147	1901	1670	1451	1042	678	376	182	0

Cont'd

P (kPa)	G (kg/m²s)	Quality -0.5	-0.4	-0.3	-0.2	-0.15	-0.1	-0.1	0	0.05	0.1	0.15	0.2	0.25	0.3	0.35	0.4	0.45	0.5	0.6	0.7	0.8	0.9	1
500	7500	20458	18003	14780	11192	9675	8411	6441	4962	3964	3498	3409	3116	2811	2426	2190	1958	1734	1517	1109	738	423	206	0
500	8000	21205	18606	15269	11571	9969	8642	6746	5268	3985	3518	3428	3135	2832	2463	2236	2010	1791	1577	1171	795	469	229	0
1000	0	6627	6028	5619	4685	4058	3564	2859	2175	1910	1438	1030	717	519	389	312	286	270	256	198	188	181	175	0
1000	50	7360	6691	6371	5523	4991	4436	3928	3323	2944	2469	2071	1752	1559	1414	1307	1230	1157	1076	876	806	804	768	0
1000	100	7975	7260	6981	6252	5685	5281	4851	4268	3386	2799	2651	2531	2415	2292	2184	2041	1891	1708	1312	1291	1250	732	0
1000	300	8422	7597	7492	7295	7089	6901	6766	6620	6215	5289	4760	4456	4120	3856	2851	2151	1924	1703	1343	1289	1215	660	0
1000	500	8611	7678	7577	7464	7327	7177	7110	7048	6818	5771	5094	4660	4233	3432	2754	2284	1979	1659	1035	825	767	589	0
1000	1000	8910	7788	7594	7466	7329	7192	7124	7022	6705	5694	5042	4634	3953	3264	2670	2035	1741	1516	958	592	452	338	0
1000	1500	9484	8304	7700	7468	7349	7230	7153	7013	6604	5532	4989	4422	3952	3236	2429	1557	1145	930	637	411	370	266	0
1000	2000	10673	9478	8187	7552	7424	7281	7192	7012	6401	5196	4720	4404	3952	3143	2259	1373	980	713	541	306	130	86	0
1000	2500	11889	10920	8962	7788	7544	7314	7202	6979	6237	5028	4668	4397	3924	2999	2081	1281	925	690	512	343	95	36	0
1000	3000	12905	11805	9731	8149	7728	7370	7206	6966	6154	4920	4647	4391	3898	2880	1955	1234	908	701	567	349	84	25	0
1000	3500	13861	12571	10456	8659	8005	7450	7179	6910	6049	4849	4628	4385	3865	2765	1797	1252	1059	1020	595	356	108	36	0
1000	4000	14783	13251	11146	9203	8342	7591	7143	6778	5752	4757	4584	4380	3794	2723	1891	1410	1292	1021	605	375	134	51	0
1000	4500	15675	13932	11816	9746	8754	7750	7141	6715	5537	4627	4477	4304	3715	2689	1953	1483	1327	1034	643	401	159	65	0
1000	5000	16537	14574	12447	10239	9182	7859	6988	6412	5107	4361	4211	3924	3338	2581	1978	1576	1363	1126	726	438	188	83	0
1000	5500	17373	15273	13033	10745	9599	8124	6794	5995	4822	4239	4085	3729	3112	2523	2017	1703	1469	1235	816	484	227	104	0
1000	6000	18184	15915	13573	11285	10064	8595	6647	5530	4654	4096	3966	3625	3050	2519	2063	1760	1555	1325	902	546	275	129	0
1000	6500	18979	16766	14101	11770	10479	8933	6351	5228	4460	3913	3804	3484	2973	2497	2115	1852	1633	1406	983	616	326	155	0
1000	7000	19755	17416	14608	12172	10857	9325	6654	4850	4232	3734	3721	3336	2867	2461	2178	1945	1707	1480	1057	681	375	180	0
1000	7500	20521	18055	15109	12524	11194	9725	7272	5409	4227	3683	3525	3287	2851	2478	2246	2006	1774	1548	1126	744	423	204	0
1000	8000	21279	18668	15629	12866	11463	9958	7773	6039	4447	3684	3536	3341	2837	2571	2306	2062	1834	1612	1190	802	470	227	0
3000	0	6583	5927	5252	4544	4205	3891	3536	3022	2429	2009	1564	1145	892	699	568	502	452	413	321	275	266	256	0
3000	50	7307	6575	5972	5386	5107	4857	4570	4135	3478	3061	2653	2266	2041	1865	1722	1614	1521	1418	1409	1400	1392	1076	0
3000	100	7888	7106	6580	6114	5897	5708	5479	5057	4121	3502	3326	3186	3051	2926	2796	2625	2475	2367	2191	1936	1587	1015	0
3000	300	8356	7476	7307	7303	7302	7300	7298	7255	6954	5922	5380	5211	4936	4635	4297	3322	3177	3173	2865	2078	1536	953	0
3000	500	8548	7674	7660	7647	7640	7634	7627	7621	7496	6486	5883	5620	5269	4807	3997	3392	3376	3324	2745	1841	1320	835	0
3000	1000	8851	7776	7578	7560	7560	7560	7518	7512	7444	6846	6208	5660	4728	4200	3745	3079	2910	2618	1925	1242	830	471	0
3000	1500	9464	8313	7824	7598	7554	7541	7471	7436	7250	6661	5980	5043	4364	3792	3422	2691	2130	1728	1080	626	499	312	0
3000	2000	10640	9563	8427	7706	7578	7548	7453	7298	6723	6026	5315	4507	3991	3485	2958	2279	1686	1211	608	373	330	216	0
3000	2500	11851	10928	9397	8034	7681	7567	7441	7158	6226	5599	4880	4175	3702	3152	2369	1726	1301	921	431	313	137	45	0

Cont'd

P (kPa)	G (kg/m²s)	Quality -0.5	-0.4	-0.3	-0.2	-0.15	-0.1	-0.1	0	0.05	0.1	0.15	0.2	0.25	0.3	0.35	0.4	0.45	0.5	0.6	0.7	0.8	0.9	1
3000	3000	12854	11900	10414	8640	7947	7643	7439	7069	5966	5339	4712	4094	3619	2963	2024	1423	1037	772	473	420	89	25	0
3000	3500	13809	12661	11230	9396	8434	7824	7437	6995	5829	5131	4586	4067	3540	2705	1715	1329	1127	1000	678	431	129	44	0
3000	4000	14738	13379	11939	10174	9013	8028	7418	6832	5753	4966	4471	4021	3424	2463	1474	1234	1228	1118	699	440	147	54	0
3000	4500	15629	14077	12608	10862	9586	8292	7365	6566	5570	4792	4348	3945	3273	2302	1514	1311	1306	1145	713	445	163	63	0
3000	5000	16488	14778	13200	11500	10262	8818	7348	6039	5258	4610	4242	3867	3121	2196	1610	1505	1405	1173	786	472	179	72	0
3000	5500	17322	15454	13765	12044	10824	9249	7402	6188	5134	4431	4136	3794	3006	2155	1712	1650	1500	1252	846	493	197	83	0
3000	6000	18136	16101	14321	12489	11252	9513	7735	6382	5070	4332	4061	3753	3042	2265	1853	1738	1590	1342	906	532	234	103	0
3000	6500	18929	16742	14849	12926	11673	9813	7950	6446	5002	4181	3931	3693	3067	2360	2043	1869	1678	1432	982	589	282	129	0
3000	7000	19703	17385	15350	13332	12053	10197	8005	6507	4694	3888	3705	3557	3084	2465	2209	2008	1755	1514	1062	656	333	155	0
3000	7500	20460	18013	15834	13724	12429	10666	8448	6526	4644	3817	3643	3459	3103	2571	2315	2073	1825	1588	1138	724	385	181	0
3000	8000	21200	18629	16299	14090	12789	11196	9144	7075	4971	3839	3645	3548	3291	2862	2413	2112	1885	1654	1205	787	437	207	0
5000	0	5951	5460	4941	4459	4230	4011	3762	3360	2628	2234	1791	1346	1083	877	731	638	571	515	405	345	341	323	0
5000	50	6644	6095	5629	5224	5030	4840	4626	4294	3606	3225	2837	2450	2224	2047	1896	1774	1666	1553	1532	1512	945	830	0
5000	100	7234	6636	6223	5891	5734	5573	5387	5065	4165	3609	3458	3315	3174	3061	2936	2803	2655	2476	2300	2148	1757	1039	0
5000	300	7680	6990	6769	6737	6722	6686	6677	6619	6280	5401	5007	4907	4741	4509	4249	4061	3786	3283	2973	2543	1823	1083	0
5000	500	7918	7164	6943	6900	6882	6829	6812	6739	6395	5662	5289	5178	5027	4588	4244	3812	3707	3503	3040	2459	1769	1061	0
5000	1000	8364	7454	7171	7014	6944	6819	6743	6595	6107	5734	5296	4957	4676	4166	3759	3447	3263	2964	2066	1433	1034	763	0
5000	1500	9068	8009	7470	7142	7025	6859	6707	6441	5779	5317	4899	4530	4074	3623	3337	2983	2569	2134	1194	913	899	744	0
5000	2000	10362	9287	8159	7346	7139	6944	6593	6110	5262	4779	4405	3984	3610	3206	2865	2557	1973	1332	668	650	650	526	0
5000	2500	11531	10599	9179	7837	7458	7195	6565	5849	4915	4515	3981	3594	3401	3067	2474	1861	1252	867	401	308	132	53	0
5000	3000	12458	11530	10191	8483	7761	7353	6543	5664	4750	4321	3782	3428	3268	2855	2085	1406	948	793	584	374	117	37	0
5000	3500	13348	12271	10990	9196	8178	7551	6527	5421	4581	4144	3693	3380	3109	2510	1688	1195	958	874	645	441	149	55	0
5000	4000	14214	12958	11651	9917	8669	7764	6476	5139	4421	3916	3540	3317	2945	2221	1437	1140	1108	1049	688	441	151	58	0
5000	4500	15045	13625	12254	10566	9102	7980	6502	5044	4317	3784	3457	3260	2799	2059	1425	1247	1242	1187	734	453	155	61	0
5000	5000	15844	14283	12804	11186	9669	8443	6655	4986	4255	3723	3454	3251	2745	1990	1470	1385	1383	1205	766	466	164	66	0
5000	5500	16626	14896	13352	11741	10379	8952	6807	5334	4253	3656	3421	3240	2717	1992	1583	1504	1459	1234	804	481	182	76	0
5000	6000	17388	15495	13856	12319	11313	9818	7558	5744	4314	3627	3415	3239	2688	2091	1812	1679	1529	1296	850	500	211	94	0
5000	6500	18126	16100	14340	12662	11743	10343	8118	5954	4356	3613	3397	3235	2711	2303	2034	1876	1611	1370	913	531	239	110	0
5000	7000	18845	16707	14796	12961	11971	10647	8504	6049	4363	3603	3445	3291	2801	2349	2242	1951	1689	1444	989	592	282	130	0
5000	7500	19549	17296	15245	13320	12236	10989	8865	6189	4478	3749	3547	3350	3051	2667	2329	2021	1764	1519	1064	656	328	154	0
5000	8000	20238	17880	15671	13711	12701	11561	9419	6556	4717	3975	3695	3482	3290	2882	2405	2074	1829	1588	1130	717	379	178	0

Cont'd

P (kPa)	G (kg/m²s)	Quality -0.5	-0.4	-0.3	-0.2	-0.15	-0.1	-0.1	0	0.05	0.1	0.15	0.2	0.25	0.3	0.35	0.4	0.45	0.5	0.6	0.7	0.8	0.9	1
6000	0	5626	5219	4798	4387	4185	3995	3777	3415	2669	2291	1859	1416	1150	941	787	686	608	547	439	348	344	327	0
6000	50	6300	5838	5443	5092	4920	4760	4575	4272	3564	3191	2812	2431	2204	2023	1871	1749	1645	1537	1229	989	942	823	0
6000	100	6873	6366	5999	5708	5567	5434	5273	4973	4079	3530	3377	3237	3089	2966	2854	2724	2598	2431	1833	1647	1511	1067	0
6000	300	7318	6710	6451	6395	6379	6330	6316	6261	5942	5126	4783	4679	4496	4269	4077	3881	3659	3315	2663	2330	1766	1179	0
6000	500	7573	6883	6586	6512	6480	6364	6310	6255	5978	5371	5005	4822	4683	4333	4066	3975	3803	3468	2874	2374	1636	1118	0
6000	1000	8080	7185	6742	6576	6502	6256	6114	6008	5633	5334	4857	4429	4177	3788	3528	3418	3322	3086	1965	1257	803	735	0
6000	1500	8817	7758	7023	6667	6585	6331	6146	5787	5138	4703	4326	3964	3637	3309	3056	2839	2550	2068	1029	785	714	707	0
6000	2000	10109	9053	7842	6970	6796	6559	6167	5531	4716	4227	3875	3532	3229	2919	2640	2383	1789	1096	532	518	439	435	0
6000	2500	11237	10324	8947	7698	7356	7038	6235	5383	4543	4030	3545	3244	3054	2797	2311	1632	930	519	370	305	107	52	0
6000	3000	12123	11219	9913	8360	7693	7264	6241	5237	4449	3882	3340	3043	2876	2560	1887	1093	571	477	472	353	122	52	0
6000	3500	12969	11949	10669	8979	7986	7458	6243	4962	4218	3651	3219	2961	2696	2235	1522	871	582	576	505	382	145	57	0
6000	4000	13791	12626	11288	9594	8324	7679	6245	4590	3787	3318	3038	2893	2570	1995	1376	988	952	952	580	384	146	59	0
6000	4500	14582	13274	11857	10119	8549	7682	6247	4578	3624	3133	2922	2814	2470	1863	1358	1154	1133	1124	622	386	147	60	0
6000	5000	15341	13920	12372	10555	8820	7811	6336	4701	3674	3115	2918	2795	2432	1792	1319	1237	1235	1130	650	390	148	64	0
6000	5500	16091	14489	12910	11165	9671	8416	6533	4793	3751	3148	2936	2816	2475	1877	1459	1363	1345	1149	698	411	167	74	0
6000	6000	16823	15039	13396	12151	11312	10207	7356	5118	3824	3169	2946	2843	2506	2049	1755	1621	1405	1192	756	438	196	90	0
6000	6500	17524	15635	13826	12525	11906	11101	8043	5370	3900	3211	2979	2886	2586	2247	2026	1760	1468	1250	818	472	223	105	0
6000	7000	18210	16212	14268	12743	11972	11239	8585	5556	4010	3305	3095	2988	2795	2492	2169	1822	1545	1314	887	528	260	123	0
6000	7500	18884	16771	14706	13013	12063	11299	8839	5779	4287	3660	3411	3187	2980	2635	2268	1901	1632	1394	960	587	299	142	0
6000	8000	19548	17309	15140	13347	12447	11537	9157	6019	4481	3966	3675	3423	3262	2860	2359	1981	1717	1479	1034	646	341	162	0
7000	0	5361	5010	4651	4293	4118	3954	3762	3426	2692	2336	1918	1485	1212	996	834	723	641	575	466	369	357	339	0
7000	50	6002	5599	5236	4926	4778	4644	4483	4198	3498	3137	2769	2397	2165	1981	1826	1706	1604	1501	1200	984	940	774	0
7000	100	6539	6094	5738	5474	5355	5245	5105	4818	3957	3401	3239	3093	2941	2820	2707	2595	2489	2302	1710	1515	1479	1097	0
7000	300	6998	6441	6104	6015	6002	5953	5940	5887	5582	4834	4494	4247	4046	3862	3632	3430	3318	3065	2402	2144	1735	1215	0
7000	500	7264	6617	6233	6123	6088	5947	5886	5865	5690	5134	4682	4316	4157	3900	3634	3469	3366	3157	2596	2213	1587	1029	0
7000	1000	7798	6930	6386	6216	6135	5799	5604	5505	5318	5070	4472	3892	3626	3347	3136	3031	3028	2838	1774	1121	735	613	0
7000	1500	8557	7520	6715	6339	6253	5886	5603	5145	4673	4301	3874	3486	3189	2964	2735	2523	2250	1728	805	488	273	259	0
7000	2000	9793	8774	7597	6676	6480	6142	5684	4952	4275	3785	3407	3122	2890	2731	2451	2023	1445	844	432	322	196	190	0
7000	2500	10882	9986	8709	7496	7142	6690	5806	4876	4104	3537	3147	2922	2723	2445	1983	1367	789	424	261	204	99	52	0
7000	3000	11730	10850	9620	8170	7523	6953	5816	4724	3981	3369	2940	2714	2491	2133	1570	967	553	425	346	263	112	51	0
7000	3500	12535	11558	10344	8740	7757	7135	5848	4567	3834	3199	2786	2565	2294	1896	1323	782	519	490	409	317	135	57	0
7000	4000	13317	12216	10929	9320	8041	7398	5938	4372	3469	2928	2645	2490	2201	1730	1228	840	734	732	470	317	136	58	0

Cont'd

P (kPa)	G (kg/m²s)	Quality -0.5	-0.4	-0.3	-0.2	-0.15	-0.1	-0.1	0	0.05	0.1	0.15	0.2	0.25	0.3	0.35	0.4	0.45	0.5	0.6	0.7	0.8	0.9	1
7000	4500	14070	12839	11469	9769	8188	7399	6061	4410	3347	2743	2515	2418	2139	1640	1200	930	872	854	492	317	137	59	0
7000	5000	14792	13465	11954	10124	8354	7427	6225	4552	3378	2696	2471	2380	2105	1591	1193	1010	995	888	521	326	138	63	0
7000	5500	15509	14000	12474	10713	9223	8025	6409	4682	3454	2710	2458	2382	2146	1673	1308	1154	1102	952	582	345	153	70	0
7000	6000	16208	14521	12931	11840	11049	10108	7226	4752	3483	2714	2470	2415	2213	1840	1539	1385	1228	1032	655	379	179	84	0
7000	6500	16875	15091	13336	12214	11696	11181	7804	4867	3535	2784	2519	2466	2330	2140	1879	1599	1311	1108	725	422	210	99	0
7000	7000	17529	15640	13763	12432	11718	11183	8065	5055	3745	3006	2708	2595	2464	2260	2014	1687	1401	1186	795	476	243	116	0
7000	7500	18170	16174	14182	12682	11740	11185	8202	5208	3974	3339	3032	2913	2779	2541	2199	1773	1489	1269	866	530	277	132	0
7000	8000	18806	16673	14610	12995	12067	11187	8424	5405	4172	3727	3483	3384	3259	2846	2288	1851	1576	1353	936	581	312	149	0
8000	0	5101	4795	4484	4175	4022	3883	3716	3403	2547	2044	1674	1295	1195	994	838	731	653	591	542	456	423	364	0
8000	50	5714	5359	5025	4744	4615	4503	4362	4081	3170	2622	2374	2169	2006	1871	1761	1667	1579	1490	1183	980	938	720	0
8000	100	6229	5834	5487	5235	5132	5039	4916	4650	3796	3239	3086	2969	2837	2708	2601	2507	2417	2281	1678	1457	1449	1087	0
8000	300	6685	6179	5792	5654	5637	5605	5597	5544	5250	4549	4207	3911	3759	3642	3458	3328	3212	2893	2068	1858	1538	1193	0
8000	500	6958	6354	5920	5763	5718	5577	5512	5484	5324	4784	4306	3829	3583	3411	3248	3096	2964	2629	2144	1877	1427	917	0
8000	1000	7518	6668	6144	5919	5765	5314	5072	5040	4997	4755	4106	3452	3103	2847	2749	2560	2331	2069	1413	944	554	511	0
8000	1500	8280	7266	6556	6124	5911	5334	5042	4774	4459	4066	3562	3137	2863	2639	2355	2001	1661	1209	643	364	205	195	0
8000	2000	9465	8470	7416	6490	6179	5626	5178	4623	4015	3483	3039	2749	2551	2345	2014	1559	1068	656	388	250	154	134	0
8000	2500	10508	9633	8457	7323	6937	6335	5386	4575	3816	3144	2769	2551	2319	1899	1514	1099	655	396	237	178	96	49	0
8000	3000	11320	10465	9316	7976	7376	6702	5426	4348	3609	2906	2535	2340	2093	1694	1253	811	524	397	307	225	111	50	0
8000	3500	12091	11136	10017	8489	7576	6794	5461	4205	3479	2798	2381	2179	1947	1616	1128	696	501	470	385	258	122	55	0
8000	4000	12839	11763	10584	9021	7836	7014	5626	4145	3241	2592	2238	2084	1893	1528	1063	702	603	577	401	258	122	56	0
8000	4500	13559	12361	11093	9494	8078	7215	5921	4248	3137	2420	2116	2037	1867	1475	1066	783	738	676	425	259	122	57	0
8000	5000	14251	12945	11568	9938	8351	7424	6106	4394	3169	2403	2120	2031	1821	1450	1147	923	859	756	470	275	125	59	0
8000	5500	14934	13466	12056	10488	9083	7990	6213	4479	3283	2478	2177	2070	1878	1570	1277	1071	988	850	535	304	139	65	0
8000	6000	15597	13983	12477	11434	10721	9893	6851	4526	3352	2510	2237	2159	1998	1721	1519	1256	1136	938	607	346	165	77	0
8000	6500	16235	14521	12879	11791	11200	10540	7172	4629	3419	2556	2432	2391	2207	2027	1794	1514	1225	1025	678	396	197	93	0
8000	7000	16859	15043	13288	12019	11214	10542	7253	4766	3593	2843	2558	2466	2287	2179	1832	1585	1316	1111	747	447	228	108	0
8000	7500	17470	15550	13689	12260	11235	10544	7292	4874	3748	3136	2935	2820	2611	2287	1980	1654	1402	1193	814	498	260	124	0
8000	8000	18075	16026	14098	12584	11555	10546	7482	4967	3931	3490	3380	3376	3257	2798	2157	1718	1479	1272	881	548	295	140	0
9000	0	4836	4571	4301	4034	3902	3783	3639	3352	2503	1977	1637	1290	1179	992	843	739	660	608	560	471	431	349	0
9000	50	5422	5114	4813	4547	4432	4335	4213	3960	3071	2528	2304	2110	1945	1810	1699	1610	1536	1457	1152	971	938	650	0
9000	100	5916	5571	5251	4988	4892	4811	4704	4462	3658	3134	2976	2841	2697	2575	2458	2373	2317	2165	1554	1306	1300	1067	0

Cont'd

P (kPa)	G (kg/m²s)	Quality -0.5	-0.4	-0.3	-0.2	-0.15	-0.1	-0.1	0	0.05	0.1	0.15	0.2	0.25	0.3	0.35	0.4	0.45	0.5	0.6	0.7	0.8	0.9	1
9000	300	6366	5916	5527	5300	5260	5239	5236	5194	4925	4243	3692	3478	3344	3257	3065	2894	2713	2334	1672	1380	1197	899	0
9000	500	6641	6100	5668	5412	5332	5205	5147	5114	4944	4270	3625	3364	3160	2999	2887	2741	2351	1983	1583	1282	904	626	0
9000	1000	7221	6432	5947	5625	5398	4936	4705	4703	4697	4204	3520	3118	2854	2661	2545	2118	1553	1143	984	729	346	311	0
9000	1500	7976	7023	6356	5856	5535	4958	4693	4467	4189	3730	3227	2850	2712	2495	2034	1429	1081	892	546	350	131	119	0
9000	2000	9111	8171	7160	6258	5863	5299	4835	4196	3569	3097	2746	2448	2312	1931	1428	1027	745	603	345	186	97	48	0
9000	2500	10108	9252	8185	7162	6749	6025	5004	4119	3339	2797	2521	2241	1942	1373	1028	809	570	348	211	136	96	48	0
9000	3000	10887	10041	8998	7755	7210	6399	5097	4045	3240	2604	2289	2038	1724	1276	952	708	508	393	282	169	103	49	0
9000	3500	11622	10683	9660	8227	7395	6453	5140	3995	3155	2487	2124	1896	1643	1354	967	650	457	419	305	184	107	54	0
9000	4000	12336	11283	10200	8756	7669	6674	5266	3983	3066	2349	1931	1750	1604	1375	982	664	558	499	331	190	108	55	0
9000	4500	13022	11857	10680	9235	7924	6936	5469	4047	3026	2249	1827	1719	1631	1385	1037	771	670	615	381	205	109	56	0
9000	5000	13683	12418	11127	9685	8259	7305	5645	4183	3080	2245	1836	1755	1663	1416	1152	908	816	717	445	239	116	57	0
9000	5500	14332	12927	11580	10180	8872	7818	5764	4272	3210	2355	1963	1856	1760	1542	1334	1076	935	801	512	281	130	62	0
9000	6000	14961	13402	11998	10989	10217	9236	6149	4331	3303	2421	2126	2045	1937	1699	1500	1219	1072	892	578	329	157	73	0
9000	6500	15570	13909	12387	11336	10646	9735	6353	4416	3344	2492	2346	2317	2197	1985	1710	1431	1170	977	646	378	186	88	0
9000	7000	16165	14403	12779	11578	10702	9737	6355	4542	3482	2788	2527	2402	2245	2070	1785	1497	1258	1058	712	426	216	103	0
9000	7500	16748	14881	13166	11824	10747	9739	6394	4637	3660	3076	2877	2745	2567	2142	1800	1557	1339	1140	778	475	248	118	0
9000	8000	17323	15340	13551	12107	10954	9741	6556	4714	3838	3419	3342	3299	3162	2736	2042	1620	1420	1218	842	525	281	134	0
10000	0	4568	4337	4103	3874	3760	3658	3534	3274	2464	1922	1596	1276	1163	991	849	748	680	625	562	474	410	282	0
10000	50	5126	4857	4591	4336	4230	4146	4040	3814	3002	2482	2256	2057	1890	1750	1641	1555	1482	1415	1139	965	886	645	0
10000	100	5597	5296	5007	4734	4637	4565	4472	4253	3512	3015	2865	2728	2582	2457	2347	2266	2213	2105	1551	1296	1211	897	0
10000	300	6039	5642	5266	4961	4891	4870	4868	4832	4599	4016	3506	3393	3315	3233	2987	2781	2593	2240	1383	1076	1021	674	0
10000	500	6318	5831	5417	5074	4965	4855	4800	4765	4636	4013	3353	3165	3038	2871	2644	2239	2002	1651	1137	848	796	522	0
10000	1000	6912	6184	5732	5328	5073	4676	4463	4376	4328	3822	3225	2936	2680	2484	2171	1342	1033	802	636	460	298	250	0
10000	1500	7650	6747	6118	5570	5212	4712	4476	4178	3843	3402	2958	2559	2393	2102	1655	938	647	547	451	253	127	86	0
10000	2000	8720	7826	6896	6030	5591	5000	4575	3974	3349	2872	2468	2106	1912	1402	972	677	480	355	303	155	95	46	0
10000	2500	9664	8829	7895	7010	6589	5726	4678	3901	3191	2623	2258	1901	1601	1035	666	533	399	280	195	126	95	47	0
10000	3000	10400	9580	8648	7587	7077	6149	4779	3891	3089	2444	2030	1701	1419	1001	647	478	388	300	256	147	97	48	0
10000	3500	11099	10200	9259	8008	7253	6254	4797	3830	3005	2327	1877	1591	1361	1062	723	525	414	364	274	151	99	51	0
10000	4000	11783	10775	9774	8533	7582	6503	4841	3728	2909	2178	1686	1470	1345	1147	870	641	492	429	291	160	101	53	0
10000	4500	12444	11327	10230	8989	7824	6787	4940	3754	2892	2088	1605	1476	1410	1262	1016	768	590	545	359	188	105	54	0
10000	5000	13081	11867	10655	9402	8114	7092	5116	3898	2977	2087	1612	1562	1539	1383	1130	876	686	639	430	229	112	56	0
10000	5500	13694	12355	11078	9834	8616	7476	5265	4034	3114	2208	1742	1692	1663	1496	1261	993	796	703	490	274	126	59	0

Cont'd

P (kPa)	G (kg/m²s)	Quality -0.5	-0.4	-0.3	-0.2	-0.15	-0.1	-0.1	0	0.05	0.1	0.15	0.2	0.25	0.3	0.35	0.4	0.45	0.5	0.6	0.7	0.8	0.9	1
10000	6000	14268	12772	11467	10502	9695	8551	5687	4147	3227	2286	1927	1902	1821	1641	1440	1183	993	842	553	317	150	70	0
10000	6500	14835	13236	11837	10808	10067	8972	5912	4241	3275	2378	2206	2200	2098	1895	1687	1382	1133	942	620	363	179	85	0
10000	7000	15399	13708	12204	11028	10083	8975	5926	4267	3390	2707	2422	2309	2182	2003	1720	1432	1212	1021	686	410	208	99	0
10000	7500	15952	14166	12567	11253	10103	8977	5940	4279	3559	2995	2729	2594	2483	2092	1733	1484	1287	1097	750	459	240	114	0
10000	8000	16496	14588	12938	11536	10351	8979	5955	4484	3783	3325	3120	2988	2864	2621	2015	1596	1393	1182	812	507	272	129	0
11000	0	4294	4095	3891	3694	3599	3513	3407	3175	2437	1880	1560	1270	1146	989	854	757	693	643	565	493	389	267	0
11000	50	4821	4588	4356	4124	4017	3938	3844	3646	2917	2416	2184	1985	1820	1673	1579	1510	1451	1375	1101	938	837	565	0
11000	100	5267	5006	4752	4492	4379	4303	4217	4027	3358	2892	2727	2589	2441	2299	2230	2182	2146	2048	1471	1039	960	741	0
11000	300	5694	5346	5002	4672	4560	4516	4505	4452	4218	3709	3392	3301	3207	2996	2872	2516	2259	1687	1316	963	652	548	0
11000	500	5966	5534	5145	4765	4640	4526	4468	4393	4236	3706	3250	3083	2957	2761	2395	1926	1663	1311	959	728	550	344	0
11000	1000	6553	5906	5430	4911	4665	4365	4197	4035	3837	3389	2981	2693	2389	2153	1682	919	791	696	477	363	245	189	0
11000	1500	7281	6484	5794	5105	4739	4389	4171	3806	3390	2982	2564	2201	1934	1567	1212	675	458	361	295	209	124	65	0
11000	2000	8285	7469	6600	5732	5270	4675	4221	3695	3122	2619	2195	1772	1484	972	738	554	345	305	228	135	94	46	0
11000	2500	9166	8371	7589	6807	6361	5371	4332	3676	3005	2461	1970	1537	1265	818	529	399	283	241	192	115	90	47	0
11000	3000	9861	9055	8268	7343	6854	5785	4446	3668	2920	2257	1695	1311	1109	802	457	322	277	276	237	126	90	48	0
11000	3500	10518	9636	8798	7680	7019	5939	4491	3619	2843	2127	1570	1251	1101	820	524	407	349	331	247	129	92	49	0
11000	4000	11153	10169	9265	8151	7358	6242	4605	3503	2765	2004	1476	1266	1160	962	733	572	434	359	274	151	97	50	0
11000	4500	11765	10675	9696	8592	7672	6551	4757	3566	2761	1952	1471	1336	1256	1133	922	699	489	408	338	186	104	51	0
11000	5000	12351	11158	10092	8934	7863	6753	4892	3707	2890	1999	1540	1491	1440	1299	1057	804	549	462	397	226	112	53	0
11000	5500	12922	11622	10478	9284	8203	7035	5020	3849	2985	2108	1677	1645	1578	1416	1181	936	664	534	450	272	126	57	0
11000	6000	13495	12064	10871	9904	9138	7915	5414	4024	3128	2210	1846	1823	1716	1518	1326	1115	920	780	529	307	146	68	0
11000	6500	14034	12509	11220	10197	9477	8290	5637	4157	3262	2360	2118	2112	2032	1743	1521	1302	1104	922	602	351	173	82	0
11000	7000	14562	12953	11560	10403	9509	8328	5655	4188	3347	2669	2349	2256	2110	1824	1591	1390	1178	994	666	399	203	97	0
11000	7500	15082	13381	11899	10634	9563	8334	5673	4209	3497	2915	2635	2511	2375	2020	1689	1451	1248	1061	729	447	233	111	0
11000	8000	15594	13784	12241	10923	9825	8435	5692	4231	3680	3152	2836	2703	2634	2467	1976	1595	1383	1159	790	493	265	126	0
12000	0	4022	3849	3671	3501	3419	3349	3259	3053	2397	1859	1535	1258	1130	988	859	766	706	660	565	494	376	224	0
12000	50	4511	4309	4111	3909	3809	3729	3634	3462	2826	2360	2111	1910	1745	1598	1505	1436	1383	1309	1069	933	818	507	0
12000	100	4924	4699	4488	4261	4147	4058	3957	3791	3213	2789	2599	2447	2293	2152	2088	2036	2008	1916	1415	985	946	708	0
12000	300	5311	5011	4728	4435	4300	4239	4176	4057	3775	3401	3187	3099	2966	2695	2591	2227	2034	1389	1132	820	636	545	0
12000	500	5533	5172	4848	4489	4333	4185	4097	3919	3659	3254	3004	2866	2685	2402	2057	1673	1341	940	716	537	263	228	0
12000	1000	6063	5518	5083	4467	4119	3776	3577	3372	3118	2733	2496	2232	1947	1675	1318	815	619	514	338	262	128	96	0

Cont'd

P (kPa)	G (kg/m²s)	Quality -0.5	-0.4	-0.3	-0.2	-0.15	-0.1	-0.1	0	0.05	0.1	0.15	0.2	0.25	0.3	0.35	0.4	0.45	0.5	0.6	0.7	0.8	0.9	1
12000	1500	6852	6169	5458	4626	4129	3854	3569	3177	2823	2464	2101	1764	1474	1094	793	536	408	320	235	175	114	54	0
12000	2000	7804	7104	6246	5206	4596	4089	3659	3172	2712	2281	1898	1497	1168	747	568	474	345	257	221	119	91	44	0
12000	2500	8606	7926	7227	6161	5502	4523	3768	3225	2688	2203	1707	1262	949	640	457	363	275	221	176	107	87	44	0
12000	3000	9263	8483	7798	6682	6060	4884	3885	3274	2659	2064	1477	1064	850	620	402	310	263	253	209	113	87	48	0
12000	3500	9873	8929	8209	7076	6416	5166	4024	3319	2654	1983	1395	1053	900	682	462	364	335	309	220	116	88	49	0
12000	4000	10395	9339	8589	7553	6877	5668	4293	3390	2687	1935	1384	1160	1050	882	687	559	419	342	260	145	94	50	0
12000	4500	10866	9735	8953	7997	7296	6103	4504	3487	2735	1952	1450	1285	1188	1067	874	684	462	363	318	181	101	51	0
12000	5000	11303	10049	9228	8306	7473	6374	4628	3605	2874	2068	1598	1465	1359	1211	995	777	510	403	376	226	109	52	0
12000	5500	11820	10479	9563	8588	7674	6576	4720	3697	2952	2165	1738	1625	1501	1343	1135	914	633	473	424	265	123	55	0
12000	6000	12614	11227	10153	9221	8470	7252	5076	3873	3098	2268	1877	1799	1673	1456	1281	1098	890	749	513	299	142	66	0
12000	6500	13206	11751	10530	9514	8770	7564	5290	3991	3239	2429	2116	2091	2020	1664	1445	1270	1076	903	588	343	169	80	0
12000	7000	13689	12152	10841	9715	8838	7643	5346	4035	3319	2652	2326	2225	2106	1800	1576	1364	1150	973	652	390	198	94	0
12000	7500	14161	12534	11149	9952	8942	7712	5403	4054	3404	2855	2556	2423	2286	1948	1653	1433	1223	1037	714	437	228	109	0
12000	8000	14662	12943	11474	10247	9213	7919	5460	4075	3533	3020	2664	2570	2496	2307	1914	1594	1374	1140	774	484	260	123	0
13000	0	3766	3617	3465	3317	3247	3184	3111	2935	2352	1850	1530	1255	1115	987	865	775	720	677	588	518	373	187	0
13000	50	4208	4039	3883	3712	3624	3555	3463	3302	2728	2293	2039	1827	1658	1496	1404	1326	1237	1143	1005	926	752	444	0
13000	100	4575	4391	4236	4050	3947	3870	3762	3597	3067	2675	2463	2279	2106	1909	1830	1749	1618	1446	1234	940	933	636	0
13000	300	4843	4613	4448	4233	4101	4018	3934	3831	3536	3175	2868	2663	2492	2124	1896	1746	1454	1179	931	746	622	506	0
13000	500	4923	4655	4500	4233	4043	3803	3654	3560	3358	3019	2708	2485	2193	1864	1584	1320	1069	716	473	397	245	208	0
13000	1000	5355	4921	4614	4095	3769	3369	3032	2832	2644	2307	1992	1724	1540	1361	1136	721	471	351	254	202	122	72	0
13000	1500	6344	5777	5070	4197	3817	3594	3201	2766	2390	2013	1697	1396	1182	937	699	476	361	293	229	162	112	50	0
13000	2000	7337	6773	5836	4656	4124	3820	3363	2852	2361	1965	1637	1277	962	638	455	387	307	243	206	113	86	44	0
13000	2500	8056	7515	6896	5685	4865	4126	3471	2940	2403	1983	1567	1149	797	504	362	309	235	192	161	102	84	44	0
13000	3000	8688	7876	7317	6269	5533	4509	3631	3022	2449	1962	1434	1031	777	562	385	290	231	228	186	107	84	45	0
13000	3500	9210	8021	7365	6395	5766	4775	3802	3091	2491	1978	1413	1065	874	681	485	376	331	287	201	111	86	46	0
13000	4000	9436	8108	7419	6533	5984	5113	4060	3223	2620	2024	1493	1222	1038	867	702	586	452	342	244	139	90	47	0
13000	4500	9495	8197	7536	6741	6225	5464	4230	3342	2784	2106	1604	1362	1176	1020	863	712	526	387	298	178	97	48	0
13000	5000	9545	8199	7622	7067	6480	5834	4420	3429	2879	2232	1789	1532	1324	1139	950	769	575	433	355	218	105	49	0
13000	5500	10034	8609	7982	7400	6731	6064	4489	3515	2935	2324	1949	1726	1520	1303	1094	904	682	518	403	255	119	54	0
13000	6000	11456	10012	9157	8347	7605	6635	4586	3609	3029	2384	2027	1894	1714	1449	1265	1109	894	735	499	292	139	65	0
13000	6500	12458	11078	9915	8897	8120	6995	4727	3679	3121	2471	2174	2110	2016	1658	1431	1278	1053	882	578	336	165	78	0
13000	7000	12882	11431	10179	9113	8280	7180	4812	3703	3206	2607	2298	2192	2090	1791	1573	1369	1136	955	641	383	194	93	0

Cont'd

P (kPa)	G (kg/m²s)	Quality -0.5	-0.4	-0.3	-0.2	-0.15	-0.1	-0.1	0	0.05	0.1	0.15	0.2	0.25	0.3	0.35	0.4	0.45	0.5	0.6	0.7	0.8	0.9	1
13000	7500	13246	11713	10405	9314	8405	7305	4870	3742	3310	2761	2431	2305	2191	1898	1640	1434	1217	1022	703	431	225	107	0
13000	8000	13772	12145	10756	9606	8630	7448	4957	3776	3396	2923	2537	2427	2360	2161	1859	1592	1365	1126	763	477	257	122	0
14000	0	3493	3365	3232	3106	3046	2994	2930	2779	2271	1812	1510	1248	1089	963	851	767	714	695	598	509	351	175	0
14000	50	3895	3750	3620	3476	3402	3343	3266	3123	2618	2211	1958	1756	1588	1423	1327	1253	1168	1070	974	807	632	350	0
14000	100	4229	4072	3948	3794	3708	3641	3551	3403	2933	2560	2336	2169	2005	1804	1708	1636	1509	1300	992	764	615	355	0
14000	300	4448	4260	4142	3970	3862	3800	3706	3630	3411	3099	2800	2552	2404	1967	1669	1554	1263	986	757	563	378	246	0
14000	500	4497	4278	4181	4004	3832	3618	3453	3399	3267	2963	2612	2295	1941	1605	1318	1124	950	626	381	322	224	164	0
14000	1000	4928	4533	4349	3958	3659	3197	2864	2705	2530	2189	1791	1508	1359	1209	980	627	434	334	223	190	116	70	0
14000	1500	5911	5399	4821	4046	3724	3394	3020	2650	2255	1847	1534	1287	1089	877	629	396	307	273	205	150	93	47	0
14000	2000	6752	6229	5421	4413	3994	3672	3200	2739	2230	1886	1520	1188	902	629	425	316	248	220	195	109	80	41	0
14000	2500	7369	6879	6351	5379	4639	4017	3363	2826	2300	1938	1498	1089	782	529	351	266	200	170	148	101	82	43	0
14000	3000	8033	7236	6834	6001	5227	4390	3551	2931	2372	1959	1477	1078	826	589	388	285	218	202	166	106	83	43	0
14000	3500	8543	7311	6865	6069	5420	4584	3679	3013	2439	2039	1546	1190	943	696	496	383	312	257	185	112	84	44	0
14000	4000	8724	7332	6886	6137	5545	4794	3790	3086	2622	2184	1688	1356	1106	871	695	596	471	330	227	135	87	44	0
14000	4500	8731	7377	6942	6292	5734	5054	3846	3189	2929	2368	1828	1489	1240	1023	866	746	586	394	282	172	94	45	0
14000	5000	8733	7394	6999	6618	6103	5568	4075	3321	3081	2520	1993	1648	1390	1164	988	840	685	480	338	210	101	47	0
14000	5500	9100	7685	7266	6926	6363	5822	4241	3364	3088	2583	2156	1850	1596	1343	1148	985	803	568	382	246	116	53	0
14000	6000	10544	9148	8464	7715	7010	6223	4288	3456	3126	2613	2254	1996	1776	1472	1280	1152	942	721	484	286	136	64	0
14000	6500	11595	10306	9186	8230	7474	6512	4416	3503	3132	2665	2333	2149	2010	1646	1413	1286	1053	866	568	332	163	77	0
14000	7000	11986	10624	9429	8450	7655	6686	4467	3523	3169	2673	2344	2172	2079	1785	1572	1396	1137	942	633	379	192	91	0
14000	7500	12314	10864	9636	8641	7821	6853	4610	3613	3242	2682	2356	2240	2133	1870	1623	1444	1217	1012	695	427	222	106	0
14000	8000	12821	11286	9967	8893	8043	7029	4837	3735	3362	2870	2449	2313	2243	2034	1810	1588	1357	1116	757	474	255	121	0
15000	0	3196	3087	2976	2868	2815	2772	2720	2595	2165	1750	1456	1221	1047	923	831	745	694	693	645	501	297	172	0
15000	50	3566	3437	3319	3207	3149	3098	3033	2910	2485	2114	1873	1695	1514	1341	1223	1152	1073	968	900	712	520	332	0
15000	100	3874	3730	3611	3497	3434	3373	3295	3163	2768	2430	2229	2087	1906	1686	1537	1472	1355	1123	871	648	494	327	0
15000	300	4082	3878	3747	3630	3543	3442	3358	3274	3111	2884	2667	2393	2193	1807	1514	1251	1128	866	644	482	351	227	0
15000	500	4184	3933	3790	3638	3517	3315	3195	3115	3003	2739	2384	1923	1657	1425	1191	1038	895	597	368	299	213	134	0
15000	1000	4678	4287	4068	3724	3482	3068	2708	2468	2251	1897	1523	1286	1204	1147	927	606	420	312	192	174	108	60	0
15000	1500	5402	4961	4532	3891	3586	3155	2674	2312	1955	1649	1367	1179	1025	850	595	368	259	233	176	135	92	43	0
15000	2000	5890	5387	4879	4196	3805	3351	2833	2464	2071	1843	1501	1178	918	664	424	281	202	190	163	106	76	39	0
15000	2500	6438	5806	5478	4946	4365	3686	3083	2705	2224	1912	1559	1171	891	618	395	272	193	149	139	107	80	41	0

Cont'd

P (kPa)	G (kg/m²s)	Quality -0.5	-0.4	-0.3	-0.2	-0.15	-0.1	-0.1	0	0.05	0.1	0.15	0.2	0.25	0.3	0.35	0.4	0.45	0.5	0.6	0.7	0.8	0.9	1
15000	3000	7244	6348	6122	5596	4858	4010	3336	2854	2322	1974	1595	1225	954	675	461	344	257	180	154	111	81	42	0
15000	3500	7886	6597	6342	5765	5039	4226	3459	2904	2340	2055	1670	1339	1062	769	557	454	360	266	185	116	82	42	0
15000	4000	8278	6675	6445	5899	5239	4502	3517	2916	2615	2270	1815	1483	1217	939	750	673	549	377	231	132	83	42	0
15000	4500	8512	6767	6565	6179	5561	4808	3552	3057	2953	2472	1951	1607	1355	1103	934	841	676	455	291	164	88	43	0
15000	5000	8629	6956	6681	6504	5999	5383	3789	3255	3188	2657	2131	1774	1495	1250	1083	944	762	524	352	204	95	45	0
15000	5500	8926	7284	6913	6707	6217	5673	3984	3297	3216	2744	2295	1947	1676	1419	1232	1065	855	605	406	244	113	52	0
15000	6000	9942	8684	7860	7163	6512	5863	4029	3339	3221	2785	2397	2063	1838	1539	1321	1180	967	739	484	283	135	63	0
15000	6500	10615	9447	8361	7475	6767	5984	4103	3419	3228	2823	2440	2165	2002	1656	1421	1300	1079	855	558	328	162	77	0
15000	7000	10992	9718	8592	7676	6946	6098	4135	3443	3286	2826	2450	2179	2068	1774	1570	1405	1160	938	623	375	191	91	0
15000	7500	11337	9941	8797	7866	7112	6222	4282	3522	3297	2831	2461	2194	2099	1845	1610	1458	1230	1013	689	424	221	105	0
15000	8000	11774	10337	9087	8074	7319	6455	4633	3670	3309	2836	2481	2218	2166	1988	1784	1576	1349	1111	753	471	253	121	0
16000	0	2883	2793	2700	2612	2571	2530	2489	2380	2020	1647	1379	1162	997	873	769	674	614	612	537	383	260	167	0
16000	50	3213	3103	3009	2911	2857	2816	2759	2664	2329	1998	1756	1586	1404	1228	1076	975	888	791	693	482	383	311	0
16000	100	3486	3359	3268	3163	3101	3054	2983	2888	2593	2295	2072	1940	1741	1521	1333	1226	1114	907	695	550	330	319	0
16000	300	3649	3473	3359	3236	3159	3080	3009	2934	2818	2597	2432	2194	2016	1688	1438	1124	978	747	508	428	325	210	0
16000	500	3683	3441	3336	3210	3112	2886	2775	2673	2545	2268	1963	1580	1362	1198	1051	934	803	574	333	272	203	127	0
16000	1000	4042	3623	3491	3323	3149	2725	2366	2089	1853	1528	1251	1076	992	948	804	587	407	288	174	154	102	59	0
16000	1500	4726	4312	4002	3586	3329	2901	2360	1945	1655	1419	1235	1071	907	743	541	357	228	172	125	115	80	39	0
16000	2000	5241	4790	4395	3873	3538	3050	2500	2166	1841	1688	1477	1188	943	704	462	312	201	147	120	105	72	36	0
16000	2500	5901	5360	5038	4546	4031	3307	2724	2446	2112	1888	1628	1298	1031	754	495	339	244	197	165	120	76	37	0
16000	3000	6667	5912	5709	5190	4449	3540	2937	2617	2282	2058	1745	1408	1139	849	597	465	370	271	190	123	78	39	0
16000	3500	7252	6155	5907	5393	4622	3772	3075	2660	2440	2199	1859	1554	1254	947	698	588	485	369	247	129	79	39	0
16000	4000	7734	6288	6048	5561	4834	4052	3170	2824	2668	2401	2011	1691	1412	1104	867	763	634	476	297	136	80	39	0
16000	4500	8088	6346	6193	5888	5220	4407	3270	2980	2932	2554	2118	1807	1543	1240	1026	901	736	543	343	163	81	40	0
16000	5000	8350	6494	6277	6217	5695	4991	3561	3223	3209	2774	2307	1979	1684	1391	1174	990	803	597	395	201	89	42	0
16000	5500	8669	6857	6463	6376	5903	5268	3783	3344	3321	2940	2470	2116	1814	1519	1289	1084	885	667	449	244	109	50	0
16000	6000	9148	7890	7094	6537	5988	5386	3873	3367	3321	2993	2586	2242	1942	1627	1389	1211	1009	765	499	283	134	63	0
16000	6500	9555	8478	7462	6654	6074	5402	3928	3388	3321	3003	2611	2301	2033	1704	1481	1339	1121	857	557	328	161	76	0
16000	7000	9926	8738	7682	6811	6188	5423	3952	3406	3395	3020	2629	2340	2057	1754	1567	1435	1199	940	618	373	190	90	0
16000	7500	10287	8963	7885	6963	6314	5492	4090	3425	3414	3039	2650	2359	2088	1830	1598	1473	1249	1018	686	422	220	105	0
16000	8000	10652	9312	8130	7145	6495	5785	4413	3445	3434	3050	2669	2380	2141	1969	1749	1554	1342	1107	751	470	253	120	0

Cont'd

P (kPa)	G (kg/m²s)	Quality -0.5	-0.4	-0.3	-0.2	-0.15	-0.1	-0.1	0	0.05	0.1	0.15	0.2	0.25	0.3	0.35	0.4	0.45	0.5	0.6	0.7	0.8	0.9	1
17000	0	2551	2479	2406	2335	2300	2276	2235	2146	1849	1547	1327	1144	993	866	761	672	608	598	494	354	257	156	0
17000	50	2800	2707	2619	2530	2485	2439	2398	2319	2046	1734	1473	1299	1154	1022	922	858	798	726	587	407	347	292	0
17000	100	2998	2886	2789	2685	2631	2566	2521	2439	2196	1878	1584	1423	1286	1150	1054	1007	946	806	581	490	300	258	0
17000	300	2970	2769	2607	2439	2347	2260	2175	2102	1972	1755	1532	1399	1286	1107	1000	941	821	659	429	390	295	192	0
17000	500	2817	2549	2374	2227	2138	2044	1917	1774	1661	1487	1308	1151	1048	958	868	802	685	534	291	243	194	118	0
17000	1000	3054	2719	2452	2318	2233	2074	1850	1597	1407	1205	1045	912	839	744	635	483	354	273	153	109	77	52	0
17000	1500	3874	3538	3124	2722	2518	2320	2043	1753	1526	1305	1187	1020	859	685	527	361	223	155	104	83	74	39	0
17000	2000	4639	4218	3790	3214	2860	2568	2288	2018	1757	1533	1435	1223	993	780	567	405	273	180	125	108	69	33	0
17000	2500	5565	5074	4638	3963	3416	2911	2529	2283	1991	1790	1637	1408	1148	885	618	462	358	288	218	136	72	35	0
17000	3000	6358	5769	5238	4406	3758	3197	2726	2415	2218	2081	1832	1562	1289	1006	719	568	483	407	302	148	73	36	0
17000	3500	6917	6047	5368	4467	3874	3398	2844	2588	2526	2337	1993	1685	1399	1114	831	694	609	533	462	193	76	36	0
17000	4000	7403	6224	5569	4621	4012	3528	2931	2765	2746	2519	2134	1807	1533	1246	978	832	702	615	489	212	77	37	0
17000	4500	7593	6226	5723	4953	4355	3694	3017	2902	2863	2619	2245	1935	1681	1380	1120	947	775	646	499	216	80	37	0
17000	5000	7689	6228	5814	5285	4769	3933	3247	3128	3110	2821	2406	2092	1833	1539	1273	1048	849	685	508	242	89	40	0
17000	5500	7871	6397	5943	5432	4936	4086	3463	3348	3330	3024	2545	2203	1931	1643	1365	1135	938	743	530	275	109	49	0
17000	6000	8132	6991	6277	5506	4986	4123	3478	3399	3370	3080	2673	2311	1984	1694	1457	1277	1069	821	577	307	135	62	0
17000	6500	8472	7405	6535	5600	5049	4154	3524	3399	3374	3087	2708	2349	2037	1733	1526	1395	1174	872	597	340	161	76	0
17000	7000	8820	7664	6746	5718	5133	4169	3580	3437	3415	3116	2719	2357	2047	1741	1562	1463	1237	947	629	376	189	90	0
17000	7500	9163	7907	6947	5876	5271	4356	3770	3517	3434	3135	2738	2367	2058	1825	1593	1490	1269	1023	683	420	219	104	0
17000	8000	9480	8235	7110	6148	5620	5075	4230	3649	3455	3155	2757	2388	2120	1952	1722	1537	1334	1104	748	468	251	120	0
18000	0	2189	2133	2078	2022	1997	1976	1950	1885	1647	1398	1213	1060	930	812	726	657	595	577	444	315	228	139	0
18000	50	2382	2308	2239	2172	2137	2103	2070	2004	1782	1532	1325	1183	1062	937	849	796	752	691	525	400	314	248	0
18000	100	2524	2435	2357	2282	2239	2192	2152	2077	1880	1632	1410	1278	1168	1040	940	892	865	757	542	478	274	233	0
18000	300	2378	2223	2101	2002	1936	1854	1777	1693	1600	1481	1325	1192	1112	991	871	759	688	580	392	375	271	174	0
18000	500	2137	1930	1790	1698	1657	1582	1487	1377	1275	1210	1096	964	895	854	749	653	545	457	274	231	184	115	0
18000	1000	2484	2220	1960	1832	1759	1689	1587	1399	1195	1049	979	854	747	652	543	409	317	269	160	136	88	47	0
18000	1500	3354	3048	2648	2304	2097	2004	1862	1606	1377	1204	1165	1011	849	695	554	383	229	198	112	73	71	35	0
18000	2000	4160	3773	3358	2874	2589	2408	2176	1855	1637	1484	1448	1259	1077	897	675	447	288	234	138	115	66	31	0
18000	2500	5115	4671	4271	3613	3118	2736	2410	2108	1885	1730	1680	1431	1241	1010	757	532	413	352	268	147	68	32	0
18000	3000	5776	5147	4697	3919	3353	2939	2529	2224	2092	2088	1863	1569	1328	1104	860	653	513	465	368	158	69	33	0
18000	3500	6200	5263	4751	3952	3428	3073	2613	2476	2473	2291	1953	1645	1395	1186	966	764	640	606	526	209	72	34	0
18000	4000	6698	5557	5016	4100	3547	3146	2683	2602	2600	2432	2107	1808	1584	1341	1080	881	705	643	601	238	74	34	0

Cont'd

P (kPa)	G (kg/m²s)	Quality -0.5	-0.4	-0.3	-0.2	-0.15	-0.1	-0.1	0	0.05	0.1	0.15	0.2	0.25	0.3	0.35	0.4	0.45	0.5	0.6	0.7	0.8	0.9	1
18000	4500	6863	5589	5164	4349	3817	3236	2917	2828	2795	2504	2176	2020	1761	1486	1188	1000	777	664	611	239	76	35	0
18000	5000	6894	5600	5215	4608	4132	3365	3148	3069	2992	2578	2354	2132	1877	1636	1342	1113	900	741	628	260	88	39	0
18000	5500	6982	5726	5328	4726	4258	3473	3458	3458	3313	2865	2532	2295	2023	1768	1410	1167	983	817	635	291	109	49	0
18000	6000	7157	6118	5497	4754	4297	3667	3557	3471	3334	2885	2620	2357	2031	1778	1494	1335	1126	869	651	324	135	62	0
18000	6500	7437	6468	5657	4756	4302	3860	3656	3485	3355	2904	2640	2363	2038	1789	1535	1437	1227	898	654	356	162	75	0
18000	7000	7750	6724	5829	4805	4340	4053	3754	3498	3374	2924	2659	2383	2046	1799	1540	1458	1261	965	667	387	190	89	0
18000	7500	8065	6948	6031	5039	4556	4247	3853	3511	3393	2945	2680	2404	2053	1809	1577	1464	1275	1034	697	423	218	104	0
18000	8000	8347	7225	6182	5286	4858	4441	3952	3525	3414	2965	2701	2423	2114	1934	1710	1515	1321	1103	746	468	249	120	0
19000	0	1786	1744	1699	1656	1639	1628	1618	1567	1393	1207	1069	964	856	741	664	630	570	528	402	281	194	116	0
19000	50	1935	1889	1843	1802	1777	1752	1711	1660	1503	1316	1154	1055	974	843	724	660	624	590	460	369	278	214	0
19000	100	2032	1983	1940	1903	1872	1830	1760	1706	1570	1388	1208	1113	1056	918	760	666	655	624	483	423	332	220	0
19000	300	1682	1612	1549	1545	1528	1462	1358	1290	1218	1115	974	854	807	763	646	534	485	452	342	333	248	156	0
19000	500	1364	1264	1167	1123	1099	1067	980	911	833	810	799	724	695	671	575	508	447	381	250	207	174	112	0
19000	1000	1882	1752	1537	1372	1286	1241	1189	1085	909	890	889	800	705	646	529	420	350	263	177	119	83	33	0
19000	1500	2838	2604	2302	2033	1827	1702	1623	1428	1225	1170	1114	986	838	737	605	406	303	244	137	83	60	31	0
19000	2000	3670	3283	2917	2593	2380	2218	2014	1679	1498	1465	1402	1226	1101	945	746	470	335	249	150	116	63	29	0
19000	2500	4468	3900	3580	3169	2832	2523	2261	1905	1694	1672	1531	1393	1246	1064	840	618	481	373	279	156	66	30	0
19000	3000	4747	4016	3725	3315	2968	2642	2332	1977	1769	1768	1610	1472	1328	1169	929	735	587	490	390	184	67	31	0
19000	3500	4918	4106	3813	3355	3013	2717	2393	2047	1917	1890	1742	1595	1391	1216	993	821	671	646	550	225	71	31	0
19000	4000	5285	4443	4086	3441	3077	2773	2470	2158	2021	2014	1875	1720	1455	1264	1098	883	710	646	587	272	72	32	0
19000	4500	5496	4642	4166	3493	3159	2813	2534	2280	2130	2127	2125	1902	1593	1455	1212	1021	823	673	588	278	75	33	0
19000	5000	5668	4833	4311	3646	3301	2910	2760	2757	2546	2342	2151	1963	1762	1648	1414	1127	897	701	638	288	88	39	0
19000	5500	5862	5120	4534	3738	3375	3017	2879	2877	2796	2587	2350	2135	1945	1771	1519	1211	1021	836	692	301	109	48	0
19000	6000	6118	5409	4659	3748	3396	3107	3059	3058	3028	2756	2485	2290	1948	1775	1531	1328	1170	893	693	333	135	61	0
19000	6500	6389	5636	4757	3765	3426	3162	3134	3123	3069	2775	2505	2348	1950	1779	1546	1438	1273	929	695	365	162	75	0
19000	7000	6653	5832	4906	3883	3540	3240	3160	3143	3087	2797	2526	2367	1953	1783	1559	1451	1287	985	696	396	190	89	0
19000	7500	6916	5989	5136	4275	3911	3493	3268	3164	3119	2815	2545	2388	2011	1787	1574	1461	1294	1048	716	430	219	103	0
19000	8000	7164	6190	5284	4511	4158	3826	3509	3204	3139	2836	2566	2409	2090	1919	1703	1502	1311	1102	745	468	248	119	0
20000	0	1367	1333	1304	1277	1261	1255	1235	1193	1092	988	921	846	761	665	573	522	472	418	321	228	154	90	0
20000	50	1628	1593	1576	1552	1522	1477	1396	1314	1222	1094	1001	951	881	747	623	547	481	424	345	270	215	152	0
20000	100	1806	1774	1772	1752	1715	1633	1508	1394	1310	1165	1044	1014	957	797	651	553	480	421	371	369	224	187	0

Concluded

P (kPa)	G (kg/m²s)	Quality -0.5	-0.4	-0.3	-0.2	-0.15	-0.1	-0.1	0	0.05	0.1	0.15	0.2	0.25	0.3	0.35	0.4	0.45	0.5	0.6	0.7	0.8	0.9	1
20000	300	1524	1476	1461	1461	1449	1379	1253	1173	1072	904	721	667	652	609	547	432	353	318	292	291	223	140	0
20000	500	1167	1090	1024	997	978	962	905	858	781	685	592	572	572	539	487	430	344	269	210	185	165	72	0
20000	1000	1538	1403	1259	1142	1086	996	936	873	750	713	712	711	667	610	485	393	358	259	190	102	77	31	0
20000	1500	2411	2193	1966	1766	1640	1468	1328	1194	1161	1161	1096	949	769	681	611	533	385	250	139	103	63	29	0
20000	2000	3269	2881	2536	2229	2049	1812	1633	1469	1396	1360	1198	1153	1029	939	825	593	411	283	167	129	62	27	0
20000	2500	3945	3350	2983	2597	2338	2012	1864	1692	1534	1369	1252	1250	1153	1124	939	808	611	428	291	159	64	28	0
20000	3000	4169	3514	3182	2767	2442	2077	1949	1770	1566	1380	1294	1293	1292	1227	1033	905	672	558	388	173	65	29	0
20000	3500	4171	3606	3286	2850	2522	2154	2014	1854	1763	1669	1581	1522	1331	1253	1128	962	813	671	582	232	70	29	0
20000	4000	4173	3765	3426	2954	2639	2294	2174	2013	1960	1959	1870	1753	1371	1280	1188	1035	856	690	583	258	72	29	0
20000	4500	4233	4009	3596	3034	2742	2472	2308	2123	2096	2096	2008	1892	1473	1425	1280	1044	871	695	585	262	75	31	0
20000	5000	4436	4270	3812	3193	2893	2659	2489	2485	2256	2120	2038	1927	1576	1571	1374	1150	887	701	692	277	88	37	0
20000	5500	4687	4581	4048	3320	3002	2825	2661	2657	2428	2146	2068	1962	1678	1669	1509	1230	996	857	693	302	109	48	0
20000	6000	4915	4686	4148	3416	3109	2950	2733	2728	2611	2172	2100	1999	1832	1671	1521	1312	1178	935	694	333	135	60	0
20000	6500	5129	4688	4157	3492	3206	3018	2820	2815	2697	2220	2116	2040	1891	1674	1534	1393	1257	958	696	366	163	74	0
20000	7000	5338	4706	4158	3532	3242	3051	2840	2835	2717	2260	2147	2083	1931	1678	1547	1400	1265	998	700	399	190	88	0
20000	7500	5548	4808	4185	3586	3298	3110	2861	2854	2736	2329	2179	2114	1983	1776	1561	1413	1274	1053	726	433	220	103	0
20000	8000	5757	4976	4232	3614	3338	3135	2882	2876	2755	2443	2255	2164	2075	1912	1697	1493	1304	1102	744	467	247	119	0

IMAGE EVALUATION TEST TARGET (QA-3)

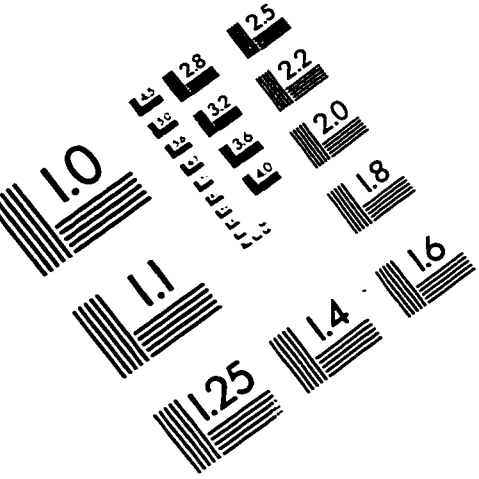

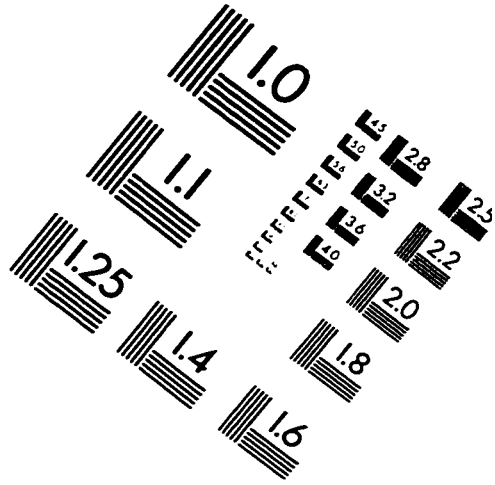

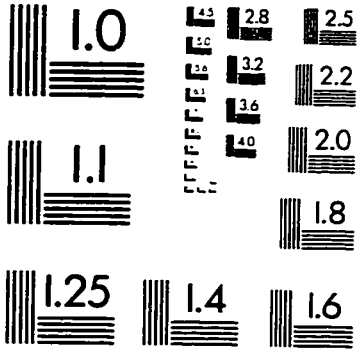

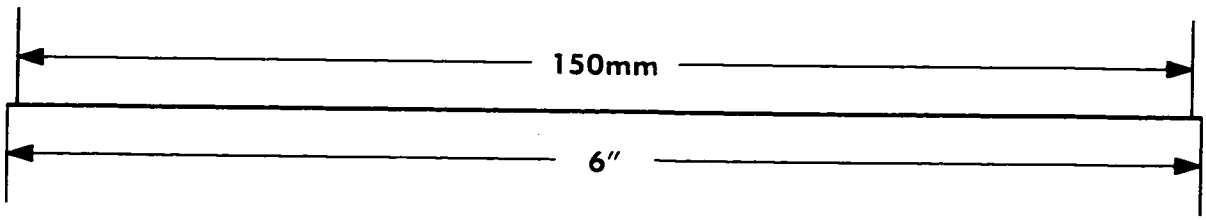

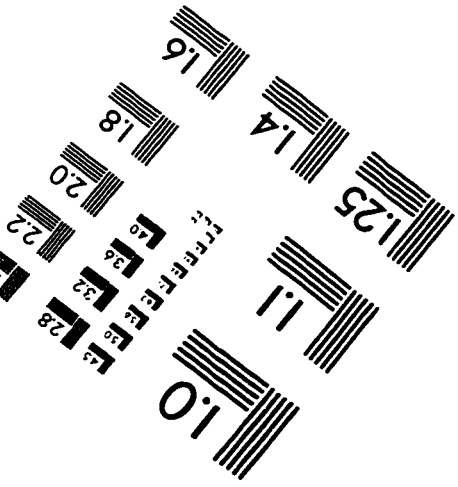

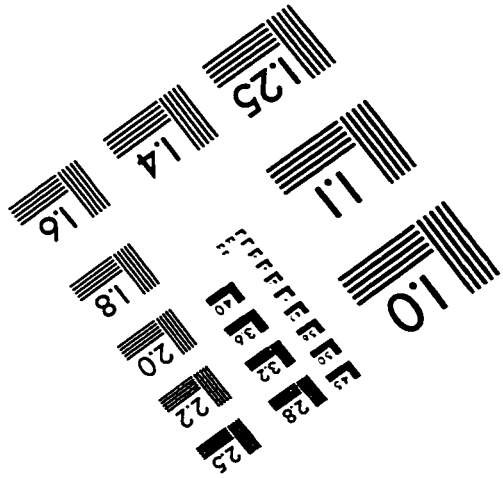

APPLIED IMAGE, Inc
1653 East Main Street
Rochester, NY 14609 USA
Phone: 716/482-0300
Fax: 716/288-5989